

DISSERTATION THESIS

Structure, activity and metabolism of human glutamate carboxypeptidase II

by
Petra Mlčochová

Scientific Supervisor: Jan Konvalinka



Department of Biochemistry
Faculty of Natural Science
Charles University



Gilead Sciences and IOCB Research Center,
Institute of Organic Chemistry and Biochemistry
Academy of Sciences of the Czech Republic

Prague 2007

ACKNOWLEDGEMENTS

Hereby, I wish to thank all my colleagues and friends who contributed to the completion of this dissertation thesis.

First of all, I want to thank Jan Konvalinka for kind advice and financial support and also for several enigmatic projects which tested my persistence and skills.

I also want to thank Anička Plechanovová, my former diploma student and my friend, for her brilliant co-operation and her bright, omnipresent comments.

My thanks also belong to the whole „NAALADase team“, especially to my colleague Pavlík Šácha, who was always there to discuss projects and find, if not answers, at least some reasonable theories. I thank Klara Hlouchová for her enthusiasm for the work and for the reason that she did not let me be the only one who was losing the plot during some long working days. And, of course, I thank Mirka Rovenská for her unforgettable „**Marvin-** from **Hitchhiker's** Guide“ mood and her ability to frequently obtain more suspicious results than me.

I cannot forget to thank Jana „Bimča“ Starková, my very good friend and also a very nice person, for her excellent assistance in my experiments and for her unflagging solicitude towards our tissue cultures.

I thank my loving family, who enabled me to finish my studies.

CONTENTS

1	ABBREVIATIONS	5
2	PREFACE.....	7
3	INTRODUCTION	10
3.1	GCPII AS AN INTERESTING MOLECULE (A GENERAL INFORMATION) ..	11
3.1.1	<i>GCPII: from DNA to protein</i>	11
3.1.2	<i>GCPII hydrolytic activities</i>	13
3.1.2.1	N-acetylated-alpha-linked acidic dipeptidase activity.....	13
3.1.2.2	Folylpoly-gamma-glutamate carboxypeptidase activity	13
3.1.3	<i>GCPII substrate specificity</i>	14
3.1.4	<i>GCPII inhibitors</i>	14
3.1.5	<i>GCPII structure</i>	16
3.1.5.1	Overall structure of GCPII	16
3.1.5.2	Active site of GCPII	20
3.2	GCPII AS A NEUROPEPTIDASE	22
3.2.1	<i>Glutamate, NAAG, GCPII and nervous system</i>	22
3.2.1.1	Glutamate-excitatory neurotransmitter.....	22
3.2.1.2	N-acetyl-aspartyl-glutamate (NAAG)	23
3.2.1.3	NAAG peptidase (= glutamate carboxypeptidase II = GCPII)	24
3.2.2	<i>Acute neurological disorders and GCPII</i>	25
3.2.2.1	Stroke.....	25
3.2.2.2	Head injury	27
3.2.2.3	Neuropathic and inflammantory pain	27
3.2.3	<i>Chronic neurological disorders and GCPII</i>	28
3.2.3.1	Schizophrenia	28
3.2.3.2	Diabetic neuropathy.....	28
3.2.3.3	Amyotrophic lateral sclerosis	28
3.3	GCPII AS A DIAGNOSTIC MARKER AND THERAPEUTIC TARGET IN THE PROSTATE CANCER	29
3.3.1	<i>GCPII as a marker of prostate cancer</i>	29
3.3.1.1	Prostate cancer in numbers	29
3.3.1.2	Markers of the prostate cancer.....	30
3.3.1.2.1	Prostatic Acid Phosphatase (PAP).....	30
3.3.1.2.2	Prostate specific antigen (PSA).....	30
3.3.1.2.3	GCPII disguised as Prostate specific membrane antigen	31
3.3.1.2.3.1	GCPII organ-specificity.....	31
3.3.1.2.3.2	GCPII cancer-specificity	35
3.3.1.2.3.3	GCPII specificity and sensitivity.....	38
3.3.1.2.3.4	Simple and cost-efficient test for GCPII and cancer prognosis.....	38
3.3.1.2.3.4.1	Serum screening	38
3.3.1.2.3.4.2	Detection of GCPII mRNA	39
3.3.1.2.3.4.3	Detection of GCPII protein: ProstaScint scan.....	39
3.3.2	<i>Therapeutic target in the prostate cancer - GCPII again</i>	40
3.3.2.1	Radioimmunotherapy	40
3.3.2.2	Immunotherapeutic approach	40
3.3.2.3	Immunotoxins.....	41

3.3.2.4	Gene therapy and enhancer/promoter of GCPII.....	42
4	DISSERTATION RESEARCH AIMS	43
5	LIST OF PUBLICATIONS	44
6	RESULTS AND DISCUSSION	47
6.1	IMPORTANCE OF AMINO ACID RESIDUES INSIDE THE ACTIVE SITE OF GCPII ..	48
6.1.1	<i>Background information</i>	48
6.1.2	<i>Summary</i>	49
6.1.3	<i>Publication I</i>	50
6.2	EXTRACELLULAR DOMAIN OF GCPII: IDENTIFICATION OF PUTATIVE PROTEOLYTIC DOMAIN	64
6.2.1	<i>Background information</i>	64
6.2.2	<i>Summary</i>	65
6.2.3	<i>Publication II</i>	66
6.2.4	<i>Postscript</i>	75
6.3	STRUCTURAL ANALYSIS OF THE BINDING SPECIFICITY OF GCPII: RATIONAL DRUG DESIGN	76
6.3.1	<i>Background information</i>	76
6.3.2	<i>Summary</i>	77
6.3.3	<i>Publication III</i>	78
6.4	GCPIII, A HUMAN HOMOLOG OF GCPII.....	85
6.4.1	<i>Background information</i>	85
6.4.2	<i>Summary</i>	86
6.4.3	<i>Publication IV</i>	87
6.5	GCPII IN HUMAN BRAIN.....	102
6.5.1	<i>Background information</i>	102
6.5.2	<i>Summary</i>	102
6.5.3	<i>Publication V</i>	104
6.6	FULL LENGTH FORM OF GCPII – PSMA AND THE ORIGIN OF ITS TRUNCATED FORM	116
6.6.1	<i>Background information</i>	116
6.6.2	<i>Summary</i>	116
6.6.3	<i>Publication VI</i>	118
7	CONCLUSIONS AND PERSPECTIVES	136
8	REFERENCES	141
9	GLOSSARY	162

1 ABBREVIATIONS

ALS	amyotrophic lateral sclerosis
AMPA	alpha-amino-3-hydroxy-5-methyl-4-isoxazolepropionate
Beta-NAAG	N-acetyl-beta-aspartyl-glutamic acid
DM1	derivate of maytansine (from ethiopian plant <i>Maytenus serrata</i>), tumor-activated immunotoxin
DNA	deoxyribonucleic acid
EGTA	ethylene glycol tetraacetic acid
FISH	Fluorescent <i>in situ</i> hybridization
FOLH1	folate hydrolase 1
GABA	γ -aminobutyric acid
GCPII	glutamate carboxypeptidase II
GCPIII	glutamate carboxypeptidase III
IC₅₀	median Inhibition Concentration
K_M	Michaelis-Menten constant
K_I	inhibition constant
LNCaP	lymph node carcinoma of the prostate
mAb	monoclonal antibody
mGluR	metabotropic glutamate receptors
mRNA	messenger ribonucleic acid
NAA	N-acetyl-aspartate
NAAG	N-acetyl-aspartyl-glutamate
NAALADase	N-acetylated-alpha-linked acidic dipeptidase
NAALADase L	N-acetylated-alpha-linked acidic dipeptidase-like protein
NMDA	N-methyl-D-aspartic acid
NMDAR	NMDA receptor
PAP	prostatic acid phosphatase
PCP	phenylcyclohexylpiperidine
PSA	prostate specific antigen
PSCA	prostate stem cell antigen
PSM[?]	truncated form of prostate specific membrane antigen at N-terminus
PSMA	prostate specific membrane antigen
PSM-C	alternatively spliced variant of PSMA
PSM-D	alternatively spliced variant of PSMA
PSM-E	alternatively spliced variant of PSMA
PSM-F	alternatively spliced variant of PSMA
2-PMPA	2-(phosphonomethyl)pentanedioic acid
QM/MM	quantum mechanics/molecular mechanics
rRNA	ribosomal RNA
RT-PCR	reverse transcriptase-polymerase chain reaction
TGF-β	transforming growth factor beta

2 PREFACE

Glutamate carboxypeptidase II (GCPII) is a type II transmembrane glycoprotein. Its expression was independently discovered in brain, prostate and also in small intestine. In the brain it is known as a N-acetylated- α -linked acidic dipeptidase (NAALADase), in the prostate as a Prostate-Specific Membrane Antigen (PSMA), in the small intestine as a folate hydrolase (FOLH1). Although NAALADase, PSMA and FOLH1 were identified as a single protein at the end and the name of the protein was standardized to glutamate carboxypeptidase II (GCPII), the researchers from different disciplines use all four known names.

GCPII is a metallopeptidase from the M28 family. It is homologous to aminopeptidases (from *Aeromonas proteolytica* and *Streptomyces griseus*), which also belong to this family. The first model of domain representation was constructed based on this homology. The first X-ray structure was determined almost one decade later. The structure of extracellular part of GCPII reveals a symmetric homodimer with each monomer containing three domains (analogous to three domains of transferrin receptor): a protease domain, an apical domain, and a helical domain. Amino acids from all three domains are involved in substrate binding. Even though GCPII protein was also crystallized with inhibitors and product of hydrolysis (glutamate), the structure with a natural substrate has not yet been determined.

GCPII is expressed in high concentration in human brain. It hydrolyzes a substrate N-acetyl-aspartyl-glutamate (NAAG), which is cleaved into N-acetyl-aspartate and glutamate. NAAG is an abundant neurotransmitter in central nervous system and together with glutamate plays a role in excitotoxic neurotransmission. Inhibition of NAAG hydrolysis by specific and potent inhibitor 2-(phosphonomethyl)pentanedioic acid (2-PMPA) showed to be neuroprotective in animal models of stroke and neuropathic pain.

Interestingly enough, experiments with GCPII knock-out mice showed that GCPII is not the only protein with NAAG-hydrolyzing activity in the brain. It was shown that at least two homologous enzymes can be detected in mice: GCPII and GCPIII. They have similar pharmacological properties and affinity for NAAG.

GCPII is also overexpressed in prostate cancer and it is used as a new prostate cancer marker. Moreover, it is intensively studied as a possible therapeutic target because it is anchored in the membrane and it is expressed in all prostate cancers and also in neovasculature of several non-prostatic solid tumors. In the benign prostate, a truncated form (PSM') of GCPII is prevalent. The ratio GCPII/PSM' increases with the prostate cancer progression and can be used for prostate cancer prognosis (tumor index).

The study of GCPII is such a broad field that also this thesis is not focused on only one aspect of this interesting protein. Published papers in this thesis are reflection of this fact.

Beginning of this thesis deals with the structure of GCPII protein, to the architecture of its active site and protein folding. Moreover, it also addresses the structural features of several inhibitors of GCPII.

Second part deals with GCPII as a biological target. It is aimed at expression of GCPII in human brain and at the direct comparison between GCPII and its close homolog GCPIII. Moreover, it also concerns the study of GCPII and PSM' trafficking in cells and the origin of PSM'.

The thesis is written as an introduction and an overview of the published papers and manuscript, which are included in the thesis. The Methods and Material part is omitted because it is described in details in the enclosed papers. In the Results and Discussion background information and summary of individual papers are presented.

3 INTRODUCTION

3.1 GCPII AS AN INTERESTING MOLECULE (a general information)

3.1.1 GCPII: from DNA to protein

DNA

GCPII gene (FOLH1) spans 62 035 base pairs, consisting of 18 exons and 19 introns. All intron-exon boundaries conform to the GT-AG rule [1], thus there is space for rich alternative splicing. Using FISH¹ analysis, the location of GCPII was found in chromosome 11, at p11.2 arm [2, 3].

GCPII promoter lies upstream of GCPII encoding gene FOLH1. It contains number of potential sites for transcription factor binding, none of which by itself is responsible for such a high expression of GCPII in prostate [1, 4].

GCPII enhancer is in the third intron. It contains 72 bp direct repeat within a 331 bp core region and activates transcription from its own and heterologous promoters in prostate cell lines. The enhancer is repressed in the presence of androgen [5, 6].

mRNA

GCPII mRNA offers various sites for alternative splicing. Until recently, three alternatively spliced forms were discovered and designated as PSM' [7, 8], PSM-C and PSM-D (Fig. 1) [7] and also variants PSMA Δ 6 [9] and PSMA Δ 18, in which complete exon 6 or 18 are excluded, respectively [10]. Recently, another two new forms of alternative splicing were found: PSM-E [11] and PSM-F in the database (on the web sites of National Center for Biotechnology Information (<http://www.ncbi.nlm.nih.gov>) in Protein: sequence database).

¹ Glossary item

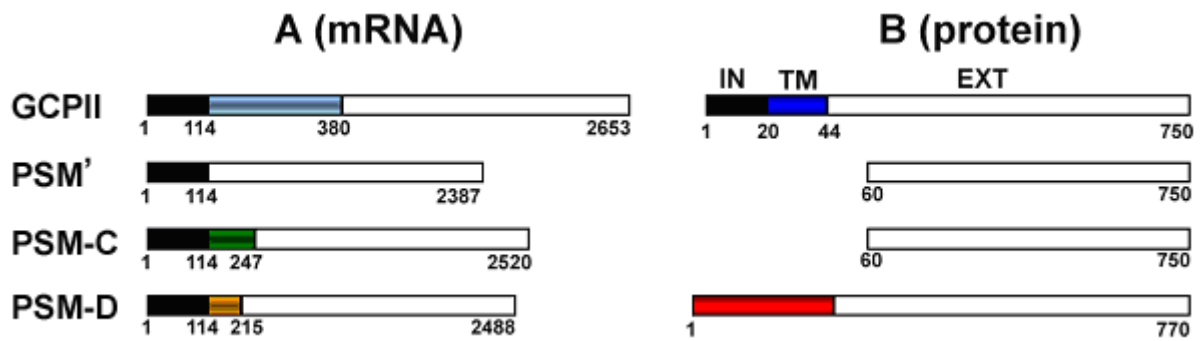


Fig. 1: cDNA sequences of GCPII and three alternatively spliced variants (PSM', PSM-C and PSM-D). **Panel A:** In PSM' bases 114-380 (pale blue box in GCPII) of genomic GCPII sequence are removed by alternative splicing. PSM-C has the same splice donor site as PSM' (nucleotide 114) but alternative acceptor site is located in intron one of GCPII; mRNA contains additional 133 nucleotides (green box). PSM-D has the same splice donor site as PSM' and an unique acceptor site within intron one. It includes a novel exon (orange box) [7]. **Panel B:** Translation of GCPII mRNA yields a 750 amino acids long protein consisting of intracellular domain (**IN**), transmembrane domain (**TM**) and large extracellular domain (**EXT**). PSM' protein lacks 59 amino acids from N-terminus compared to GCPII (full length form). PSM-C protein is predicted to be identical to PSM'. PSM-D protein is predicted to be a protein with novel 21 amino acids on the N-terminus (red box).

PSM' is the most often described alternatively spliced variant. It lacks 266 nucleotides near 5' end and the translated protein has no intracellular and transmembrane domain. It was detected only in the prostate and in no other tissue [8]. Its importance in normal prostate and prostate cancer will be discussed elsewhere (see chapter: 3.3.1.2.3.4.2).

Translation of PSM-C mRNA variant would yield protein identical to PSM'. Translation of PSM-D mRNA would yield a protein of 97kDa, without transmembrane domain and with different amino acids at N-terminus of the protein compared to GCPII [7].

PROTEIN

Glutamate carboxypeptidase II (EC 3.4.17.21) belongs to the M28 family of metallopeptidases on the basis of sequence homology to the aminopeptidases of this family.

GCPII is a membrane type II glycoprotein with short intracellular N-terminus and large extracellular domain containing active site and possessing hydrolytic activity [12]. It is a 750 amino acids long protein with molecular weight of 100kDa. The structure of GCPII will be discussed later (see chapter 3.1.5).

3.1.2 GCPII hydrolytic activities

3.1.2.1 N-acetylated-alpha-linked acidic dipeptidase activity

GCPII is able to cleave N-acetyl-aspartyl-glutamate (NAAG), a neurotransmitter (see chapter 3.2.1.2) (Fig. 2) [13]. It cleaves off the C-terminal glutamate and thus releases it into the synapse. Biological significance of this cleavage is discussed in detail elsewhere (see chapter 3.2 GCPII as a neuropeptidase).

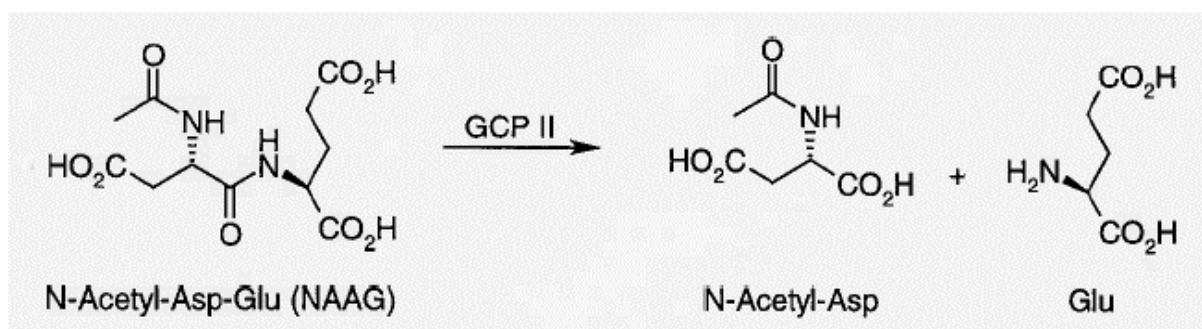


Fig. 2: Hydrolysis of the substrate N-acetyl-aspartyl-glutamate (NAAG) by GCPII to yield N-acetyl-aspartyl (NAA) and neurotransmitter glutamate (Glu).

3.1.2.2 Folylpolo-gamma-glutamate carboxypeptidase activity

This activity was characterized in the brush border of intestinal mucosa and converts folylpoly-gamma-glutamate into the folate (Fig. 3) that is ready for intestinal uptake [14]. This activity is responsible for cleavage of methotrexatepolyglutamate and thus it is important for its uptake and metabolism [15]. Due to this activity, GCPII can also be a target for activation of peptide prodrug in prostate cancer. Methotrexate-based peptide analogs were analysed to identify new GCPII-specific substrate. However, the longer γ -linked analogs of methotrexate were not significantly hydrolysed into methotrexate. Moreover, these analogs were transported into cell via folate transport mechanism independent of GCPII hydrolysis and thus might not be preferred agents for targeting GCPII activity [16].

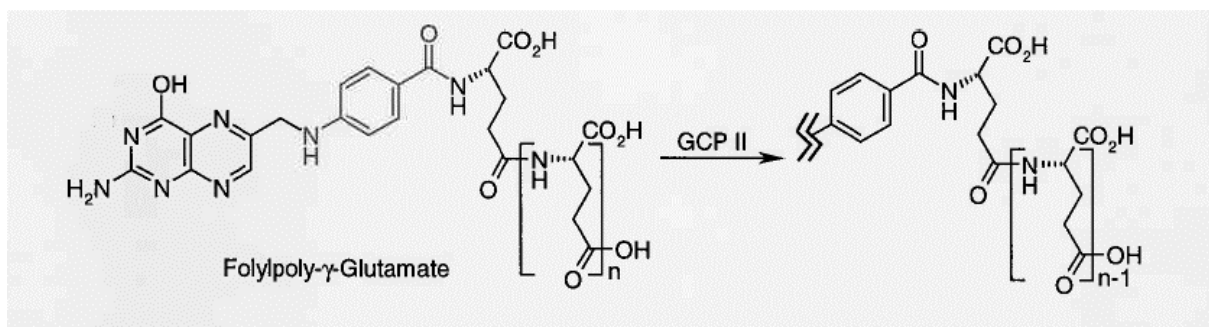


Fig. 3: Cleavage of foylpolypoly-gamma-glutamate by GCPII.

3.1.3 GCPII substrate specificity

Generally, dipeptides are much better substrates than those with longer chain, alpha-linked peptides are better than gamma-linked and peptides containing C-terminal glutamate are the best substrates of all [13]. Using libraries of all possible dipeptides, new substrates for GCPII were discovered [17]. They were indentified as: Ac-Glu-Met, Ac-Asp-Met, Ac-Ala-Glu, and Ac-Ala-Met, yet dipeptides containing Met as a C-terminal amino acid showed two order of magnitude loss in binding to GCPII (Table 1) [17].

Substrate	K_M [μM]	k_{cat} [s^{-1}]	k_{cat}/K_M [$\text{s}^{-1}/\text{mmol}^{-1}$]
Ac-Asp-Glu	0.43 ± 0.1	0.59 ± 0.16	1372
Ac-Glu-Glu	<5.0	0.78 ± 0.08	ND
Ac-Ala-Glu	ND	ND	ND
Ac-Glu-Met	53.0 ± 5.9	0.29 ± 0.01	5.5
Ac-Asp-Met	24.8 ± 3.9	0.07 ± 0.002	2.8
Ac-Ala-Met	303 ± 41	0.01 ± 0.001	0.03

Table 1: Example of kinetic parameters of GCPII for different dipeptides from peptide libraries. ND, not determined. Modified from [17].

3.1.4 GCPII inhibitors

GCPII is inhibited by polyvalent anions such as phosphate, sulphate [13], and by compounds chelating divalent cations (like EGTA), which is a common feature of metallopeptidases. Interestingly enough, GCPII activity was also inhibited by bestatin and puromycin (aminopeptidase inhibitors) [13].

Studying derivates of NAAG and glutamate and their inhibition efficiency on GCPII revealed effective inhibitors N-succinyl-Glu-OH, N-fumaryl-Glu-OH (K_I 0.9 and 0.4 μM , respectively) (Fig. 4) [18], noncompetetive inhibitor quisqualic acid and competitive inhibitor beta-NAAG (N-acetyl-aspartyl-beta-linked-glutamate) (Fig. 4) [19].

In the panel of hydroxyphosphinyl derivatives [20] and urea-based inhibitors of GCPII [21], the most potent inhibitor of GCPII 2-(phosphonomethyl)pentanedioic acid (2-PMPA) (K_I of 300pM) (Fig. 4) was discovered [20]. Further analysis showed that for a good inhibition potency the inhibitor should contain acidic moiety in propionic acid portion. None of the new designed inhibitors was so efficient as 2-PMPA [22].

Practical application of GCPII inhibition as a therapeutical tool (see chapter 3.2 GCPII as a neuropeptidase), requires efficient orally bioavailable inhibitor and because 2-PMPA meets only one of these criteria (efficiency), 2-(thioalkyl)pentanedioic acids were synthesised. The inhibition by these compounds was dependent on the number of methylene units between the thiol group and pentanedioic acid. Although none of these compounds are as efficient as 2-PMPA, very potent inhibitor 2-(3-mercaptopropyl)pentanedioic acid (2-MPPA, IC_{50} 90nM) (Fig. 4) was found to be orally bioavailable in rats and showed efficacy in an animal model of neuropathic pain following oral administration [23]. These thiol based inhibitors were further modified to contain at the P1' position benzyl moiety. 3-(2-carboxy-5-mercaptopentyl)-benzoic acid (IC_{50} 15nM) (Fig. 4) was more potent than 2-MPPA. However, the replacement of 2-carboxyethyl group with 3-carboxybenzyl group in 2-PMPA resulted in significant loss of inhibitor potency [24].

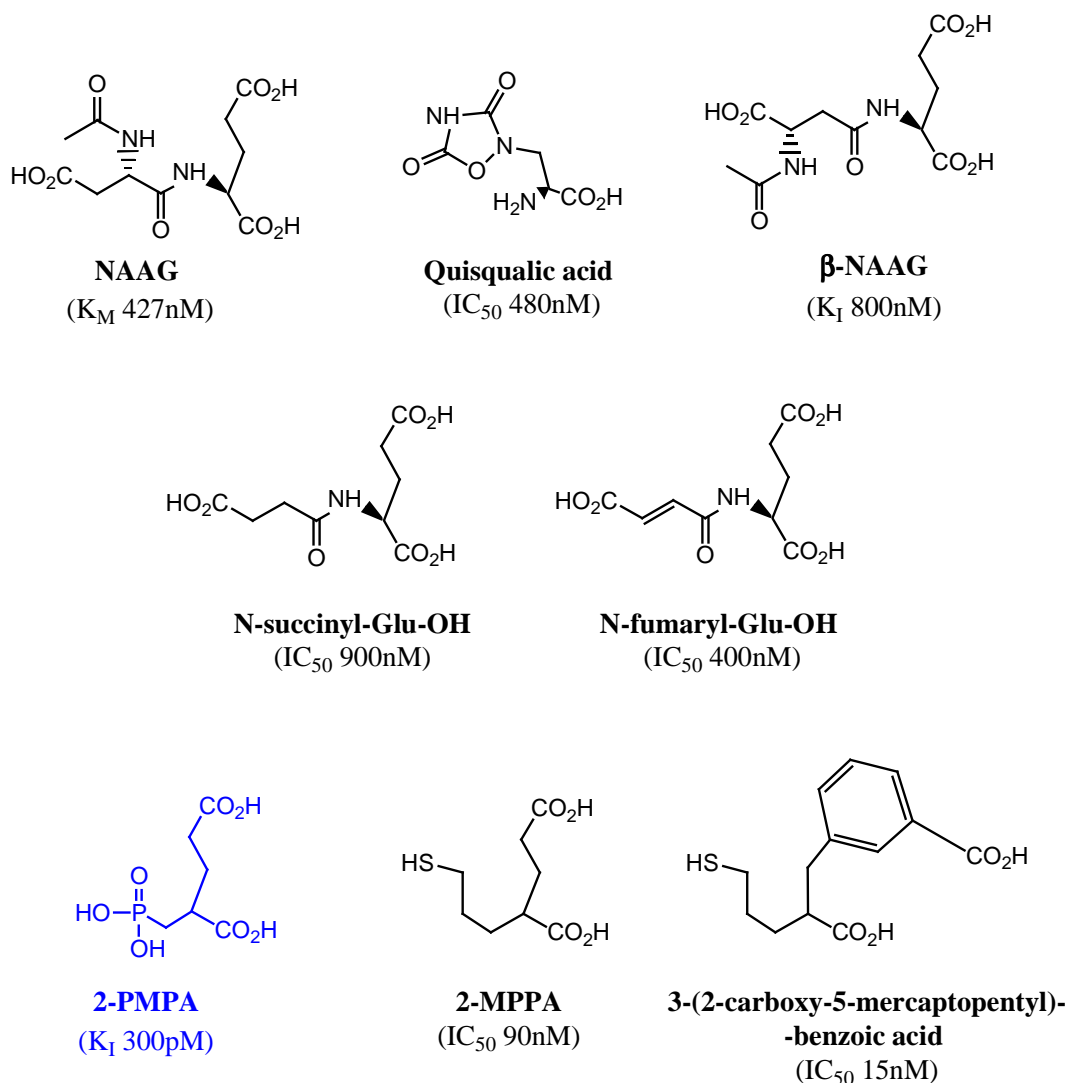


Fig. 4: Examples of the most potent inhibitors of GCPII. Inhibition constants are expressed as IC_{50} or K_I values in nmolar (picomolar) concentration. For the substrate N-acetyl-aspartyl-glutamate (**NAAG**) K_M value is shown. The most potent inhibitor 2-(phosphonomethyl)pentanedioic acid (**2-PMPA**) is depicted in blue. **2-MPPA**: 2-(3-mercaptopropyl)pentanedioic acid. **β -NAAG**: (N-acetyl-aspartyl-beta-linked-glutamate).

3.1.5 GCPII structure

3.1.5.1 Overall structure of GCPII

The structure of extracellular part of GCPII reveals a symmetric homodimer with each monomer containing three domains (analogous to three domains of transferrin receptor): a **protease domain** (residues 57-116 and 352-590), an **apical domain** (residues 117-351), and a **helical domain** (residues 591-750) [25, 26]. Amino acids from all three domains are involved in substrate binding. The dimer interface of GCPII is large (total of 2457 \AA^2) [26], suggesting

thus that monomer would dissociate from GCPII only upon partial unfolding and perhaps that is why the only active species of GCPII *in vitro* seems to be a dimer [27] (Fig. 5).

The **protease domain** is most closely related to the domain of aminopeptidase from *Aeromonas proteolytica* [25, 26]. The domain contains a central seven-stranded mixed β -sheet surrounded by ten α -helices [26].

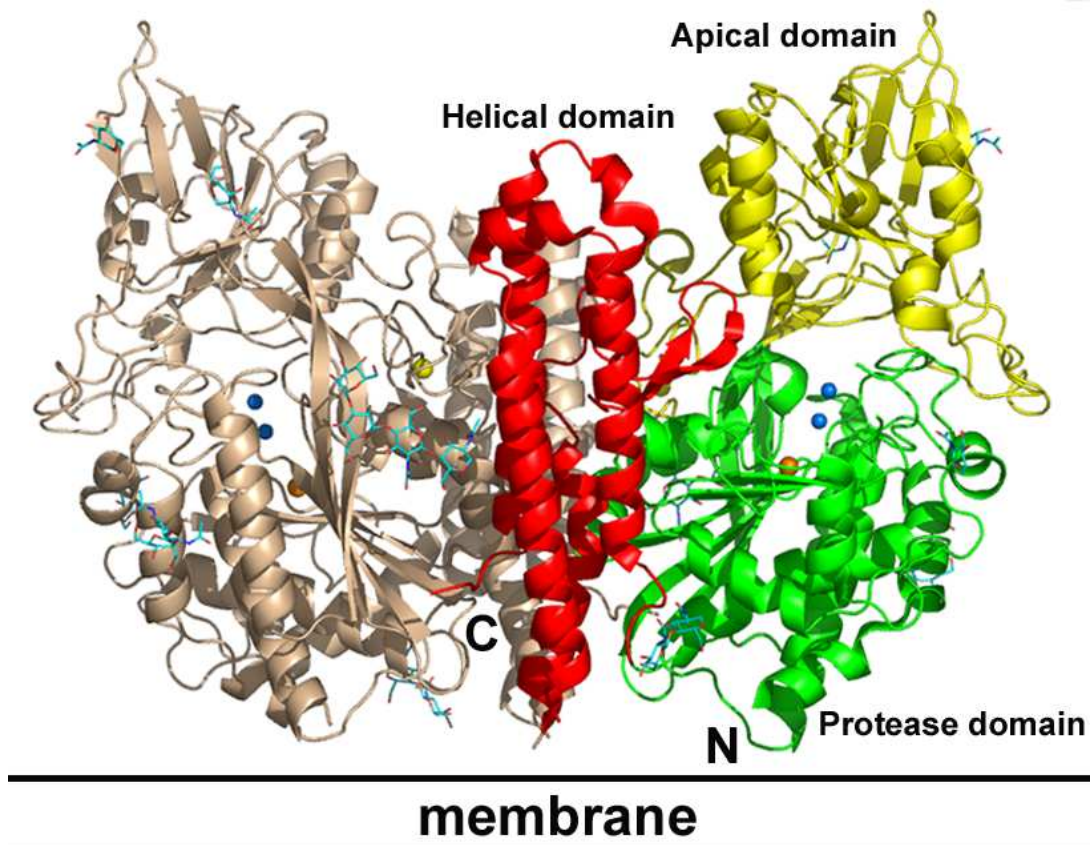


Fig. 5: Three-dimensional representation of GCPII dimer. One monomer is shown in wheat colour, the other is coloured according to domain organisation. In the active site there are zinc ions (blue spheres), calcium ions (yellow spheres), and also chloride ions (orange spheres). Seven carbohydrate side chains located in the electron density map are shown in line representation. N- and C-terminus of this extracellular domain is labeled as N and C, respectively.

Inserted between first and second strand of the central β -sheet of the protease domain is the **apical domain**. It covers the active site and creates a substrate binding funnel between the domains [26] (Fig. 5).

The **helical** (or C-terminal) **domain** has a main feature consisting of up-down-up-down four-helices bundle. There are also two loops; first one (residues 676-690) creates contact with protease domain through hydrogen bonds. The second loop (residues 692-704), which also makes a several hydrogen bonds to protease domain, is a part of the „glutarate

sensor“. „Glutarate sensor“ is a hairpin containing residues Lys699 and Tyr700, which are directly involved in the specific substrate binding. This second loop is flexible and its conformation changes in the crystal structures depending on ligand bound in the S1' position of the active site [26, 28] (Fig. 6, panel A, B). Helical domain also forms a dimer interface, which comprise mostly of helical domain of one monomer and protease and apical domains of the other. There are also two intermolecular salt-bridges formed between Arg662 of one monomer in helical domain and Asp666 of helical domain of other monomer [26].

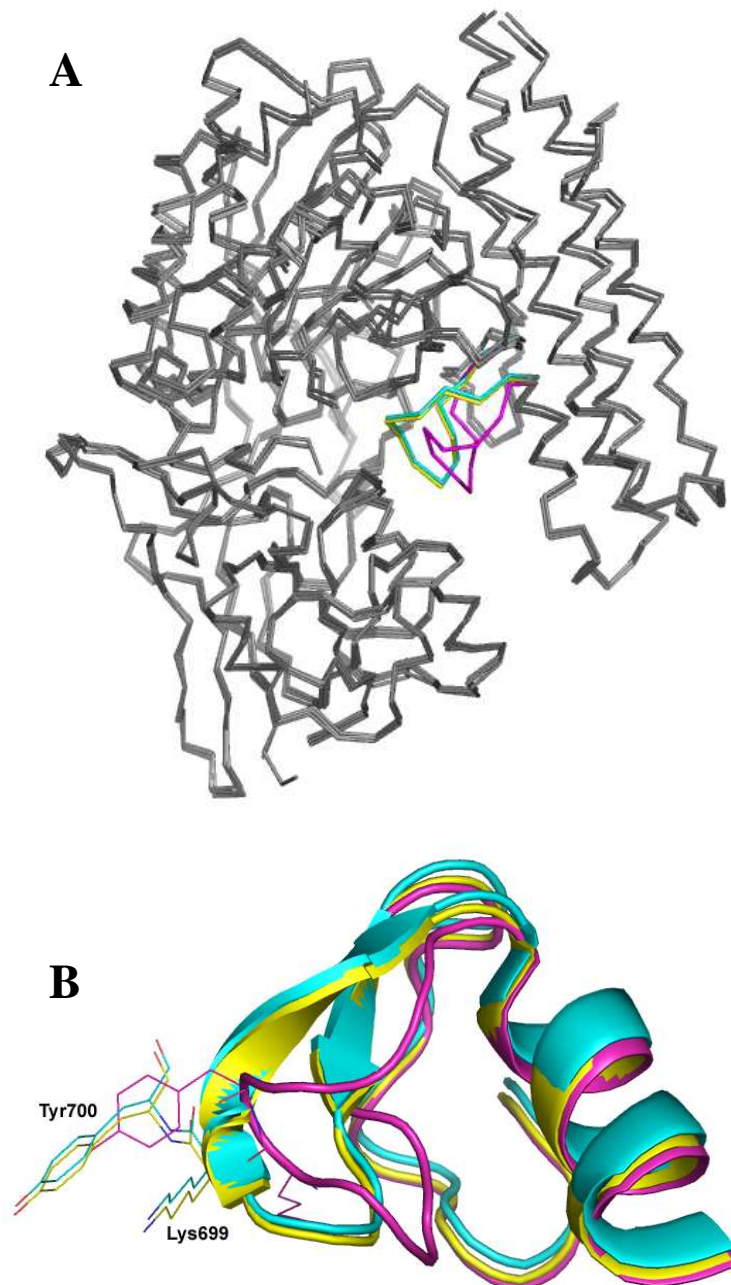


Fig. 6: „Glutarate sensor“ in the GCPII structure. Amino acid residues 692-704 create a flexible loop that is involved in substrate binding. **Panel A:** The GCPII structures available from the RSCB PDB were superimposed. The C α -traces are shown in ribbon representation. Colour-coding used for „glutarate sensor“ is depicted in cyan for GCPII/GPI-18431 (GCPII inhibitor) structure, in yellow for GCPII/glutamate structure and in magenta for

GCPII/phosphate structure. Residues Lys699 and Tyr700 create a part of this loop. They directly bind ligands in S1' site. If the S1' site is not occupied by a ligand (structure GCPII/phosphate; magenta), the loop change its position in the active site. **Panel B:** Detailed picture of „glutarate sensor“. Different position of the loop highlights the movement of Lys699 and Tyr700 (in line representation) in the structure of GCPII/phosphate. Colour-coding is the same as in panel A.

In the GCPII structure a calcium ion is also located. Two domains (protease and apical) co-operate in its binding. The Ca^{2+} is too distant from active site to be involved in enzyme catalysis. Its role is more likely to hold protease and apical domain together through coordinative interaction. Possibly, it is involved in dimerization by stabilizing the loop 272-279 which has three tyrosins (272, 277, 279) (Fig. 7). These tyrosins form hydrophobic pocket, which is entered by side chain of Tyr733 of the other monomer in the dimer (Fig. 7). Moreover, Tyr277 forms an intermolecular hydrophobic interaction with N-acetyl group of N-acetyl-glucosamine of the sugar chain attached to Asn638. This contact of sugar chain and protease domain is one of the few structurally well-defined cases of a protein-carbohydrate contact involved in homodimerization of a protein (Fig. 5) [26].

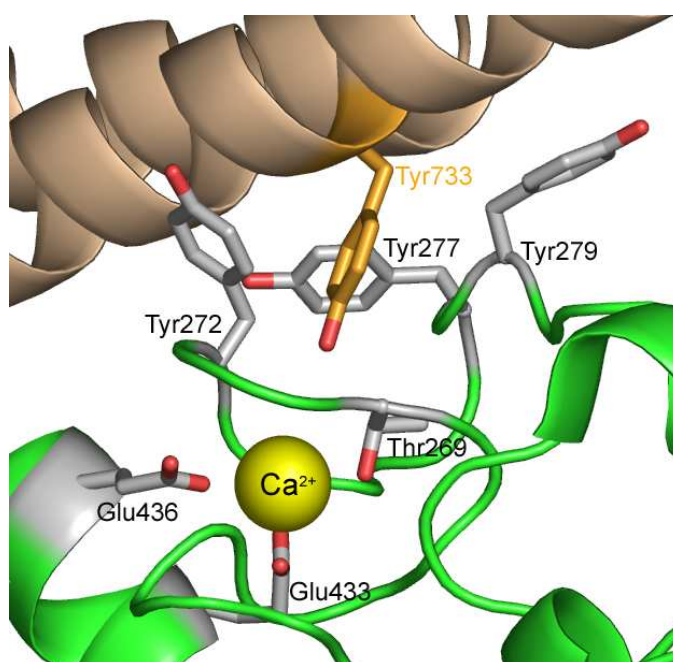


Fig. 7: Function of Ca^{2+} ion is still not understood. Ion Ca^{2+} is coordinated by two glutamates and threonine. Three tyrosins (in gray colour) in one monomer form a hydrophobic pocket, which is entered by side chain of Tyr733 of the other monomer in the dimer (depicted in orange). This interaction can play a role in dimerization. Monomers of GCPII dimer are coloured in green and wheat.

Another ion in the GCPII structure is Cl^- ion. It seems that it has stabilizing role and holds Arg534 in favorable conformation for substrate binding [26].

3.1.5.2 Active site of GCPII

Approximately 20Å long funnel leads from the GCPII surface to the active site that contains two zinc ions. One zinc ion (Zn1) is tetrahedrally coordinated by Glu425, His553 and by a bridging ligand Asp387. This aspartate also coordinates other zinc ion (Zn2) together with Asp453 and His377. The catalytic zinc center in free state has a single water molecule bridging two zinc ions (Fig. 8). Interestingly, the distance between zinc ions is changing from 3.30Å, in the free state, to 3.65 and 3.78Å, respectively, in the complexes with phosphate and GPI-18431 [26].

Asp387 in the active site forms a peptide bond in *cis* conformation with its neighbouring Pro388, which is common in binuclear zinc peptidases [26].

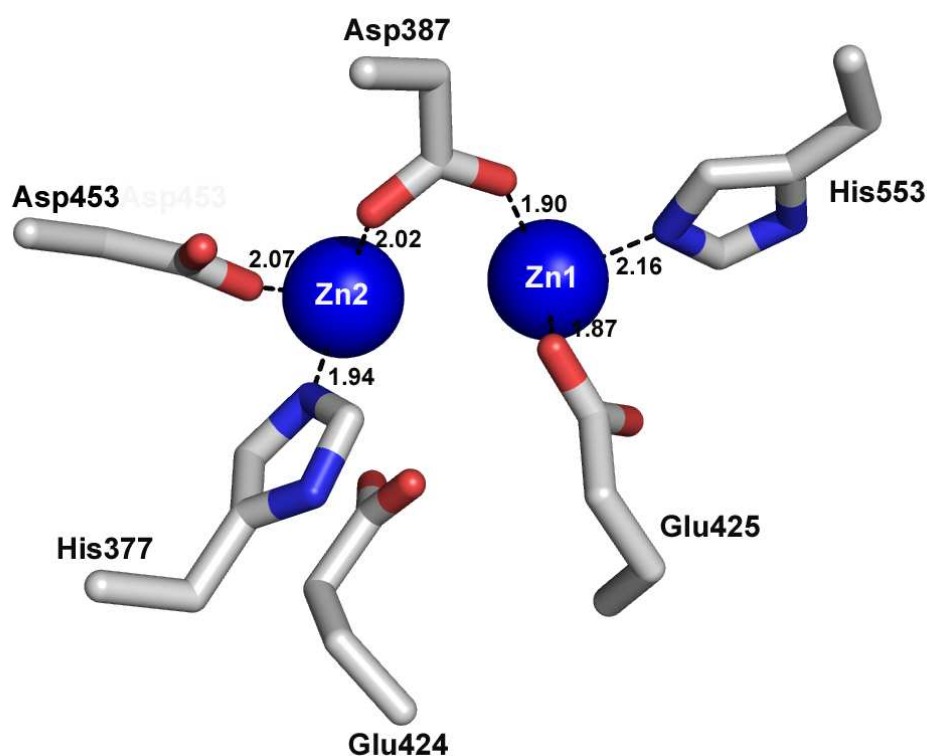


Fig. 8: Active site of GCPII. Zinc ions are depicted in blue. Each metal ion is tetrahedrally coordinated by histidine, acidic amino acid and by a bridging ligand Asp387. Glu424, a possible catalytic acid/base of GCPII, is also depicted.

In the catalytic mechanism Glu424 plays a prominent role. It is a probable catalytic acid/base of GCPII. As a proton shuttle it abstracts a proton from the water between zinc ions and transfers the proton to the amino group of glutamate, possibly during substrate cleavage. The activated water molecule then attacks carbonyl group of aspartate in the substrate (Fig. 9) [26]. This catalytic mechanism is similar to those discovered in other carboxypeptidases [29].

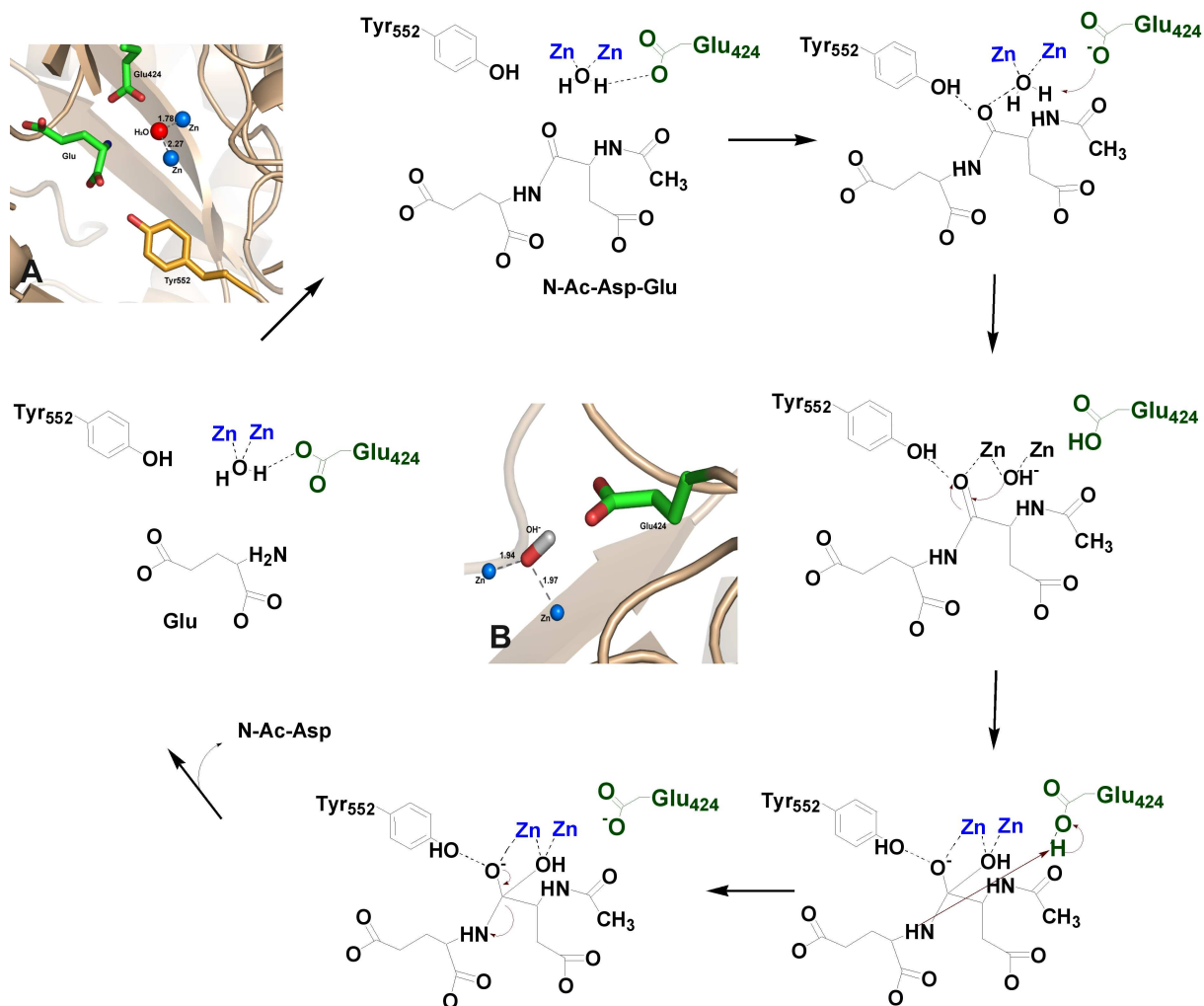


Fig. 9: The catalytic mechanism of GCPII. Catalytic pathway was suggested on the basis of proposed catalytic mechanism of aminopeptidases from *Aeromonas proteolytica* [29] and *Streptomyces griseus* [30]. Tyr552 can play an important role in stabilizing the transition state during catalysis (Tyr246 plays similar role in aminopeptidase from *Streptomyces griseus* [30]). Dashed lines indicate stabilizing interaction and/or hydrogen bond in the catalysis. Inserted **panel A**: a product of hydrolysis L-glutamate (green) is located in the active site together with Glu424 (green), Tyr552 (orange), and water molecule between two zinc ions (blue spheres). Inserted **panel B**: a catalytic acid/base Glu424 (in green) of GCPII is shown together with activated water molecule between two zinc ions (blue spheres).

3.2 GCPII AS A NEUROPEPTIDASE

The expression of GCPII is not as tissue-restricted as was expected a few years ago [31-37]. Yet there are still several tissues with higher GCPII expression. One of these tissues is the brain. The function of this enzyme is known there, contrary to other tissues. Moreover, GCPII seems to play a role in neuropathologies where excessive amount of glutamate was detected.

3.2.1 Glutamate, NAAG, GCPII and nervous system

3.2.1.1 Glutamate-excitatory neurotransmitter

Glutamate is primary excitatory neurotransmitter in the human nervous system and it plays role in neurodevelopment and, unfortunately, also in neurodegeneration. It acts postsynaptically on three ionotropic receptors (Table 2), named after their preferentially agonists² [38]. These receptors have incorporated ion channels permeable for cations.

Glutamate also binds to metabotropic receptors (Table 2), which are linked to G-proteins³ and operate by releasing second messenger into the cytoplasm or influence ion channels through releasing G-protein subunits within the membrane [39].

There are also other ligands, except glutamate, which bind to the glutamate receptors [40-42]. Among them an endogenous dipeptide **N-acetyl-aspartyl-glutamate (NAAG)** can be found.

^{2,3} Glossary item

Name	Type	Group	Function
NMDA	ionotropic		calcium influx into post-synaptic cell, a signal crucial for induction of LTP and LTD (long-term potentiation and long-term depression)
APMA	ionotropic		mediate fast synaptic transmission in the CNS
kainate	ionotropic		synaptic plasticity
mGlu1	metabotropic	I	activates adenylate cyclase; increases activity of phospholipase C; inhibits K ⁺ channels
mGlu5	metabotropic	I	
mGlu2	metabotropic	II	inhibits adenylate cyclase; inhibits voltage-gated Ca ²⁺ channels; activates K ⁺ channels
mGlu3	metabotropic	II	
mGlu4	metabotropic	III	inhibits adenylate cyclase; inhibits voltage-gated Ca ²⁺ channels
mGlu6	metabotropic	III	
mGlu7	metabotropic	III	
mGlu8	metabotropic	III	

Table 2: Glutamate receptors. The classification of mGlu receptors is determined by their similarities in coupling mechanism, molecular structure, sequence homology and the pharmacology of the receptors.

3.2.1.2 N-acetyl-aspartyl-glutamate (NAAG)

NAAG is the most prevalent and widely distributed peptide neurotransmitter in the mammalian nervous system [43-45].

Specific antibodies against NAAG showed wide distribution of the peptide through the mammalian brain, spinal cord, sensory neurons [46-49], and mammalian retina [50-53]. NAAG seems to be strictly located in neurons containing a variety of amine neurotransmitters including glutamate, GABA [44], although, in glial cells cultures moderate micromolar concentrations of NAAG were also found [54]. It is concentrated into synaptic vesicles [55, 56] and released by depolarization-induced, calcium-dependent manner [57, 58]. NAAG is hydrolyzed (enzymatically inactivated) by glutamate carboxypeptidase II in the synaptic cleft [59]. However, it is also directly taken back to neurons [60].

NAAG novel receptor was identified by receptor binding studies, which showed binding of NAAG at NMDA receptor binding sites (IC₅₀ values: glutamate, 0.4 mM; NAAG, 8.8 mM) in rat forebrain membranes [61]. NAAG is a low-potency agonist² of NMDA receptors, but not kainate or AMPA receptors [62-64]. Interestingly enough, NAAG also acts as an antagonist⁴ of NMDA receptors at low concentration (below 20μM) [65-67].

NAAG was also detected as a selective agonist of mGluR3 receptors with a potency that rivaled glutamate [68, 69]. One role of NAAG in the nervous system is to activate

^{2,4} Glossary item

presynaptic mGluR3 receptors and thus suppress synaptic release of itself and mainly glutamate [70]. It also activates postsynaptic mGluR3 and decreases the cAMP levels via inhibitory G protein in neuron and astrocytes (Table 2). The downstream consequences of this process are not well established [71, 72].

The NAAG neurotransmission action is summarized in Fig. 10.

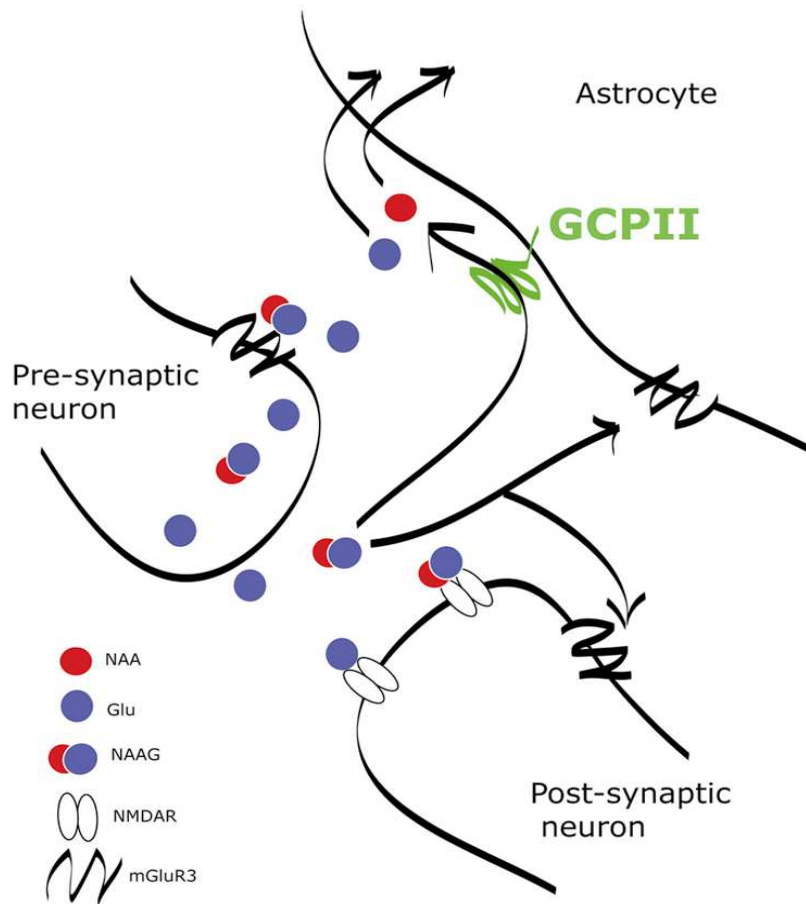


Fig. 10: Illustration of the NAAG neurotransmission. After release, at the post-synaptic membrane, NAAG attenuates excitability by competing with glutamate for binding at NMDA receptors or by the activation of post-synaptic mGluR3. At the pre-synaptic membrane, it activates inhibitory mGluR3 to attenuate further release of neurotransmitter, including glutamate and NAAG. NAAG is removed from the synaptic cleft by hydrolysis into glutamate and NAA catalysed by GCPII (at astrocyte membrane). The reaction products are taken up by astrocytes. Glutamate and NAAG can be also taken back to pre-synaptic neuron.

3.2.1.3 NAAG peptidase (= glutamate carboxypeptidase II = GCPII)

GCPII cleaves N-acetyl-aspartyl-glutamate in the synaptic cleft into glutamate and N-acetyl-aspartate (NAA) (Fig. 10) and the reaction products can act in neurotransmission or can be taken back to pre-synaptic neurons or astrocytes.

The peptidase activity of GCPII is widely distributed throughout the nervous system, consistent with the distribution of NAAG [66, 73, 74]. NAAG peptidase activity has been located to extracellular space of plasma membrane of isolated retinal cells, cultures containing mouse brain neurons and glia⁵, mouse brain glia cultured alone, and nonmyelinating Schwann cells⁵ [54, 75-77]. GCPII is concentrated in glia, namely astrocytes⁵ [78].

If NAAG is cleaved, glutamate is released and thus concentration of excitotoxic neurotransmitter is increasing. On the other hand, if GCPII is inhibited and NAAG is not cleaved, it binds to NMDA receptors [62, 64] and also to pre-synaptic metabotropic glutamate receptors, where it negatively influences releasing of glutamate into synapse [70].

Inhibitors of GCPII can be valuable therapeutic tool in neurological diseases, because they indirectly decrease excitotoxic glutamate. Moreover, they influence and enhance a natural regulatory process (decreasing glutamate) in contrast to other strategies, which chronically activate or inhibit receptors in a manner which is unrelated to ongoing neurotransmissions and which is almost always accompanied by side effects.

3.2.2 Acute neurological disorders and GCPII

3.2.2.1 Stroke

Ischemic injury is the cause of excitotoxic nerve-cell death which occurs in the area of insult and also in nervous tissues in surroundings. Excessive levels of glutamate, overstimulation of NMDA receptors and influx of Ca^{2+} into the cell are the major factor of nerve-cell death [79].

In 1999 Slusher *et al.* proposed a new strategy for the treatment of stroke by inhibition of GCPII. Use of selective inhibitor 2-(phosphonomethyl)pentanedioic acid (2-PMPA) (Fig. 4) showed to be neuroprotective in neuronal culture model of stroke and in rats after transient middle cerebral artery occlusion⁶ [80].

Neuroprotection during ischemia is caused by inhibition of GCPII hydrolyzing activity (2-PMPA), increase of NAAG and decrease of glutamate, through the action of NAAG on the metabotropic glutamate receptors [80-82].

Moreover 2-PMPA does not induce the learning and memory deficit and neurotoxic properties of NMDA receptor antagonists and has no effect on glutamate levels in normal

^{5,6} Glossary item

non-ischemic rats [80]. The neuroprotective effects of 2-PMPA were also confirmed in peripheral neuropathies [83], retinal ganglion⁷ cell death caused by excessive glutamate receptors activation [84] and in spinal cord injury [85].

Another interesting discovery was that the neuroprotection mediated through GCPII inhibition appears to be dependent on the presence of glial cells in the neuronal/glial culture [86, 87]. Interestingly, increasing concentration of NAAG (caused by GCPII inhibition) can activate mGluR3 receptors, expressed by astrocytes, which control release of transforming growth factor beta (TGF- β) that have a neuroprotective effect in neurodegenerative disorders (Fig. 11) [88]. Neuroprotection was reversed by antagonist of mGluR3 receptor and also by use of neutralizing antibodies against TGF- β . Taken together, these results suggest involvement of glial mGlu receptors in NAAG and 2-PMPA mediated neuroprotection [86, 87].

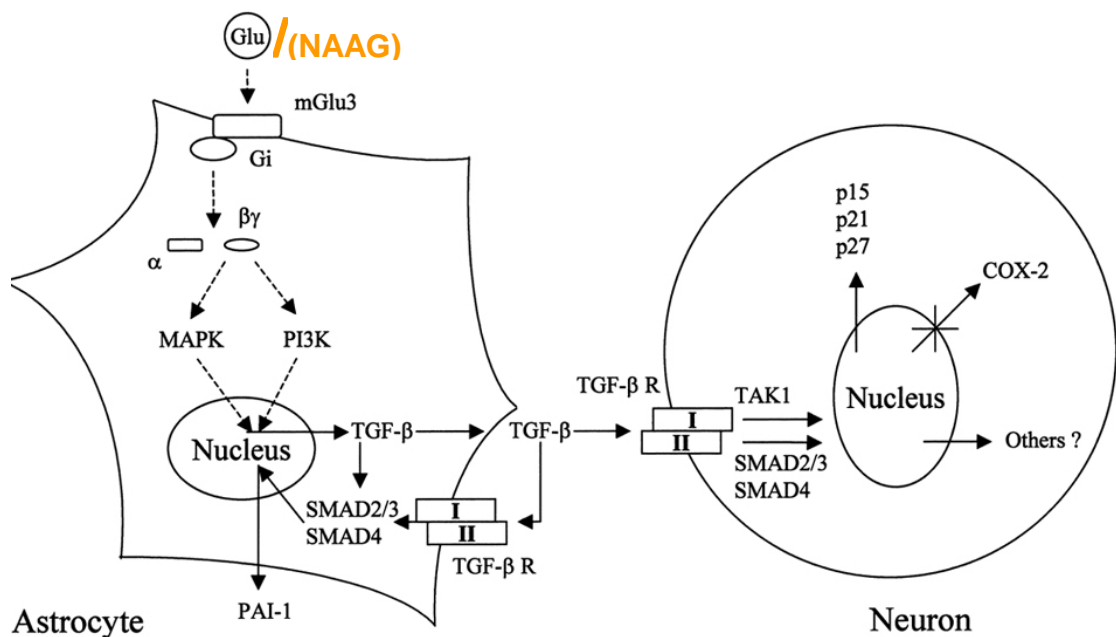


Fig. 11: The neuroprotective effect of transforming growth factor- β (TGF- β). Activation of glial mGlu3 receptors causes the release of TGF- β , through the activation of mitogen-activated protein kinase (MAPK) and PI-3-K pathways. TGF- β released from astrocytes may exert its neuroprotective effect in glial cells by inducing an expression of the serpin PAI-1 (plasminogen activator inhibitor type 1), which is then released from the astrocyte (left panel), and by acting in neurons through a set of high affinity serine-threonine kinases (TGF- β R I and TGF- β R II), which signal to the nucleus through the activation of transcriptional factors (SMAD2/3, SMAD4) or through the activation of transforming growth factor kinase 1 (TAK1). Downstream events include the induction of cell cycle proteins (p15, p21, and p27) or the inhibition of cyclooxygenase-2 (COX-2) expression. Other factors, still unknown, might contribute to TGF- β -induced neuroprotection (right panel). Modified from [39].

⁷ Glossary item

3.2.2.2 Head injury

Traumatic brain injury⁸ is followed by secondary injury associated with excessive elevation of extracellular glutamate and following cell death occurs [89]. Neurons and glial cells in the hippocampus, a brain area associated with learning and memory, are exceptionally sensitive to trauma-induced excitotoxic cell death [90].

In an animal model of fluid percussion⁹, the inhibition of GCPII reduced glutamate concentration and the loss of degenerating neurons and astrocytes. Use of metabotropic glutamate receptor antagonists LY-341495 completely abolished the neuroprotecting activity of GCPII inhibition and probably effect of NAAG on mGlu3 receptors [91, 92]. The data support the hypothesis that GCPII inhibition might decrease magnitude and duration of excitotoxic events associated with brain injury and represent thus new therapeutic target in brain injury.

3.2.2.3 Neuropathic and inflammatory pain

Increased glutamate concentration in the spinal cord and primary afferent nerves¹⁰ plays an important role in acute and chronic pain. Ectopic discharges¹¹ from afferent nerves in the site of nerve injury are responsible for the development of hypersensitivity, hyperalgesia¹² and allodynia¹³ (abnormal pain sensation) in patients with painful neuropathies [93].

Mechanical allodynia induced in inflammatory model (formalin test or carrageenan injection¹⁴) is mediated by spinal NMDA receptors-dependent mechanism [94]. Using low levels of selective GCPII inhibitor 2-PMPA (1-100µg) caused accumulation of small amount of NAAG, which acts as an antagonist on NMDA receptors and has an anti-allodynic effect (attenuating the level of mechanical allodynia). At higher doses (300µg) this effect disappears because of accumulation of larger amount of NAAG, which acts now as an agonist on NMDA receptors [95, 96, 97].

Even though there are two controversial studies about analgetic effect of GCPII inhibition through the NAAG effect on pre-synaptic mGlu receptors [98, 99], orally bioavailable GCPII inhibitor (2-(3-mercaptopropyl)pentanedioic acid (IC50 90nM); see Fig. 4) exhibited efficiency in an animal model of neuropathic pain [23].

⁸⁻¹⁴ Glossary item

3.2.3 Chronic neurological disorders and GCPII

3.2.3.1 Schizophrenia

Schizophrenia is a chronic brain disorder where alternations in dopaminergic and glutamatergic transmission seem to play an important role [100-102]. One theory of schizophrenia is the glutamate theory, which involves hypofunction of the glutamate neurotransmitter system where also NMDA and mGluR II receptors belong. [103-105]. Even though NAAG acts on both these receptors and GCPII inhibition seems to be an interesting therapeutic approach, all studies published to date are inconclusive [102, 106, 107].

3.2.3.2 Diabetic neuropathy

Diabetic neuropathy¹⁵ is a common complication of diabetes. It damages the nerves that allow to feel sensations such as pain [108, 109]. Glutamate excitotoxicity is believed to be a prominent mechanism involved in diabetic neuropathy [110].

GCPII inhibitor (2-PMPA) in model of diabetic neuropathy showed that the prevention of glucose-induced programmed cell death and positive effect on neuropathic hyperalgesia, nerve dysfunction of both myelinated and unmyelinated fibers, was specific and was mediated by NAAG agonist activity on mGluR3 receptor [111, 112].

3.2.3.3 Amyotrophic lateral sclerosis

Amyotrophic lateral sclerosis (ALS) is a progressive and fatal degeneration of motor neurons in the spinal cord and cerebral cortex [113]. Glutamate excitotoxicity has been implicated as a mechanism of motor neuron death in this disease [114].

In ALS patient, NAAG levels are elevated [114] and in addition GCPII activity is upregulated [115]. The inhibition of GCPII by 2-PMPA and 2-MPPA decreased death of motor neurons and glia in the animal model of ALS. This neuroprotective effect is mediated through the limiting glutamate levels (originating from NAAG) when glutamate uptake is abnormal [116].

¹⁵ Glossary item

3.3 GCPII AS A DIAGNOSTIC MARKER AND THERAPEUTIC TARGET IN THE PROSTATE CANCER

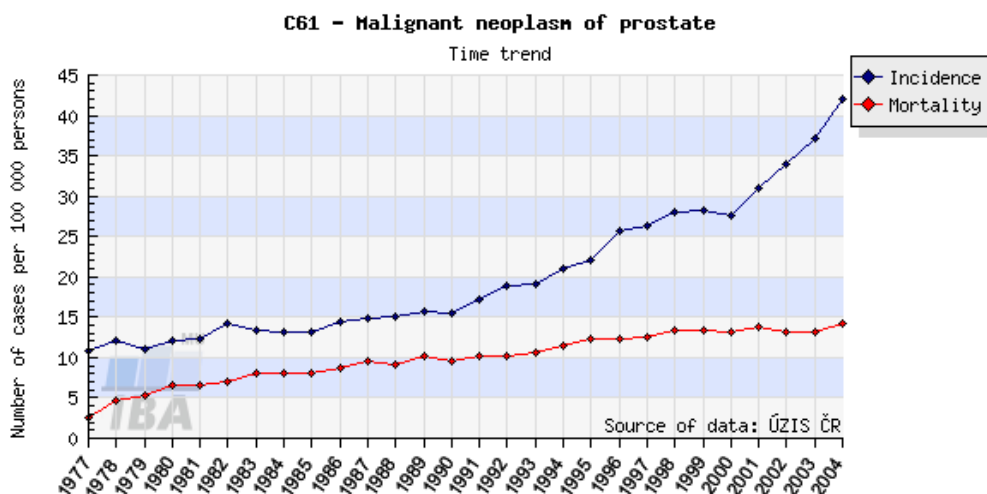
GCPII is overexpressed in prostate cancer and it is used as a new prostate cancer marker with its pros and cons. Moreover, it is studied as a possible therapeutic marker of the prostate because it is anchored in the membrane and it is expressed in all prostate cancers and also in neovasculature of several non-prostatic solid tumors.

3.3.1 GCPII as a marker of prostate cancer

3.3.1.1 Prostate cancer in numbers

Prostate cancer is the second most prevalent cancer in the Czech Republic. At least in 15% of men over age 50 oncogenic changes in prostate tissue were detected. Worldwide occurrence of this cancer is increasing by about 3% every year.

Czech Republic takes 40th place in the incidence of prostate cancer (source from Epidemiology of malignant tumors in the Czech Republic; www.svod.cz [117]).



Graph 1: Time trend of crude incidence (number of new cases per 100 000 persons) **and crude mortality** (number of deaths on a diagnosis per 100 000 persons); (source from <http://www.svod.cz>).

It can be seen that the incidence and mortality is still increasing (Graph 1). Individuals with prostate cancer lose 8-9 years of their life span and although this type of cancer is sometimes called an indolent and incidental cancer, only 70% of prostate cancer patients have 10-year survival compared to general population [118].

With the aging population the incidence of the prostate cancer increases. However, the increased incidence can be partially attributed to novel methods in earlier detections.

The tumors of epithelial cells belong to the most common type of prostate cancer. The leading two tumors are: carcinoma¹⁶ of the prostate and benign hyperplasia¹⁷ (malignant tumor of epithelial cells and benign adenoma, respectively).

The majority of prostate carcinoma represents adenocarcinomas¹⁸ from prostatic epithelial cells (over 95%) [119].

3.3.1.2 Markers of the prostate cancer

Some tumor markers have diagnostic values and we call them *diagnostic markers*. They distinguish cancerous disease from other abnormalities in the prostate. Some markers have prognostic values: they are called *prognostic markers*; they should independently predict the biological behavior and outcome of prostate cancer [118].

3.3.1.2.1 Prostatic Acid Phosphatase (PAP)

It is a non-specific phosphomonoesterase secreted into seminal plasma under androgen control [120]. PAP represents only a small portion of the total acid phosphatases in the serum of normal men, thus cross reactivity during screening is observed with serum acid phosphatases. It is also not a prostate specific marker; it is synthesized by granulocytes, spleen and pancreas [121]. Limited ability to detect early prostate cancer, high false negative results and elevation of PAP in already advanced disease, lead to current replacement of PAP by prostate specific antigen.

3.3.1.2.2 Prostate specific antigen (PSA)

It is a serine protease secreted by prostate epithelial cells and it is a normal component of the ejaculate [122-124]. PSA was detected in serum of men with benign and malignant prostatic diseases and it is widely used as a tumor marker. Even though it was believed to be prostate specific, it was also detected in other body tissues [125-129], cancers of non-prostatic origin [130, 131] and also in serum of normal women [130-132].

¹⁶⁻¹⁸ Glossary item

PSA testing is used normally in hospitals as a standard test [133] for prostate cancer patients and detects pathologically organ-confined prostate cancer in large number of cases. Nevertheless, it is not disease-specific, elevated levels can be found in a small portion of normal males and in 25-85% of patients with benign prostatic hyperplasia (BPH) and prostatitis [134]. Moreover, PSA serum levels are downregulated by the absence of testosterone (stimulates cancer cell growth) during androgen-deprivation therapy, which is normally used for reducing the male hormones [135]. Thus it makes the diagnosis more difficult.

3.3.1.2.3 GCPII disguised as Prostate specific membrane antigen

An ideal diagnostic tumor marker SHOULD [118]:

- Meet general tumor marker criteria but also be an organ-specific and cancer-specific
- Have high sensitivity
- Have high specificity and reproducibility
- Be practical; simple, cost-efficient test
- Predict the prognosis

AN IDEAL PROSTATE CANCER MARKER HAS NOT YET BEEN DISCOVERED.

3.3.1.2.3.1 GCPII organ-specificity

Although GCPII is mostly expressed in brain, prostate, kidney and small intestine [31, 33, 35, 136, 137], it was also detected in other organs [32, 36].

It is very disturbing that different studies very often show different results of tissue localization of the enzyme (Table 3). In many examples 7E11 antibody, which recognizes cytosolic N-terminus of GCPII, was used [31-33, 35-37]. Only in half of these studies new antibodies against extracellular part of GCPII were applied [33, 34, 37, 138, 139]. Also the methods of protein detection are different and could have an influence on final results (Table 3).

GCPII does not seem to be located strictly into the prostate tissue, it can be found in many other normal tissues through the human body. But there are only three tissues (kidney proximal tubules, prostate and duodenum) in which all studies showed consistent results (Table 3). It is not surprising since these tissues express high concentration of GCPII and thus

even antibodies with low sensitivity can detect the protein. Interestingly, three studies did not observe expression in human brain [35, 36, 138], although there are several other studies, which agree with each other in positive expression of GCPII protein in human brain [33, 137, 139, 140]. Moreover, the brain localization was also confirmed by activity measurement [141].

Even though the results of tissue localization are not consistent (because of different antibodies and detection methods used), it can be concluded that GCPII is not strictly prostate specific (Table 3).

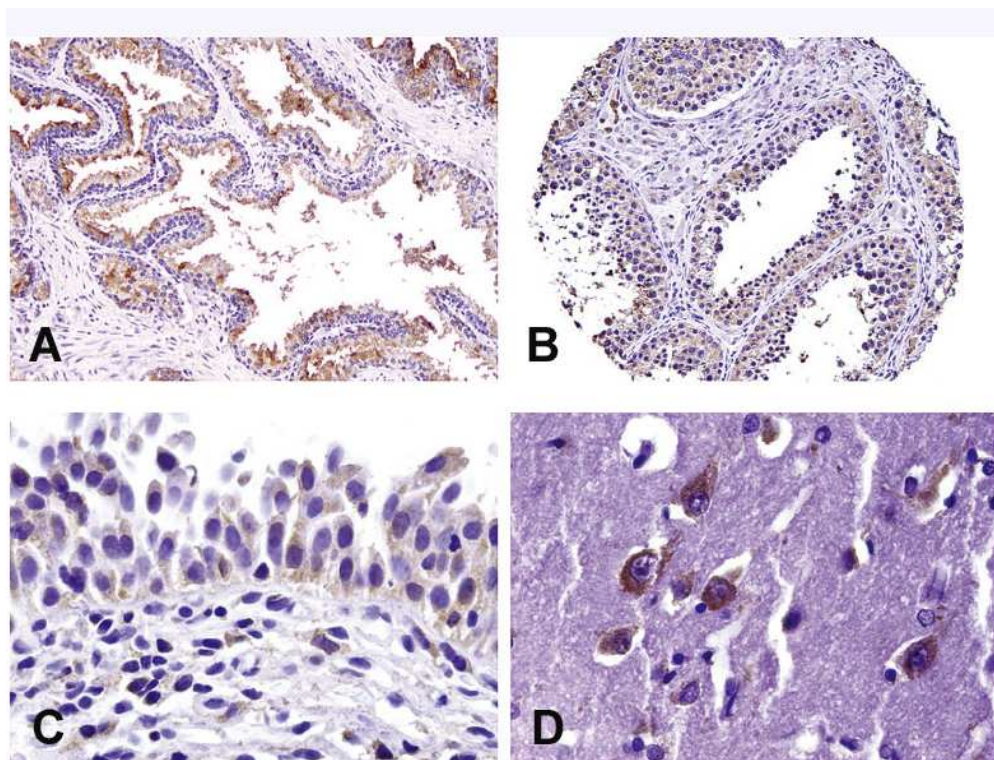
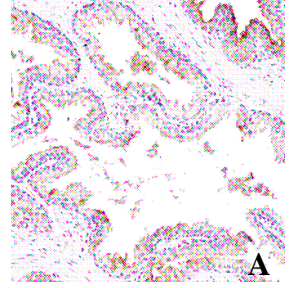


Fig. 12: GCPII staining in different human tissues. A. Benign prostate tissue, weak to moderate GCPII staining, apical to cytoplasmic pattern. B. Testis; cytoplasmic staining. C. Urothelium of the urinary bladder; cytoplasmic staining. D. Brain tissue; cytoplasmic staining. Adopted from [139].

tissue	adrenal glands	adipocyte	bladder	bone marrow	brain	breast	capillaries	cardiac muscle	cerebellum	cervix	colon	duodenum	endometrium	endothelium	esophagus	eye	fallopian tube	frontal cortex	gallbladder	ganglion cell in the gastrointestinal tract	heart	ileum	kidney-glomerulus	kidney-proximal tubule	kidney-distal tubule	kidney-Henle loop	liver	lung	references
	0				0			Y			0											0	Y	0	0	0	0	0	Lopes <i>et al.</i> [35] ²
				Y	0			0			0															0	0	Troyer <i>et al.</i> [137] ¹	
	0		0	0	0	0			0	0	Y	Y				0		0		0		0	0			0		Silver <i>et al.</i> [36] ²	
												Y																Liu <i>et al.</i> [34] ²	
	0		0		0	Y					Y	Y			0							0	0	Y	0		0	0	Chang <i>et al.</i> [138] ²
							0																Y					Dumas <i>et al.</i> [31] ²	
						Y																						Gala <i>et al.</i> [32] ²	
	Y		Y		Y	Y					Y				Y		Y										Y	0	Sokoloff <i>et al.</i> [37] ³
	0	Y		Y	0					0	0		Y	0	0		0		0		Y		0				Y	0	Kinoshita <i>et al.</i> [33] ¹
													Y	0	0		0		0		Y		0				0	0	Mhaweck-Faucegia <i>et al.</i> [139] ^{2,4}



tissue	lymph node	myometrium	nerve	ovary	pancreas	pancreas-islets	pancreas-acini	parathyroid gland	peripheral ganglion	prostate	prostate-stroma	salivary gland	skeletal mus	seminal fluid	seminal vesicles	serum	skin	skin gland	small intestine	smooth muscle	smooth muscle in prostate, bladder, intestine	spleen	stomach	striated muscle	testis	thymus	thyroid gland	urine	urothelium		
references				0	0					Y			Y				0	Y	0			0	0		0					Lopes <i>et al.</i> [35] ²	
				0						Y	0	Y	0	Y		0			Y											Troyer <i>et al.</i> [137] ¹	
	0				0				0	Y	0		0			0							0		0	0				Silver <i>et al.</i> [36] ²	
										Y														0							Liu <i>et al.</i> [34] ²
				0	0					Y			Y				0							0	0	0	0				Chang <i>et al.</i> [138] ²
																															Dumas <i>et al.</i> [31] ²
																													Y		Gala <i>et al.</i> [32] ²
				Y						Y				Y							Y								Y		Sokoloff <i>et al.</i> [37] ³
				Y						Y						0				Y		Y		Y							Kinoshita <i>et al.</i> [33] ¹
0	0	0	0	0	0	Y	0	0		Y		0					0		0	0		0	0		Y	0	0		Y	Mhaweck-Fauceglia <i>et al.</i> [139] ^{2,4}	

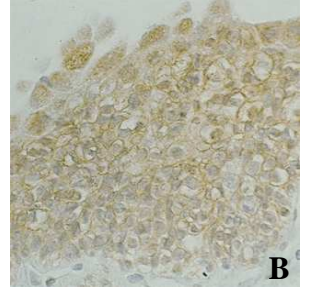


Table 3: GCPII expression in different human tissues. Y, protein expression detected. 0, no expression detected. ¹, western blot; ², immunohistochemistry; ³, dual-monoclonal sandwich assay; ⁴, tissue microarray. Inserted pictures: immunohistochemistry of **A**, prostatic tissue, adopted from [139] and **B**, urothelium, adopted from [32]. Different studies used different antibodies. **7E11-C5.3** (widely used as 7E11) applied: [31-33, 35-37, 137, 138]. **J591**: [34, 138]. **J415**: [138]. **PEQ226.5**: [37, 138]. **PM2J004.5**: [138]. **24.4E6**: [33]. **Y-PSMA-1**: [139].

3.3.1.2.3.2 GCPII cancer-specificity

Results from GCPII expression in malignant tissues are summarized in Table 4.

New study concerning detection in normal (Table 3) and malignant (Table 4) tissues was published recently [139]. This study analysed 3161 benign and malignant tumors for GCPII presence. GCPII was expressed in 154 (5.4%) from 2174 malignant tumors. The only brain tumor positive tissue for GCPII was glioblastoma multiforme in 3/148 of brain cases overall. And finally all 846 benign tumors were negative for GCPII [139].

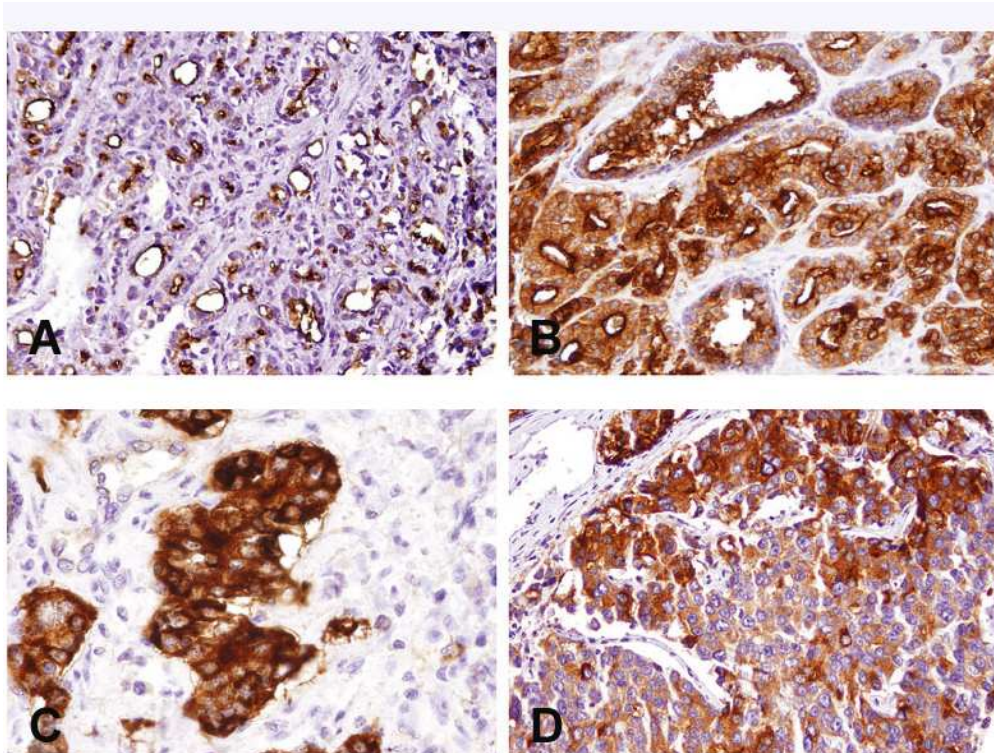


Fig. 13: GCPII expression in prostate adenocarcinoma. A. Apical pattern. B. Apical/cytoplasmic. C. Cytoplasmic with membranous accentuation. D. Cytoplasmic only. Adopted from [139].

	malignant tissue																	references				
	adrenal gland	bladder	breast	colon	connective tissue	esophagus	gallbladder	kidney	larynx	liver	lung	ovary	pancreas	prostate	salivary gland	skin	small intestine		stomach	testis	thyroid	urinary bladder
	0	0	0				0			0			Y		0							Lopes <i>et al.</i> [35]
	0	0	0						0	0			Y									Troyer <i>et al.</i> [137]
	0		0				0						Y									Silver <i>et al.</i> [36]
	0	0	0	0			0			0		0	Y		0				0			Chang <i>et al.</i> [138] ¹
	Y																					Chang <i>et al.</i> [142] ²
							Y															Dumas <i>et al.</i> [31]
	Y																					Gala <i>et al.</i> [32]
			Y																			Sokoloff <i>et al.</i> [37]
	Y	Y	Y	Y		Y	Y			Y	0		Y			Y	Y	Y				Kinoshita <i>et al.</i> [33]
	0	Y	0	Y		Y	Y	Y	Y			Y	Y	Y	Y				0	Y	Y	Mhaweck-Fauceglia <i>et al.</i> [139]

Table 4: Expression of GCPII in different malignant tissue. Y, protein expression detected. 0, no expression detected. Methods used for GCPII determination are the same as in protein detection from normal tissues. ¹, Chang *et al.* [142] used immunohistochemistry, and antibodies 7E11, J591, J415. ², Chang *et al.* [138] used immunohistochemistry, and antibodies 7E11, PM2J004.5, PEQ226.5, J591, J415.

Moreover, the neovasculature of several solid tumors was also GCPII positive, as shown in Table 5. For these studies different antibodies detecting N-terminus [31, 36] or extracellular part of GCPII [139] or combination of both [34, 138, 142] were used. Interestingly, no GCPII positivity was detected in benign tissue [138, 142] except benign kidney [142] and also only small number of prostate cancer neovasculature showed GCPII staining (only 2 from 12) [138].

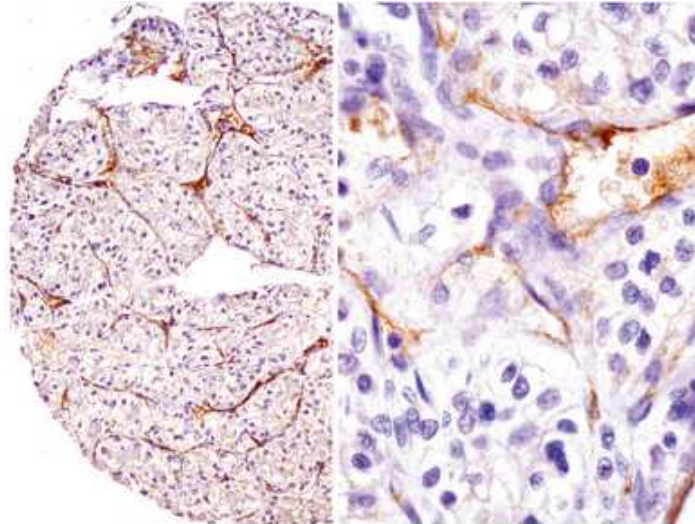


Fig. 14: Example of GCPII expression in neovasculature in clear cell carcinoma of kidney. Note that the tumor cells are negative for GCPII. Adopted from [139].

carcinoma neovasculature	bladder	blood vessels	breast	colon	glioblastoma multiforme	kidney	lung	metastatic carcinoma to liver	neuroendocrine carcinoma	pancreas	prostate carcinoma	sarcoma	skin	testis	references
	Y			Y		Y					0				
Y		Y	Y		Y	Y	Y								Liu <i>et al.</i> [34]
					Y										Dumas <i>et al.</i> [31]
Y	0	Y	Y	Y	Y	Y		Y	Y	Y	Y	Y	Y	Y	Chang <i>et al.</i> [138]
Y					Y ¹	Y			Y			Y	Y		Chang <i>et al.</i> [142]
					Y										Mhaweck-Fauceglia <i>et al.</i> [139]

Table 5: GCPII expression in carcinoma neovasculature. ¹, benign kidney was the only benign tissue that was GCPII positive. Different antibodies were used for detection.

The last published study detected only small samples of GCPII positive neovasculature. Tissue microarrays¹⁹ used in this study (described in [143]), where limited stroma is usually seen, makes the evaluation of GCPII expression in neovasculature difficult.

The expression of GCPII in neovasculature is a very interesting issue, because antibodies against GCPII can be used for delivery of a variety of agents aimed at destroying tumor neovasculature.

3.3.1.2.3.3 GCPII specificity and sensitivity

Sensitivity refers to the test's ability to identify people who have the disease. Specificity refers to the test's ability to identify people who do not have the disease. Most tumor markers are not sensitive or specific enough to be used for cancer screening.

The sensitivity and specificity of GCPII to distinguish adenocarcinoma of prostate from all other tumor types was 66% and 95%, respectively. However, in the differential diagnosis between prostate carcinoma and urothelial carcinoma of the bladder, the specificity is lower (83%) but the sensitivity is the same (66%) [139].

EVEN THOUGH GCPII IS EXPRESSED IN SEVERAL OTHER TYPES OF MALIGNANCIES, IT REMAINS A SENSITIVE AND SPECIFIC MARKER FOR PROSTATE CARCINOMA.

3.3.1.2.3.4 Simple and cost-efficient test for GCPII and cancer prognosis

3.3.1.2.3.4.1 Serum screening

Testing the cancer markers directly from serum (true for PSA) would be easier way and also less expensive, but there are controversial data concerning the presence and diagnostic relevance of GCPII in human serum [144-147]. Thus GCPII is neither used as a serum diagnostic nor serum-screening marker.

¹⁹ Glossary item

3.3.1.2.3.4.2 Detection of GCPII mRNA

GCPII mRNA expression is not prostate specific [32, 136, 142, 148-150]. Interestingly enough, it was not detected in normal (non-tumor) vasculature [142].

The reverse transcriptase-polymerase chain reaction (RT-PCR) can be an important molecular tool for its sensitivity and specificity [151-155]. Even though the GCPII as a PCR marker has some advantage over the PSA during hormone deprivation therapy [156], GCPII RT-PCR (compared with RT-PCR of serum PSA) is still inadequate for detection of all patients with prostate carcinoma and metastasis²⁰ [153, 157].

A strategy using GCPII and PSA RT-PCR assays in combination showed correlation with pathologic stage, sensitivity 67% in predicting circulating prostatic cells and specificity 91% [158-161].

RNAse protection assay showed higher expression of GCPII mRNA in prostate cancer compared to normal or benign prostate [8, 153, 162]. Also *in situ* hybridization studies showed trend in increasing GCPII expression with Gleason score²¹ [163]. But none of these studies did take into account existence of all alternatively spliced variants: GCPII (PSMA), PSM', PSM-C, PSM-D and PSM-E [4, 11], which can cause false positive results.

The most relevant splice variant PSM' (see chapter 3.1.1), lacking 266 nucleotides at the 5' end [8], represents together with GCPII a tumor index GCPII/PSM'. This index increases from normal to cancerous prostate. The ratio is also higher in the metastasis compared to normal prostate but did not change between tumor and benign tissues [7, 8].

3.3.1.2.3.4.3 Detection of GCPII protein: ProstaScint scan

GCPII protein levels are approximately 50-fold higher in normal and diseased prostate than in non-prostatic studied tissues [37]. Its expression increases from benign hyperplasia of the prostate to high-grade intraepithelial neoplasia²² or adenocarcinoma of the prostate [164, 165-167]. GCPII expression is higher in poorly differentiated and metastatic tumors [166] and its increase correlates with tumor grade (Gleason score), biochemical recurrence, pathological stage, and in primary tumors predicts disease outcome [166-168].

²⁰⁻²² Glossary item

In 1999 a radiographic test that uses murine antibody 7E11 linked to ¹¹¹indium (¹¹¹indium-capromab pendetide = ProstaScint) was approved by US Food and Drug Administration.

ProstaScint is noninvasive scan and can differentiate patients with organ localized disease from those with metastatic prostate cancer [169, 170]. Its cost is approximately \$2 000 [169]. In high-risk metastatic prostate cancer this scan have demonstrated a specificity and sensitivity of 70-90% and 60-80%, respectively, which is in true better than the accuracy of current CT scans (Computerized Axial Tomography) and MRI (Magnetic Resonance Imaging) [168, 169].

An important study in 2003 showed that the ProstaScint scan does not predict biochemical control after radiation therapy [171].

3.3.2 Therapeutic target in the prostate cancer - GCPII again

3.3.2.1 Radioimmunotherapy

In the terms of an *in vivo* targeting by radioimmunotherapy and cell killing, GCPII can be a nearly ideal molecule, because it is anchored in the membrane and is expressed in all prostate cancers [36, 156, 165]. The most used monoclonal antibody (mAb) for radioimmunotherapy is J591 stably bound to alpha-emitting radioisotope ²¹³Bi [172-174] or to beta-emitting particles ¹¹¹In, ¹³¹I, ⁹⁰Y, and ¹⁷⁷Lu [175, 176, 177-179].

Alpha-emitting and also beta-emitting mAb construct specifically targeted LNCaP cells and also prostate cancer *in vivo* [172, 174, 177] and showed no side effect [173].

Phase I radioimmunotherapy trials were started in patients with progressing hormone independent prostate cancer and J591 (labeled with ¹¹¹In) targeted bone and/or soft tissue lesion in 98% of patients [176, 179]. Selective targeting of antibody to tumor was seen [175].

3.3.2.2 Immunotherapeutic approach

Active non-specific immunotherapy, which uses the responses of immune system, is mostly used in cancer immunotherapy.

Dendritic cell based immunotherapy is a promising approach to increase tumor antigen-specific T-cell responses in cancer patients. This approach uses peptides from GCPII

and evokes responses of cell-mediated immunity [180-187]. T-cells were also stimulated by recombinant and native GCPII [188, 189]. In all these studies T-cells were stimulated and immune response was observed.

Since the tumor is trying to escape the immune system by down-regulation of target antigen, it seems better to generate T-cell response by several prostate-specific antigens in the same time. A study using PSCA, PAP, PSA and GCPII resulted in significant cytotoxic T-cell responses against all prostate-specific antigens tested [190].

Another interesting approach is generation of artificial T-cell receptors [191-194] or DNA vaccinations with plasmid coding for GCPII [195, 196].

Interestingly enough, prostate cancer patients immunized with plasmid coding for GCPII [197], or extracellular portion of GCPII [189, 198], or only with a part of extracellular domain [199] induced anti-GCPII humoral immune response and also produced specific antibodies which could not be detected in healthy men, women and patients before the vaccination [200].

3.3.2.3 Immunotoxins

Using antibodies specific to tumors conjugated with toxins is a very elegant method. Use of monoclonal antibodies to GCPII showed to be specific and effective. J591 linked to maytansine derivate (DM1, from ethiopian shrug *Maytenus serrata*) showed to be effectively delivered to GCPII positive cells *in vitro* and *in vivo* [201] and to xenograft tumor tissue. It blocked tumor growth and elaboration of osteoblastic lesions [202].

Another toxin, ricine A-chain [203] and its deglycosylated form [204] were cross-linked to different monoclonal antibodies of GCPII. The toxic effect on LNCaP cells and spheroids was observed [203]. They also inhibited growth of LNCaP tumor xenografts without toxicity in mice [204]. One of the recent attempts used recombinant immunotoxin containing single-chain antibody fragment against GCPII conjugated to truncated form of *Pseudomonas* exotoxin A, which binds to GCPII positive cells and reduces the viability by 50% at concentration of 20pM, while the GCPII negative cells remain unaffected [205].

3.3.2.4 Gene therapy and enhancer/promoter of GCPII

Transcription activity of GCPII enhancer/promoter is prostate specific [206]. When GCPII enhancer/promoter is combined with a cytosine deaminase gene for suicide-driven gene therapy, GCPII enhancer/promoter drives the cytosine deaminase toxicity in GCPII expressing cells and non-prostatic cells are not significantly affected [207]. Elimination of tumors when expressing cytosine deaminase under the regulatory control of GCPII enhancer/promoter was detected in mice bearing prostatic cell line transfected with enhancer/promoter of GCPII [208]. Cytosine deaminase gene suicide therapy is based on conversion of nontoxic prodrug 5-fluorocytosine into cytotoxic 5-fluorouracil. Also another suicide gene thymidine kinase, when coupled to GCPII enhancer/promoter, showed strong inhibitory effect on tumor growth in mice [209].

4 DISSERTATION RESEARCH AIMS

The principal aims of the studies presented in this thesis were:

- Analysis of possible domain representation of GCPII; the significance of these domains in protein folding and enzyme activity
- Analysis of the substrate specificity of GCPII by site-directed mutagenesis; molecular modeling; kinetic characterization
- Localization and trafficking of GCPII and its truncated form PSM' in cells and tissues

5 LIST OF PUBLICATIONS

- I. Mlčochová P, Plechanovová A, Bařinka C, Mahadevan D, Saldanha JW, Rulíšek L, Konvalinka J.
Mapping of the active site of glutamate carboxypeptidase II by site-directed mutagenesis.
FEBS J 2007; 274:4731-41.
- II. Bařinka C, Mlčochová P, Šácha P, Hilgert I, Majer P, Slusher BS, Hořejší V, Konvalinka J.
Amino acids at the N- and C-termini of human glutamate carboxypeptidase II are required for enzymatic activity and proper folding.
Eur J Biochem 2004; 271:2782-90.
- III. Bařinka C, Rovenská M, Mlčochová P, Hlouchová K, Plechanovová A, Majer P, Tsukamoto T, Slusher BS, Konvalinka J, Lubkowski J.
Structural insight into the pharmacophore pocket of human glutamate carboxypeptidase II.
J Med Chem 2007; 50:3267-73.
- IV. Hlouchová K, Bařinka C, Klusák V, Šácha P, Mlčochová P, Majer P, Rulíšek L, Konvalinka J.
Biochemical characterization of human glutamate carboxypeptidase III.
J Neurochem 2007; 101:682-96.
- V. Šácha P, Zámečník J, Bařinka C, Hlouchová K, Vícha A, Mlčochová P, Hilgert I, Eckschlager T, Konvalinka J.
Expression of glutamate carboxypeptidase II in human brain.
Neuroscience 2007; 144:1361-72.
- VI. Mlčochová P, Bařinka C, Konvalinka J.
Prostate-Specific Membrane Antigen and its truncated form PSM'.
Manuscript in preparation

Another publication (not included in thesis)

Rovenská M, Hlouchová K, Šácha P, Mlčochová P, Horák V, Zámečník J, Bařinka C, Konvalinka J.

Tissue expression and enzymologic characterization of human prostate specific membrane antigen and its rat and pig orthologs.

Prostate 2007, accepted September 2007

6 RESULTS AND DISCUSSION

6.1 Importance of amino acid residues inside the active site of GCPII

6.1.1 Background information

GCPII is a metallopeptidase from the peptidase family M28. Based on the alignment of GCPII sequence to aminopeptidases *Aeromonas proteolytica* and *Streptomyces griseus*, five putative amino acids coordinating the zinc ions in the active site were identified. It has been shown that mutation in these residues (His377, Asp387, Glu425, Asp453 and His553) abolished the GCPII activity. The mutation in the putative substrate-binding residues influenced but did not abolish the GCPII activity [210]. Reliability of assignment of zinc binding residues was confirmed by the crystal structures of GCPII published in 2005 and 2006 [25, 26]. Nevertheless, the identity of substrate-binding residues is still not confirmed, because crystal structure of GCPII in complex with the naturally occurring substrate, N-acetyl-aspartyl-glutamate (NAAG), has not yet been published.

We created a computational model of GCPII/NAAG complex on the basis of crystal structure of GCPII with inhibitor GPI-18431 (Fig. 15) [26]. We found several important amino acid residues in the active site, which bind the substrate and performed the mutagenesis study to confirm this model.

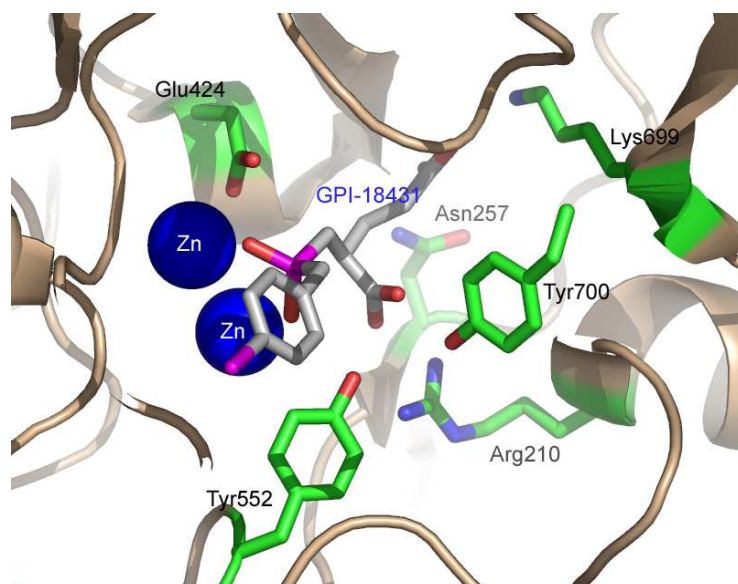


Fig. 15: Active site of GCPII with bound inhibitor GPI-18431.

6.1.2 Summary

We performed detailed analysis of amino acid residues inside the active site of glutamate carboxypeptidase II using site-directed mutagenesis.

Firstly, we designed QM/MM model of GCPII/NAAG complex (GCPII in complex with N-acetyl-aspartyl-glutamate) based on known crystal structure of GCPII in complex with the inhibitor. The structural arrangement and the interactions between enzyme and substrate in S1' pocket of GCPII/NAAG model is highly similar to crystal structure of GCPII/glutamate.

In the S1 pocket, Arg534, Arg536, and Asn519 interact with the aspartate side chain of NAAG. Mutation in these residues caused a decrease in turnover number and thus they seem to be much more important for substrate turnover than for substrate binding.

On the other hand, mutation in residues of S1' site showed dramatic increase in Michaelis-Menten constant value (compared to wild-type). These amino acids binding glutamate of NAAG are thus critical for substrate/inhibitor recognition and binding.

Mapping of the active site of glutamate carboxypeptidase II by site-directed mutagenesis

Petra Mičochová^{1,2*}, Anna Plechanovová^{1,2*,†}, Cyril Bařínka^{1,‡}, Daruka Mahadevan³, Jose W. Saldanha⁴, Lubomír Rulíšek¹ and Jan Konvalinka^{1,2}

1 Gilead Sciences and IOCB Research Centre, Institute of Organic Chemistry and Biochemistry, Academy of Sciences of the Czech Republic, Prague, Czech Republic

2 Department of Biochemistry, Faculty of Science, Charles University, Prague, Czech Republic

3 Department of Medicine, Hematology/Oncology, Arizona Cancer Center, Tucson, AZ, USA

4 National Institute for Medical Research, Division of Mathematical Biology, London, UK

Keywords

active site; metallopeptidase; mutagenesis; NAALADase; prostate specific membrane antigen

Correspondence

J. Konvalinka, Institute of Organic Chemistry and Biochemistry, Academy of Sciences of the Czech Republic, Flemingovo n. 2, 166 10 Praha 6, Czech Republic
Fax: +420 220 183578
Tel: +420 220 183218
E-mail: konval@uochb.cas.cz

*These authors contributed equally to this work

Present address

†College of Life Sciences, University of Dundee, UK

‡Center for Cancer Research, National Cancer Institute at Frederick, MD, USA

(Received 18 April 2007, revised 15 June 2007, accepted 11 July 2007)

doi:10.1111/j.1742-4658.2007.06021.x

Human glutamate carboxypeptidase II [GCPII (EC 3.4.17.21)] is a membrane-bound metallopeptidase expressed in several tissues, including the prostate, brain, small intestine, and kidney [1–5]. Although the function of GCPII in prostate remains unclear, it is well known that this protein is overexpressed in pros-

Human glutamate carboxypeptidase II [GCPII (EC 3.4.17.21)] is recognized as a promising pharmacological target for the treatment and imaging of various pathologies, including neurological disorders and prostate cancer. Recently reported crystal structures of GCPII provide structural insight into the organization of the substrate binding cavity and highlight residues implicated in substrate/inhibitor binding in the S1' site of the enzyme. To complement and extend the structural studies, we constructed a model of GCPII in complex with its substrate, *N*-acetyl-L-aspartyl-L-glutamate, which enabled us to predict additional amino acid residues interacting with the bound substrate, and used site-directed mutagenesis to assess the contribution of individual residues for substrate/inhibitor binding and enzymatic activity of GCPII. We prepared and characterized 12 GCPII mutants targeting the amino acids in the vicinity of substrate/inhibitor binding pockets. The experimental results, together with the molecular modeling, suggest that the amino acid residues delineating the S1' pocket of the enzyme (namely Arg210) contribute primarily to the high affinity binding of GCPII substrates/inhibitors, whereas the residues forming the S1 pocket might be more important for the 'fine-tuning' of GCPII substrate specificity.

tate cancer [6–8]; hence, GCPII is a putative target for prostate cancer diagnosis and treatment [9–11].

In the brain, GCPII is expressed in astrocytes and cleaves *N*-acetyl-L-aspartyl-L-glutamate (NAAG), a neuropeptide, releasing *N*-acetyl-L-aspartate and free glutamate [12], the most potent excitatory

Abbreviations

AccQ, 6-aminoquinolyl-*N*-hydroxysuccinimidyl carbamate; NAAG, *N*-acetyl-L-aspartyl-L-glutamate; NAALADase, *N*-acetylated- α -linked-acidic dipeptidase; 2-PMPA, 2-(phosphonomethyl)pentanedioic acid; QM/MM, quantum mechanics/molecular mechanics; rhGCPII, recombinant human glutamate carboxypeptidase II (extracellular part, amino acids 44–750).

neurotransmitter in the central nervous system. Several potent inhibitors of GCPII act in a neuroprotective fashion in animal models of neurological disorders associated with high levels of glutamate, such as stroke and neuropathic pain [13–17]. GCPII also acts as a folate hydrolase and cleaves γ -linked glutamates from folyl-poly γ -glutamates, thus participating in the absorption of dietary folates in the small intestine [18].

For both activities of GCPII, the presence of oligosaccharides on the protein surface [19,20] and two zinc(II) ions complexed in the active site is essential. Based on the homology of GCPII with aminopeptidases from *Streptomyces griseus* and *Vibrio proteolytica* His377, Asp387, Glu425, Asp453, and His553 were proposed to coordinate the active-site zinc(II) ions and these predictions were later confirmed by mutational analysis experiments [21]. In the same study, Speno *et al.* [21] also targeted putative substrate binding residues (as predicted from the sequence alignment with the *Vibrio* aminopeptidase). The change in these residues negatively influenced but did not abolish GCPII activity.

Until recently, the only available structural data on GCPII consisted of models based on its homology with the transferrin receptor and members of M28 family [22–24]. However, structure–activity analysis using deletion mutants of the GCPII ectodomain showed that the putative protease domain itself supports neither proteolytic activity, nor the correct folding of the enzyme [25]. These biochemical observations were later rationalized by X-ray structures of the unliganded ectodomain of GCPII revealing that all three extracellular domains of GCPII cooperate to form the active site and substrate binding cavity of GCPII [26,27].

A more detailed insight into the active site was obtained by an analysis of crystal structures of the extracellular part of GCPII complexed with small molecules [28]. The structure with bound glutamate (Fig. 1) reveals that the previous predictions of its binding in the GCPII active site [21,23,26] were inaccurate. By contrast to the available models, L-glutamate is bound in the S1' site via its α -carboxylate group, which forms a salt bridge with Arg210 and hydrogen bonds with the hydroxyl groups of Tyr552 and Tyr700. Furthermore, the γ -carboxylate of glutamate forms a strong salt bridge with Lys699 and the hydrogen bond with Asn257 [28] (Fig. 2A). Although the information about the S1' pocket is rather detailed, very little is known about the architecture of the S1 site. Mesters *et al.* [28] suggest that the S1 pocket is defined by Asn519, Arg534, Arg536, Arg463, and Ser454.

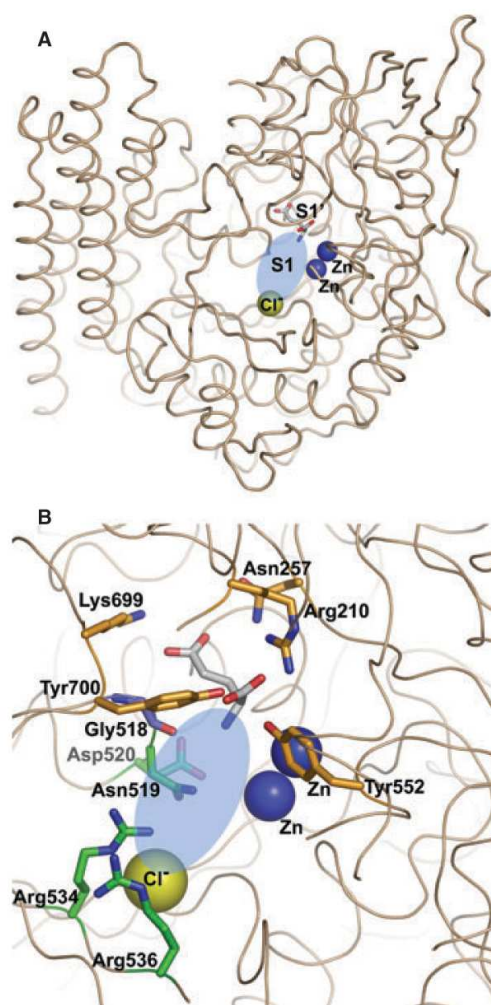


Fig. 1. Overall structure of the GCPII extracellular domain (designed from the structure of GCPII in complex with glutamate [28] using PYMOL molecular graphics system, version 0.97 (DeLano Scientific, San Carlos, CA, USA). (A) Ectodomain of GCPII in ribbon representation. Glutamate (the product of cleavage of the substrate NAAG) resides in the S1' pocket of GCPII. The predicted S1 site is delineated by a blue oval near two zinc ions (blue spheres) and a chloride ion (yellow sphere). (B) A detailed look inside the active site of GCPII. The blue oval outlines the predicted GCPII S1 site. Amino acid residues defining the S1' site are colored in orange, predicted S1 site residues are in green, and Gly518, which binds the free amino group of glutamate, is in slate color. Zinc ions (blue) and chloride ion (yellow) are depicted as spheres.

2-(Phosphonomethyl)pentanedioic acid (2-PMPA), the one of the most potent and specific inhibitors of GCPII published so far [29], includes a phosphonate

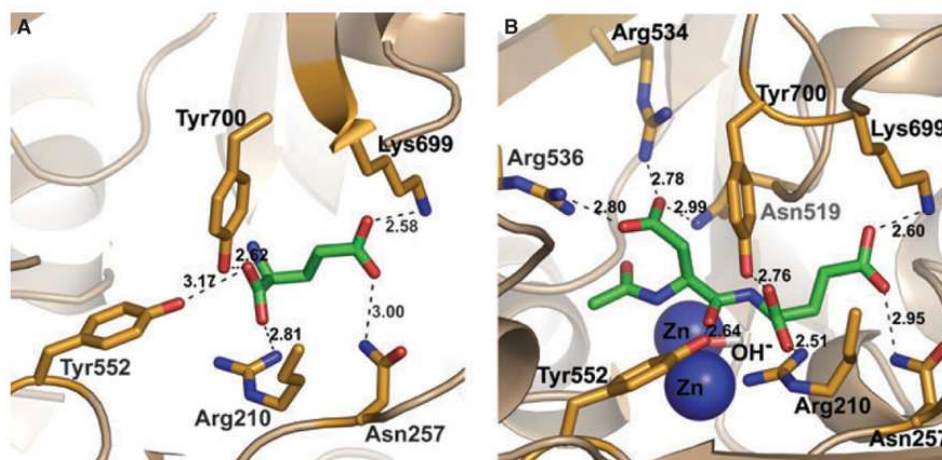


Fig. 2. Active site of GCPII with bound product (L-glutamate) and a natural substrate (NAAG). (A) Amino acid residues in the S1' substrate binding pocket. L-glutamate (depicted here in green) is held in the active site via interactions with several amino acid residues (shown in orange). The α -carboxylate group of glutamate accepts hydrogen bonds from the hydroxyl groups of Tyr552 (distance of 3.17 Å) and Tyr700 (2.62 Å) and forms a salt bridge with Arg210 (2.81 Å). The γ -carboxylate group is recognized through an ionic interaction with Lys699 (2.58 Å) and through a hydrogen bond with the side-chain amide of Asn257 (3.00 Å). This picture was designed from the structure of GCPII in complex with glutamate [28] using PYMOL molecular graphics system, version 0.97 (DeLano Scientific). (B) The optimized QM/MM structure of NAAG bound in the active site of GCPII. The carbonyl group of L-aspartate from NAAG (depicted in green) accepts a hydrogen bond from the hydroxyl group of Tyr552 (distance 2.64 Å). The β -carboxylate group of L-aspartate forms strong salt bridges with two arginines, Arg534 and Arg536 (2.78 Å and 2.80 Å, respectively), and a hydrogen bond with Asn519 (2.99 Å). The structural arrangement of the glutamate part of NAAG within the S1' pocket closely resembles the arrangement observed in the crystal structure of the rhGCPII/glutamate complex, with all principal interactions conserved. Zinc ions (blue) and the hydroxyl between them are also depicted. This picture was designed from the model of GCPII in complex with NAAG using PYMOL molecular graphics system, version 0.97 (DeLano Scientific).

group chelating the active site zinc ions and a glutarate moiety (pentanedioic acid) that binds to the glutamate recognition site of GCPII (the S1' site) [28]. The majority of GCPII inhibitors have a glutarate moiety as a common denominator and differ only in their zinc-binding groups. Attempts to substitute the glutarate residue of the inhibitor led to significant decrease of inhibition potency *in vitro* [14,29–31]. The first successful improvement in efficiency by modifying the glutarate moiety of GCPII inhibitors was achieved by introducing the 3-carboxybenzyl group to the P1' side chain of the inhibitor together with the sulfhydryl zinc-binding moiety [32].

To analyze the binding mode of the substrate/inhibitor to the active site of GCPII on a molecular level, we performed a structure–activity analysis of the residues participating in substrate/inhibitor binding in the S1' pocket, as identified by X-ray structure analysis, and the residues predicted to participate in binding in the S1 pocket of the enzyme. The latter residues were identified both from the available crystal structures and the quantum mechanics/molecular mechanics (QM/MM) calculations of the substrate bound in the GCPII active site as

reported here. Finally, the results of QM/MM calculations are used *a posteriori* to qualitatively elucidate the observed changes in k_{cat} and K_{m} values and provide some insight into the reaction mechanism of this prime pharmaceutical target.

Results

Site-directed mutagenesis

Based on the crystal structure of the recombinant human glutamate carboxypeptidase II (rhGCPII)/glutamate complex [28], as well as the QM/MM model of the rhGCPII/NAAG complex (see below), 12 mutations of amino acids delineating the substrate binding cavity of GCPII were designed and introduced into the GCPII ectodomain (rhGCPII; amino acids 44–750) using site-directed mutagenesis. Individual amino acid changes were created by modifying the rhGCPII sequence using two complementary oligonucleotide primers harboring the desired mutation (Table 1). The presence of individual mutations and the accuracy of the whole rhGCPII sequence were verified by dideoxynucleotide-terminated sequencing.

Table 1. Sequences of primers used for site-directed mutagenesis. Mutagenic bases are shown in bold.

Mutation	Nucleotide sequence (5'- to 3')
R210A	GGGAAAGTTTTC CGC GGAAATAAGGTTAAAAATG CATTTTTAACTTATTTC CGC GAAAACTTTCC
R210K	GGGAAAGTTTTC AG GGAAATAAGGTTAAAAATGC GCATTTTAACTTATTTC CT TGAAAACTTTCC
N257D	GTCACGCGTGG A GATATCCTAAATCTGAATGG CCATTCAGATTTAGGATAT C TCCACGCTGGAC
G518P	GGATAAGCAAATGGGAT CCCA AATGATTTTGAGGTG CACCTCAAATCATT TGGG GATCCCAATTTGCTTATCC
N519D	GCAAATGGGAT CCGG A GAC GATTTTGAGG CCTCAAAT CTC CCGATCCCAATTTGC
N519V	GGATAAGCAAATGGGAT CCGG A TTG ATTTTGAGGTGTTCC GAACACCTCAAAT CA ACT CCG GATCCCAATTTGCTTATCC
D520N	GCAAATGGGAT CTGG AAAT AA TTTGGAGGTGTTCTTC GAAGAACACCTCAAAT ATT TTCCAGATCCCAATTTGC
R534L	GGAAATGCTTCAGG CTAG CGCATCTACTAAAAATTGG CCAATTTTGTAGTATACCGT GTAG CCCTGAAGCAATTCC
R536L	GCTTCAGGCAGAG CTCT GATATAAAATTTGG CCAATTTTGTAGTAT ACAG AGCTCTGCTGAAGC
Y552I	CAGCGGCTAT CCACTG ATT CA CAGTGTCTATGAAAC GTTTCATAGACACT GTGA ATCAGTGGATAGCCGCTG
K699S	CAAGCAGCCACA ACTCA TATGACAGGGGAGTC GACTCCCTGCAT ATGA TTGTTGGCTGCTTG
Y700F	GCAGCCACA CAAGT TCG CA GAGGGGAGTCATTCC GGAATGACTCCCT GCA ACTTGTGTGGCTGC

Mutant protein expression and purification

Schneider's S2 cells were used for heterologous overexpression of wild-type rhGCPII (wt rhGCPII) as well as for the expression of rhGCPII mutants. Immunoblot analysis confirmed that all rhGCPII mutants were efficiently secreted into culture media (Fig. 3), suggesting correct protein folding. The expression levels of the individual rhGCPII mutants were comparable (in the range 0.8–1.7 $\mu\text{g}\cdot\text{mL}^{-1}$) and were approximately four- to eight-fold lower than wt rhGCPII expression (6 $\mu\text{g}\cdot\text{mL}^{-1}$; data not shown). In subsequent experiments, kinetic/inhibition parameters for the mutants with high specific activities (R534L, R536L, and Y552I) were determined using the conditioned media. wt rhGCPII and the remaining nine mutants, which exhibited lower specific activities, were expressed on a large scale and purified as described in the Experimental procedures.

Mutational analysis of the S1' site

The previously reported crystal structure of the rhGCPII/glutamate complex [28] indicates that the α -carboxylate of the S1'-bound glutamate interacts with Arg210, Tyr552, and Tyr700, whereas the γ -carboxyl-

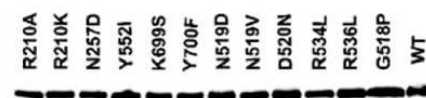


Fig. 3. Expression of individual mutant proteins. Recombinant protein expression was induced with 1 mM CuSO_4 in stably transfected S2 cell lines. Culture medium containing the expressed protein was harvested on the third day after induction. Proteins were resolved on a 10% SDS/PAGE gel, electroblotted onto a nitrocellulose membrane, and immunostained as described in Experimental procedures. The band intensities were recorded using a charge-coupled device camera. Amount of proteins applied: R210A (11 ng), R210K (11.9 ng), N257D (9 ng), Y552I (11 ng), K699S (8.4 ng), Y700F (8.2 ng), N519D (8.7 ng), N519V (9 ng), D520N (12 ng), R534L (8 ng), R536L (12 ng), G518P (13 ng). Purified wt rhGCPII (12.5 ng) is shown for comparison.

Table 2. Kinetic parameters of NAAG hydrolysis for wt and mutant forms of rhGCPII. Michaelis–Menten values (K_m) for NAAG hydrolysis were determined by a nonlinear least squares fit of the initial velocity versus concentration of the substrate and compared with wild-type enzyme. The concentrations of mutant proteins used for calculation of turnover number (k_{cat}) were determined by quantification from a western blot.

Mutation	K_m (μM)	k_{cat} (s^{-1})	k_{cat}/K_m ($\text{mmol}^{-1}\cdot\text{s}^{-1}$)
Wild-type ^{a,c}	1.15 ± 0.57	1.1 ± 0.2	957
Residues in the S1' substrate binding site			
R210A ^{a,b}	294 ± 15	0.023 ± 0.001	0.08
R210K ^{a,b}	801 ± 124	0.130 ± 0.020	0.16
N257D ^{a,b}	68.10 ± 19.7	0.320 ± 0.080	4.70
Y552I ^{c,d}	0.15 ± 0.036	0.014 ± 0.001	93.3
K699S ^{a,b}	40.50 ± 22.9	0.270 ± 0.060	6.67
Y700F ^{a,b}	45.70 ± 6.6	0.075 ± 0.003	1.64
Residues in the predicted S1 substrate binding site			
N519D ^{a,b}	27.60 ± 0.300	0.078 ± 0.005	2.83
N519V ^{a,c}	0.67 ± 0.066	0.036 ± 0.001	53.7
D520N ^{a,c}	2.30 ± 0.180	0.007 ± 0.001	3.04
R534L ^{c,d}	0.14 ± 0.072	0.100 ± 0.040	714
R536L ^{c,d}	0.18 ± 0.005	0.010 ± 0.005	55.6
Residue binding free amino group of L-glutamate			
G518P ^{a,c}	2.20 ± 0.028	0.090 ± 0.020	40.9

^a Kinetic parameters were measured using purified protein.

^b Kinetic parameters were determined by an HPLC assay. ^c Kinetic parameters were determined by a radioenzymatic assay. ^d Kinetic parameters were determined using the culture medium of the protein expressing cells.

ate group is hydrogen bonded by the side chains of Asn257 and Lys699 (Fig. 2A). In the present study, the glutamate-binding residues of GCPII were mutated as follows: Arg210 (to Ala210 or Lys210), Asn257 (to Asp257), Tyr552 (to Ile552), Lys699 (to Ser699) and Tyr700 (to Phe700) (Tables 1 and 2).

The mutations of the glutamate-binding residues led to a dramatic increase in the Michaelis–Menten constant value (compared to wild-type), ranging from approximately 35-fold (for the K699S mutant) to an almost 700-fold increase for the R210K mutation (Table 2). The only exception was the Y552I mutant, which exhibited an eight-fold decrease in the K_m value. On the other hand, in most cases the mutations resulted in a relatively minor decrease in k_{cat} value, again with the exception of Y552I, which exhibited the largest decrease (approximately 80-fold) in k_{cat} detected in this series. The catalytic efficiencies of all the mutated proteins studied decreased by one to four orders of magnitude, which can be attributed mainly to the significant decrease in substrate binding (K_m values) (Table 2 and Fig. 4A).

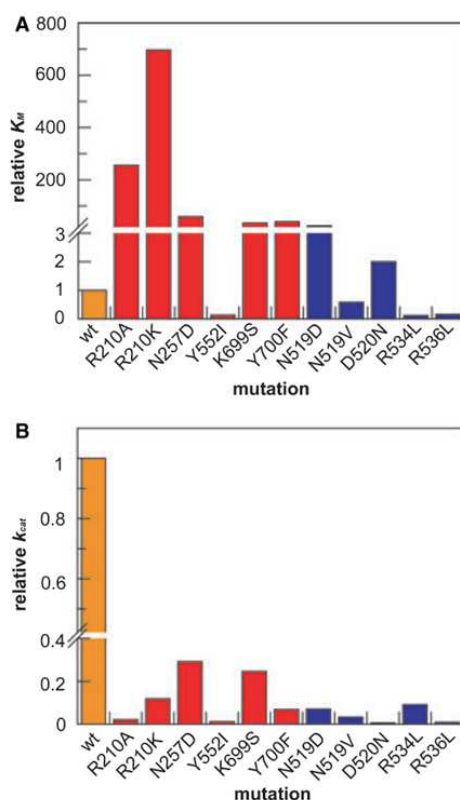


Fig. 4. Relative K_m and k_{cat} values for individual mutant proteins. Relative values of kinetic parameters of NAAG hydrolysis for mutant proteins with a substitution in the S1' site are shown as red columns, whereas blue columns are used for proteins with a mutation in the predicted S1 pocket. (A) Relative K_m values. (B) Relative k_{cat} values.

A model of the rhGCPII/NAAG complex: identification of residues delineating the S1 pocket

QM/MM calculations of the rhGCPII/NAAG complex yielded the equilibrium structure corresponding to the NAAG moiety bound in the active site of GCPII prior to its hydrolytic cleavage. All the details of the model structure, including the partial charges in all atoms used in the MM part, can be found in the PDB file deposited in the Supplementary material. A detailed structure of the GCPII active site with NAAG bound is depicted in Fig. 2B.

The structural arrangement and the enzyme–substrate interactions within the S1' pocket closely resemble the arrangement observed in the crystal structure of the rhGCPII/glutamate complex, with all principal (polar) interactions preserved. In the S1 pocket, Arg534, Arg536, and Asn519 interact with the aspartate side chain from NAAG, whereas Tyr552 forms a hydrogen bond with the peptide bond oxygen (Fig. 2B).

It can be observed that the NAAG molecule geometry differs from that of a free dipeptide and resembles the activated species. For example, the peptide bond hydrogen deviates from planarity by 25°. This is not quite surprising because the OH[−] moiety coordinated between two zinc(II) ions is expected to initiate the hydrolytic cleavage of the NAAG peptide bond and the formation of the tetrahedral intermediate results in the nonplanarity of a peptide bond.

The structural aspects of the NAAG binding mode enable us to discuss the possible changes in the values of K_m caused by the amino acid substitutions. It is more difficult to utilize the model structure for discussions of k_{cat} values because these are directly related to the transition state structures and the corresponding free energy barriers, which are not yet available.

Mutational analysis of the S1 site

The model of the rhGCPII/NAAG complex suggests that GCPII most likely interacts with the N-terminal part of the substrate via the side chains of Asp453, Asn519, Arg534, and Arg536 (Fig. 2B). To verify this model experimentally, the N519D, N519V, R534L, and R536L mutants were constructed and kinetically characterized and the results are summarized in Table 2 and Fig. 4.

In general, mutations of the S1 residues interacting with the substrate led to a significant decrease in k_{cat} values (Fig. 4B), whereas the changes in K_m values were rather modest. Not surprisingly, the changes observed in the kinetic parameters were largely depen-

dent on the nature of the amino acid newly introduced. When Asn519 was mutated to aspartate, the N519D mutant exhibited a 24-fold increase in K_m compared to the wt rhGCPII. On the other hand, the Asn to Val mutation at the same position did not lead to a significant change in the K_m value. The corresponding k_{cat} values were approximately 14-fold (for N519D) and 30-fold (for N519V) lower than that of the wild-type enzyme. Both Arg534 and Arg536 were individually mutated to leucine. These mutations were unexpectedly associated with a moderate decrease in the K_m values as well as a pronounced decrease in the turnover number for both mutants.

Amino acid residues binding free amino group of L-glutamate

The free amino group of glutamate is bound through carbonyl oxygen of Gly518 and with a water molecule that is hydrogen-bonded to Tyr552. As discussed above, the mutation Y552I leads to the decrease of both the K_m and k_{cat} values. The mutation of Gly518 to Pro led to a slight increase of the K_m value and one order of magnitude decrease of the k_{cat} value (Table 2).

Analysis of inhibitor binding to the mutated proteins

Inhibition constants (K_i) for 2-PMPA [33], were determined for seven mutant proteins, and the data are summarized in Table 3. Compared with those of the wild-type enzyme, the K_i values for the rhGCPII mutants with S1' amino acid substitutions were

Table 3. K_i values for 2-PMPA. Inhibition constants for 2-PMPA were measured using HPLC and radioenzymatic assays as described in Experimental procedures. *N*-acetyl-L-aspartyl-L-methionine was used as the substrate for wt rhGCPII, whereas NAAG was used for all the mutant proteins.

Mutation	K_i (nM)
Wild-type	0.18 ± 0.03
Residues in the S1' substrate binding site	
R210A	22 000 ± 1,000
N257D	626 ± 46
K699S	32.7 ± 5.40
Y700F	49.7 ± 2.60
Residues in the predicted S1 substrate binding site	
N519D	5.6 ± 0.4
N519V ^a	1.8 ± 0.3
R534L ^a	0.5 ± 0.1

^a K_i values were determined by a radioenzymatic assay.

increased by two- to five orders of magnitude. The highest increase was observed for the R210A mutant protein, which showed a K_i value five orders of magnitude higher. Of the mutations outside the S1' pocket, the N519D, N519V, and R534L mutations resulted in an increase in the K_i value compared to the wt rhGCPII (30-fold, 11-fold, and 2.5-fold, respectively).

Discussion

The present study aimed to analyze the binding pocket of human GCPII using molecular modeling and site-directed mutagenesis analysis. Guided by the previously determined crystal structure of GCPII, we set out to complement the available structural data by a functional analysis of the GCPII mutants. Additionally, the QM/MM calculations of the NAAG binding mode in the GCPII active site enabled us to predict the structure and enzyme-substrate interactions in the S1 binding site. Such a detailed information cannot be obtained from the crystal structure; however, the complete description of the reaction mechanism by QM/MM modeling is beyond the scope of the present study, and the structural insights obtained are used in the qualitative way.

The biochemical data clearly indicate that interactions in S1' pocket are indispensable for high affinity substrate or inhibitor binding. In this respect, Arg210 is the most important residue. Somewhat surprisingly, the mutation R210K leads to dramatic increase of K_m and decrease of k_{cat} . Arg210 apparently fulfills a dual role in the architecture of the S1' site. First, it interacts directly with an α -carboxylate of the C-terminal substrate residue, assuring GCPII selectivity as a carboxypeptidase. Second, it is important for maintaining productive architecture of the S1' site of GCPII, including the positioning of the Tyr552 side chain. Despite similarities between lysine and arginine residues, the lysine side chain could not fully substitute Arg210 as the N- ϵ group, contrary to the arginine guanidinium group, can not simultaneously engage both the α -carboxylate of NAAG and the Tyr552 hydroxyl group. Consequently, it is likely that the R210K mutation leads to rearrangement of Tyr552 and/or active-site bound NAAG, resulting in observed changes in kinetic parameters of GCPII.

The importance of the S1' subsite for the ligand binding is also documented by previously published structure-activity data on GCPII inhibitors showing that the glutarate part of various inhibitors, which presumably targets in the S1' pocket [28], is very sensitive to any structural change [29,30,34]. Moreover, a change in the α -carboxylate group is more disruptive

than a change in the γ -carboxylate group [32,34,35]. The glutarate moiety is also present in 2-PMPA, one of the most potent inhibitors of GCPII published to date ($K_i = 0.3$ nM) [29], and the α -carboxylate group, which has been shown to interact with Arg210, renders this structural feature indispensable for potent inhibitor binding.

The only residue in the S1' site which does not seem to be critical for substrate binding is Tyr552. The OH group of Tyr552 forms a weak hydrogen bond with the α -carboxylate group of C-terminal glutamate and with the carbonyl group of the Asp-Glu peptide bond (in the QM/MM model). Tyr552 could play a more important role in transition state stabilization, which might explain why the mutagenesis of this residue leads to such a dramatic decrease in k_{cat} value.

It should be noted that, in addition to polar interactions, there are also nonpolar interactions that might contribute to the substrate/inhibitor binding (Phe209, Leu428, C. Bařinka, unpublished results), which are not analyzed in this study.

The important role of the S1' residues is also supported by the fact that all of them are conserved in the GCPII homolog GCPIII and in the mammalian GCPII orthologs (Table 4) and that the ability of these enzymes to bind NAAG is highly similar to that of GCPII [36] (M. Rovenska, K. Hlouchova, P. Šacha, P. Ml̄ochova, V. Horak, J. Zameenik, C. Bařinka & J. Konvalinka, unpublished results). On the other hand, the GCPII homolog *N*-acetylated- α -linked-acidic dipeptidase L (NAALADase L), which does not cleave NAAG [37], has only two (out of five) of these residues conserved (Arg210 and Tyr552). It can be postulated that NAALADase L cannot bind NAAG with enough affinity for cleavage due to the absence of certain important residues in the S1' site.

To identify the residues delineating the S1 binding pocket, a QM/MM analysis of the interaction between the enzyme and its natural substrate was performed. Previous inhibition studies revealed that the S1 pocket

appears to be large, and a wide variety of substituents are tolerated at the N-terminus of a phosphonate or phosphinate analogue without a significant loss in inhibitor potency [34,38]. We have recently shown that the S1 pocket is critical for GCPII specificity (only Glu and Asp are tolerated in the P1 position of the *N*-acetylated substrate) [19]. In agreement with structure-activity relationship analysis, our findings confirm that the S1 pocket tolerates more variability and does not contribute substantially to affinity of the substrate binding.

Interestingly, the mutations of Arg534 and Arg536 lead to decreases in K_m . It can be speculated that the enzyme is able to compensate for the lost interaction of one arginine. The side chain of Arg536 adopts two different conformations in the crystal structure of ligand-free GCPII [27]. Additionally, when the crystal structures of GCPII complexes with glutamate, inhibitor GPI-18431, and phosphate are superimposed, both Arg534 and Arg536 appear to adopt different conformations depending on the bound ligand [28], suggesting that the enzyme might compensate for the lost ionic interaction in the S1 pocket by a rearrangement of the side chains of these amino acids.

Observed changes in GCPII kinetic parameters might not result only from disruption of the predicted direct interactions between enzyme and substrate; indeed, the amino acid substitutions might elicit unpredicted long-range rearrangements, possibly leading to major changes in the tertiary structure of the enzyme. These more complex effects could be documented by the unpredicted decrease in turnover number caused by the D520N mutation or by the different effects of substituting Asn519 with either Asp or Val. Speno *et al.* [21] reported mutations in amino acid residues located far from the active site of the enzyme, which nonetheless caused dramatic effects on the proteolytic activity (K499E, K500E). Furthermore, it should be noted that amino acid substitutions in the vicinity of the Zn ions (Arg210, Tyr552, Asn519, Asp520, and Arg536) have a more profound effect on k_{cat} in general

Table 4. The sequence alignment of human GCPII with its homologs and mouse and rat orthologs. GCPII was aligned with its homologs GCPIII, NAALADase L, and with orthologs, mouse and rat GCPII. Amino acid residues in the active site, which are changed compared to human GCPII, are depicted in bold.

Residues	S1'					S1			
	R210	N257	Y552	K699	Y700	N519	D520	R534	R536
Human GCPII	R	N	Y	K	Y	N	D	R	R
Human GCPIII	R	N	Y	K	Y	S	D	R	R
Human NAALADase L	R	S	Y	V	V	S	D	D	A
Mouse GCPII	R	N	Y	K	Y	N	D	R	R
Rat GCPII	R	N	Y	K	Y	N	D	R	R

than do substitutions farther away (Lys699, Asn257), most likely due to distortion of the coordination sphere of the active-site zincs.

Our results indicate that the binding of the glutarate part of the inhibitor in the S1' pocket contributes to the inhibition effect of the specific inhibitor 2-PMPA [29]. This notion can be supported by the fact that the R210A mutant has the least ability to bind substrate and also exhibits the largest effect on inhibition by 2-PMPA. The decreased binding affinity of 2-PMPA is also observed for the N519D and N519V mutants. Although Asn519 does not directly interact with the glutarate moiety of the inhibitors, its side-chain amide forms a weak H-bond with one of the phosphonate oxygen atoms of 2-PMPA [39] contributing to the inhibitor binding.

Conclusions

In conclusion, we report a detailed analysis of the active site of glutamate carboxypeptidase II using site-directed mutagenesis as a tool. Amino acid residues important for substrate/inhibitor binding were determined from the crystal structures of GCPII with inhibitors and glutamate, and from a QM/MM model of the rhGCPII/NAAG complex. The results suggest that residues in the S1' site are critical for substrate/inhibitor binding. It appears that amino acids in the S1 site are relevant for substrate turnover and may play a role in the enzyme's mechanism of action. The data presented here show that the glutarate part of inhibitor is essential for the affinity to the GCPII, whereas the S1 pocket of the enzyme allows for higher substrate/inhibitor diversity.

Experimental procedures

Reagents

SF900II medium, fetal bovine serum, pCoHygro plasmid, Hygromycin-B, Defined Lipid Concentrate, and Yeastolate Ultrafiltrate were purchased from Invitrogen (San Diego, CA, USA). Horseradish peroxidase conjugated goat secondary serum against mouse antibody, and SuperSignal West Dura Chemiluminescence Substrate were obtained from Pierce (Rockford, IL, USA). AccQ Fluor reagent was obtained from Waters (Milford, MA, USA). Cupric sulfate (CuSO_4), EDTA, potassium phosphate, sodium chloride, sodium borate, L-glutamine, L-arginine, L-glutamate, NAAG, and D-glucose were purchased from Sigma (St Louis, MO, USA). Formic acid was obtained from Lachema (Brno, Czech Republic). 2-Amino-2-(hydroxymethyl)-1,3-propanediol was purchased from USB (Cleveland, OH,

USA). Lentil lectin Sepharose was obtained from Amersham Biosciences (Uppsala, Sweden) and ^3H -NAAG substrate was obtained from Perkin-Elmer (Boston, MA, USA).

Site-directed mutagenesis

Site-directed mutagenesis was carried out using the Quik-Change Site-Directed Mutagenesis Kit (Stratagene, La Jolla, CA, USA). The pMTNAEXST plasmid [19] was used as a template, and each mutation was introduced by two complementary oligonucleotide primers harboring the desired mutation. The presence of individual mutations was verified by dideoxynucleotide-terminated sequencing. Nucleotide sequences of the primers used for individual amino acid changes are shown in Table 1.

Stable transfection of *Drosophila* S2 cells and large scale expression of mutant forms of rhGCPII

Transfection, stable cell line generation and expression of all mutant forms of rhGCPII were performed essentially as previously described [19] only the induction conditions were altered (to 1 mM CuSO_4).

Purification of mutant forms of rhGCPII

Mutant forms of rhGCPII were purified as previously described for wt rhGCPII [19] with minor modification for individual mutants described in the Supplementary material.

Western blotting and protein quantification

Proteins were resolved by SDS/PAGE, electroblotted onto a nitrocellulose membrane, probed with an GCPII mouse antibody (GCP-04, $1 \text{ mg}\cdot\text{mL}^{-1}$; 1 : 5000) overnight at room temperature, and visualized and quantified using SuperSignal West Dura Chemiluminescence Substrate [25].

Radioenzymatic assay

Radioenzymatic assay using ^3H -NAAG substrate (radio-labeled on the terminal glutamate) was performed as described previously [19], with minor modifications, using 20 mM Mops, 20 mM NaCl, pH 7.4 as a reaction buffer and the kinetic constants determined as previously described [19].

Kinetic constant determination by HPLC assay

To determine Michaelis–Menten kinetics, the NAAG concentration was varied to cover the range 0.3–6 K_m . Typically, the substrate was mixed with 20 mM Mops, 20 mM NaCl, pH 7.4 and the reaction was started by the addition of

enzyme to a final volume of 120 μ L. After a 15–30 min incubation at 37 $^{\circ}$ C, the reaction was stopped with 60 μ L of stopping buffer (67 mM sodium borate, 33 mM EDTA, pH 9.2, containing 16 μ M L-arginine as an internal standard). Released glutamate was derivatized by the addition of 20 μ L of 2.5 mM AccQ Fluor reagent dissolved in acetonitrile. Thirty microlitres of the sample were then injected onto a Luna C18 column (250 \times 4.6 mm, 5 μ m, Phenomenex, Torrance, CA, USA) mounted to a Waters Alliance 2795 system equipped with a Waters 2475 fluorescence detector. Fluorescence was monitored at $\lambda_{EX}/\lambda_{EM} = 250/395$ nm.

Determination of inhibition constants

Measurements of inhibition constants for 2-PMPA were carried out with varying concentrations of the inhibitor while keeping the enzyme concentration fixed. The final enzyme concentrations used for individual mutants were: 12 nM for K699S, 10 nM for N257D, 150 nM for R210A, 38 nM for Y700F, 67 nM for N519D, 20 nM for N519V, 1 nM for R534L, and 32 nM for wt rhGCPII. Enzyme was preincubated with the inhibitor in reaction buffer (20 mM Mops, 20 mM NaCl, pH 7.4) for 10 min at 37 $^{\circ}$ C, and the reaction was started by the addition of NAAG to a final concentration of 60 μ M (for mutant N519D), 100 μ M (for mutants K699S, N257D, and Y700F), 600 μ M (for mutant R210A) or 100 nM (for mutants N519V, and R534L). *N*-acetyl-L-aspartyl-L-methionine (50 μ M) was used as a substrate for wt rhGCPII. Following a 20–40 min incubation at 37 $^{\circ}$ C, the reaction mixture was derivatized with AccQ Fluor reagent and product formation was quantified by HPLC with fluorimetric detection. K_i values for mutants N519V and R534L were obtained by using the radioenzymatic assay. The ratio of reaction rates of the inhibited reaction to the uninhibited reaction (v_i/v_0) was plotted against inhibitor concentration, and the apparent inhibition constant [$K_{I(app)}$] was determined from a nonlinear fit to Morrison's equation for tight-binding inhibitors [40] using GRAFIT software (Erihtacus Software Ltd, Horley, UK). For mutant proteins N257D and R210A, tight-binding inhibition was not observed under the conditions used; therefore, IC_{50} values were determined. Inhibition constant (K_i) values were calculated using the Cheng and Prusoff relationship, which assumes a competitive inhibition mechanism. However, the mode of inhibition was not determined for either of the mutant proteins because it was assumed that the inhibition mechanism would not be changed by the mutations introduced.

Molecular modelling

QM/MM calculations were based on the 2.0 Å structure of GCPII in complex with inhibitor (S)-2-(4-iodobenzylphosphonomethyl)-pentanedioic acid (GPI-18431, PDB code 2C6C).

Prior to QM/MM modeling, three missing loops (12 amino acids in total, Thr334-Phe337, Trp541-Phe546, Lys655-Ser656) were added using the GCPII structure at 3.5 Å resolution (protein databank code 1Z8L) as a template [26]. Then, a total of approximately 100 atoms not resolved in side chains (i.e. missing from the crystal structure) were added using standard libraries. Finally, hydrogen atoms were added to the crystal structure, and the model, including hydrogen atoms, was solvated in a truncated octahedral box. The positions of all the hydrogen atoms, all nonhydrogen atoms added as described above, and solvent water molecules were then optimized by a 180-ps simulated annealing (i.e. molecular dynamics simulation, using constant volume and periodic boundary conditions) followed by a conjugate gradient energy minimization of their positions. We assumed the normal protonation state at pH 7 for all amino acids. For the His residues, the protonation status was decided from a detailed study of the hydrogen-bond network around the residue and the solvent accessibility. Thus, His82, 347, 377, 553, and 573 were assumed to be protonated on the N ^{δ 1} atom; His112, 124, 295, 396, 475, 689, and 697 on the N ^{ϵ 2} atom; and His345 and 618 were considered to be protonated on both nitrogens.

The initial model for the QM/MM calculations of the rhGCPII/NAAG complex was obtained by replacement of the inhibitor with NAAG, such that the orientation and binding of the glutamate residue is identical to the crystal structure of the rhGCPII/glutamate complex, and the *N*-acetyl-L-aspartate part of the substrate is positioned in the cavity originally filled with the iodobenzyl part of inhibitor in the rhGCPII/GPI-18431 crystal structure. This structure has been subjected to QM/MM minimization. The quantum region consisted of side chains of Arg210, Asn257, His377, Asp387, Glu424, Glu425, Asp453, Asn519, Tyr552, His553, Lys699, Tyr700, two zinc(II) ions including the bridging H₂O/OH⁻ moiety and the molecule of NAAG. The details of QM and MM parts of QM/MM protocol are provided in the Supplementary material.

Acknowledgements

We thank Jana Starkova for excellent technical assistance and Hillary Hoffman for critical proofreading of the manuscript. This work has been supported by grants from the Ministry of Education of the Czech Republic (Research Center for New Antivirals and Antineoplastics-IM0508 and Research Center for Complex Molecular Systems and Biomolecules LC 512).

References

- 1 Israeli RS, Powell CT, Corr JG, Fair WR & Heston WD (1994) Expression of the prostate-specific membrane antigen. *Cancer Res* **54**, 1807–1811.

- 2 Kinoshita Y, Kuratsukuri K, Landas S, Imaida K, Rovito PM Jr, Wang CY & Haas GP (2006) Expression of prostate-specific membrane antigen in normal and malignant human tissues. *World J Surg* **30**, 628–636.
- 3 Troyer JK, Beckett ML & Wright GL Jr (1995) Detection and characterization of the prostate-specific membrane antigen (PSMA) in tissue extracts and body fluids. *Int J Cancer* **62**, 552–558.
- 4 Dumas F, Gala JL, Berteau P, Brasseur F, Eschwege P, Paradis V, Lacour B, Philippe M & Loric S (1999) Molecular expression of PSMA mRNA and protein in primary renal tumors. *Int J Cancer* **80**, 799–803.
- 5 Lopes AD, Davis WL, Rosenstraus MJ, Uveges AJ & Gilman SC (1990) Immunohistochemical and pharmacokinetic characterization of the site-specific immunconjugate CYT-356 derived from antiprostata monoclonal antibody 7E11-C5. *Cancer Res* **50**, 6423–6429.
- 6 Bostwick DG, Pacelli A, Blute M, Roche P & Murphy GP (1998) Prostate specific membrane antigen expression in prostatic intraepithelial neoplasia and adenocarcinoma: a study of 184 cases. *Cancer* **82**, 2256–2261.
- 7 Kinoshita Y, Kuratsukuri K, Newman N, Rovito PM, Kaumaya PT, Wang CY & Haas GP (2005) Targeting epitopes in prostate-specific membrane antigen for antibody therapy of prostate cancer. *Prostate Cancer Prostatic Dis* **8**, 359–363.
- 8 Ross JS, Sheehan CE, Fisher HA, Kaufman RP Jr, Kaur P, Gray K, Webb I, Gray GS, Mosher R & Kallakury BV (2003) Correlation of primary tumor prostate-specific membrane antigen expression with disease recurrence in prostate cancer. *Clin Cancer Res* **9**, 6357–6362.
- 9 Gong MC, Chang SS, Sadelain M, Bander NH & Heston WD (1999) Prostate-specific membrane antigen (PSMA)-specific monoclonal antibodies in the treatment of prostate and other cancers. *Cancer Metastasis Rev* **18**, 483–490.
- 10 Mincheff M, Altankova I, Zoubak S, Tchakarov S, Botev C, Petrov S, Krusteva E, Kurteva G, Kurtev P, Dimitrov V *et al.* (2001) In vivo transfection and/or cross-priming of dendritic cells following DNA and adenoviral immunizations for immunotherapy of cancer – changes in peripheral mononuclear subsets and intracellular IL-4 and IFN-gamma lymphokine profile. *Crit Rev Oncol Hematol* **39**, 125–132.
- 11 Todorova K, Ignatova I, Tchakarov S, Altankova I, Zoubak S, Kyurkchiev S & Mincheff M (2005) Humoral immune response in prostate cancer patients after immunization with gene-based vaccines that encode for a protein that is proteasomally degraded. *Cancer Immun* **5**, 1.
- 12 Robinson MB, Blakely RD, Couto R & Coyle JT (1987) Hydrolysis of the brain dipeptide N-acetyl-L-aspartyl-L-glutamate. Identification and characterization of a novel N-acetylated alpha-linked acidic dipeptidase activity from rat brain. *J Biol Chem* **262**, 14498–14506.
- 13 Chen SR, Wozniak KM, Slusher BS & Pan HL (2002) Effect of 2-(phosphono-methyl)-pentanedioic acid on allodynia and afferent ectopic discharges in a rat model of neuropathic pain. *J Pharmacol Exp Ther* **300**, 662–667.
- 14 Majer P, Jackson PF, Delahanty G, Grella BS, Ko YS, Li W, Liu Q, Maclin KM, Polakova J, Shaffer KA *et al.* (2003) Synthesis and biological evaluation of thiol-based inhibitors of glutamate carboxypeptidase II: discovery of an orally active GCP II inhibitor. *J Med Chem* **46**, 1989–1996.
- 15 Slusher BS, Vornov JJ, Thomas AG, Hurn PD, Harukuni I, Bhardwaj A, Traystman RJ, Robinson MB, Britton P, Lu XC *et al.* (1999) Selective inhibition of NAALADase, which converts NAAG to glutamate, reduces ischemic brain injury. *Nat Med* **5**, 1396–1402.
- 16 Zhou J, Neale JH, Pomper MG & Kozikowski AP (2005) NAAG peptidase inhibitors and their potential for diagnosis and therapy. *Nat Rev Drug Discov* **4**, 1015–1026.
- 17 Neale JH, Olszewski RT, Gehl LM, Wroblewska B & Bzdega T (2005) The neurotransmitter N-acetylaspartylglutamate in models of pain, ALS, diabetic neuropathy, CNS injury and schizophrenia. *Trends Pharmacol Sci* **26**, 477–484.
- 18 Pinto JT, Suffoletto BP, Berzin TM, Qiao CH, Lin S, Tong WP, May F, Mukherjee B & Heston WD (1996) Prostate-specific membrane antigen: a novel folate hydrolase in human prostatic carcinoma cells. *Clin Cancer Res* **2**, 1445–1451.
- 19 Barinka C, Rinnova M, Sacha P, Rojas C, Majer P, Slusher BS & Konvalinka J (2002) Substrate specificity, inhibition and enzymological analysis of recombinant human glutamate carboxypeptidase II. *J Neurochem* **80**, 477–487.
- 20 Barinka C, Sacha P, Sklenar J, Man P, Bezouska K, Slusher BS & Konvalinka J (2004) Identification of the N-glycosylation sites on glutamate carboxypeptidase II necessary for proteolytic activity. *Protein Sci* **13**, 1627–1635.
- 21 Speno HS, Luthi-Carter R, Macias WL, Valentine SL, Joshi AR & Coyle JT (1999) Site-directed mutagenesis of predicted active site residues in glutamate carboxypeptidase II. *Mol Pharmacol* **55**, 179–185.
- 22 Rawlings ND & Barrett AJ (1997) Structure of membrane glutamate carboxypeptidase. *Biochim Biophys Acta* **1339**, 247–252.
- 23 Rong SB, Zhang J, Neale JH, Wroblewski JT, Wang S & Kozikowski AP (2002) Molecular modeling of the interactions of glutamate carboxypeptidase II with its potent NAAG-based inhibitors. *J Med Chem* **45**, 4140–4152.
- 24 Mahadevan D & Saldanha JW (1999) The extracellular regions of PSMA and the transferrin receptor contain

- an aminopeptidase domain: implications for drug design. *Protein Sci* **8**, 2546–2549.
- 25 Barinka C, Mlčochová P, Sacha P, Hilgert I, Majer P, Slusher BS, Horejsi V & Konvalinka J (2004) Amino acids at the N- and C-termini of human glutamate carboxypeptidase II are required for enzymatic activity and proper folding. *Eur J Biochem* **271**, 2782–2790.
- 26 Davis MI, Bennett MJ, Thomas LM & Bjorkman PJ (2005) Crystal structure of prostate-specific membrane antigen, a tumor marker and peptidase. *Proc Natl Acad Sci USA* **102**, 5981–5986.
- 27 Barinka C, Starková J, Konvalinka J & Lubkowski J (2007) A high-resolution structure of ligand-free human glutamate carboxypeptidase II. *Acta Crystallograph Sect F Struct Biol Cryst Commun* **63**, 150–153.
- 28 Mesters JR, Barinka C, Li W, Tsukamoto T, Majer P, Slusher BS, Konvalinka J & Hilgenfeld R (2006) Structure of glutamate carboxypeptidase II, a drug target in neuronal damage and prostate cancer. *EMBO J* **25**, 1375–1384.
- 29 Jackson PF, Cole DC, Slusher BS, Stetz SL, Ross LE, Donzanti BA & Trainor DA (1996) Design, synthesis, and biological activity of a potent inhibitor of the neuropeptidase N-acetylated alpha-linked acidic dipeptidase. *J Med Chem* **39**, 619–622.
- 30 Jackson PF, Tays KL, Maclin KM, Ko YS, Li W, Vitharana D, Tsukamoto T, Stoermer D, Lu XC, Wozniak K *et al.* (2001) Design and pharmacological activity of phosphinic acid based NAALADase inhibitors. *J Med Chem* **44**, 4170–4175.
- 31 Stoermer D, Liu Q, Hall MR, Flanary JM, Thomas AG, Rojas C, Slusher BS & Tsukamoto T (2003) Synthesis and biological evaluation of hydroxamate-based inhibitors of glutamate carboxypeptidase II. *Bioorg Med Chem Lett* **13**, 2097–2100.
- 32 Majer P, Hin B, Stoermer D, Adams J, Xu W, Duvall BR, Delahanty G, Liu Q, Stathis MJ, Wozniak KM *et al.* (2006) Structural optimization of thiol-based inhibitors of glutamate carboxypeptidase II by modification of the P1' side chain. *J Med Chem* **49**, 2876–2885.
- 33 Rojas C, Frazier ST, Flanary J & Slusher BS (2002) Kinetics and inhibition of glutamate carboxypeptidase II using a microplate assay. *Anal Biochem* **310**, 50–54.
- 34 Kozikowski AP, Zhang J, Nan F, Petukhov PA, Grąjkowska E, Wroblewski JT, Yamamoto T, Bzdega T, Wroblewska B & Neale JH (2004) Synthesis of urea-based inhibitors as active site probes of glutamate carboxypeptidase II: efficacy as analgesic agents. *J Med Chem* **47**, 1729–1738.
- 35 Oliver AJ, Wiest O, Helquist P, Miller MJ & Tenniswood M (2003) Conformational and SAR analysis of NAALADase and PSMA inhibitors. *Bioorg Med Chem* **11**, 4455–4461.
- 36 Hlouchová K, Barinka C, Klusak V, Sacha P, Mlčochová P, Majer P, Rulisek L & Konvalinka J (2007) Biochemical characterization of human glutamate carboxypeptidase III. *J Neurochem* **101**, 682–696.
- 37 Pangalos MN, Neefs JM, Somers M, Verhasselt P, van der Bekkers MHL, Fraiponts E, Ashton D & Gordon RD (1999) Isolation and expression of novel human glutamate carboxypeptidases with N-acetylated alpha-linked acidic dipeptidase and dipeptidyl peptidase IV activity. *J Biol Chem* **274**, 8470–8483.
- 38 Tsukamoto T, Flanary JM, Rojas C, Slusher BS, Valiaeva N & Coward JK (2002) Phosphonate and phosphinate analogues of N-acylated gamma-glutamylglutamate. Potent inhibitors of glutamate carboxypeptidase II. *Bioorg Med Chem Lett* **12**, 2189–2192.
- 39 Barinka C, Rovenska M, Mlčochová P, Hlouchová K, Plechanovová A, Majer P, Tsukamoto T, Slusher BS, Konvalinka J & Lubkowski J (2007) Structural insight into the pharmacophore pocket of human glutamate carboxypeptidase II. *J Med Chem* **50**, 3267–3273.
- 40 Morrison JF (1969) Kinetics of reversible inhibition of enzyme-catalysed reactions by tight-binding inhibitors. *Biochim Biophys Acta* **185**, 269–286.

Supplementary material

The following supplementary material is available online:

Doc S1. QM/MM procedure and quantum chemical calculation, purification of GCPII mutants.

Model S1. QM/MM model of rhGCPII/NAAG (.pdb format).

This material is available as part of the online article from <http://www.blackwell-synergy.com>

Please note: Blackwell Publishing is not responsible for the content or functionality of any supplementary materials supplied by the authors. Any queries (other than missing material) should be directed to the corresponding author for the article.

Supplementary Material

Purification of Mutant Forms of rhGCPII

The purification protocol consisted of initial dialysis and three chromatographic steps: QAE-Sephadex A50 (Pharmacia, Fine Chemicals AB, Uppsala, Sweden) batch chromatography, chromatography on a Source 15S column (HR10/10, Amersham Pharmacia Biotech AB, Uppsala, Sweden), and affinity chromatography using Lentil Lectin Sepharose. Minor changes in the composition of buffers used during purification were made for some of the mutant proteins. MOPS buffer, instead of Tris buffer, was used throughout the purification of mutant proteins R210A, R210K, and Y700F. For mutants R210A and Y700F, a different pH (pH 7.0 and 6.5, respectively) was used during the first two chromatographic steps. Purification of mutants K699S and N257D was completed by gel permeation chromatography using a Superdex HR200 column (16/60; Pharmacia, NJ, USA) preequilibrated with 20mM MOPS, 300mM NaCl, pH 7.4 (for N257D) or with 20mM MOPS, pH 7.4 (for K699S). Proteins were separated at a flow rate of 1 ml/min and absorbance was monitored at 220 and 280 nm. For all mutants, the fractions containing the recombinant GCPII were concentrated, aliquoted, and stored at -80°C until further use.

QM/MM procedure

All QM/MM calculations were carried out with the COMQUM program [1, 2]. In the current version, it uses Turbomole 5.7 [3] for the QM part and AMBER 8 [4] with the Cornell force field [5] for the MM part. In this approach, the protein and solvent are split into three subsystems; the QM region (system 1) contains the most interesting atoms and is relaxed by QM/MM forces. System 2 consists of all the residues within 8\AA of any atom in system 1 and is relaxed by a full MM minimization at each step of the QM/MM geometry optimization. Finally, system 3 contains the remaining part of the protein and surrounding solvent

molecules and is kept fixed at the original (crystallographic) coordinates. In the quantum chemical calculations, the QM system is represented by a wave function, whereas all the other atoms are represented by an array of partial point charges, one for each atom, taken from Amber libraries. In this way, the polarization of the quantum chemical system by the surroundings is included in a self-consistent manner. In the MM calculations for the QM/MM forces and energies, all atoms are represented by the Amber force field. When there is a bond between systems 1 and 2 (a junction), the quantum region is truncated by hydrogen atoms, the positions of which are linearly related to the corresponding carbon atoms in the full system (the hydrogen link approach) [1, 6]. In order to avoid overpolarization of the quantum system, point charges on atoms in the MM region bound to junction atoms are zeroed, and the remaining charges on the truncated amino acid are adjusted to keep the fragment neutral. The actual charges used for all atoms can be found in the sample PDB file in the supplementary material (last column).

The total energy is calculated as:

$$E_{\text{tot}} = E_{\text{QM}} + E_{\text{MM123}} - E_{\text{MM1}}$$

Here, E_{QM} is the QM energy of the quantum system truncated by hydrogen atoms, excluding the self-energy of the surrounding point charges. E_{MM1} is the MM energy of the quantum system, still truncated by hydrogen atoms, but without any electrostatic interactions. Finally, E_{MM123} is the MM energy of all atoms in the system with the original atoms at the junctions and with the charges of the quantum system set to zero (to avoid double-counting of the electrostatic interactions). By using this approach, which is similar to the one used in the ONIOM method [7], errors caused by the truncation of the quantum system should cancel out. The calculated forces are the gradient of this energy, but owing to the differing junctions in the various calculations, they have to be corrected using the chain rule.

Quantum chemical calculations

All quantum chemical calculations were performed with density functional theory (DFT). Geometry optimizations were carried out at the Becke–Perdew86 (BP86) level [8, 9]. These calculations were sped up by expanding the Coulomb interactions in an auxiliary basis set, the resolution-of-identity (RI) approximation [10, 11]. They employed the 6–31G* basis set on all atoms except Zn, for which we used the DZP basis set of Schäfer *et al.* [12, 13].

References

1. Ryde U (1996) The coordination of the catalytic zinc ion in alcohol dehydrogenase studied by combined quantum-chemical and molecular mechanics calculations. *Journal of Computer-Aided Molecular Design* **10**, 153-164.
2. Ryde U & Olsson MHM (2001) Structure, strain, and reorganization energy of blue copper models in the protein. *International Journal of Quantum Chemistry* **81**, 335-347.
3. Treutler O & Ahlrichs R (1995) Efficient Molecular Numerical-Integration Schemes. *Journal of Chemical Physics* **102**, 346-354.
4. Case DA, Pearlman DA, Caldwell JW, Cheatham TE, III., Wang J, Ross WS, Simmerling CL, Darden TA, Merz KM, Stanton RV, Cheng AL, Vincent JJ, Crowley M, Tsui V, Gohlke H, Radmer RJ, Duan Y, Peters J, Massova I, Seibel GL, Singh UC, Weiner PK & Kollman PA (2002) *AMBER 7*. University of California, San Francisco, CA.
5. Cornell WD, Cieplak P, Bayly CI, Gould IR, Merz KM, Ferguson DM, Spellmeyer DC, Fox T, Caldwell JW & Kollman PA (1995) A 2Nd Generation Force-Field for the Simulation of Proteins, Nucleic-Acids, and Organic-Molecules. *Journal of the American Chemical Society* **117**, 5179-5197.
6. Reuter N, Dejaegere A, Maigret B & Karplus M (2000) Frontier bonds in QM/MM methods: A comparison of different approaches. *Journal of Physical Chemistry A* **104**, 1720-1735.
7. Svensson M, Humbel S, Froese RDJ, Matsubara T, Sieber S & Morokuma K (1996) ONIOM: A multilayered integrated MO+MM method for geometry optimizations and single point energy predictions. A test for Diels-Alder reactions and Pt(P(t-Bu)(3))(2)+H-2 oxidative addition. *Journal of Physical Chemistry* **100**, 19357-19363.
8. Becke AD (1988) Density-Functional Exchange-Energy Approximation with Correct Asymptotic-Behavior. *Physical Review A* **38**, 3098-3100.
9. Perdew JP (1986) Density-Functional Approximation for the Correlation-Energy of the Inhomogeneous Electron-Gas. *Physical Review B* **33**, 8822-8824.
10. Eichkorn K, Treutler O, Ohm H, Haser M & Ahlrichs R (1995) Auxiliary Basis-Sets to Approximate Coulomb Potentials. *Chemical Physics Letters* **240**, 283-289.
11. Eichkorn K, Weigend F, Treutler O & Ahlrichs R (1997) Auxiliary basis sets for main row atoms and transition metals and their use to approximate Coulomb potentials. *Theoretical Chemistry Accounts* **97**, 119-124.
12. Hehre WJ, Radom L, Schleyer PvR & Pople JA (1986) *Ab Initio Molecular Orbital Theory*. Wiley-Interscience, NY.
13. Schafer A, Huber C & Ahlrichs R (1994) Fully Optimized Contracted Gaussian-Basis Sets of Triple Zeta Valence Quality for Atoms Li to Kr. *Journal of Chemical Physics* **100**, 5829-5835.

6.2 Extracellular domain of GCPII: identification of putative proteolytic domain

6.2.1 Background information

In 2004, there was still no 3D-structure of GCPII, when Rawlings and Barrett proposed their structural model of GCPII. Their schematic model was composed of several domains: **intracellular domain** (amino acids 1-19); **transmembrane domain** (20-43) and **extracellular domain** further divided into *domains C* (amino acids 44-149) and *D* (150-273) with unknown function; huge *domain E* (274-586) possessing catalytic center of GCPII (relative to other metallopeptidases); and *domain F* (587-750) with an unknown function (Fig. 16). Amino acid sequences (145-175 and 249-273) rich in proline and glycine were found in the polypeptide chain and were believed to be linkers between two domains [12].

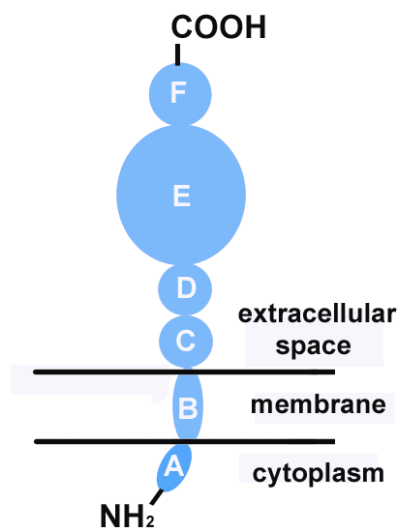


Fig. 16: Schematic diagram of GCPII structure. Proposed by Rawlings and Barrett [12].

In 2002, Barinka *et al.* proved that the recombinant extracellular domain is active and determined kinetic parameters of this „truncated“ recombinant protein [17]. However, little if anything was known about the role of individual domains, their role in activity and proper folding.

6.2.2 Summary

Insect cells were transfected with a plasmids coding for full length, truncated, and tagged GCPII constructs and corresponding proteins were expressed into the culture medium (except for full length form of GCPII which is membrane bound).

We monitored the expression using immunodetection on western blot, but this particular step required design of a new monoclonal antibody, which would allow us to study also the smallest protein construct – catalytic domain (amino acids 274-586). This catalytic domain expressed in *Escherichia coli* was used to select clones immunoreactive against an epitope within this sequence. Importantly, all of the variants used in this study comprise the putative catalytic domain.

Moreover, we measured hydrolytic activity of all constructs (by their ability to cleave N-acetyl-aspartyl-glutamate).

Any change at C-terminus (truncation or tag) caused significant decrease in activity and removal of more than 15 amino acids from its end completely abolished the activity. Also the secretion to the media was negatively influenced which suggests incorrect protein folding in the cells.

The N-terminus of GCPII is also required for enzymatic activity and correct folding. Deletion of more than 60 amino acids resulted in inactive protein.

All data show that almost the whole extracellular part of GCPII is required for the proteolytic activity and thus the proposed homology model of GCPII with independent domains may be incorrect and should be interpreted with circumspection (see postscript).

My contribution to this study was the expression of protein constructs in insect cells, immunodetection, and activity measurement.

6.2.3 Publication II

Eur. J. Biochem. **271**, 2782–2790 (2004) © FEBS 2004

doi:10.1111/j.1432-1033.2004.04209.x

Amino acids at the N- and C-termini of human glutamate carboxypeptidase II are required for enzymatic activity and proper folding

Cyril Bařinka¹, Petra Mlřochov^{1,2}, Pavel řcha^{1,2}, Ivan Hilgert³, Pavel Majer⁴, Barbara S. Slusher⁴, Vclav Hořejř³ and Jan Konvalinka^{1,2}

¹Institute of Organic Chemistry and Biochemistry, Academy of Sciences of the Czech Republic, Prague, the Czech Republic; ²Department of Biochemistry, Faculty of Natural Science, Charles University, Prague, the Czech Republic; ³Institute of Molecular Genetics, Academy of Sciences of the Czech Republic, Prague, the Czech Republic; ⁴Guilford Pharmaceuticals Inc., Baltimore, MD, USA

Human glutamate carboxypeptidase II (GCPII) is a co-catalytic metallopeptidase and its putative catalytic domain is homologous to the aminopeptidases from *Vibrio proteolyticus* and *Streptomyces griseus*. In humans, the enzyme is expressed predominantly in the nervous system and the prostate. The prostate form, termed prostate-specific membrane antigen, is overexpressed in prostate cancer and is used as a diagnostic marker of the disease. Inhibition of the form of GCPII expressed in the central nervous system has been shown to protect against ischemic injury in experimental animal models. Human GCPII consists of 750 amino acids, and six individual domains were predicted to constitute the protein structure. Here, we report the analysis of the contribution of these putative domains to the structure/function of recombinant human GCPII. We cloned 13 mutants of human GCPII that are truncated or extended at one or both the N- and C-termini of the GCPII sequence.

The clones were used to generate stably transfected *Drosophila* Schneider's cells, and the expression and carboxypeptidase activities of the individual protein products were determined. The extreme C-terminal region of human GCPII was found to be critical for the hydrolytic activity of the enzyme. The deletion of as few as 15 amino acids from the C-terminus was shown to completely abolish the enzymatic activity of GCPII. Furthermore, the GCPII carboxypeptidase activity was abrogated upon removal of more than 60 amino acid residues from the N-terminus of the protein. Overall, these results clearly show that amino acid segments at the N- and C-termini of the ectodomain of GCPII are essential for its carboxypeptidase activity and/or proper folding.

Keywords: NAALADase; PSMA; metallopeptidase; prostate cancer; mutagenesis.

Human glutamate carboxypeptidase II (GCPII; EC 3.4.17.21) is a 750 amino acid type II transmembrane glycoprotein. Its expression is restricted mainly to the nervous system, prostate, small intestine, and kidney [1–3]. The GCPII form expressed in the brain, termed *N*-acetylated- α -linked acidic dipeptidase, plays an import-

ant role in neurotransmission, as it cleaves *N*-acetyl-L-aspartyl-L-glutamate (NAAG), the most abundant peptidic transmitter within the human central nervous system [4], and terminates its activity [5]. Inhibition of the brain form of GCPII has been shown to be neuroprotective in animal models of stroke, neuropathic pain, or amyotrophic lateral sclerosis [6–8]. The physiological role of GCPII in the prostate is unknown [9]. Expression of this protein is upregulated in prostate cancer (where it is termed prostate specific membrane antigen, PSMA) and is exploited both as a diagnostic modality of, and a therapeutic target for, carcinomas of prostatic origin [10–12]. The enzyme represents a promising target of therapeutic intervention under various pathological conditions.

GCPII belongs to the M28 peptidase family, which encompasses co-catalytic metallopeptidases requiring two zinc ions for catalytic activity, such as aminopeptidases from *Streptomyces griseus* and *Vibrio proteolyticus* [13]. Additionally, the homology of human GCPII with the transferrin receptor has been reported, with sequence identities of 30.3%, 30.2% and 24.0% for the protease-like, apical, and helical domains of the transferrin receptor, respectively [14]. Rawlings & Barrett made

Correspondence to J. Konvalinka, Institute of Organic Chemistry and Biochemistry, Academy of Sciences of the Czech Republic, Flemingovo n. 2, 166 10 Praha 6, the Czech Republic.

Fax: + 420 2 20183 257, Tel.: + 420 2 20183 218,

E-mail: konval@uochb.cas.cz

Abbreviations: ERAD, endoplasmic reticulum-associated degradation; GCPII, human glutamate carboxypeptidase II; NAAG, *N*-acetyl-L-aspartyl-L-glutamate; rhGCPII, recombinant human glutamate carboxypeptidase II; Z-Leu-Leu-Leucinal (Z-LLnL, MG132), *N*-benzyloxycarbonyl-L-leucyl-L-leucyl-L-leucinal; Z-Leu-Leu-Norvalinal (Z-LLnV, MG115), *N*-benzyloxycarbonyl-L-leucyl-L-leucyl-L-norvalinal.

Enzyme: human glutamate carboxypeptidase II (EC 3.4.17.21).

(Received 26 March 2004, revised 3 May 2004,

accepted 7 May 2004)

predictions about the domain structure and the putative catalytic site of GCPII [16]. Similarly to the transferrin receptor, GCPII probably exists as a homodimer under physiological conditions and the dimerization seems to be essential for its hydrolytic activity [15]. The protein is proposed to consist of six domains: the N-terminal cytoplasmic tail (amino acids 1–18), the helical transmembrane region (amino acids 19–43), and four extracellular domains spanning amino acids 44–150 (domain C), 151–274 (domain D), 275–586 (domain E), and 587–750 (domain F). While the domain spanning amino acids 275–586 is believed to be the catalytic domain, the importance/function of the three remaining extracellular domains is unknown [16]. The putative catalytic domain of GCPII is homologous to aminopeptidases from *S. griseus* and *V. proteolyticus* whose crystal structures have been solved at 1.75 Å and 1.8 Å resolution, respectively [17,18]. By analogy with the *Vibrio* aminopeptidase and the alignment of partial amino acid sequences from human GCPII, human transferrin receptor, yeast aminopeptidase Y, *S. griseus* aminopeptidase, and *Caenorhabditis elegans* mGCP fragment, His377, Asp387, Glu425, Asp453 and His553 were proposed to be the zinc ligands of GCPII [16]. To experimentally verify these amino acid assignments, Speno *et al.* [19] mutated the putative zinc ligands, putative substrate-binding residues and other amino acids situated in the vicinity of these residues. The results confirmed the importance of the amino acid residues, all located at the putative catalytic domain, for the GCPII hydrolytic activity and substrate binding.

Recently, a 3D model of the extracellular region of rat GCPII has been published [20]. In addition to the model of the ligand-free protein, the authors docked several GCPII inhibitors into the GCPII-binding pocket and proposed/analyzed the amino acid residues involved in the ligand–protein interactions. All of the residues identified are situated within the segment spanning Arg212 to Arg538, i.e. the putative catalytic domain (domain E) and the D domain of rat GCPII. The contribution of domains C and F to the GCPII hydrolytic activity/inhibitor binding remains to be established.

The 3D structure of GCPII has not yet been solved and virtually nothing is known about the significance of the individual putative GCPII domains for the carboxypeptidase activity and/or proper folding of the protein. In this work we report cloning and expression of GCPII mutants truncated or extended at both N- and C-termini. We analyzed the expression of individual mutants in *Drosophila* Schneider's S2 cells and their corresponding hydrolytic activities, and identified the minimal catalytically competent fragment. We show that the C-terminal end is necessary for GCPII enzymatic activity and that any polypeptide truncated beyond Lys59 (from the N-terminus) is inactive and probably misfolded.

Materials and methods

Expression plasmids

All of the GCPII variants used in this study are schematically depicted in Fig. 1.

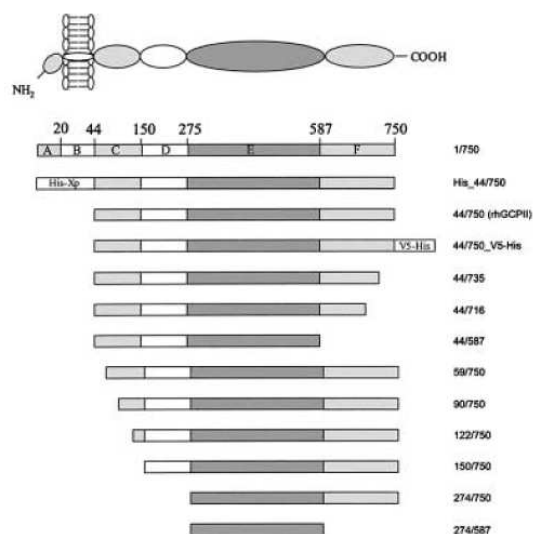


Fig. 1. Schematic diagram of the human glutamate carboxypeptidase II (GCPII) domain structure and GCPII variants used in this study. The figure shows wild-type human GCPII and its truncated or tagged variants. Individual domains are as described previously [16]: A, intracellular segment; B, transmembrane domain; E, putative catalytic domain; polypeptides spanning amino acids 44–150 (domain C), 151–274 (domain D), and 587–750 (domain F) represent domains of unknown function; His, histidine tag; V5, V5 epitope; Xp, Xpress epitope. Numbers before or after a slash correspond to the first or the last amino acid of the truncated variant, respectively, as compared to the full-length wild-type protein.

Truncated constructs. The pMTNAEXST plasmid, described previously [21], was used as the template for generating truncated GCPII constructs. Corresponding primer pairs (20 pmol each), together with 3 U of *Pfu* polymerase (Promega) and 1 ng of the template plasmid, were employed in amplification reactions according to the manufacturer's protocol. The primer sequences, together with thermal cycling parameters, are described in Table 1. Generally, 30 PCR cycles were used for the sequence amplification.

The individual PCR fragments were purified by gel electrophoresis, digested with *Bgl*III/*Xho*I and cloned into pMT/BiP/V5-His A (Invitrogen), in-frame with the BiP leader peptide.

Full-length construct. Sequences of primers and cycling conditions used for generation of the full-length construct (transmembrane, spanning amino acids 1–750) are described in Table 1. The pcDNA3.1/GCPII plasmid [21] was used as a template. The PCR product was digested with *Kpn*I/*Xho*I endonucleases and cloned into a pMT/V5-His A plasmid (Invitrogen).

C-terminally tagged construct. The C-terminally tagged construct was generated similarly to the 44/750 variant. The only exception was usage of the reverse primer (complementary to the C-terminal part of GCPII) that was devoid

Table 1. Primer sequences and thermal cycling parameters.

Variant	Primer pairs (5' → 3')	Cycling conditions		
1-750	AAAGGTACCAAAGATGTGGAATCTCCTTCACG ATTCTCGAGTCATTAGGCTACTTCACTCAAAG	30 s/94 °C;	1 min/57 °C;	5 min/72 °C
44/750	AAACTCGAGAGATCTAAATCCTCCAATGAAGC ATTCTCGAGTCATTAGGCTACTTCACTCAAAG	1 min/94 °C;	1 min/54 °C;	4 min/72 °C
44/735	AAACTCGAGAGATCTAAATCCTCCAATGAAGC ATTCTCGAGTCATTATGCAACATAAAATCTGTCTCTT	30 s/94 °C;	1 min/54 °C;	4 min/72 °C
44/716	AAACTCGAGAGATCTAAATCCTCCAATGAAGC AAACTCGAGTTATTATTCAATATCAAACAGAG	30 s/94 °C;	1 min/56 °C;	4 min/72 °C
59/750	AAAAGATCTAAAGCATTCTTTGGATGAATTG ATTCTCGAGTCATTAGGCTACTTCACTCAAAG	1 min/94 °C;	1 min/54 °C;	4 min/72 °C
90/750	AAAAGATCTTTTCAGCTTGCAAAGCAA ATTCTCGAGTCATTAGGCTACTTCACTCAAAG	1 min/94 °C;	1 min/57 °C;	4 min/72 °C
122/750	AAAAGATCTAAGACTCATCCAACTAC ATTCTCGAGTCATTAGGCTACTTCACTCAAAG	1 min/94 °C;	1 min/54 °C;	4 min/72 °C
150/750	AAAAGATCTGGATATGAAAAATGTTTCGG ATTCTCGAGTCATTAGGCTACTTCACTCAAAG	30 s/94 °C;	1 min/56 °C;	4 min/72 °C
274/750	ACACTCGAGAGATCTGCAAATGAATATG ATTCTCGAGTCATTAGGCTACTTCACTCAAAG	30 s/94 °C;	1 min/57 °C;	4 min/72 °C
274/587	AAACTCGAGAGATCTAAATCCTCCAATGAAGC CACCTCGAGTTATTATAGCTCAAACACCATCC	30 s/94 °C;	1 min/56 °C;	3 min/72 °C
44/587	AAACTCGAGAGATCTAAATCCTCCAATGAAGC CACCTCGAGTTATTATAGCTCAAACACCATCC	30 s/94 °C;	1 min/56 °C;	3 min/72 °C
44/750_V5-His	AAACTCGAGAGATCTAAATCCTCCAATGAAGC AAACTCGAGGGCTACTTCACTCAAAG	1 min/94 °C;	1 min/57 °C;	4 min/72 °C

of a stop codon, and consequently, the PCR product could be cloned into the pMT/BiP/V5-His A in-frame with the C-terminal V5-His epitope.

N-terminally tagged construct. The DNA sequence encoding the GCPII variant (amino acids 44-750) in the pMTNAEXST plasmid was excised by digestion with *Bgl*II and *Xho*I restriction enzymes and ligated into *Bam*HI/*Xho*I sites in a pcDNA4/HisA vector (Invitrogen). The resulting plasmid was digested with *Nco*I/*Xho*I endonucleases and the GCPII-coding sequence, N-terminally flanked with His-tag and Xpress epitope, was cloned into the *Nco*I/*Xho*I-digested pMTBiP/V5-His A vector in-frame with the BiP leader peptide. The resulting plasmid was designated pMTHis-NA44/750.

The identities of all sequences were verified by dideoxynucleotide-terminal sequencing using an ABI Prism BigDye Terminator Cycle Sequencing Ready Reaction Kit v2.0 (Perkin-Elmer) and an ABI Prism 310 Genetic Analyzer (PE Corporation).

Transfection of insect cells and generation of stable cell lines

Schneider's S2 cells (Invitrogen) were maintained in SF900II medium (Gibco) supplemented with 10% (v/v) fetal bovine serum (complete medium; Gibco) at 22-24 °C. Stable cell lines expressing individual mutants were generated by cotransfection with 19 µg of the expression plasmid and 1 µg of a pCoHYGRO selection vector (Invitrogen), using a kit for calcium phosphate-mediated transfection (Invitrogen). Stable transfectants were selected by culture of the cells

in complete medium [SF900II + 10% (v/v) fetal bovine serum] supplemented with 400 µg·mL⁻¹ Hygromycin B (Invitrogen).

Expression of GCPII variants

Stably transfected S2 cells were transferred into six-well plates and grown in serum-free SF900II medium to a density of 8 × 10⁶ cells·mL⁻¹. At this point, protein expression was induced with 0.5 mM CuSO₄ (final concentration) (Sigma). Three days later, conditioned media and cells were harvested by centrifugation and stored at -70 °C until further use.

Cell lysates

The cell pellets were resuspended in 50 mM Tris/HCl, pH 7.4, containing 100 mM NaCl and a protease inhibitor cocktail (MiniEDTAFree; Roche), to a concentration of 40 × 10⁶ cells per mL, sonicated three times (20 s each, 10 µm amplitude) on ice (Soniprep 150; Sanyo), and subjected to centrifugation at 15 000 g for 10 min. The supernatant fraction is referred to as the cell lysate.

Total RNA isolation

Total RNA from stably transfected S2 cells (with protein expression induced by addition of 0.5 mM CuSO₄) was isolated using Trizol Reagent (Gibco), according to the manufacturer's protocol, with 5 × 10⁶ cells as the starting material. Isolated total RNA was dissolved in RNase-free water to a concentration of 1 µg·µL⁻¹.

RT-PCR

To eliminate contaminating chromosomal DNA, 1 µg of total RNA was incubated with DNase I (1 U; Gibco) for 30 min at room temperature in a total volume of 10 µL. One microlitre of EDTA (25 mM, pH 8.0) was then added and DNase I inactivated at 65 °C for 10 min. The RNA was further amplified using a pair of sequence-specific primers (forward primer, 5'-ATTCAAGACTCCTTCAA GAGCGTGGCGTGGC-3'; reverse primer, 5'-GCTCA AACACCATCCCTCCTCGAACCTGGG-3') with cycling conditions comprising 30 min at 55 °C followed by 25 cycles of 30 s at 94 °C, 30 s at 55 °C, and 60 s at 72 °C. The reaction products were analyzed on a 1% (w/v) agarose gel, and a positive signal identified as a 549 bp band.

Proteasome inhibition

Stably transfected S2 cells were cultured in SF900II medium supplemented with 10% (v/v) fetal bovine serum, and protein expression was induced with 0.5 mM CuSO₄ at a density of 8×10^6 cells mL⁻¹. Twelve hours postinduction, lactacystine (10 µM final concentration), *N*-benzyloxycarbonyl-L-leucyl-L-leucyl-L-norvalinal (*Z*-Leu-Leu-Norvalinal, Z-LLnV, MG115; 50 µM final concentration), or *N*-benzyloxycarbonyl-L-leucyl-L-leucyl-L-leucinal (*Z*-Leu-Leu-Leucinal, Z-LLnL, MG132; 50 µM final concentration) was added to the medium and incubation continued for additional 0, 4, 8 or 12 h. The cells were counted, harvested by centrifugation at 500 *g* for 5 min, and frozen at -70 °C until further use.

Antibodies

Hybridomas secreting mAbs (clones GCP-01, GCP-02 and GCP-04, all IgG1) were prepared by standard methods from mice (F1 hybrids of BALB/c and B10.A strains) immunized with recombinant human GCPII (rhGCPII, a major fragment corresponding to the extracellular domain, i.e. amino acid residues 44–750), prepared as described previously [21].

SDS/PAGE and Western blotting

Proteins were resolved by SDS/PAGE [0.1% SDS, 13% polyacrylamide (w/w/v)] and electroblotted onto a nitrocellulose membrane. The membrane was probed with the GCP-02 anti-rhGCPII mouse monoclonal antibody (1 mg·mL⁻¹) at a 1 : 5000 dilution, followed by incubation with a 1 : 20 000 dilution of horseradish peroxidase-conjugated goat anti-mouse immunoglobulin (Pierce) for 2 h, then developed using a West DuraTM chemiluminescence substrate (Pierce).

NAAG-hydrolyzing activities

Radioenzymatic assays using ³H-labelled NAAG (radio-labeled at the terminal glutamate) were performed as described previously [5], with minor modifications. Briefly, 50 mM Tris/HCl, pH 7.4 (at 37 °C), containing 20 mM NaCl and 20 µL of the GCPII sample, were preincubated for 15 min at 37 °C in a final volume of 225 µL. A 25 µL

mixture of 950 nM 'cold' NAAG (Sigma) and 50 nM ³H-labelled NAAG (51.9 Ci·mmol⁻¹; New England Nuclear) was added to each tube and incubation continued for 20 min. The reaction was stopped with 250 µL of ice-cold 200 mM sodium phosphate, pH 7.4, after which the released glutamate was separated from the substrate by ion exchange chromatography and quantified by liquid scintillation.

Determination of kinetic parameters

Michaelis–Menten (saturation) kinetics were measured in a reaction setup similar to that used for the activity measurements (see above) with substrate concentrations ranging from 0.025 to 50 µM NAAG. Initial velocity measurements for each concentration point were carried out in triplicate. Typical turnover of the substrate did not exceed 25%. *K_m* and *k_{cat}* values were determined by a nonlinear least-squares fit of the initial velocity vs. substrate concentration using a GRAFIT software package (Erithacus Software Limited).

Large scale expression and purification

The 44/750 variant was expressed in large quantities in spinner flasks and purified by a combination of ion-exchange chromatography, Lentil-Lectin Sepharose chromatography and chromatofocusing, as described previously [21].

Results

Expression and secretion of truncated variants of GCPII

To analyze the contribution of individual domains of human GCPII (as proposed by Rawlings & Barrett [16]) to its carboxypeptidase activity and/or folding, 13 variants encoding the polypeptide chains truncated or extended at one or both N- or C-termini were constructed (Fig. 1) and the resulting plasmids were used for transfection of *Drosophila* Schneider's S2 cells. The expression and carboxypeptidase activities of the individual constructs were analyzed both in cell lysates and conditioned media, and the results are summarized in Fig. 2 and Table 2, respectively.

Of the 13 variants, only 274/587 (the putative catalytic domain) and 274/750 (the polypeptide spanning the putative catalytic domain and the C-terminal-most domain) were not detected in Western blots of the cell lysates, even though the mAb used in the experiment targets an epitope within these sequences (data not shown). The remainder of the constructs were expressed and immunoreactive bands of expected relative molecular weights observed. Analysis of conditioned media revealed that the majority of the constructs detectable in the cell lysates were secreted into the medium. The only exception was the 150/750 variant, which was retained intracellularly. Additionally, and not surprisingly, neither of the variants absent from the cell lysates (274/587 and 274/750) were detected in the conditioned media.

To quantify the amount of the individual GCPII variants, the signal intensities of the blots were recorded with a CCD camera and analyzed using the AIDA image-analyzing software, version 3.28.001 (Raytest Isotopenmessgerate, Straubenhardt, Germany). Subsequently, calculations of the

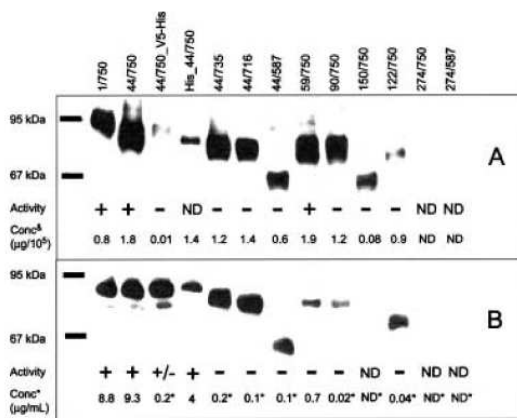


Fig. 2. Western blot analysis of the expression of human glutamate carboxypeptidase II (GCPII) variants in S2 cells. Stably transfected S2 cells were grown in serum-free SF900II medium. Protein expression was induced with 500 μM CuSO₄ and conditioned media and cells were harvested 3 days later. Some of the conditioned media, marked with an asterisk (*), were concentrated ×20 using a Microcon ultracentrifugation device (Millipore) prior to Western blot analysis. The proteins were resolved by SDS/PAGE (13% gel), electroblotted onto a nitrocellulose membrane, and immunostained as described in the Materials and methods. Relative band intensities were recorded using a CCD camera, and the concentrations of individual variants was calculated from a calibration curve of known 44/750 concentrations. Carboxypeptidase activities of individual GCPII variants were determined using 100 nM *N*-acetyl-L-aspartyl-L-glutamate (NAAG) as a substrate. (A) Expression of GCPII variants in S2 cells. The cell lysates were mixed with an equal volume of the denaturing SDS buffer and loaded onto a single lane. Activity levels are indicated as follows: (+), measurable NAAG-hydrolyzing activity; (+/-), extremely low activity; (-), no activity; ND, not determined. Conc^A, expression levels of the individual variants in stably transfected induced cells (μg per 10⁵ cells). *To visualize and quantify the individual variants in one blot, different numbers of cells were loaded for each mutant. (B) Expression of GCPII variants in conditioned media. Conditioned media were mixed with an equal volume of the denaturing SDS buffer and 10 μL of the mixture was loaded onto a single lane. Activity levels are indicated as follows: (+), measurable NAAG-hydrolyzing activity; (+/-), extremely low activity; (-), no activity; ND, not determined. Conc^B, amount of the individual variant in the conditioned medium prior to concentration (μg·mL⁻¹).

protein quantities from the standard calibration curve of known GCPII (the purified 44/750 variant) concentrations were performed.

Marked differences in the expression levels of the individual variants were observed in both cell lysates and conditioned media. The highest expression levels in the conditioned media were ≈10 μg·mL⁻¹ for the 44/750 and 1/750 variants. A decrease of more than 80-fold in the secretion of recombinant protein was associated with the deletion of the C-terminal part(s) of the protein, even though the intracellular expression levels remained fairly constant. Likewise, deletions within the N-terminal part of the polypeptide resulted in a noticeable decrease in secretion efficiency, as the amounts of the 59/750, 90/750, and

Table 2. Specific activities of the human glutamate carboxypeptidase II (GCPII) variants and wild-type recombinant human glutamate carboxypeptidase II (rhGCPII). Stably transfected S2 cells were grown in serum-free SF900II medium and protein expression was induced with 500 μM CuSO₄. Three days later, the cells and conditioned media were harvested and processed as described in the Materials and methods. Conditioned media were dialyzed and concentrated, if desired. Carboxypeptidase activities of the individual variants were determined using 100 nM *N*-acetyl-L-aspartyl-L-glutamate (NAAG) as a substrate and related to the amounts of the immunoreactive proteins, as determined by Western blot densitometry, using purified rhGCPII as a standard. ND, not detected.

Construct	Cell lysates (nmol·s ⁻¹ ·mg ⁻¹)	Conditioned medium (nmol·s ⁻¹ ·mg ⁻¹)
1/750	1.5	5.4
His_44/750	ND	4.1
44/750	6.7	27.7
44/750_V5-His	<0.001	0.002
44/735	<0.001	<0.001
44/716	<0.001	<0.001
44/587	<0.001	<0.001
59/750	0.003	4.0
90/750	<0.001	<0.001
122/750	<0.001	<0.001
150/750	<0.001	ND
274/750	ND	ND
274/587	ND	ND

122/750 variants in the medium were ≈14-, 600-, and 250-times lower as compared to the 44/750 variant. Moreover, the 150/750 variant was not secreted at all (Fig. 2).

Analysis of the DNA transcription of mutants 274/587 and 274/750

Regarding the 274/587 and 274/750 variants, no protein products of the expected relative molecular masses were observed in Western blots of either cell lysates or the conditioned media. To analyze whether the cells were really transfected with the plasmids encoding the corresponding GCPII variants and that the DNA was transcribed, we isolated genomic DNA and total RNA from the induced cells and performed PCR or RT-PCR assays, respectively. The experiments using GCPII-specific primers confirmed plasmid integration into the genome of Schneider S2 cells and functional transcription of GCPII-coding sequences (data not shown).

Inhibition of proteasome degradation

As the mRNAs encoding the 274/587 and 274/750 variants, but no corresponding protein products, were detected in the induced, stably transfected S2 cells, we attempted to distinguish between two possible alternatives: either the protein was not translated at all, or it was aberrantly folded and consequently degraded by the endoplasmic reticulum-associated degradation system (ERAD), a ubiquitin-proteasome dependent pathway [22]. To investigate this further, we used three different proteasome inhibitors to block the degradation activity of the cells. The proteasome

was inhibited 12 h postinduction by addition of the commercially available inhibitors lactacystine, Z-Leu-Leu-Norvalinal or Z-Leu-Leu-Leucinal to the S2 cells stably transfected with 274/587 and 274/750. The presence of recombinant proteins in cell lysates was analyzed at 0, 4, 8 and 12 h following the addition of inhibitors. No immunoreactive bands of expected molecular mass were observed in the cell lysates at any of the time-points (data not shown).

Analysis of carboxypeptidase activities of the individual truncated mutants of GCPII

The carboxypeptidase activities against NAAG, a naturally occurring substrate of GCPII, were analyzed both in conditioned media and the cell lysates. The results are summarized in Fig. 2 and Table 2. Out of the 11 variants with detectable levels of expression, only five GCPII constructs were found to be enzymatically active. These were the 1/750 (the transmembrane full-length protein), the 44/750 (the whole ectodomain of GCPII, rhGCPII), the 59/750 and the His₄₄/750 variants. An extremely low level of NAAG-hydrolyzing activity, < 0.01% of the 44/750 variant, was associated with the 44/750_V5-His variant, and no proteolytic activity could be detected with variants N-terminally truncated beyond Lys59 or truncated at the C-terminus. These results clearly show that polypeptide stretches situated both N- and C-terminally of the putative catalytic domain are indispensable for GCPII carboxypeptidase activity.

To further characterize the hydrolytical activities of the GCPII variants, we determined the kinetic parameters (K_m and k_{cat}) of the mutants towards NAAG. The data are summarized in Table 3. The kinetic constants for the 44/750_V5-His protein construct could not be determined owing to a very low specific activity of the truncated enzyme. The Michaelis constants of all the constructs tested were comparable, ranging from 81 nM to 472 nM for the 59/750 and 1/750 variants, respectively. In terms of both k_{cat} and K_m , the full-length 1/750 variant showed values similar to the ectodomain-spanning 44/750 mutant, confirming that the ectodomain is a fully active form of the enzyme. Further truncation at the N-terminus, or addition of the V5-His tag at the C-terminus, significantly compromises the proteolytic activity of the variants, by affecting the turnover number rather than substrate binding (Table 3).

Table 3. Kinetic characterization of the human glutamate carboxypeptidase II (GCPII) variants and wild-type recombinant human glutamate carboxypeptidase II (rhGCPII). The kinetic parameters against N-acetyl-L-aspartyl-L-glutamate (NAAG) were determined by saturation kinetics for the mutated variants, and wild-type rhGCPII. k_{cat} values were calculated from known concentrations of the individual proteins, as determined by Western blot densitometry.

Construct	k_{cat} (s ⁻¹)	K_m (nM)	k_{cat}/K_m (μM ⁻¹ ·s ⁻¹)
44/750 (rhGCPII)	5.4 ± 0.3	160 ± 44	33.7 ± 15.4
1/750	8.5 ± 0.4	472 ± 88	18.1 ± 5.1
His ₄₄ /750	0.80 ± 0.05	127 ± 47	6.6 ± 4.0
59/750	1.00 ± 0.04	81 ± 11	12.7 ± 2.2

Discussion

Within the last decade, GCPII has been recognized as a promising pharmacological target, and much effort has been invested in developing compounds and strategies targeting or manipulating this enzyme under various pathological conditions. Surprisingly, the 'basic' biochemical characterization of GCPII at the protein level, which might simplify and rationalize the development of modalities useful in clinical practice, is lagging behind the drug discovery activities. Here, we report mapping of the individual predicted domains of human GCPII with regard to their contributions to the GCPII enzymatic activity and folding.

The first critical, important step for analyzing all the GCPII variants used in this study was the development of specific antibodies against human GCPII. As polyclonal rabbit anti-GCPII immunoglobulin cross-reacted slightly with Schneider's autologous S2 cell proteins, and because this cross-reactivity might have interfered with the detection of GCPII variants (especially when the expression level of the variant was very low), several clones of mouse mAbs, specifically recognizing human GCPII, were produced. A polypeptide spanning the putative catalytic domain of human GCPII (amino acids 274–587) expressed in *Escherichia coli* was used to select clones immunoreactive against an epitope within this sequence (data not shown), as all of the variants used in this study comprise the putative catalytic domain.

Carboxypeptidase activities of each of the GCPII constructs that were modified at the C-terminus (either truncated or modified with the V5-His epitope) were either absent or extremely low. An intact C-terminus is therefore indispensable for GCPII enzymatic activity, as the removal of as few as 15 amino acids from the C-terminus completely abolished NAAG-hydrolyzing activity (the 44/736 variant), and the C-terminal extension (addition of the V5-His tag in the case of the 44/750_V5-His variant) reduced the activity by a factor of > 10⁴. Furthermore, C-terminal modifications also negatively influenced secretion of the truncated variants into the culture medium, suggesting the importance of the C-terminus for the correct folding and procession of GCPII throughout the secretory pathway. These data imply that the putative F domain of GCPII (amino acids 587–750) (Fig. 1), as predicted by Rawlings & Barret [16], might represent an integral part of the GCPII fold, and cannot be deleted without adverse effects on the structure/function of GCPII.

Recently, it has been shown that human GCPII exists in the form of a dimer and that the dimerization is critical for its carboxypeptidase activity [15]. Interestingly, the dimerization of the human transferrin receptor is mediated via contacts of the amino acids forming a helical segment near the C-terminus. As the human transferrin dimerization domain has been reported to be homologous with the C-terminal end of human GCPII [14], it is conceivable that manipulation of the GCPII C-terminus could disrupt the structure of this potential dimerization interface, thus abolishing the enzymatic activity of the protein. Unfortunately, as a result of extremely low yields of the mutants modified at the C-terminus, we were not able to identify an oligomeric status of the variants and confirm these assumptions experimentally.

In contrast to our results, Meighan *et al.* [23] reported expression of the hydrolytically active full-length GCPII flanked with the FLAG-tag at the C-terminus in an HEK293 human embryonic kidney cell line. The authors concluded that this C-terminally modified protein retains hydrolytic activity similar to the wild-type enzyme isolated from LNCaP cells, the cell line naturally expressing GCPII. This discrepancy is difficult to explain. It could be hypothesized that the observed inhibition might be sequence specific, i.e. that either the presence of the 6-His tag compromises carboxypeptidase activity of the 1/750_V5-His construct in an unidentified specific manner or that the inhibition might depend on the length of an epitope attached.

The sequence at the N-terminus of the protein was also shown to be required for the activity and/or secretion of the GCPII carboxypeptidase. As for the N-terminally modified variants, the absence of the intracellular and transmembrane domains does not influence carboxypeptidase activity of GCPII and neither does the attachment of the His-Xpress epitope at the N-terminus of the 44/750 variant. However, the protein was rendered inactive following the deletion of more than 60 amino acids from the N-terminus. Moreover, the amounts of recombinant protein secreted into the media were substantially lower for the variants truncated further at the N-terminus (as compared to the 44/750 variant), and the 150/750 construct was not secreted at all.

The specific activities of the mutants secreted into the medium were generally higher than those retained intracellularly (Table 2). These differences could be attributed to the presence of incorrectly or partially folded protein species in the intracellular fraction, while the extracellular protein consists exclusively of a properly folded enzyme. However, the cause for three orders of magnitude specific activity difference in the case of mutant 59/750 is not clear at present.

The ER is responsible for the quality control of newly synthesized polypeptide chains. Nascent proteins with only a partial fold are cycled via the calnexin-calreticulin-glucosidase I and II system within the ER lumen, providing space and time for the unfolded/partially folded proteins to acquire the correct 3D conformation. The proteins that fail to attain their native conformation are subsequently degraded by the ERAD system [24–26]. As the 150/750 variant was clearly detectable in the cell lysate, but absent from the conditioned medium, it is plausible that the 150/750 variant was not able to fold correctly and consequently was retained in the ER and not allowed to proceed further along the secretory pathway.

Two of the GCPII variants studied, namely the 274/750 and 274/587 constructs, were detected neither in the cell lysates nor in the conditioned media, although the corresponding mRNAs were detected by RT-PCR. Our failure to detect expression of these GCPII variants, even after proteasome inhibition, cannot be explained unequivocally, but may be a result of the fact that mRNAs encoding the respective proteins are not, for an unknown reason, translated in S2 cells. Another possibility could be that the proteasome inhibition was not complete. Similar phenomena were described for the EL4 mouse cell line that was formerly reported to be adapted to conditions of total

proteasome inhibition [27]. Additionally, an increase in the proteolytic activity of different cell degradation systems, for example tripeptidyl peptidase II, might compensate for the inhibited proteasome activity [28,29]. Yet another explanation might be that proteasome inhibitors exercise more general effects on the overall metabolism of S2 cells, resulting in an overall decrease of protein synthesis or increase in protein degradation. This interpretation is supported by our control experiment with proteasome inhibition of the S2 cells expressing the 44/587 variant, which lowered, rather than increased, the expression levels of the recombinant protein (data not shown). Similar, negative effects of proteasome inhibitors on recombinant protein expression (reduction of luciferase and beta-galactosidase activity in tissue culture cells treated with proteasome inhibitors) were recently reported by Deroo & Archer [30].

Unexpectedly, the 1/750 variant of GCPII, i.e. full-length transmembrane protein, was detected in the conditioned medium. This observation contradicts the analysis of conditioned media of LNCaP cells or HEK cells stably transfected with full-length human GCPII, in which 'shedding' of GCPII was not detected (data not shown). We attempted to identify the cleavage site recognized by an unknown 'shedase' by the N-terminal sequencing, but no sequence was recovered, apparently as a result of the blocking of the N-terminal amino acid. Subsequent Western blot analysis, exploiting the 7E11 mAb recognizing the first six amino acids of the full-length GCPII [31], revealed the absence of the immunoreactive epitope (i.e. the N-terminal end of GCPII) in the species 'shed' into the medium, but not in the species expressed on the cell surface (data not shown). Taken together, S2 cells probably express an unidentified peptidase capable of specific cleavage of the 1/750 variant, releasing soluble protein into the culture medium.

Kinetic parameter comparison of the individual enzymatically active GCPII variants did not reveal any significant differences in either the binding or the turnover of the substrate. The submicromolar values of the Michaelis constants are in good agreement with the data reported previously for both rat and human enzymes [5,32–35].

In conclusion, we analyzed the contribution of the N- and C-terminal regions of GCPII to its enzymatic properties and structure/folding. The results clearly show that the amino acids at the extreme C-terminus of GCPII are crucial for the hydrolytic activity of the enzyme and, furthermore, that no more than 60 amino acids can be deleted from the N-terminus without compromising the carboxypeptidase activity of GCPII. These data thus indicate that current GCPII homology models should be interpreted with some caution, as they might lack elements indispensable for the enzymatic activity of GCPII.

Acknowledgements

The authors wish to thank Jana Starková and Taťána Mrázková for excellent technical assistance. This work (performed under the research project Z4055 905) was supported by grant IAA5055108 from the Grant Agency of the Academy of Science of the Czech Republic, grant 301/03/0784 from the Grant Agency of the Czech Republic and by research support from Guilford Pharmaceuticals.

References

- Chang, S.S., Reuter, V.E., Heston, W.D., Bander, N.H., Grauer, L.S. & Gaudin, P.B. (1999) Five different anti-prostate-specific membrane antigen (PSMA) antibodies confirm PSMA expression in tumor-associated neovasculature. *Cancer Res.* **59**, 3192–3198.
- Silver, D.A., Pellicer, I., Fair, W.R., Heston, W.D. & Cordon-Cardo, C. (1997) Prostate-specific membrane antigen expression in normal and malignant human tissues. *Clin. Cancer Res.* **3**, 81–85.
- Troyer, J.K., Beckett, M.L. & Wright, G.L. Jr (1995) Detection and characterization of the prostate-specific membrane antigen (PSMA) in tissue extracts and body fluids. *Int. J. Cancer* **62**, 552–558.
- Coyle, J.T. (1997) The nagging question of the function of N-acetylaspartylglutamate. *Neurobiol. Dis.* **4**, 231–238.
- Robinson, M.B., Blakely, R.D., Couto, R. & Coyle, J.T. (1987) Hydrolysis of the brain dipeptide N-acetyl-L-aspartyl-L-glutamate. Identification and characterization of a novel N-acetylated alpha-linked acidic dipeptidase activity from rat brain. *J. Biol. Chem.* **262**, 14498–14506.
- Chen, S.R., Wozniak, K.M., Slusher, B.S. & Pan, H.L. (2002) Effect of 2-(phosphono-methyl)-pentanedioic acid on allodynia and afferent ectopic discharges in a rat model of neuropathic pain. *J. Pharmacol. Exp. Ther.* **300**, 662–667.
- Ghadge, G.D., Slusher, B.S., Bodner, A., Canto, M.D., Wozniak, K., Thomas, A.G., Rojas, C., Tsukamoto, T., Majer, P., Miller, R.J., Montti, A.L. & Roos, R.P. (2003) Glutamate carboxypeptidase II inhibition protects motor neurons from death in familial amyotrophic lateral sclerosis models. *Proc. Natl Acad. Sci. USA* **100**, 9554–9559.
- Slusher, B.S., Vornov, J.J., Thomas, A.G., Hurn, P.D., Harukuni, I., Bhardwaj, A., Traystman, R.J., Robinson, M.B., Britton, P., Lu, X.C., Tortella, F.C., Wozniak, K.M., Yudkoff, M., Potter, B.M. & Jackson, P.F. (1999) Selective inhibition of NAALADase, which converts NAAG to glutamate, reduces ischemic brain injury. *Nat. Med.* **5**, 1396–1402.
- Bostwick, D.G., Pacelli, A., Blute, M., Roche, P. & Murphy, G.P. (1998) Prostate specific membrane antigen expression in prostatic intraepithelial neoplasia and adenocarcinoma: a study of 184 cases. *Cancer* **82**, 2256–2261.
- Lamb, H.M. & Faulds, D. (1998) Capromab pendetide. A review of its use as an imaging agent in prostate cancer. *Drugs Aging* **12**, 293–304.
- Lodge, P.A., Jones, L.A., Bader, R.A., Murphy, G.P. & Salgaller, M.L. (2000) Dendritic cell-based immunotherapy of prostate cancer: immune monitoring of a phase II clinical trial. *Cancer Res.* **60**, 829–833.
- Mincheff, M., Tchakarov, S., Zoubak, S., Loukinov, D., Botev, C., Altankova, I., Georgiev, G., Petrov, S. & Meryman, H.T. (2000) Naked DNA and adenoviral immunizations for immunotherapy of prostate cancer: a phase I/II clinical trial. *Eur. Urol.* **38**, 208–217.
- Rawlings, N.D. (1998) Introduction: Metallopeptidases and their clans. In *Handbook of Proteolytic Enzymes* (Barrett, A.J., Rawlings, N.D. & Woessner, J.F., eds), pp. 989–991. Academic Press, New York.
- Lawrence, C.M., Ray, S., Babyonyshev, M., Galluser, R., Borhani, D.W. & Harrison, S.C. (1999) Crystal structure of the ectodomain of human transferrin receptor. *Science* **286**, 779–782.
- Schulke, N., Varlamova, O.A., Donovan, G.P., Ma, D.S., Gardner, J.P., Morrissey, D.M., Arrigale, R.R., Zhan, C.C., Chodera, A.J., Surowitz, K.G., Maddon, P.J., Heston, W.D.W. & Olson, W.C. (2003) The homodimer of prostate-specific membrane antigen is a functional target for cancer therapy. *Proc. Natl Acad. Sci. USA* **100**, 12590–12595.
- Rawlings, N.D. & Barrett, A.J. (1997) Structure of membrane glutamate carboxypeptidase. *Biochim. Biophys. Acta* **1339**, 247–252.
- Chevrier, B., Schalk, C., Dorchymont, H., Rondeau, J.M., Tarnus, C. & Moras, D. (1994) Crystal structure of *Aeromonas proteolytica* aminopeptidase – a prototypical member of the co-catalytic zinc enzyme family. *Structure* **2**, 283–291.
- Greenblatt, H.M., Almog, O., Maras, B., SpunginBialik, A., Barra, D., Blumberg, S. & Shoham, G. (1997) *Streptomyces griseus* aminopeptidase: X-ray crystallographic structure at 1.75 angstrom resolution. *J. Mol. Biol.* **265**, 620–636.
- Speno, H.S., Luthi-Carter, R., Macias, W.L., Valentine, S.L., Joshi, A.R. & Coyle, J.T. (1999) Site-directed mutagenesis of predicted active site residues in glutamate carboxypeptidase II. *Mol. Pharmacol.* **55**, 179–185.
- Rong, S.B., Zhang, J., Neale, J.H., Wroblewski, J.T., Wang, S. & Kozikowski, A.P. (2002) Molecular modeling of the interactions of glutamate carboxypeptidase II with its potent NAAG-based inhibitors. *J. Med. Chem.* **45**, 4140–4152.
- Barinka, C., Rinnova, M., Sacha, P., Rojas, C., Majer, P., Slusher, B.S. & Konvalinka, J. (2002) Substrate specificity, inhibition and enzymological analysis of recombinant human glutamate carboxypeptidase II. *J. Neurochem.* **80**, 477–487.
- Doherty, F.J., Dawson, S. & Mayer, R.J. (2002) The ubiquitin-proteasome pathway of intracellular proteolysis. *Essays Biochem.* **38**, 51–63.
- Meighan, M.A., Dickerson, M.T., Glinskii, O., Glinsky, V.V., Wright, G.L. & Deutscher, S.L. (2003) Recombinant glutamate carboxypeptidase II (prostate specific membrane antigen-PSMA) – cellular localization and bioactivity analyses. *J. Protein Chem.* **22**, 317–326.
- Hampton, R.Y. (2002) ER-associated degradation in protein quality control and cellular regulation. *Curr. Opin. Cell Biol.* **14**, 476–482.
- Jarosch, E., Lenk, U. & Sommer, T. (2003) Endoplasmic reticulum-associated protein degradation. *Int. Rev. Cytol.* **223**, 39–81.
- Yoshida, Y. (2003) A novel role for N-glycans in the ERAD system. *J. Biochem. (Tokyo)* **134**, 183–190.
- Princiotta, M.F., Schubert, U., Chen, W.S., Bennink, J.R., Myung, J., Crews, C.M. & Yewdell, J.W. (2001) Cells adapted to the proteasome inhibitor 4-hydroxy-5-iodo-3-nitrophenylacetyl-Leu-Leu-leucinal-vinyl sulfone require enzymatically active proteasomes for continued survival. *Proc. Natl Acad. Sci. USA* **98**, 513–518.
- Geier, E., Pfeifer, G., Wilm, M., Lucchiari-Hartz, M., Baumeister, W., Eichmann, K. & Niedermann, G. (1999) A giant protease with potential to substitute for some functions of the proteasome. *Science* **283**, 978–981.
- Wang, E.W., Kessler, B.M., Borodovsky, A., Cravatt, B.F., Bogyo, M., Ploegh, H.L. & Glas, R. (2000) Integration of the ubiquitin-proteasome pathway with a cytosolic oligopeptidase activity. *Proc. Natl Acad. Sci. USA* **97**, 9990–9995.
- Deroo, B.J. & Archer, T.K. (2002) Proteasome inhibitors reduce luciferase and beta-galactosidase activity in tissue culture cells. *J. Biol. Chem.* **277**, 20120–20123.
- Troyer, J.K., Feng, Q., Beckett, M.L. & Wright, G.L. Jr (1995) Biochemical characterization and mapping of the 7E11-C5.3 epitope of the prostate-specific membrane antigen. *Urol. Oncol.* **1**, 29–37.
- Luthi-Carter, R., Barczak, A.K., Speno, H. & Coyle, J.T. (1998) Hydrolysis of the neuropeptide N-acetylaspartylglutamate (NAAG) by cloned human glutamate carboxypeptidase II. *Brain Res.* **795**, 341–348.
- Luthi-Carter, R., Barczak, A.K., Speno, H. & Coyle, J.T. (1998) Molecular characterization of human brain N-acetylated

- alpha-linked acidic dipeptidase (NAALADase). *J. Pharmacol. Exp. Ther.* **286**, 1020–1025.
34. Serval, V., Barbeito, L., Pittaluga, A., Cheramy, A., Lavielle, S. & Glowinski, J. (1990) Competitive inhibition of N-acetylated-alpha-linked acidic dipeptidase activity by N-acetyl-L-aspartyl-beta-linked L-glutamate. *J. Neurochem.* **55**, 39–46.
35. Slusher, B.S., Robinson, M.B., Tsai, G., Simmons, M.L., Richards, S.S. & Coyle, J.T. (1990) Rat brain N-acetylated alpha-linked acidic dipeptidase activity. Purification and immunologic characterization. *J. Biol. Chem.* **265**, 21297–21301.

6.2.4 Postscript

X-ray structures provide evidence these days that the extracellular part of GCPII composes of three domains. These domains cooperate to form an active site and all of them are essential for the GCPII hydrolytic activity (see Fig. 5) [25, 26], which explains why both N- and C-terminus truncation of GCPII have such a devastating effect on protein stability and activity.

6.3 Structural analysis of the binding specificity of GCPII: rational drug design

6.3.1 Background information

It was shown that inhibitors of GCPII are neuroprotective during ischemia in animal models [80] and so they appear to be a promising pharmacological tool. The most potent inhibitor of GCPII, 2-(phosphonomethyl)pentanedioic acid (2-PMPA) was discovered already in 1996 [20]. Unfortunately, phosphonate (and also phosphinate) functional group is poorly orally bioavailable and thus new functional groups for GCPII inhibition were searched for. Interestingly, the glutarate moiety of potent GCPII inhibitors seems to be the most important in inhibitor's affinity towards GCPII and any change in the moiety leads to a decrease in inhibitor potency [22, 23, 212].

Until recently, consecutive changes of different functional groups of known potent inhibitors were the only way how to identify new effective bioavailable inhibitor of GCPII [23, 24]. The crystal structure of GCPII became available only in 2005 [25]. Since the published structure showed free enzyme without any ligand inside the active site, it was of limited use for inhibitor design.

In 2006, further GCPII structures with bound glutamate, phosphate and GPI-18431 inhibitor (Fig. 17) were published [26]. It was the first available tool for rational design of new inhibitors.

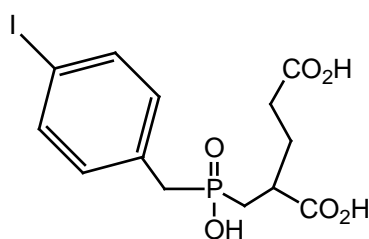


Fig. 17: Chemical formula of (S)-2-(4-iodobenzyl-phosphonomethyl)-pentanedioic acid (GPI-18431).

It was just a first step in a long journey; there are a lot of GCPII inhibitors displaying different inhibition constants and affinity to the studied enzyme.

In our study, we combined the biochemical data with crystal structures of several inhibitors and analyzed the structural features of the pharmacophore pocket of human GCPII.

6.3.2 Summary

Even though 2-PMPA, GPI-18431 inhibitor and glutamate bind in S1' pocket in a similar way, their inhibition constants are very different: 0.3nM, 100nM, and 428 μ M for 2-PMPA, GPI-18431, and glutamate, respectively. It seems that higher affinity of 2-PMPA is mediated more strongly through the interaction with zinc ions and phosphonate moiety than through interaction of enzyme with the glutamate moiety.

In the GCPII/2-PMPA complex, phosphonate oxygens (replaced by a methylene group in phosphinate compounds) form a hydrogen bond with side chain of Asn519, but this interaction contributes only partially to the high affinity of this inhibitor. It is very likely that under physiological conditions oxygen atom of phosphonate can be deprotonated in the vicinity of the zinc ions, resulting in the double negatively charged phosphonate group, which interacts with positively charged zinc ions with greater avidity than e.g. phosphinate group.

In GCPII/QA (quisqualic acid) complex, the inhibitor mimics glutamate binding, but shows greater potency than glutamate. It seems that additional hydrogen bonds participate in binding of QA oxadiazolidine ring to GCPII. This ring is engaged in more van der Waals interactions with side chains of Phe209 and Leu428 and these hydrophobic interactions are decreasing K_i value.

Interestingly, practically constant spacing between side chains of Phe209 and Leu428 (in all available structures) define a narrow channel, which limits the size and placement of potential inhibitors in the S1' site.

Moreover, oxadiazolidine ring in QA is negatively charged at physiological pH whereas the heterocyclic rings of other studied inhibitors (willardiine, AMPA) are neutral. From the IC_{50} values it seems highly probable that electrostatic interactions between inhibitor and enzyme are also important for effective binding (IC_{50} 9.5 μ M for quisqualic acid, 67 μ M for willardiine and more than 10mM for AMPA).

The presented data can be used for the development of new GCPII inhibitors, which might be orally bioavailable with preserved high potency.

My contribution to this work was a measurement of the inhibition constant of quisqualic acid and willardiine and determination of the inhibition mode in the case of quisqualic acid.

Structural Insight into the Pharmacophore Pocket of Human Glutamate Carboxypeptidase II[‡]Cyril Bařinka,[†] Miroslava Rovenska,^{‡,§} Petra Mlcchova,^{‡,§} Klara Hlouchova,^{‡,§} Anna Plechanovova,^{‡,§} Pavel Majer,[#] Takashi Tsukamoto,[#] Barbara S. Slusher,[#] Jan Konvalinka,^{‡,§} and Jacek Lubkowski^{*,†}

Center for Cancer Research, National Cancer Institute at Frederick, Frederick, Maryland 21702, Gilead Sciences and IOCB Research Centre, Institute of Organic Chemistry and Biochemistry, Academy of Sciences of the Czech Republic, Flemingovo n. 2, Prague, Czech Republic, Department of Biochemistry, Faculty of Natural Science, Charles University, Hlavova 2030, Prague, Czech Republic, and MGI Pharma, Inc., 6611 Tributary Street, Baltimore, Maryland 21224

Received February 2, 2007

Inhibition of glutamate carboxypeptidase II (GCPII) has been shown to be neuroprotective in multiple preclinical models in which dysregulated glutamatergic transmission is implicated. Herein, we report crystal structures of the human GCPII complexed with three glutamate mimetics/derivatives, 2-(phosphonomethyl)pentanedioic acid (2-PMPA), quisqualic acid (QA), and L-serine *O*-sulfate (L-SOS), at 1.72, 1.62, and 2.10 Å resolution, respectively. Despite the structural differences between the distal parts of the inhibitors, all three compounds share similar binding modes in the pharmacophore (i.e., S1') pocket of GCPII, where they are stabilized by a combination of polar and van der Waals interactions. The structural diversity of the distal parts of the inhibitors leads to rearrangements of the S1' site that are necessary for efficient interactions between the enzyme and an inhibitor. The set of structures presented here, in conjunction with the available biochemical data, illustrates a flexibility of the GCPII pharmacophore pocket and highlights the structural features required for potent GCPII inhibition. These findings could facilitate the rational structure-based drug design of new GCPII inhibitors in the future.

1. Introduction

The development of novel neuroprotective agents attracts considerable interest because the existing therapies often lack desired efficacy and selectivity.¹ One recently identified pharmacologically exploitable target/marker protein is glutamate carboxypeptidase II (GCPII,[¶] EC 3.4.17.21), a membrane-bound metallopeptidase expressed predominantly in the human nervous system, the brush border of the small intestine, proximal renal tubules, and prostate parenchyma.^{2,3} Within the nervous system, GCPII is expressed primarily on astrocyte and Schwann cell membranes with the catalytic ectodomain facing the extracellular milieu. There, it hydrolyzes *N*-acetylaspartylglutamate (NAAG), the most abundant neuropeptide in the mammalian brain, and liberates free glutamate.⁴ Excessive (or dysregulated) glutamatergic transmission is associated with various pathophysiological conditions including traumatic brain injury, stroke, neuropathic and inflammatory pain, amyotrophic lateral sclerosis (ALS), and schizophrenia.^{5–8} NAAG itself is an agonist at the group II metabotropic glutamate receptors (mGluR3) on glia and neurons.⁹ Activation of mGluR3

affects a wide spectrum of cellular functions, including the release of neuroprotective trophic factors or the inhibition of glutamate release.^{10,11} Consequently, the inhibition of GCPII provides protection in the animal models presumably because of decreasing levels of free glutamate and increasing NAAG concentrations.

GCPII has a strong preference for substrates with glutamate at the C-terminal position.¹² Not surprisingly then, the first GCPII inhibitors identified were glutamate/NAAG mimetics/derivatives, such as quisqualic acid (QA) and *N*-fumaryl glutamate.^{13,14} Demands for a more specific and potent inhibitor were met by the synthesis of 2-(phosphonomethyl)pentanedioic acid (2-PMPA, $K_i = 0.3$ nM),¹⁵ which is currently one of the most extensively studied GCPII inhibitors. Subsequently, many novel GCPII-specific compounds of different chemistries have been designed and synthesized. At present, most of the substrate-based GCPII inhibitors include a glutamate moiety linked to a zinc-binding group such as phosphonate, phosphinate, hydroxamate, urea, phosphoamidate, and thiol.^{16–20} Additionally, despite the presumed low tolerance of the GCPII pharmacophore pocket for the structural changes of an inhibitor, conformationally constrained NAAG mimetics or P1'-carboxylbenzyl-containing analogues were shown to possess inhibitory activity toward GCPII.^{21,22}

Recently reported crystal structures of GCPII revealed that the extracellular part of the enzyme is organized into the three domains spanning amino acids 57–116 and 352–590 (the protease-like domain), 117–351 (the apical domain), and 591–750 (the C-terminal domain) and that amino acid residues from all the three domains are required for high-affinity substrate/inhibitor binding.^{23,24} These structural findings, in conjunction with SAR analysis reported previously, provided useful information for the rational structure-based design of new GCPII inhibitors.

Available crystallographic data on GCPII represent a major step toward our understanding of structural features of the

[‡] Accession numbers: Atomic coordinates of the present structures together with the experimental diffraction amplitudes have been deposited at the RCSB Protein Data Bank with accession numbers 2PVW (the complex with 2-PMPA), 2OR4 (the complex with quisqualate), and 2PVV (the complex with L-serine *O*-sulfate).

^{*} To whom correspondence should be addressed. Address: Macromolecular Crystallography Laboratory, 539 Boyles Street, National Cancer Institute at Frederick, Frederick, Maryland 21702. Phone: 301-846-5494. Fax: 301-846-7517. E-mail: jacek@ncifer.gov.

[†] National Cancer Institute at Frederick.

[‡] Academy of Sciences of the Czech Republic.

[§] Charles University.

[#] MGI Pharma.

[¶] Abbreviations: GCPII, glutamate carboxypeptidase II; NAAG, *N*-acetyl-L-aspartyl-L-glutamate; 2-PMPA, (*R,S*)-2-(phosphonomethyl)pentanedioic acid; QA, quisqualic acid, 2-amino-3-(3,5-dioxo[1,2,4]oxadiazolidin-2-yl)propionic acid; rhGCPII, recombinant human glutamate carboxypeptidase II; PEG, polyethylene glycol; AMPA, 2-amino-3-(3-hydroxy-5-methyl-4-isoxazolyl)propionic acid; Glu, glutamic acid; SAR, structure–activity relationship; PSMA, prostate-specific membrane antigen; L-SOS, L-serine *O*-sulfate; L-SOP, L-serine *O*-phosphate; K_i , inhibition constant.

Table 1. Data Collection and Refinement Statistics

	rhGCPII/2-PMPA	rhGCPII/QA	rhGCPII/L-SOS
Data Collection Statistics			
wavelength (Å)	1.000	1.000	1.5478
space group	<i>I</i> 222	<i>I</i> 222	<i>I</i> 222
unit-cell parameters <i>a</i> , <i>b</i> , <i>c</i> (Å)	101.8, 130.8, 159.4	102.0, 130.4, 159.5	101.6, 130.2, 159.0
resolution limits (Å)	30.0–1.72 (1.78–1.72) ^a	50.0–1.62 (1.68–1.62) ^a	30.0–2.10 (2.18–2.10) ^a
no. of unique reflections	111281 (10238)	129603 (9922)	60304 (5928)
redundancy	9.8 (6.0)	11.0 (5.7)	4.8 (4.8)
completeness (%)	98.6 (91.7)	96.7 (74.8)	98.9 (98.4)
<i>I</i> / σ (<i>I</i>)	15.1 (3.5)	28.2 (2.7)	15.4 (3.7)
<i>R</i> _{merge}	0.126 (0.495)	0.070 (0.465)	0.097 (0.505)
Refinement Statistics			
resolution limits (Å)	15.0–1.72 (1.76–1.72)	30.0–1.62 (1.66–1.62)	30.0–2.10 (2.16–2.10)
total no. of reflections	105604	123053	57236
no. of reflections in working set	100055 (5998)	116532 (6550)	54175 (3972)
no. of reflections in test set	5549 (344)	6521 (360)	3061 (217)
<i>R</i> / <i>R</i> _{free}	0.183 (0.232)/0.207 (0.288)	0.185 (0.272)/0.218 (0.337)	0.176 (0.203)/0.212 (0.274)
total no. of non-H atoms	6217	6825	6329
no. of non-H protein atoms	5678	5871	5804
no. of ions	4	4	4
no. of water molecules	521	937	510
average <i>B</i> factor (Å ²)			
protein atoms	34.0	25.6	29.2
waters	43.1	39.9	36.3
inhibitor	30.7	23.8	25.1
rmsd			
bond length (Å)	0.019	0.019	0.021
bond angle (deg)	1.80	1.79	1.80
planarity (Å)	0.009	0.009	0.009
chiral center (Å ³)	0.132	0.124	0.125
gaps in the structure	42–55, 541–543, 654–655	42–55, 152–155, 541–543	42–55, 654–655

^a Values in parentheses correspond to the highest resolution shells.

enzyme, but the insight into the S1' (i.e., pharmacophore) pocket of GCPII is still quite limited. This is due to the fact that all available X-ray structures of GCPII have the S1' site either empty or occupied by a glutarate moiety. To obtain deeper understanding of the flexibility of the S1' pocket and to define the structural features required for potent GCPII inhibition more precisely, we determined crystal structures of human GCPII in complex with three glutamate analogues/mimetics harboring distinct S1' binding moieties. The set of structures presented here characterizes structural adjustments of the S1' pocket that are necessary to accommodate inhibitors with varied moieties in the P1' position. The availability of the crystallographic data on GCPII complexed structurally diversified inhibitors could thus facilitate development of novel GCPII specific inhibitors with enhanced activity in the future.

2. Experimental Section

2.1. Inhibitors. QA (2-amino-3-(3,5-dioxo[1,2,4]oxadiazolidin-2-yl)propionic acid) was obtained from Fluka (Fluka, 99% TLC). The stock solution was prepared by dissolving 1 mg of the inhibitor in 66 μ L of 100 mM NaOH (80 mM final concentration). (*R,S*)-2-(phosphonomethyl)pentanedioic acid (2-PMPA, a racemic form) was synthesized as described previously,¹⁵ and the inhibitor was dissolved in distilled water to a final concentration of 50 mM. L-Serine *O*-sulfate (L-SOS), L-serine *O*-phosphate (L-SOP), and (S)-willardiine were purchased from Sigma (St. Louis, MO).

2.2. rhGCPII Expression and Purification. The extracellular domain of human glutamate carboxypeptidase II (rhGCPII, amino acids 44–750) was overexpressed in *Drosophila* Schneider S2 cells and purified to homogeneity as described previously.¹² The protein was dialyzed against 20 mM Tris-HCl, 100 mM NaCl, pH 8.0, and concentrated to 10 mg/mL using an YM50 Centricron ultrafiltration device (Millipore). The protein concentration was determined with the Bio-Rad protein assay kit, using the bovine serum albumin as a standard.

2.3. Crystallization and Data Collection. The protein solution was mixed with the inhibitor stock solutions at 10:1 ratio

(resulting in an approximate 50-fold molar excess of the inhibitor), and the droplets were set up by combining 2 μ L of the rhGCPII-inhibitor mixture and 2 μ L of the reservoir solution containing 33% (v/v) pentaerythritol propoxylate PO/OH 5/4, 1–3% (w/v) PEG 3350, and 100 mM Tris-HCl, pH 8.0. The orthorhombic crystals of approximately 0.4 mm \times 0.4 mm \times 0.2 mm (*I*222 space group with one rhGCPII molecule per asymmetric unit) were grown using the hanging drop vapor diffusion method at 293 K, typically within 1 week. For the X-ray experiments, crystals were frozen in a stream of liquid nitrogen directly from hanging drops. The diffraction data for rhGCPII/2-PMPA and rhGCPII/QA were collected at 100 K using synchrotron radiation at the SER-CAT beamlines (sectors 22BM and 22ID) at the Advanced Photon Source (Argonne, IL) with the X-ray wavelength of 1.0 Å, and the images were recorded on MAR charge-coupled device detectors. The diffraction data for the rhGCPII/L-SOS complex were collected in-house at 100 K using X-radiation ($\lambda_{Cu} = 1.5478$ Å) generated by the rotating anode operating at 100 kV and 50 mA (Rigaku-Ru200), and reflection intensities were recorded on the MAR345 image plate detector (MAR Research, Hamburg, Germany). In all cases, the diffraction intensities were collected from single crystals and processed using the HKL2000 software package.²⁵

2.4. Structure Determination and Refinement. Since the crystals of rhGCPII/inhibitor complexes were isomorphous with a previously reported crystal of the ligand-free rhGCPII,²⁶ this structure (RSCB PDB code 2O0T) served as the initial solution. The structures were refined and manually rebuilt using the programs Refmac5²⁷ and Xtalview,²⁸ respectively. During the refinement, 5% of the randomly selected reflections were kept aside for cross-validation (*R*_{free}). The quality of the final models was evaluated using the program PROCHECK²⁹ distributed with the CCP4i suite, version 2.2.³⁰ Ramachandran analysis of the final models classified all residues but one, Lys207, as having either the most favorable or allowed conformations. Despite supposedly unfavorable conformations, all atoms of Lys207 are well defined in the electron density peaks. The final statistics for the data collection and the structure refinement are summarized in Table 1.

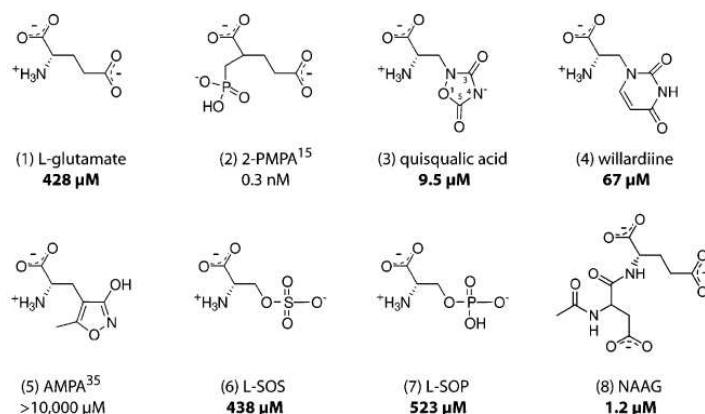


Figure 1. Chemical definitions of glutamate analogues: (1) L-Glu; (2) 2-PMPA, (*R,S*)-2-phosphonomethylpentanedioic acid; (3) quisqualic acid, 2-amino-3-(3,5-dioxo[1,2,4]oxadiazolidin-2-yl)propionic acid; (4) willardiine, 2-amino-3-(2,4-dioxo-3,4-dihydro-2*H*-pyrimidin-1-yl)propionic acid; (5) AMPA, 2-amino-3-(3-hydroxy-5-methyl-4-isoxazolyl)propionic acid; (6) L-SOS, L-serine *O*-sulfate; (7) L-SOP, L-serine *O*-phosphate; (8) NAAG, *N*-acetylaspartylglutamate. Inhibition concentration values (and the K_M value in the case of NAAG) are taken from the published data^{15,37} or determined in our laboratory (shown in bold).

2.5. Determination of Inhibition Concentration Values (IC_{50}).

The inhibition concentration values of rhGCPII were determined using the radioenzymatic assay with [³H]NAAG (radiolabeled on the terminal glutamate). Briefly, rhGCPII (30 ng/mL) was preincubated in the presence of increasing concentrations of inhibitors in 50 mM MOPS, 20 mM NaCl, pH 7.4, for 15 min at 37 °C. The reaction was initiated by adding 20 μL of the mixture of 0.95 μM NAAG (Sigma) and 50 nM [³H]NAAG (50 Ci/mmol in Tris buffer, Perkin-Elmer) to a total reaction volume of 200 μL . After 20 min, the reaction was terminated by adding 200 μL of 200 mM potassium phosphate solution, pH 7.4. The glutamate was separated from the reaction mixture by ion-exchange chromatography and quantified by liquid scintillation. Duplicate reactions were carried out for each experimental point. The IC_{50} values were calculated from plots of v/v_0 (ratio of individual reaction rates to the rate of an uninhibited reaction) versus inhibitor concentration using the GraFit program (version 5.0.4, Erithacus Software Limited).

2.6. Mode of rhGCPII Inhibition by Quisqualate (QA).

By use of 0.16–40 μM NAAG and QA concentrations of 0, 26, and 75 μM , the mode of inhibition was determined in the reaction setup described above. Initial inhibition velocities for each concentration point were measured in duplicate, and the mode of inhibition was determined from the double-reciprocal plot of velocity versus substrate concentration.

3. Results

3.1. Overall Structure Comparison. The structures of rhGCPII/2-PMPA, rhGCPII/QA, and rhGCPII/L-SOS were refined at resolutions of 1.72, 1.62, and 2.10 Å with crystallographic *R* factors equal to 0.183 ($R_{\text{free}} = 0.207$), 0.185 ($R_{\text{free}} = 0.218$), and 0.176 ($R_{\text{free}} = 0.212$), respectively (Table 1). The overall fold of rhGCPII in all three structures is nearly identical, as illustrated by the root-mean-squared deviation of 0.19 Å (for the 685 equivalent C α pairs), 0.23 Å (for the 690 equivalent C α pairs), and 0.21 Å (for the 692 equivalent C α pairs) between the ligand-free rhGCPII structure and rhGCPII/2-PMPA, rhGCPII/QA, and rhGCPII/L-SOS complexes, respectively.

3.2. Inhibitor Interactions in the S1' Pocket. As glutamate mimetics/derivatives, L-SOS, QA, and 2-PMPA each bind to the S1' pocket of GCPII in a mode similar to that of glutamate. In all complexes, the positive peaks in the $F_o - F_c$ maps clearly showed the location of the inhibitor molecules as well as the surrounding residues from the enzyme (Figure 2).

3.2.1. rhGCPII/2-PMPA Complex. The glutamate fragment of 2-PMPA forms six hydrogen bonds with the side chains of

Arg210, Asn257, Tyr552, Lys699, and Tyr700. Additional hydrogen bonds (2.6 and 2.5 Å) are formed by the α - and γ -carboxylate groups of 2-PMPA and the water molecules. Two oxygen atoms of the inhibitor phosphonate moiety coordinate the active-site Zn²⁺ ions with the Zn \cdots O–P distances of 2.0 and 2.1 Å. Furthermore, one of the phosphonate oxygen atoms forms H-bonds with the hydroxyl group of Tyr552 (2.7 Å) and Ne2 of His553 (3.1 Å). The second phosphonate oxygen interacts with the carboxylate groups of Glu424 (2.8 and 3.2 Å), Asp453 (3.1 Å), and Ne2 of His377 (3.3 Å). The third phosphonate oxygen is stabilized by a weak H-bond with the side chain amide of Asn519 (3.4 Å). The intermolecular contacts between 2-PMPA and rhGCPII are schematically depicted in Figure 3A (and Figure S1 of Supporting Information), and the inhibitor–protein distances are listed in Table T1 in Supporting Information.

3.2.2. rhGCPII/QA Complex. QA is a mimetic of glutamate in which the γ -carboxylate of glutamate is replaced by the 1,2,4-oxadiazolidine ring (Figure 1). In the rhGCPII/QA complex, the α -carboxylate group of QA interacts with the side chains of Arg210, Tyr552, and Tyr700 in a fashion similar to that described for the rhGCPII/2-PMPA complex. The free amino group of quisqualate interacts with the Glu424 γ -carboxylate, the main chain carbonyl group of Gly518, and two water molecules. The oxadiazolidine ring is wedged between Gly427, Leu428, and Gly518 on one side and the side chain of Phe209 on the opposite side of the pharmacophore pocket. Two H-bonds formed by the γ -carboxyl group of 2-PMPA with Lys699 and Asn257 are also present in the QA complex through the ring nitrogen atom N4 (N4 \cdots Ne1, 3.2 Å) and the carbonyl oxygen at position 3 (O3 \cdots N δ 2, 2.8 Å), respectively. Each of these atoms is also hydrogen-bonded to a water molecule that is furthermore stabilized by its interactions with the Leu259 carbonyl oxygen (3.2 Å) and the side chains of Asn257 and Lys699. Additionally, the exocyclic oxygen bound to C5 accepts hydrogen bonds from the main-chain amide of Gly518 (2.9 Å) and from the hydroxyl group of Ser517 (3.3 Å, Figure 3B and Supporting Information Figure S2 and Table T2). To accommodate the bulky oxadiazolidine ring, the S1' pocket of GCPII undergoes a subtle rearrangement. Compared to the rhGCPII/2-PMPA complex, the side chain of Asn257 is rotated by 70° (with a positional difference of 2.2 Å for N δ 2 atoms) and the

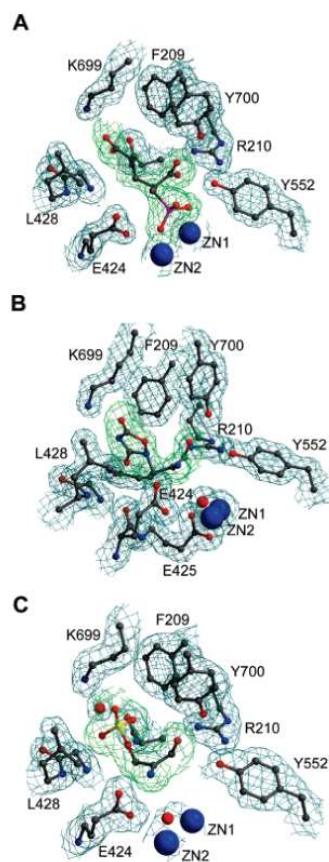


Figure 2. Representative electron density maps of the S1' site in rhGCPII: S1'-bound 2-(S)-PMPA (A), QA (B), and L-SOS (C). Selected amino acids of GCPII are shown in ball-and-stick representation, while Zn²⁺ ions are depicted as blue spheres. The $F_o - F_c$ omit electron density map around an inhibitor is contoured at the 2σ level (green) and the $2F_o - F_c$ difference electron density map at the 1σ level (blue). The picture was generated using MOLSCRIPT⁴¹ and Bobsript⁴² and rendered with PovRay.⁴³

loop containing Gly518 is displaced from its native conformation in the S1' site (Figure 3D).

3.2.3. rhGCPII/L-SOS Complex. The binding mode of L-SOS in the S1' pocket of rhGCPII is analogous to the QA binding described above. The α -amino acid fragments of both ligands structurally overlap and are stabilized by a similar set of interactions with the enzyme (Figure 3C and Supporting Information Figure S3 and Table T3). The distal sulfate group could be superimposed onto the QA oxadiazolidine ring; its oxygen atoms interact with the amino groups of Lys699 (O2...N ϵ 1, 3.0 Å) and Asn257 (O1...N δ 2, 2.9 Å) and are further hydrogen-bonded to a water molecule (O1...O, 3.1 Å; O3...O, 3.0 Å). L-SOS features a tetragonal configuration at the sulfur atom in place of the planar QA oxadiazolidine ring or planar configuration at the glutamate C δ . This spatial arrangement elicits slight movement of the Phe209 side chain to avoid possible steric clashes (Figure 3D).

3.3. Inhibition Concentration Values of Glutamate Mimetics. Inconsistent results have been reported regarding the inhibition mode and potency of QA as an inhibitor of GCPII.^{31,32} We determined that QA is a competitive inhibitor of GCPII with an inhibition concentration of 9.5 μ M (Figures 1 and 4).

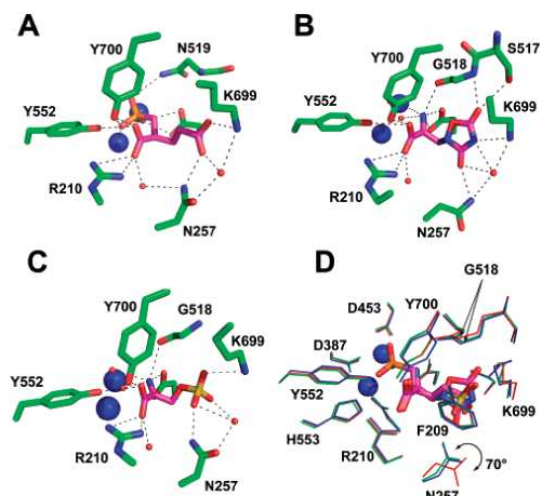


Figure 3. Inhibitor binding to the S1' pocket of rhGCPII: schematic representation of the S1' pocket of rhGCPII complexed with 2-(S)-PMPA (A), QA (B), and L-SOS (C). The N, O, and P atoms are colored in blue, red, and orange, respectively. The carbon atoms are shown in green (rhGCPII) or magenta (the S1'-bound QA/2-PMPA/L-SOS). The Zn²⁺ ions and water molecules are represented by the blue and red spheres, respectively. Hydrogen-bonding interactions between the S1'-bound inhibitor(s) and the rhGCPII residues are shown as dashed lines. The H-bonding distances are summarized in Supporting Information Tables T1–T3. The superposition of the rhGCPII S1' sites observed in complex with 2-PMPA, QA, and L-SOS is shown in panel D. The residues in the rhGCPII/2-PMPA, rhGCPII/QA, and rhGCPII/L-SOS complexes are shown in green, red, and blue, respectively. Note the rotation of the Asn257 side chain and slight shift of Phe209, Gly518, Lys699, and Tyr700. The picture was generated using PyMOL.⁴⁴

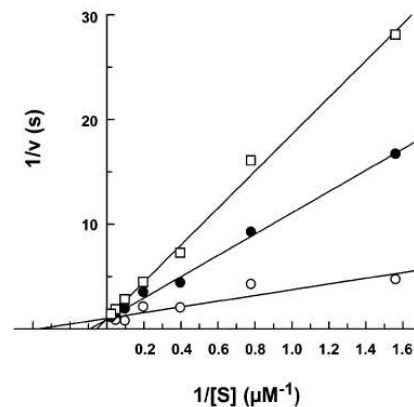


Figure 4. Double-reciprocal plot depicting inhibition mechanism of rhGCPII by quisqualate (QA). The mode of inhibition was determined by measuring rhGCPII hydrolyzing activity at a NAAG concentration range of 0.16–40 μ M, in the absence (O) or in the presence of 26 μ M QA (●) or 75 μ M QA (□), employing the radioenzymatic assay described in the Experimental Section.

These biochemical findings are in agreement with the structural data presented here that clearly show the QA binding to the S1' pocket of rhGCPII. Furthermore, the results of our kinetic experiments demonstrate that compared to QA, glutamate, L-SOS, and L-serine *O*-phosphate are at least 50 times less potent inhibitors of rhGCPII with IC₅₀ values 428, 438, and 523 μ M, respectively (Figure 1).

4. Discussion

At present, 2-PMPA is the most extensively studied inhibitor of GCPII, with proven efficacy in models of ischemic brain injury, neuropathic pain, and amyotrophic lateral sclerosis (for a review, see ref 4). The superposition of the rhGCPII/2-PMPA structure with the rhGCPII/glutamate and rhGCPII/GPI18431 complexes published recently²⁴ reveals that the binding modes of the glutamate fragments of these compounds within the S1' pocket are virtually identical. Yet the inhibitory potencies of the three compounds span more than 6 orders of magnitude with K_i values of 0.3 nM, ~100 nM, and 428 μ M for 2-PMPA, GPI18431, and glutamate, respectively. Consequently, the higher affinity of 2-PMPA against GCPII can only be attributed to the strong interactions between the active site zinc ions and the phosphonate moiety as well as a set of supplementary interactions between the phosphonate and the enzyme.

In general, the replacement of a phosphonate oxygen of 2-PMPA by an alkyl/aryl functionality increases inhibition constants of such derivatives more than 100-fold.¹⁸ In the rhGCPII/2-PMPA complex, the "extra" phosphonate oxygen/hydroxyl group (replaced by a methylene group in phosphinate compounds) forms a weak hydrogen bond with the side chain amide of Asn519. Although this interaction might partially contribute to a higher affinity of 2-PMPA, it is more likely that other factors play an even more prominent role. It should be noted that the phosphonate group of 2-PMPA could release two protons in aqueous solutions (reaching a formal charge of -2), with the calculated values $pK_{a1} \approx 1.8$ and $pK_{a2} \approx 8.5$. It is plausible that under physiological conditions both oxygen atoms of phosphonate will be deprotonated in the vicinity of the active-site zinc ions. As a result, the doubly negatively charged phosphonate group ($R-PO_3^{2-}$) could interact with the positively charged zinc ions with greater avidity than the phosphinate group ($R_{1,2} = PO_2^{-}$), thus contributing to the observed increased potency of phosphonate versus phosphinate compounds.

Results reported by Vitharana et al.³³ indicate that the potent inhibition of GCPII is attributable only to the (*S*)-form of the two 2-PMPA enantiomers, whose absolute configuration is analogous to L-glutamate and is >300 times more active than the (*R*)-enantiomer. Consistent with this report, only 2-(*S*)-PMPA was detected in the structure of rhGCPII/2-PMPA described here, even though the protein was cocrystallized with the racemic form of 2-PMPA. To explain the different activities of the two 2-PMPA enantiomers, we constructed a model of the rhGCPII/2-(*R*)-PMPA complex based on the structure of rhGCPII/2-(*S*)-PMPA complex (data not shown). Assuming that the binding mode of the phosphonate group in the GCPII active site is the same for both enantiomers, the inversion of groups around the C α (glutamate) atom in 2-(*R*)-PMPA prevents interaction between the C α -carboxylate of the ligand and the Arg210 of the enzyme. Furthermore, the same carboxylate group becomes closely positioned to the negatively charged Glu425 γ -carboxylate, resulting in steric clashes and charge repulsions. According to our model, a more complex rearrangement of the GCPII active site would be needed to accommodate the (*R*)-enantiomer, which would likely lead to an increase of the K_i value.

In the structure of the rhGCPII/QA complex, the inhibitor mimics a glutamate-like binding mode and the nearly isosteric positioning of both molecules is aided by the atypical pyramidal geometry of the heterocyclic nitrogen atom carrying the amino acid side chain^{34–36} (Figure 3D). Since the α -amino acid fragments of the ligands structurally overlap, the increased potency of QA versus glutamate can be attributed to the distal

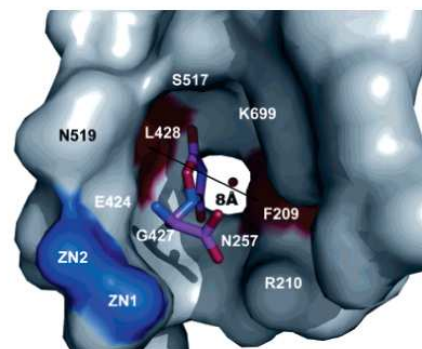


Figure 5. Schematic representation of a narrow channel contributing to the S1' pocket, with the size restricted by the side chains of Phe209 and Leu428. The S1' pocket of GCPII, defined by the residues Phe209, Arg210, Asn257, Glu424, Gly427, Leu428, Gly518, Lys699, and Tyr700, has dimensions of approximately 8 Å × 8 Å × 8 Å. The invariant positions of the Phe209 and Leu428 side chains (red) restrict the width of the pocket and, consequently, the size and placement of an S1'-bound inhibitor. The rhGCPII residues forming the S1' pocket are represented by their solvent accessible surfaces. The S1'-bound QA molecule is shown in stick representation. The residues "capping" the S1' pocket were omitted for clarity.

portions of the inhibitors. Compared to the glutamate γ -carboxylate, the oxadiazolidine ring in QA forms four additional hydrogen bonds with rhGCPII (Figure 3 and Supporting Information Table S1). Also, when compared to the side chain of glutamate, the oxadiazolidine ring is engaged in more extensive van der Waals interactions with the side chains of Phe209 and Leu428. Thus, both the polar and hydrophobic interactions contribute to the observed decrease of the quisqualate inhibition concentration value.

In contrast to the potent inhibitory properties of QA ($IC_{50} = 9.5 \mu$ M), other glutamate bioisosteres, such as AMPA and willardiine, bind GCPII with lower affinity [$IC_{50} > 10$ mM for AMPA^{37,38} and $IC_{50} = 67 \mu$ M for (*S*)-willardiine (Figure 1)]. It is noted that the acidity of the heterocyclic ring in QA is very close to that of the glutamate γ -carboxyl group ($pK_a(QA) = 4.2$; $pK_a(Glu) = 4.4$).³⁵ The heterocyclic moieties of the other bioisosteres are substantially more basic with pK_a values of 9.3 and 10.1 for willardiine and AMPA, respectively.^{39,40} Consequently, the oxadiazolidine ring in QA is negatively charged at physiological pH whereas the heterocyclic rings of the other bioisosteres are neutral. Weaker GCPII inhibition by the latter compounds indicates the importance of electrostatic interactions between an inhibitor and the enzyme.

Our data suggest that the S1' site is capable of the subtle-to-pronounced structural adjustments necessary to accommodate structurally different ligands. For example, the rearrangement of the S1' site, represented by the displacement of a loop harboring Gly518 or repositioning of the Asn257 side chain, is evident from the rhGCPII/QA structure. Similarly, slight variations could be observed in the positions of the Phe209 and Tyr700 side chains (up to ~0.5 Å) in the rhGCPII/L-SOS complex when compared to the 2-PMPA structure. At the same time, flexibility of the S1' site is limited by the overall fold of the enzyme, as all three GCPII extracellular subdomains contribute to substrate recognition. Particularly interesting is the virtually constant spacing between the side chains of the Phe209 and Leu428 located at the beginning of helices $\alpha 5$ (residues 210–219) and $\alpha 9$ (residues 429–445), respectively. These two side chains define a narrow channel with a diameter of approximately 8.0 Å (Figure 5), thus imposing limits on the

size and placement of a potential inhibitor molecule in the S1' site.

In summary, the work presented here analyzes structural features of the pharmacophore pocket of human GCPII. A limited plasticity of the S1' pocket, observed in the described structures, supports conclusions drawn from the previous SAR studies that pointed toward structural rigidity of the GCPII pharmacophore (i.e., S1') pocket¹⁸ on one hand but at the same time led to discovery of P1'-modified compounds with potent inhibitory activities toward GCPII.^{21,22} In addition, the data presented here could be exploited for the development of the novel GCPII inhibitors using the rational structure-based drug design approach. As an example, it might be feasible to substitute the γ -carboxylate group of a glutamate-containing inhibitor with a heterocyclic ring derived from a glutamate bioisoster, such as quisqualic acid or willardiine. Such modifications could improve the pharmacokinetic profile of a resulting compound (because of increased lipophilicity) as well as enhance its potency toward GCPII.

Note Added in Proof. During the editorial review of the manuscript, two of the GCPII complexes presented here were concurrently reported by Mesters and colleagues.⁴⁵

Acknowledgment. We thank Jana Starkova for excellent technical assistance. We acknowledge the use of beamlines 22BM and 22ID of the Southeast Regional Collaborative Access Team (SER-CAT), located at the Advanced Photon Source (APS), Argonne National Laboratory. Use of the APS was supported by the U.S. Department of Energy, Office of Science, Office of Basic Energy Sciences, under Contract No. W-31-109-Eng-38. The project was supported by the Intramural Research Program of the National Institutes of Health, National Cancer Institute, Center for Cancer Research (C.B. and J.L.). J.K., M.R., K.H., P.M., and A.P. were supported in part by the Ministry of Education of the Czech Republic (Research Centre for new Antivirals and Antineoplastics, Grant 1M0508).

Supporting Information Available: Figures S1–S3 and Tables T1–T3 that detail intermolecular interactions between rhGCPII and a corresponding inhibitor. This material is available free of charge via the Internet at <http://pubs.acs.org>.

References

- Doble, A. The role of excitotoxicity in neurodegenerative disease: implications for therapy. *Pharmacol. Ther.* **1999**, *81*, 163–221.
- Sacha, P.; Zámecnik, J.; Barinka, C.; Hloučhova, K.; Vicha, A.; Mlcochova, P.; Hilgert, I.; Eckschlager, T.; Konvalinka, J. Expression of glutamate carboxypeptidase II in human brain. *Neuroscience* **2007**, *144*, 1361–1372.
- Troyer, J. K.; Beckett, M. L.; Wright, G. L., Jr. Detection and characterization of the prostate-specific membrane antigen (PSMA) in tissue extracts and body fluids. *Int. J. Cancer* **1995**, *62*, 552–558.
- Neale, J. H.; Olszewski, R. T.; Gehl, L. M.; Wroblewska, B.; Bzdęga, T. The neurotransmitter *N*-acetylaspartylglutamate in models of pain, ALS, diabetic neuropathy, CNS injury and schizophrenia. *Trends Pharmacol. Sci.* **2005**, *26*, 477–484.
- Carpenter, K. J.; Sen, S.; Matthews, E. A.; Flatters, S. L.; Wozniak, K. M.; Slusher, B. S.; Dickenson, A. H. Effects of GCP-II inhibition on responses of dorsal horn neurons after inflammation and neuropathy: an electrophysiological study in the rat. *Neuropeptides* **2003**, *37*, 298–306.
- Ghadge, G. D.; Slusher, B. S.; Bodner, A.; Canto, M. D.; Wozniak, K.; Thomas, A. G.; Rojas, C.; Tsukamoto, T.; Majer, P.; Miller, R. J.; Monti, A. L.; Roos, R. P. Glutamate carboxypeptidase II inhibition protects motor neurons from death in familial amyotrophic lateral sclerosis models. *Proc. Natl. Acad. Sci. U.S.A.* **2003**, *100*, 9554–9559.
- Slusher, B. S.; Vormov, J. J.; Thomas, A. G.; Hurn, P. D.; Harukuni, I.; Bhardwaj, A.; Traystman, R. J.; Robinson, M. B.; Britton, P.; Lu, X. C.; Tortella, F. C.; Wozniak, K. M.; Yudkoff, M.; Potter, B. M.; Jackson, P. F. Selective inhibition of NAALADase, which converts NAAG to glutamate, reduces ischemic brain injury. *Nat. Med.* **1999**, *5*, 1396–1402.
- Olszewski, R. T.; Bukhari, N.; Zhou, J.; Kozikowski, A. P.; Wroblewski, J. T.; Shamimi-Noori, S.; Wroblewska, B.; Bzdęga, T.; Vicini, S.; Barton, F. B.; Neale, J. H. NAAG peptidase inhibition reduces locomotor activity and some stereotypes in the PCP model of schizophrenia via group II mGluR. *J. Neurochem.* **2004**, *89*, 876–885.
- Wroblewska, B.; Wroblewski, J. T.; Pshenichkin, S.; Surin, A.; Sullivan, S. E.; Neale, J. H. *N*-Acetylaspartylglutamate selectively activates mGluR3 receptors in transfected cells. *J. Neurochem.* **1997**, *69*, 174–181.
- Thomas, A. G.; Liu, W.; Olkowski, J. L.; Tang, Z.; Lin, Q.; Lu, X. C.; Slusher, B. S. Neuroprotection mediated by glutamate carboxypeptidase II (NAALADase) inhibition requires TGF- β . *Eur. J. Pharmacol.* **2001**, *430*, 33–40.
- Bruno, V.; Wroblewska, B.; Wroblewski, J. T.; Fiore, L.; Nicolletti, F. Neuroprotective activity of *N*-acetylaspartylglutamate in cultured cortical cells. *Neuroscience* **1998**, *85*, 751–757.
- Barinka, C.; Rinnova, M.; Sacha, P.; Rojas, C.; Majer, P.; Slusher, B. S.; Konvalinka, J. Substrate specificity, inhibition and enzymological analysis of recombinant human glutamate carboxypeptidase II. *J. Neurochem.* **2002**, *80*, 477–487.
- Serval, V.; Galli, T.; Cheramy, A.; Glowinski, J.; Lavielle, S. In vitro and in vivo inhibition of *N*-acetyl-L-aspartyl-L-glutamate catabolism by *N*-acylated L-glutamate analogs. *J. Pharmacol. Exp. Ther.* **1992**, *260*, 1093–1100.
- Subasinghe, N.; Schulte, M.; Chan, M. Y.; Roon, R. J.; Koerner, J. F.; Johnson, R. L. Synthesis of acyclic and dehydroaspartic acid analogues of Ac-Asp-Glu-OH and their inhibition of rat brain *N*-acetylated alpha-linked acidic dipeptidase (NAALAD dipeptidase). *J. Med. Chem.* **1990**, *33*, 2734–2744.
- Jackson, P. F.; Cole, D. C.; Slusher, B. S.; Stetz, S. L.; Ross, L. E.; Donzanti, B. A.; Trainor, D. A. Design, synthesis, and biological activity of a potent inhibitor of the neuropeptidase *N*-acetylated alpha-linked acidic dipeptidase. *J. Med. Chem.* **1996**, *39*, 619–622.
- Kozikowski, A. P.; Nan, F.; Conti, P.; Zhang, J.; Ramadan, E.; Bzdęga, T.; Wroblewska, B.; Neale, J. H.; Pshenichkin, S.; Wroblewski, J. T. Design of remarkably simple, yet potent urea-based inhibitors of glutamate carboxypeptidase II (NAALADase). *J. Med. Chem.* **2001**, *44*, 298–301.
- Wone, D. W.; Rowley, J. A.; Garofalo, A. W.; Berkman, C. E. Optimizing phenylethylphosphonamides for the inhibition of prostate-specific membrane antigen. *Bioorg. Med. Chem.* **2006**, *14*, 67–76.
- Jackson, P. F.; Tays, K. L.; Maclin, K. M.; Ko, Y. S.; Li, W.; Vitharana, D.; Tsukamoto, T.; Stoermer, D.; Lu, X. C.; Wozniak, K.; Slusher, B. S. Design and pharmacological activity of phosphinic acid based NAALADase inhibitors. *J. Med. Chem.* **2001**, *44*, 4170–4175.
- Majer, P.; Jackson, P. F.; Delahanty, G.; Grella, B. S.; Ko, Y. S.; Li, W.; Liu, Q.; Maclin, K. M.; Polakova, J.; Shaffer, K. A.; Stoermer, D.; Vitharana, D.; Wang, E. Y.; Zakrzewski, A.; Rojas, C.; Slusher, B. S.; Wozniak, K. M.; Burak, E.; Limsakun, T.; Tsukamoto, T. Synthesis and biological evaluation of thiol-based inhibitors of glutamate carboxypeptidase II: discovery of an orally active GCP II inhibitor. *J. Med. Chem.* **2003**, *46*, 1989–1996.
- Stoermer, D.; Liu, Q.; Hall, M. R.; Flanary, J. M.; Thomas, A. G.; Rojas, C.; Slusher, B. S.; Tsukamoto, T. Synthesis and biological evaluation of hydroxamate-based inhibitors of glutamate carboxypeptidase II. *Bioorg. Med. Chem. Lett.* **2003**, *13*, 2097–2100.
- Ding, P.; Miller, M. J.; Chen, Y.; Helquist, P.; Oliver, A. J.; Wiest, O. Syntheses of conformationally constricted molecules as potential NAALADase/PSMA inhibitors. *Org. Lett.* **2004**, *6*, 1805–1808.
- Majer, P.; Hin, B.; Stoermer, D.; Adams, J.; Xu, W.; Duval, B. R.; Delahanty, G.; Liu, Q.; Stathis, M. J.; Wozniak, K. M.; Slusher, B. S.; Tsukamoto, T. Structural optimization of thiol-based inhibitors of glutamate carboxypeptidase II by modification of the P1' side chain. *J. Med. Chem.* **2006**, *49*, 2876–2885.
- Davis, M. I.; Bennett, M. J.; Thomas, L. M.; Bjorkman, P. J. Crystal structure of prostate-specific membrane antigen, a tumor marker and peptidase. *Proc. Natl. Acad. Sci. U.S.A.* **2005**, *102*, 5981–5986.
- Mesters, J. R.; Barinka, C.; Li, W.; Tsukamoto, T.; Majer, P.; Slusher, B. S.; Konvalinka, J.; Hilgenfeld, R. Structure of glutamate carboxypeptidase II, a drug target in neuronal damage and prostate cancer. *EMBO J.* **2006**, *25*, 1375–1384.

- (25) Otwinowski, Z.; Minor, W. Processing of X-ray Diffraction Data Collected in Oscillation Mode. In *Methods in Enzymology*; Carter Jr., C. W., Sweet, R. M., Eds.; Academic Press: New York 1997; Vol. 276, pp 307–326.
- (26) Barinka, C.; Starkova, J.; Konvalinka, J.; Lubkowski, J. A high-resolution structure of ligand-free glutamate carboxypeptidase II. *Acta Crystallogr. F* **2007**, *63*, 150–153.
- (27) Murshudov, G. N.; Vagin, A. A.; Lebedev, A.; Wilson, K. S.; Dodson, E. J. Efficient anisotropic refinement of macromolecular structures using FFT. *Acta Crystallogr. D* **1999**, *55*, 247–255.
- (28) McRee, D. E. XtalView/Xfit. A versatile program for manipulating atomic coordinates and electron density. *J. Struct. Biol.* **1999**, *125*, 156–165.
- (29) Laskowski, R. A.; McArthur, M. W.; Moss, D. S.; Thornton, J. M. PROCHECK: a program to check the stereochemical quality of protein structures. *J. Appl. Crystallogr.* **1993**, *26*, 283–291.
- (30) Collaborative Computational Project, Number 4. "The CCP4 Suite: Programs for Protein Crystallography". *Acta Crystallogr. D* **1994**, *50*, 760–763.
- (31) Serval, V.; Barbeito, L.; Pittaluga, A.; Cheramy, A.; Lavielle, S.; Glowinski, J. Competitive inhibition of N-acetylated-alpha-linked acidic dipeptidase activity by N-acetyl-L-aspartyl-beta-linked L-glutamate. *J. Neurochem.* **1990**, *55*, 39–46.
- (32) Robinson, M. B.; Blakely, R. D.; Coyle, J. T. Quisqualate selectively inhibits a brain peptidase which cleaves N-acetyl-L-aspartyl-L-glutamate in vitro. *Eur. J. Pharmacol.* **1986**, *130*, 345–347.
- (33) Vitharana, D.; France, J. E.; Scarpetti, D.; Bonneville, G. W.; Majer, P.; Tsukamoto, T. Synthesis and biological evaluation of (R)- and (S)-2-(phosphonomethyl)pentanedioic acids as inhibitors of glutamate carboxypeptidase II. *Tetrahedron: Asymmetry* **2002**, *13*, 1609–1614.
- (34) Flippen, J. L.; Gilardi, R. D. Quisqualic acid. *Acta Crystallogr. B* **1976**, *32*, 951–953.
- (35) Boden, P.; Bycroft, B. W.; Chhabra, S. R.; Chiplin, J.; Crowley, P. J.; Grout, R. J.; King, T. J.; McDonald, E.; Rafferty, P.; Usherwood, P. N. The action of natural and synthetic isomers of quisqualic acid at a well-defined glutamatergic synapse. *Brain Res.* **1986**, *385*, 205–211.
- (36) Jackson, D. E.; Bycroft, B. W.; King, T. J. Crystallographic studies and semi-empirical MNDO calculations on quisqualic acid and its analogs. Systems containing unusual pyramidal heterocyclic ring nitrogens. *J. Comput.-Aided Mol. Des.* **1989**, *2*, 321–328.
- (37) Tiffany, C. W.; Cai, N. S.; Rojas, C.; Slusher, B. S. Binding of the glutamate carboxypeptidase II (NAALADase) inhibitor 2-PMPA to rat brain membranes. *Eur. J. Pharmacol.* **2001**, *427*, 91–96.
- (38) Robinson, M. B.; Blakely, R. D.; Couto, R.; Coyle, J. T. Hydrolysis of the brain dipeptide N-acetyl-L-aspartyl-L-glutamate. Identification and characterization of a novel N-acetylated alpha-linked acidic dipeptidase activity from rat brain. *J. Biol. Chem.* **1987**, *262*, 14498–14506.
- (39) Matzen, L.; Engesgaard, A.; Ebert, B.; Didriksen, M.; Frolund, B.; Krogsgaard-Larsen, P.; Jaroszewski, J. W. AMPA receptor agonists: synthesis, protolytic properties, and pharmacology of 3-isothiazolol bioisosteres of glutamic acid. *J. Med. Chem.* **1997**, *40*, 520–527.
- (40) Hill, R. A.; Wallace, L. J.; Miller, D. D.; Weinstein, D. M.; Shams, G.; Tai, H.; Layer, R. T.; Willins, D.; Uretsky, N. J.; Danthi, S. N. Structure-activity studies for alpha-amino-3-hydroxy-5-methyl-4-isoxazolepropanoic acid receptors: acidic hydroxyphenylalanines. *J. Med. Chem.* **1997**, *40*, 3182–3191.
- (41) Kraulis, P. E. MOLSCRIPT: a program to produce both detailed and schematic plots of protein structures. *J. App. Crystallogr.* **1991**, *24*, 946–950.
- (42) Esnouf, R. M. Further additions to MolScript version 1.4, including reading and contouring of electron-density maps. *Acta Crystallogr. D* **1999**, *55*, 938–940.
- (43) Merritt, E. A.; Murphy, M. E. Raster3D version 2.0. A program for photorealistic molecular graphics. *Acta Crystallogr. D* **1994**, *50*, 869–873.
- (44) DeLano, W. L. *The PyMOL Molecular Graphics System*; Delano Scientific: Palo Alto, CA, 2002.
- (45) Mesters, J.R.; Henning, K.; Hilgenfeld, R. Human glutamate carboxypeptidase II inhibition: structures of GCPII in complex with two potent inhibitors, quisqualate and 2-PMPA. *Acta Crystallogr. D* **2007**, *63*, 508–513.

JM070133W

6.4 GCPIII, a human homolog of GCPII

6.4.1 Background information

Genomic mapping of the human GCPII gene revealed its localization into chromosome 11 but from the beginning the localization was not properly defined and the gene was located using FISH method in both q and p arms of chromosome 11 [1, 213]. In the end it was shown that GCPII is located in the p arm, and homologs of GCPII: glutamate carboxypeptidase III (GCPIII) and NAALADase „like” peptidase (NAALADase L) were shown to reside in the q arm [3, 214].

GCPII sequence has a 67% identity and 81% similarity to GCPIII; and 35% identity and 54% similarity to NAALADase L. Phylogenetic analysis showed that GCPII and GCPIII are the most related proteins from this group. GCPIII also possesses the hydrophobic transmembrane domain and it is also type II membrane protein [3].

It is well established that GCPII is important in neurotransmission and neuronal damage connected with excessive glutamate release (see chapter 3.2 “GCPII as a neuropeptidase“), therefore Bacich *et al.* generated mice with disrupted gene for GCPII (Folh1^{-/-} mice; knock-out mice) to study the morphological changes in their brain. These knock-out mice were behaviorally similar to the wild-type, although less susceptible to stroke and peripheral neuropathies [83]. Activity measurements in tissues from brain revealed residual NAAG-hydrolyzing peptidase activity, although GCPII expression was not detected immunohistochemically. A new peptidase was postulated to be responsible for this residual cleavage. It was suggested that it could be a homolog of GCPII, because this new peptidase was sensitive to GCPII inhibitors [215]. Bzdega *et al.* showed at least two homologous enzymes with similar pharmacological properties and affinity for NAAG in mice: GCPII and GCPIII. Mouse GCPII and GCPIII showed similar K_M and V_{max} values (1.4 μ M and 54 pmol/min/mg; 3.5 μ M and 71 pmol/min/mg, respectively) [216, 217]. Since these two mouse homologs are very similar it is likely that also human GCPII and GCPIII will show high sequence similarity.

Nevertheless, since GCPII is such an important pharmacological target in the neurotransmission and neurological damage, detailed characterisation of human GCPIII, a very close homolog of GCPII, is very important.

We asked several questions: 1) Can GCPIII complement for GCPII activity in knock-out mice or human cells? 2) Are GCPII targeted inhibitors also active against GCPIII? 3) Can GCPIII have a distinct biological role?

6.4.2 Summary

We prepared recombinant glutamate carboxypeptidase III in insect cells and purified it to near homogeneity.

We compared the substrate specificity of GCPII and GCPIII using peptide substrates of general formula Ac-X-Glu-OH and Ac-Asp-X-OH (where X stands for any of 20 standard amino acids). GCPII shows strong preference for Ac-Asp-Glu-OH and Ac-Glu-Glu-OH, however, this is not true for GCPIII. Others substrates in the Ac-X-Glu-OH library are cleaved with approximately equal rates by both studied enzymes. In the Ac-Asp-X-OH library, GCPIII does not significantly hydrolyze any substrate except for Ac-Asp-Glu-OH (NAAG). In contrast, GCPII cleaves Ac-Asp-Ala-OH and Ac-Asp-Met-OH.

Comparison of kinetic constants of both homologs showed that GCPIII less efficiently cleaves Ac-Asp-Glu-OH (NAAG), Ac-Glu-Glu-OH and β -NAAG. The pH dependences are also different; GCPIII has pH optimum in the neutral region, while GCPII optimum is shifted to basic pH. Moreover, the difference in activities between GCPII and GCPIII increases with pH value.

Different substrate specificities and more acidic pH optimum for GCPIII can be caused by the structure of binding cavity. We created a structural model that suggested that the surface of the binding cavity of GCPIII is less positively charged in comparison to GCPII.

Inhibition studies showed that inhibitors of GCPII are also effective for GCPIII; K_I value for 2-PMPA is identical (0.9nM for GCPII and 0.8nM for GCPIII). Nevertheless, there are some modest differences in inhibitor potency between GCPII and GCPIII, which can be explained again by structural model, by the change in polarity and also by the change in geometry of the binding cavity (which is smaller by approximately 30% in GCPIII).

We show that GCPIII hydrolyzing activity is significant enough to compensate for the GCPII activity in GCPII knock-out mice. Even though the substrate specificities are distinct, the inhibition and pharmacological profiles of GCPII and GCPIII are similar. These observations can help in search for biological significance of GCPIII, which is still unknown.

I partially participated in expression of GCPIII and kinetic measurement.

6.4.3 Publication IV

Journal of Neurochemistry, 2007, **101**, 682–696

doi:10.1111/j.1471-4159.2006.04341.x

Biochemical characterization of human glutamate carboxypeptidase III

Klára Hlouchová,*† Cyril Bařinka,*¹ Vojtěch Klusák,* Pavel Šácha,*† Petra Mlčochová,*† Pavel Majer,‡ Lubomír Rulišek* and Jan Konvalinka*†

**Institute of Organic Chemistry and Biochemistry, Academy of Sciences of the Czech Republic, Prague, Czech Republic*

†*Department of Biochemistry, Faculty of Natural Science, Charles University, Prague, Czech Republic*

‡*MGI Pharma Inc., Baltimore, Maryland, USA*

Abstract

Human glutamate carboxypeptidase II (GCP_{II}) is a transmembrane metallopeptidase found mainly in the brain, small intestine, and prostate. In the brain, it cleaves *N*-acetyl-L-aspartyl-glutamate, liberating free glutamate. Inhibition of GCP_{II} has been shown to be neuroprotective in models of stroke and other neurodegenerations. In prostate, it is known as prostate-specific membrane antigen, a cancer marker. Recently, human glutamate carboxypeptidase III (GCP_{III}), a GCP_{II} homolog with 67% amino acid identity, was cloned. While GCP_{II} is recognized as an important pharmaceutical target, no biochemical study of human GCP_{III} is available at present. Here, we report the cloning, expression, and characterization of recombinant human GCP_{III}. We show that GCP_{III} lacks dipeptidylpeptidase IV-like activity, its activity is dependent on

N-glycosylation, and it is effectively inhibited by several known inhibitors of GCP_{II}. In comparison to GCP_{II}, GCP_{III} has lower *N*-acetyl-L-aspartyl-glutamate-hydrolyzing activity, different pH and salt concentration dependence, and distinct substrate specificity, indicating that these homologs might play different biological roles. Based on a molecular model, we provide interpretation of the distinct substrate specificity of both enzymes, and examine the amino acid residues responsible for the differences by site-directed mutagenesis. These results may help to design potent and selective inhibitors of both enzymes.

Keywords: folate hydrolase, metallopeptidase, molecular modeling, *N*-acetylated- α -linked-acidic dipeptidase II, neurodegeneration, prostate-specific membrane antigen. *J. Neurochem.* (2007) **101**, 682–696.

Glutamate carboxypeptidase II (GCP_{II}, EC 3.4.17.21), also known as *N*-acetylated- α -linked-acidic dipeptidase (NAALADase), is a type-II transmembrane metallopeptidase found in a variety of human tissues, primarily in the central nervous system, small intestine, and prostate (Israeli *et al.* 1994; Troyer *et al.* 1995; Silver *et al.* 1997; Chang *et al.* 1999; Renneberg *et al.* 1999; Sokoloff *et al.* 2000). In the brain, it hydrolyzes the peptide neurotransmitter *N*-acetyl-L-aspartyl-glutamate (NAAG), thus liberating free glutamate (Robinson *et al.* 1987). Inhibition of GCP_{II} has been shown to be neuroprotective in animal models of stroke, neuropathic pain and other neurodegenerative states (Slusher *et al.* 1999; Harada *et al.* 2000; Zhang *et al.* 2002; Ghadge *et al.* 2003), and thus it is being considered and tested as a potential therapeutic target (Subasinghe *et al.* 1990; Jackson *et al.* 1996; Nan *et al.* 2000; Whelan 2000; Neale *et al.* 2005; Tsukamoto *et al.* 2005; Zhou *et al.* 2005). In the small intestine, GCP_{II} has been shown to facilitate the absorption

Received August 31, 2006; revised manuscript received October 26, 2006; accepted November 3, 2006.

Address correspondence and reprint requests to Jan Konvalinka, Institute of Organic Chemistry and Biochemistry, Academy of Sciences of the Czech Republic, Flemingovo n. 2, 166 10 Praha 6, Czech Republic. E-mail: konval@uochb.cas.cz

¹The present address of Cyril Bařinka is the Center for Cancer Research, NCI, Frederick, MD 21702, USA.

Abbreviations used: β -NAAG, *N*-acetyl-L-aspartyl- β -linked L-glutamate; 2-PMPA, 2-phosphonomethyl-pentanedioic acid; AccQ, 6-aminoquinolyl-*N*-hydroxysuccinimidyl carbamate; DPP IV, dipeptidyl peptidase IV; HPLC, high-performance liquid chromatography; KO, knock-out; MD, molecular dynamics; MOPS, 3-[*N*-morpholino]propanesulfonic acid; NAAG, *N*-acetyl-L-aspartyl-L-glutamate; NAALADase, *N*-acetylated- α -linked-acidic dipeptidase; OPA, *o*-phthalaldehyde; rhGCP, recombinant human glutamate carboxypeptidase; RMSD, root mean square deviation; SASA, solvent accessible surface area.

of folates by cleaving off the terminal glutamate from poly-gamma-glutamated folates (Pinto *et al.* 1996). In prostate, the physiological role of GCPII is unknown. However, as its expression increases significantly in prostate cancer, it is used as a prostate cancer diagnostic marker (prostate-specific membrane antigen) (Murphy *et al.* 1995; Gregorakis *et al.* 1998; Xiao *et al.* 2001; Schmidt *et al.* 2003).

The notion that GCPII hydrolyzes NAAG *in vivo* was based entirely on cellular response following the application of GCPII inhibitors. To test whether or not GCPII is the only protein with NAAG-hydrolyzing activity, two different groups constructed GCPII knock-out (KO) mice (Bacich *et al.* 2002; Tsai *et al.* 2003). While Tsai *et al.* reported that the deletion of GCPII gene in mice is lethal with embryos failing to develop past mid-term, Bacich *et al.* showed that GCPII KO mice develop normally to adulthood and exhibit a normal range of neurological responses and behaviors.

The results of Bacich *et al.* (2002) suggest that another NAAG-hydrolyzing enzyme might compensate for the missing activity of GCPII. Furthermore, Bacich *et al.* report that two potent inhibitors of GCPII inhibited the NAAG peptidase activity in the brains of GCPII KO mice, in which no GCPII was detected immunohistochemically. Therefore, the existence of a not-yet-identified GCPII homolog, which would compensate for the missing activity, was suggested.

In 1999, Pangalos *et al.* cloned two novel human peptidases, which are closely related to GCPII – NAALADase II [glutamate carboxypeptidase III (GCPIII)] and NAALADase L (Pangalos *et al.* 1999). While NAALADase L was unable to hydrolyze NAAG in transient transfection experiments, transient transfection of GCPIII cDNA confers NAAG-hydrolyzing activity to COS cells, just as had been shown for GCPII. The amino acid sequence of GCPIII was calculated to be 67% identical and 81% similar to that of GCPII (Pangalos *et al.* 1999) (see Fig. 1). The physiological role of this enzyme is unknown. Expression studies using RT-PCR and northern blot hybridization show that GCPIII mRNA is highly expressed in ovary and testes as well as within discrete brain areas (Pangalos *et al.* 1999). As there is no antibody specific to GCPIII available, the expression of the enzyme in various tissues is not known.

Glutamate carboxypeptidase II is increasingly recognized as an important potential pharmaceutical target. However, a detailed biochemical study of its closely related homolog GCPIII is still missing. So far, only mouse GCPIII has been cloned and partially characterized (Bzdega *et al.* 2004). It was reported that Chinese hamster ovary cells transfected with rat GCPII or mouse GCPIII expressed NAAG-hydrolyzing activity with similar V_{max} and K_M values (although V_{max} comparison is not very significant, as levels of protein expression by the transfected cells were not known). GCPIII mRNA levels were similar in brains obtained from wild-type mice and GCPII KO mice. Two potent inhibitors of GCPII, 2-phosphonomethyl-pentanedioic acid (2-PMPA, see

Table 3) and FN6 (4,4'-phosphinobis-butane-1,3 dicarboxylic acid), inhibit the NAAG peptidase activity in the brains of GCPII KO mice. Furthermore, it was shown that they are similarly potent inhibitors of rat GCPII and mouse GCPIII. The authors concluded that the nervous system cells express at least two homologous enzymes with similar pharmacological properties and affinity for NAAG (Bzdega *et al.* 2004). However, careful enzymatic characterization of GCPIII and its direct comparison with GCPII have not been provided.

In this article, we set out to analyze a human GCPII homolog on a molecular level to establish whether or not it could contribute to the NAAG-hydrolyzing activity and whether or not current GCPII inhibitors are able to block this activity completely. To this end, we present the expression, purification, and enzymologic characterization of human GCPIII, analysis of its substrate specificity, pH and ionic strength dependence and homology modeling followed by molecular dynamic simulations of its 3D structure, based on the recently solved 3D structure of human GCPII (Davis *et al.* 2005; Mesters *et al.* 2006).

Experimental procedures

Cloning of recombinant human glutamate carboxypeptidase III

Three different clones (EHS 1001-6454448, IHS 1382-8426921, MHS 1010-7508719), containing either partial or full-length GCPIII cDNA were purchased from Open Biosystems (Huntsville, AL, USA) and plasmid DNA was isolated from individual bacterial cultures. Subsequent sequencing revealed that the IHS1382 clone contained full-length GCPIII cDNA with no mutations and frameshifts, in contrast to the information found in the Open Biosystems database (<http://www.openbiosystems.com>). This clone was therefore used as a template for PCR reactions.

To clone the extracellular part of GCPIII (amino acids 36–740), the cDNA isolated from the IHS1382 clone was PCR-amplified using the primer pair FNAIEXST (5'-AAAGGATCCGAAACGACCACTTCTGTGCGCTATCATC-3') and RNAII (5'-TTTCTCGAGCTATAATACTTCTTTCAGAGTTCTGCTG-3'), with 30 cycles of: 94°C, 30 s; 63°C, 30 s; and 72°C, 4 min. The resulting PCR product was cloned into *BglII/XhoI* sites in the pMT/BiP/V5-HisA plasmid (Invitrogen, San Diego, CA, USA) in frame with the BiP signal sequence for extracellular secretion, and the expression plasmid was designated pMTBiP_NAIlexst. The sequence of the recombinant construct was subsequently verified by DNA sequencing.

Construction of rhGCPII(N519S) and rhGCPIII(S519N) mutants

Mutations N519S and S509N were introduced into pMTNAEXST (Barinka *et al.* 2002) and pMTBiP_NAIlexst, respectively, using the QuikChange Site-Directed Mutagenesis Kit (Stratagene, La Jolla, CA, USA). Primers of the following nucleotide sequence were used for the mutagenesis: FNAIN519S (5'-GCAAATTGGGATCTGGAAGTGATTTTGGAGGTGTTCTTCC-3') and RNAIN519S (5'-GGAAGAACACCTCAAATCACTTCCAGATCCCAATTTGC-3')

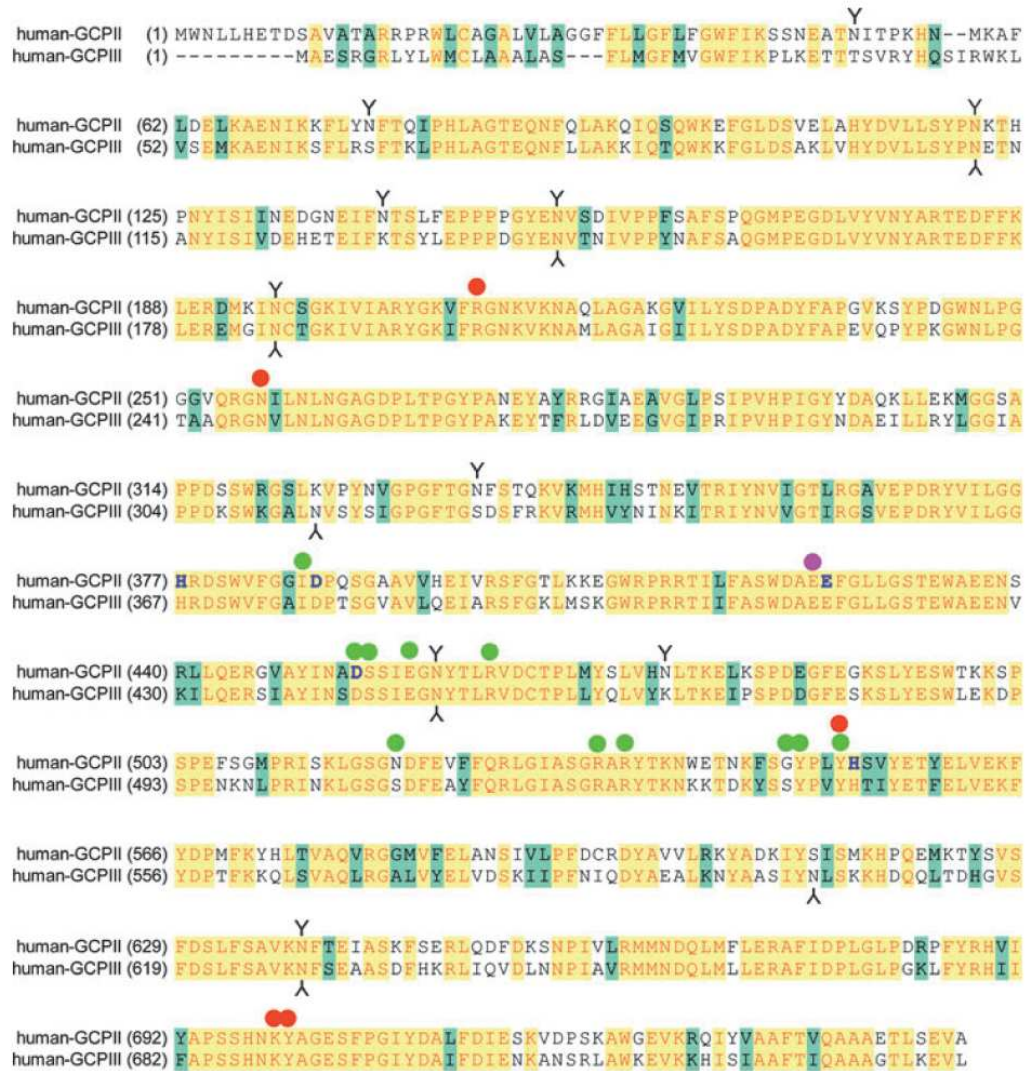


Fig. 1 Alignment of the human GCPII (E.C. 3.4.17.21) and GCPIII protein sequences (using clustal method with PAM250 residue weight table; gap penalty 3). Green ball: proposed residues interacting with the glutamate residue of the substrate in the S1 pocket; red ball:

proposed residues interacting with the glutamate residue of the substrate in the S1' pocket; purple ball: proposed proton shuttle catalytic base; blue residue symbol: zinc ligands; Y: potential N-glycosylation sites (Mesters et al. 2006).

for construction of recombinant human GCPII (rhGCPII) (N509S); FNAIIS509N (5'-CAATAAGCTGGGATCTGGAAATGACTTTG-AAGCTTATTTTC-3') and RNAIIS519N (5'-GAAAATAAGCTTCAAAGTCATTCCAGATCCCAGCTTATTG-3') for construction of rhGCPIII (S509N). The sequences of the recombinant constructs were subsequently verified by DNA sequencing.

The mutant recombinant proteins, designated rhGCPII(N519S) and rhGCPIII (S509N), were expressed in *Drosophila* Schneider's S2 cells and partially purified analogically to rhGCPIII as described below.

Stable transfection of *Drosophila* S2 cells

The *Drosophila* Schneider's S2 cells were grown in SF900II medium (Gibco, Rockville, MD, USA) until they reached a density of $2-4 \times 10^6$ cells/mL. The transfection was performed using the calcium phosphate transfection kit (Invitrogen) using 1 μ g of pCoHYGRO DNA and 19 μ g of pMTBiP_NAIIexst. The calcium phosphate solution was removed 16 h post-transfection and fresh SF900II medium supplemented with 10% fetal bovine serum was added (a complete medium). The cells were grown for one additional day and then the medium was replaced with the complete

medium containing 300 µg/mL Hygromycin B (Invitrogen). The selection medium was changed every 4–5 days. Extensive cell death of non-transfected cells was evident after about 1 week, and cells resistant to Hygromycin B started to grow out 3–4 weeks post-transfection.

Recombinant human GCPIII expression and purification

Large-scale expression of rhGCPIII in SF900II medium was carried out essentially as previously described for the rhGCPII construct (Barinka *et al.* 2002). Following cell harvest by centrifugation (500 g for 10 min), the conditioned medium was dialyzed 3× for 12 h at 4°C against 10 vols of 20 mmol/L 3-[*N*-morpholino]propanesulfonic acid (MOPS), 20 mmol/L NaCl, pH 6.5. The dialyzed medium was mixed with QAE-Sephadex A50 (6 g/L media, Pharmacia, New York, NY, USA) pre-equilibrated in 20 mmol/L MOPS, pH 6.5 (buffer A). The resulting slurry was stirred for 40 min at 24°C and filtered through a sintered glass filter. The retained QAE-Sephadex was washed with 100 mL buffer A. The pooled flow-through fractions were centrifuged at 15 000 g for 10 min at 4°C, filtered through a 0.22 µm filter, and applied onto a Source 15S column (HR10/10, Pharmacia) pre-equilibrated with buffer A at 24°C. The rhGCPIII was eluted with a linear 0–0.5 mol/L NaCl gradient in buffer A. The fractions containing rhGCPIII were pooled, mixed with an equal volume of 100 mmol/L Tris–HCl, 0.8 mol/L NaCl, 2 mmol/L CaCl₂, 2 mmol/L MnCl₂, pH 7.4, and loaded onto a Lentil Lectin-Sepharose (Amersham Biosciences, Uppsala, Sweden) column (C10/10, Pharmacia) equilibrated with 20 mmol/L Tris–HCl, 0.5 mol/L NaCl, 1 mmol/L CaCl₂, 1 mmol/L MnCl₂, pH 7.4 at 4°C. The column was washed extensively, and rhGCPIII was eluted with 20 mmol/L Tris–HCl, 0.5 mol/L NaCl, 0.3 mol/L α-methyl-D-mannoside (Sigma, Praha, Czech Republic), pH 7.4. Fractions containing rhGCPIII were concentrated to a final volume of 2–3 mL using Centriprep YM-50 filters (Millipore, Billerica, MA, USA) and loaded onto a Superdex HR200 column (16/60; Pharmacia) pre-equilibrated with 20 mmol/L MOPS, 100 mmol/L NaCl, pH 7.4. The column was operated by AKTAEplorer FPLC system (AP Biotech, Little Chalfont, UK). Proteins were separated at a flow-rate of 0.5 mL/min and absorbance was monitored at 280 nm. The final protein preparation was concentrated to approximately 200 µg/mL and stored at –70°C until further use.

During purification, rhGCPIII was tracked by sodium dodecyl sulfate–polyacrylamide gel electrophoresis, western blot and radioenzymatic activity assay (see below).

Recombinant human GCPII expression and purification

The extracellular part of human GCPII, which spans amino acids 44–750, was cloned into the pMT/BiP/V5-His A plasmid (Invitrogen), and the recombinant protein (designated rhGCPII) was expressed in *Drosophila* Schneider's S2 cells and purified as described previously (Barinka *et al.* 2002).

Recombinant human GCPII and GCPIII carboxypeptidase activity determination

Radioenzymatic assay

Radioenzymatic assays using ³H-NAAG (radiolabeled on the terminal glutamate) were performed as described previously

(Robinson *et al.* 1987), with minor modifications (Barinka *et al.* 2002). Briefly, 20 mmol/L MOPS, 20 mmol/L NaCl, pH 7.4 (if not stated otherwise) and 10 µL of enzyme solution were pre-incubated for 5 min at 37°C in a final volume of 180 µL. About 20 µL mixture of 0.95 µmol/L 'cold' NAAG (Sigma) and 50 mmol/L ³H-NAAG (50 Ci/mmol in Tris buffer, Perkin–Elmer, Wellesley, MA, USA) were added to each tube and incubation continued for 20 min. The reaction was stopped with 200 µL ice-cold 200 mmol/L sodium phosphate, pH 7.4; free glutamate was separated from the unreacted substrate by ion exchange chromatography, and quantified by liquid scintillation. If not stated otherwise, two duplicate reactions were performed for each measurement.

HPLC assay

Enzymatic reactions were performed in 20 mmol/L MOPS, 20 mmol/L NaCl, pH 7.4 (if not stated otherwise) in a total reaction volume of 120 µL. After incubation for 20 min at 37°C, the reaction was stopped by 60 µL 33 mmol/L EDTA, 66 mmol/L sodium borate, pH 9.2; and the released amino acids were derivatized using 20 µL of 6-aminoquinolyl-*N*-hydroxysuccinimidyl carbamate (AccQ)-Fluor reagent (Waters, Milford, NH, USA) dissolved in acetonitrile. An amount of 50 µL of the resulting mixture was applied to a Luna C18(2)-column (250 × 4.6 mm, 5 µm, Phenomenex, Torrance, CA, USA) mounted to a Waters Alliance 2795 system equipped with a Waters 2475 fluorescence detector and the products were separated using a 20–100% gradient of buffer B (60% acetonitrile, 40% buffer A) in buffer A (140 mmol/L sodium acetate, 17 mmol/L triethanolamine pH 5.05). The run time was 10 min.

Detection of reaction products by *o*-phthalaldehyde modification

80 mg *o*-phthalaldehyde (OPA) (Sigma) was dissolved in 500 µL methanol and transferred into 40 mL of 0.8 mol/L sodium borate, pH 10.0, containing 90 mg *N*-acetyl cysteine (Sigma). This OPA solution (100 µL) was added to an equal volume of the reaction mixtures, vortexed, and left at 24°C for 10 min. Fluorescence was measured on a Perkin–Elmer LS-3B fluorimeter (excitation at 330 nm, emission at 450 nm). If not stated otherwise, two duplicate reactions were performed for each measurement.

Screening of potential substrates

The substrates of general formulae Ac-X-Glu-OH or Ac-Asp-X-OH were prepared by solid phase peptide synthesis on a 2-chlorotrityl-chloride resin (Novabiochem, Darmstadt, Germany) as described previously (Barinka *et al.* 2002).

The individual compounds from the above-mentioned libraries were dissolved in 10% aqueous dimethylsulfoxide (Sigma). An amount of 10 µL of the enzyme (final concentration approximately 4.5 µg/mL, for rhGCPII reaction with Ac-Asp-Glu-OH and Ac-Glu-Glu-OH 0.45 µg/mL) was added to the buffered substrate solutions in a total volume of 100 µL (100 µmol/L individual compound, 20 mmol/L MOPS, 20 mmol/L NaCl pH 7.4). The reactions were allowed to proceed for 1 h at 37°C (the substrate conversion did not exceed 20%), stopped by the addition of 100 µL OPA solution and analyzed spectrofluorimetrically as described above.

The hydrolysis of all substrates from the libraries containing Pro or Lys was inspected by amino acid analysis on Biochrom 20 (Pharmacia Biotech, Uppsala, Sweden). About 100 µL reactions in

20 mmol/L MOPS, 20 mmol/L NaCl, pH 7.4 with 1 mmol/L substrate and 63 µg/mL enzyme concentrations were allowed to react for 1 h at 37°C. Hydrolysis of Ac-Pro-Glu-OH and Ac-Lys-Glu-OH was also determined by high-performance liquid chromatography (HPLC) as described above. A final enzyme concentration of approximately 3.4 µg/mL in 20 mmol/L MOPS, 20 mmol/L NaCl, pH 7.4 was reacted with 100 µmol/L substrate for 20 min at 37°C in a final volume of 120 µL (the substrate conversion did not exceed 5%).

Determination of kinetic parameters for NAAG, β-NAAG, and Ac-Glu-Glu-OH

The kinetics of substrate hydrolysis were determined by HPLC assay [NAAG, *N*-acetyl-L-aspartyl-β-linked L-glutamate (β-NAAG), and Ac-Glu-Glu-OH] and/or radiometric assay (NAAG), as described above. Typically, nanomolar enzyme concentrations were used to hydrolyze 0.4–400 µmol/L substrate in 20 mmol/L MOPS, 20 mmol/L NaCl, pH 7.4 (if not stated otherwise) for 20 min at 37°C. The substrate conversion did not exceed 20% and a total of 8–12 substrate concentration points were used for each determination.

pH Dependence of rhGCPII and rhGCPIII NAAG-hydrolyzing activity

To measure the pH dependence profile, the following selection of 20 mmol/L buffer, 10 mmol/L NaCl was used: citrate pH 4.0–5.0, 2-morpholinoethanesulfonic acid pH 5.0–6.5, MOPS 6.5–8.5, *N*-cyclohexyl-2-aminoethanesulfonic acid 8.5–10, *N*-cyclohexyl-3-aminopropanesulfonic acid 10–11. The profile was measured by fluorescence of products modified by OPA and by radiometric assay as described above.

For the fluorimetric assay, 100 µmol/L NAAG was reacted with approximately 0.5 µg/mL rhGCPII or 5 µg/mL rhGCPIII in a total volume of 100 µL for 1 h at 37°C. For the radiometric assay, reactions contained approximately 30 ng/mL of rhGCPII or 200 ng/mL of rhGCPIII and 100 nmol/L NAAG and proceeded for 20 min at 37°C.

Dependence of rhGCPII and rhGCPIII NAAG-hydrolyzing activity on NaCl concentration

The effect of NaCl concentration on rhGCPII and rhGCPIII enzyme kinetics of NAAG-hydrolysis was measured at 20, 50, 100, and 150 mmol/L NaCl concentrations in 20 mmol/L MOPS, pH 7.4. The radiometric assay described above was used with nanomolar enzyme concentrations so that the substrate conversion did not exceed 20%.

Determination of inhibition constants

Recombinant human glutamate carboxypeptidase III (80 ng/mL) or rhGCPII (20 ng/mL) was pre-incubated with differing inhibitor concentrations in 20 mmol/L MOPS, 20 mmol/L NaCl, pH 7.4, for 15 min at 37°C in a final volume of 180 µL. The radiometric assay described above was then used to measure the activities. The IC_{50} values were determined from the plots of v_i/v_0 (the ratio of individual reaction rates to rate of uninhibited reaction) against the inhibitor concentration using GraFit (version 5.0.4; Erithacus Software Ltd, Horley, UK) and used for the calculation of K_i values by the Morrison's formula for competitive inhibitors (Morrison 1969).

Dipeptidylpeptidase IV-like activity

Dipeptidyl peptidase IV (DPP IV) activity of rhGCPIII and rhGCPII was determined by fluorescent analysis of the Gly-Pro-AMC hydrolysis on a GENios TECAN reader (excitation at 360 nm, emission at 465 nm). Assays were initiated by the addition of enzyme (final concentration of 50 µg/mL) to the buffered substrate solutions (100 µmol/L Gly-Pro-AMC, 150 mmol/L glycine, pH 8.5) in a total reaction volume of 100 µL and monitored for 22 h at 37°C. C6 rat glial cells (cell lysate, final protein concentration of 100 µg/mL) were used as a positive control (Kato *et al.* 1978; Sedo *et al.* 1998).

In parallel, DPP IV activity was analyzed on HPLC using a similar assay as for carboxypeptidase activity (described above). Reactions were initiated by addition of 10 µmol/L Gly-Pro-AMC to the enzyme solution (final enzyme concentration approximately 5 µg/mL) in 20 mmol/L MOPS, 20 mmol/L NaCl, pH 7.4 in a total reaction volume of 60 µL. After incubation for 20 min at 37°C, the reaction was stopped by 30 µL 33 mmol/L EDTA, 66 mmol/L sodium borate, pH 9.2. The fluorescence of AMC was inspected by excitation at 335 nm, emission at 450 nm.

Recombinant human GCPIII and GCPII deglycosylation

An amount of 1 µL of PNGase F (NEB, 1000 U/µL) was used to deglycosylate 6 µg of native rhGCPIII and rhGCPII in 20 mmol/L MOPS, 20 mmol/L NaCl, pH 7.4. The deglycosylation took place at 37°C for 15 h in total volume of 100 µL.

Mass spectrometry

Matrix-assisted laser desorption/ionization (MALDI) mass spectra of rhGCPIII and rhGCPII were inspected by MALDI-TOF spectrometer Reflex4 (Bruker Daltonics, Bremen, Germany) using sinapic acid (Sigma) as the matrix.

Molecular modeling of GCPIII

- Protein(s) setup. All molecular dynamics (MD) simulations were based on the 2.0-Å structure of GCP II complexed with the inhibitor, 2-(4-iodobenzylphosphonomethyl)-pentanedioic acid (RCSB Protein Data Bank accession number 2C6C) (Mesters *et al.* 2006). Prior to MD simulations, three missing loops (consisting of 12 amino acids in total, Thr334-Phe337, Trp541-Phe546, Lys655-Ser656) were added using the GCP II structure at 3.5 Å resolution as a template (Davis *et al.* 2005). Then, a total number of ~100 atoms not resolved in side chains (i.e., missing in the structure coordinate file) were added by leap module of AMBER 8 (Case *et al.* 2004), using standard libraries. Finally, hydrogen atoms were added to the crystal structure and the system was solvated in a truncated octahedral box. The positions of (i) all the hydrogen atoms, (ii) all non-hydrogen atoms added to the original crystal structure as described above and (iii) all atoms of solvent water molecules were then optimized by a 300-ps simulated annealing (i.e., MD simulation at varying temperature under constant volume and periodic boundary conditions; for a detailed protocol, see below) followed by a conjugate gradient energy minimization of their positions. We assumed the normal protonation state at pH 7 for all amino acids (i.e., Glu, Asp in their deprotonated – anionic – form, and Lys, Arg in the protonated – cationic – form). For the His residues, the protonation status was decided from a detailed study of the hydrogen-bond network around the residue and the solvent

accessibility. Thus, in GCP II, His 82, 347, 377, 553, and 573 were assumed to be protonated on the N^{δ1} atom, His 112, 124, 295, 396, 475, 689, and 697 on the N^{ε2} atom, whereas His 345 and 618 were considered to be protonated on both nitrogens.

- The initial GCPIII structure was then obtained by a replacement of the respective amino acid residues, preserving the GCPII geometry of main chain atoms, and using the side chain templates from standard Amber library (leap module). The protonation states of histidines were assumed as follows: His 82, 377, 553, and 731 were assumed to be protonated on the N^{δ1} atom, His 112, 134, 295, 625, 647, 689, and 697 on the N^{ε2} atom, whereas His 345 and 618 were considered to be protonated on both nitrogens. Finally, to improve a poor description of electrostatics in the local environment of binuclear zinc(II) site, the default Amber charges were replaced by the ESP-fitted ones for ~60 atoms comprising the active site – Zn₂(His)₂(Asp)₂(Glu)(OH) system.

- Molecular dynamics simulations. All MD simulations have been carried out with AMBER 8 (Case *et al.* 2004) program, using the Cornell force field (all_amin03.in) (Cornell *et al.* 1995). For a solvation model, explicit TIP3P water molecules were used with the boundaries of the truncated octahedron 9.0 Å outside any atom of the protein (resulting in the 105 × 105 × 105 Å box size, total number of ~73 000 atoms in the simulation). The simulated annealing protocol consisted of 45 ps of heating the system up to 370 K, 150 ps of constant temperature simulation at 370 K, and 105 ps cooling the system to 0 K (with the time step of 1.5 fs). A cut-off for the non-bond interactions of 8.0 Å was employed. The bonds involving hydrogens were kept fixed at their equilibrium values by the SHAKE algorithm and dielectric constant of 1.0 was used in all simulations. Each MD simulation was then followed by the minimization of the resulting structure with the solvent molecules removed, except for 10 Å solvation shell of the protein, yielding the final structures that we refer to in this work. During the minimization, no cut-off has been used for non-bond interactions.

- Structure analysis. The final equilibrium structures of the two proteins obtained from the MD simulations were compared with respect to the overall fold, root mean square deviation (RMSD), cavity volume and cavity polarity. The disposable volume around the ligand was estimated by the program SURFNET (Laskowski 1995) with the following parameters: calculating the gaps between protein and inhibitor with grid separation 1 Å, minimum and maximum radius for gap spheres being 1.2 and 20 Å, respectively. The cavity surface was visualized using Pymol (DeLano 2002) and colored according to the vacuum electrostatic potential. Change in polarity of the cavity surface was estimated by comparing the solvent accessible surfaces of the charged functional groups (Arg, Lys, Glu, Asp) in the cavity using vmd program suite (Humphrey *et al.* 1996).

Results

Cloning, expression, and purification of human GCPIII

Three clones containing the human GCPIII sequence were identified by search in the Open Biosystems database, and the clone IHS 1382-8426921, spanning the full-length cDNA for GCPIII, was used for subsequent cloning. The sequence coding for the predicted extracellular part of GCPIII (rhGCPIII, amino acids 36–740) was PCR-amplified and

cloned into pMTBiP/V5-His A *Drosophila* expression vector, in frame with the BiP signal sequence that directs secretion of the protein into the medium. rhGCPIII was efficiently secreted by the stably transfected S2 cells, and the enzyme was purified from the conditioned medium using ion-exchange chromatography on QAE-Sephadex A50, ion-exchange chromatography on a Source 15S column, and affinity chromatography on Lentil Lectin-Sepharose, exploiting the predicted *N*-glycosylation of GCPIII for the purification (Barinka *et al.* 2004b). Finally, the protein was purified by gel filtration on a Superdex HR200 column. The final purity of the protein was higher than 70% with a yield of approximately 1 mg of rhGCPIII per liter of media (Fig. 2, panel d). The protein was recognized by monoclonal antibody GCP-04 (Fig. 2, panel c), which was raised against rhGCPII (Barinka *et al.* 2004a).

Activity and substrate specificity of rhGCPIII when compared with rhGCPII

The availability of pure, active rhGCPIII enabled detailed analysis of its substrate specificity in direct comparison with its homolog rhGCPII. A panel of dipeptides of general formulae Ac-X-Glu-OH and Ac-Asp-X-OH (X stands for any naturally occurring L amino acid) was used for the analysis of the specificity of rhGCPIII in the S1 and S1' subsites (Barinka *et al.* 2002). Identical amounts of rhGCPII and rhGCPIII were used in the cleavage reaction (with the exception of Ac-Asp-Glu-OH and Ac-Glu-Glu-OH hydrolysis by rhGCPII, in which the enzyme was 10 times more diluted). The cleavage of the C-terminal amino acid was analyzed fluorimetrically using OPA derivatization, except for the substrates containing proline or lysine (those were analyzed by amino acid analysis and/or HPLC assay following product derivatization by an AccQ-Fluor reagent; hydrolysis of these substrates was normalized to the cleavage of NAAG, which was used as a control). The products of the dipeptide hydrolysis were detected as an increase in fluorescence at $\lambda(\text{EX})/\lambda(\text{EM}) = 330/450$ nm. The results of the assays are summarized in Figs 2a and b.

In agreement with earlier studies reported by our laboratory, rhGCPII was found to cleave Ac-Asp-Glu-OH (NAAG) and Ac-Glu-Glu-OH more efficiently by at least one order of magnitude than other compounds in the tested peptide libraries. However, this was not the case for rhGCPIII. The hydrolysis of Ac-Asp-Glu-OH and Ac-Glu-Glu-OH seems to be significantly less efficient than for rhGCPII. Other substrates in the Ac-X-Glu-OH library are hydrolyzed with approximately equal rates by rhGCPII and rhGCPIII. In the Ac-Asp-X-OH library, rhGCPIII does not significantly hydrolyze any substrate except for NAAG under the conditions selected. In contrast, rhGCPII effectively hydrolyzes Ac-Asp-Ala-OH and Ac-Asp-Met-OH as well. To verify that the enzyme responsible for the hydrolysis

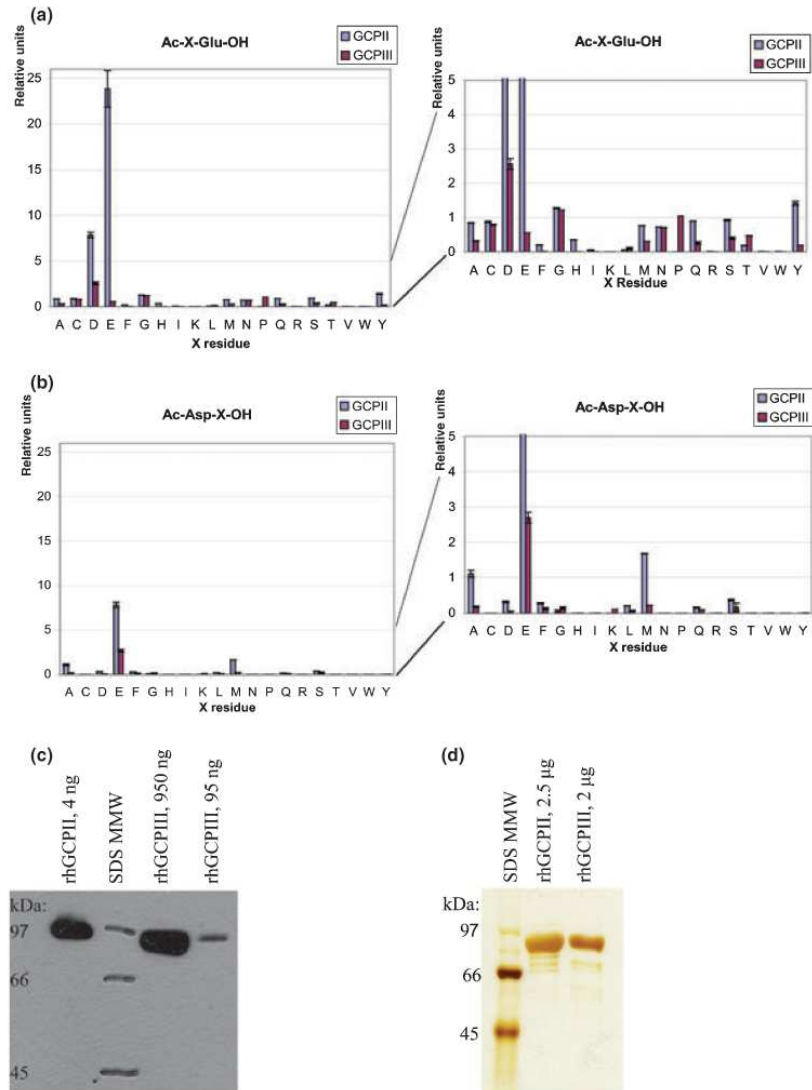


Fig. 2 Comparison of substrate specificities of rhGCP II and rhGCP III in the P1 (panel a) and P1' (panel b) positions. Substrates of the general formula Ac-X-Glu-OH and Ac-Asp-X-OH (X standing for any naturally occurring amino acid except for Lys or Pro) were reacted with an enzyme (final concentration approximately 4.5 µg/mL, for rhGCP II reaction with Ac-Asp-Glu-OH and Ac-Glu-Glu-OH 0.45 µg/mL) and the products were detected spectrofluorimetrically after derivatization with *o*-phthalaldehyde. Cleavage of the substrates containing Lys or Pro was analyzed by amino acid analysis and/or HPLC assay following product derivatization by an AccQ-Fluor reagent. Hydrolysis of these substrates was recalculated relative to NAAg, which was used as a

control. On the right-hand side of both panels, the lower range (below 5 relative units) is expanded to allow for a better comparison between GCP II and GCP III enzymatic activities against the less favored substrates. Panel c: western blot of purified rhGCP II and rhGCP III with monoclonal antibody GCP-04. Indicated amounts of protein were resolved by 10% SDS-PAGE, electroblotted onto a nitrocellulose membrane, probed with the antibody GCP-04 and visualized by HRP-labeled anti-mouse antibody. Panel d: purity of rhGCP II and rhGCP III. Indicated amounts of protein were resolved by 11% SDS-PAGE and visualized by silver staining.

Table 1 Direct comparison of NAAG, β -NAAG and Ac-Glu-Glu-OH hydrolysis by rhGCPII and rhGCPIII

Substrate	GCPII			GCPIII		
	K_M (nmol/L)	k_{cat} (per second)	k_{cat}/K_M [$10^5/s/(mol/L)$]	K_M (nmol/L)	k_{cat} (per second)	k_{cat}/K_M [$10^5/s/(mol/L)$]
NAAG	1200 \pm 500	1.1 \pm 0.2	9.3 \pm 4.9 ^{ab}	370 \pm 70	0.11 \pm 0.01	3.0 \pm 0.6 ^b
Ac-Glu-Glu-OH	2600 \pm 800	3.7 \pm 0.4	14.1 \pm 4.5 ^a	3640 \pm 1080	0.29 \pm 0.02	0.8 \pm 0.2 ^a
β -NAAG	1400 \pm 200	0.30 \pm 0.01	2.1 \pm 0.3 ^a	5200 \pm 1000	0.15 \pm 0.01	0.3 \pm 0.1 ^a

Nanomolar enzyme concentrations were used to hydrolyze 0.4–400 μ mol/L concentration of the analyzed substrate in 20 mmol/L MOPS, 20 mmol/L NaCl, pH 7.4. Enzyme kinetics of substrate hydrolysis was determined by HPLC assay ^a(NAAG, β -NAAG and Ac-Glu-Glu-OH) and/or radiometric assay ^b(NAAG).

reactions was rhGCPII/rhGCPIII rather than a host factor copurified with the enzyme (e.g., traces of *Drosophila* beta galactosidase protein, EC 3.2.1.23, were identified in the final rhGCPIII preparation by N-terminal sequencing), control reactions in the presence of the GCPII-specific inhibitor 2-PMPA (Jackson *et al.* 1996; Bzdega *et al.* 2004) were performed. No substrate hydrolysis was detected (data not shown).

Direct comparison of the enzymatic activity on cognate substrates was performed using NAAG, Ac-Glu-Glu-OH, and β -NAAG (refer to Pharmacological profile of rhGCPIII section). The substrates were cleaved by purified, titrated rhGCPII and rhGCPIII in 20 mmol/L MOPS, 20 mmol/L NaCl, pH 7.4 (see Experimental procedures section). The results are summarized in Table 1. The cleavage of the identified substrates by both enzymes follows Michaelis–Menten kinetics. The rhGCPIII K_M and k_{cat} constants for NAAG hydrolysis are 370 nmol/L and 0.11/s, respectively, suggesting that the catalytic efficiency of rhGCPIII for NAAG-hydrolysis is about threefold lower than that of rhGCPII in this particular set of conditions. The catalytic efficiency of rhGCPIII for Ac-Glu-Glu-OH is about 18-fold lower than that of rhGCPII.

DPP-IV-like activity of rhGCPII and rhGCPIII

Pangalos *et al.* (1999) reported a DPP-IV-like activity of COS cells transfected by GCPII and GCPIII cDNAs. We have previously shown (Barinka *et al.* 2002) that purified rhGCPII reveals no measurable hydrolysis of a typical fluorogenic substrate of DPP-IV, Gly-Pro-AMC (Kato *et al.* 1978; Sedo *et al.* 1998). Similarly, under the conditions described in the Experimental procedures section, we detected negligible DPP-IV-like activity (turnover lower than 0.01/s) using purified rhGCPIII.

Site-directed mutagenesis around the active site: NAAG-hydrolyzing activity of rhGCPII(N519S) and rhGCPIII(S509N)

In an effort to explain the differences in the proteolytic activities of rhGCPII and rhGCPIII, the amino acid residues of GCPII involved in the recognition of substrate/inhibitors [(Mesters *et al.* 2006) and Mlcochova *et al.*, unpublished

data] were compared with the corresponding residues in the GCPIII protein sequence (see Fig. 1). The only noticeable difference between the two enzymes was the residue at position 519 (509 for GCP III), which is asparagine in GCPII and serine in GCPIII. As Asn519 has been proposed to bind the *N*-acetyl-aspartate part of NAAG (Mesters *et al.* 2006), recombinant proteins introducing the corresponding amino acid exchange in GCPII (N519S) and GCPIII (S509N) were cloned, expressed, and partially purified, and their NAAG-hydrolyzing activities were characterized. Results are summarized in Table 2. While mutation N519S of rhGCPII caused an approximately 10-fold decrease in K_M , the mutation S509N of rhGCPIII did not significantly change the value of K_M . Both mutations brought about a decrease in k_{cat} values in comparison with the wild-type proteins.

pH Dependence of rhGCPII and rhGCPIII

The pH dependence of NAAG hydrolysis by rhGCPII and rhGCPIII was measured in the pH range 4.0–11.0 at a saturating substrate concentration (100 μ mol/L, by both the radiometric assay and fluorescence measurement using OPA derivatization, see Experimental procedures section for details) as well as at sub- K_M substrate concentration (100 nmol/L, the radiometric assay). The corresponding curves could thus be approximated as the pH dependence of k_{cat}/K_M (Fig. 3, panel a) and k_{cat} (panel b) for individual enzymes. rhGCPII shows a significant decrease in K_M

Table 2 Kinetic parameters for rhGCPII, rhGCPIII, rhGCPII(N519S) and rhGCPIII(S509N) NAAG hydrolysis

Recombinant protein	K_M (nmol/L)	k_{cat} (per second)	k_{cat}/K_M [$10^5/s/(mol/L)$]
rhGCPII	1200 \pm 500	1.1 \pm 0.2	9.3 \pm 4.9
rhGCPIII	370 \pm 70	0.11 \pm 0.01	3.0 \pm 0.6
rhGCPII(N509S)	100 \pm 30	0.42 \pm 0.02	41 \pm 12
rhGCPIII(S509N)	410 \pm 110	0.026 \pm 0.002	0.6 \pm 0.2

NAAG hydrolysis was measured using the radiometric assay (see Experimental procedures section). Nanomolar enzyme concentrations were used to hydrolyze 0.4–400 μ mol/L concentration of the analyzed substrate in 20 mmol/L MOPS, 20 mmol/L NaCl, pH 7.4.

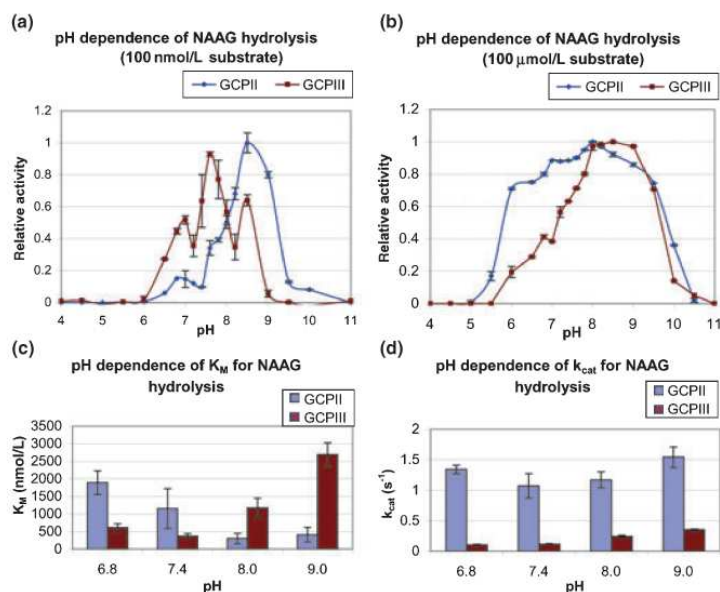


Fig. 3 pH dependence of rhGCPII and rhGCPIII NAAG-hydrolyzing activity. The pH dependence of NAAG hydrolysis by rhGCPII and rhGCPIII was measured using the following selection of 20 mmol/L buffer, 20 mmol/L NaCl: citrate pH 4.0–5.0, MES pH 5.0–6.5, MOPS 6.5–8.5, CHES 8.5–10, CAPS 10–11. Panels a and b: pH dependence curve for rhGCPII (blue) and rhGCPIII (red) measured with 100 nmol/L (panel a) and 100 μ mol/L (panel b) substrate concentration. For the fluorimetric assay, 100 μ mol/L NAAG was reacted with approximately 0.5 μ g/mL rhGCPII or 5 μ g/mL rhGCPIII. For the radiometric assay, reactions of less than 0.5 μ g/mL enzyme with 100 nmol/L NAAG were used. The dependency curves were derived statistically from two

independent measurements, each comprising of duplicate reactions. Panels c and d: kinetic constants (K_M , panel c; k_{cat} , panel d) of NAAG hydrolysis in pH values of 6.8, 7.4, 8.0 and 9.0. Enzyme kinetics of NAAG hydrolysis was determined by HPLC assay and/or radiometric assay. Nanomolar enzyme concentrations were used to hydrolyze 0.4–400 μ mol/L concentration of the analyzed substrate. The substrate conversion did not exceed 20% and a total of 8–12 substrate concentration points measured in duplicates were used for single determination. Typically, two independent measurements were performed to determine an average value.

from pH 6.8 to 9.0, while the k_{cat} value over the pH region is almost constant. On the contrary, pH dependence values for rhGCPIII suggest a more acidic pH optimum for K_M (around 7.4; Fig. 3, panel c) and an apparent increase in k_{cat} value between pH 6.0 and 9.0 (Fig. 3, panels b and d). At selected pH values, the kinetic constants for NAAG-hydrolysis by the enzymes were determined. The overall catalytic efficiency optimum of rhGCPII is shifted to basic pH, compared with the optimum of rhGCPIII, which is around pH 7.4 (Fig. 3, panel a). Taken together, rhGCPIII shows a more pronounced pH dependence than rhGCPII and the difference in activities between rhGCPII and rhGCPIII increases with pH value.

Dependence of rhGCPII and rhGCPIII NAAG-hydrolyzing activity on salt concentration

The effect of NaCl on rhGCPII and rhGCPIII NAAG-hydrolyzing activity was assayed at concentrations of 20, 50, 100, and 150 mmol/L NaCl (Fig. 4). Interestingly, rhGCPII and rhGCPIII show opposite dependence of K_M on the NaCl

concentration: while rhGCPII binds its substrate better in higher salt concentrations (a few fold decrease in the K_M value between 20 and 50 mmol/L NaCl), rhGCPIII has a higher affinity for NAAG at 20 mmol/L than at 50 mmol/L NaCl (Fig. 4a). The value of k_{cat} changes significantly only for rhGCPIII at the concentrations of NaCl tested (Fig. 4b), while the k_{cat} for GCPII remains nearly constant. The overall catalytic efficiency (expressed as k_{cat}/K_M) of NAAG hydrolysis is not significantly affected by NaCl concentration for rhGCPIII, while for rhGCPII it increases significantly from 20 to 150 mmol/L NaCl concentrations.

Pharmacological profile of rhGCPIII

As GCPIII activity was suggested to be a compensatory NAAG-hydrolyzing activity in GCPII KO mice (Bacich *et al.* 2002) and only limited data exists whether or not this homolog is inhibited by compounds targeting GCPII, we set out to directly compare the inhibition pattern of rhGCPIII and GCPII. To this end, we analyzed rhGCPIII inhibition by general metalloproteinase inhibitors (EDTA, 1,10-phenanthr-

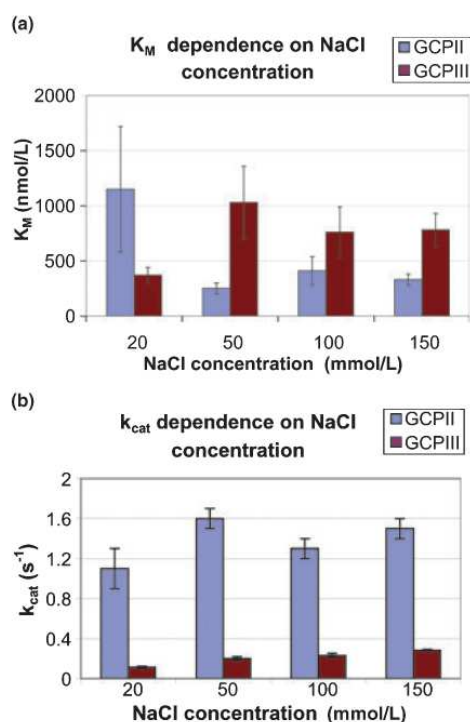


Fig. 4 Dependence of rhGCPII and rhGCPIII NAAG-hydrolyzing activity on NaCl concentration. Panels a and b: the effect of NaCl concentration on rhGCPII and rhGCPIII NAAG-hydrolyzing activity was measured in 20, 50, 100, and 150 mmol/L NaCl concentration in 20 mmol/L MOPS, pH 7.4. The radiometric assay described above was used with nanomolar enzyme concentrations so that the conversion of substrate did not exceed 20%.

oline), substrate analogs (β -NAAG), and phosphonate, phosphinate- or thiol-based compounds designed as GCPII inhibitors (Jackson *et al.* 1996; Tsukamoto *et al.* 2002, 2005; Majer *et al.* 2003, 2006).

Consistent with the notion that GCPIII is a cocatalytic metallopeptidase and that its hydrolytic activity is metal-ion-dependent, all of the chelating agents tested completely abolished its proteolytic activity (data not shown). Surprisingly, β -NAAG, a conformational analog of NAAG that is reported to be a competitive inhibitor of GCPII with a K_I value of 0.7 μ mol/L (Serval *et al.* 1990), turned out to be hydrolyzed by both rhGCPIII and rhGCPII quite efficiently. The cleavage of this 'substrate-inhibitor' by both enzymes follows Michaelis–Menten kinetics with kinetic constants $K_M = 1.4$ μ mol/L, $k_{cat} = 0.3/s$ and $K_M = 5.2$ μ mol/L, $k_{cat} = 0.15/s$ for rhGCPII and rhGCPIII, respectively (see Table 1).

To extend these inhibition studies, IC_{50} values for seven different inhibitors, originally designed as GCPII-specific

inhibitors, were assessed using rhGCPII and III and the radioenzymatic assay. First, we determined that 2-PMPA is a competitive inhibitor of rhGCPIII with a K_I of 0.9 nmol/L, and this compound was subsequently used for the active-site titration of rhGCPIII (data not shown). The IC_{50} values for other inhibitors were then utilized for calculation of K_I values using Morrison's formula for competitive inhibitors (Morrison 1969), and the results are summarized in Table 3. Reflecting the sequence and likely structural (see below) similarity between rhGCPII and rhGCPIII, the potencies (i.e., K_I values) of all the compounds against the two peptidases are comparable. The only noticeable differences were observed for inhibition constants of inhibitors I-2 (RS), (S), and (R), which show several fold lower K_I values for rhGCPIII than rhGCPII. Additionally, it is interesting to note that the (S)-enantiomer of I-2, which has a stereochemical configuration analogous to L-glutamate of NAAG, is more potent in terms of rhGCPII/rhGCPIII inhibition than the corresponding (R)-form. This finding is consistent with GCPII (and supposedly GCPIII) preferences for L-amino acid-containing substrates as well as data for the inhibition constants of (R,S)-enantiomers of 2-PMPA (Robinson *et al.* 1987; Vitharana *et al.* 2002). Taken together, the pharmacological profiles for both NAAG-peptidases are quite similar and inhibitors designed against GCPII also effectively inhibit rhGCPIII activity. It could therefore be hypothesized that *in vivo* administration of GCPII/GCPIII inhibitors would completely abolish total NAAG-peptidase activity in the targeted area.

Mass spectrometry

The mass of the polypeptide backbone of both rhGCPII and rhGCPIII calculated from the known amino acid sequence is 79.8 kDa. Mass spectrometry analysis showed that the molecular weight of the recombinant glycosylated proteins rhGCPII and rhGCPIII is approximately 89.1 kDa in both cases. For both proteins, post-translational modifications represent approximately 9.3 kDa, while the number of potential N-glycosylation sites in GCPII and GCPIII is 10 and 7, respectively (Fig. 1).

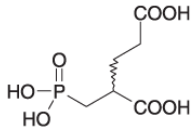
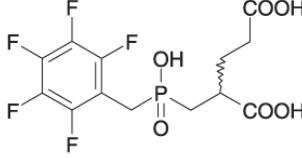
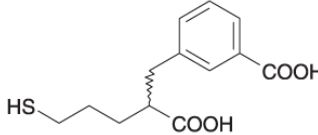
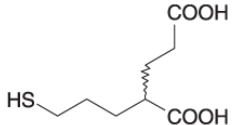
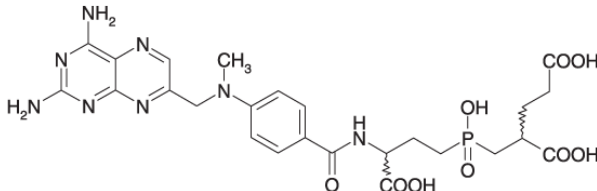
Role of N-glycosylation

It has been shown for GCPII that its N-glycosylations are vital for the carboxypeptidase activity (Barinka *et al.* 2002, 2004b; Ghosh and Heston 2003). To determine the role of N-glycosylation on GCPIII activity, rhGCPIII was deglycosylated using PNGase F. Similarly to GCPII, deglycosylation of the native protein completely abolished its carboxypeptidase activity (data not shown).

Molecular modeling of GCPIII structure

As shown in Fig. 1, the amino acid sequence of GCPIII is 67% identical and 81% similar to that of GCPII. Such a high level of sequence similarity implies a high level of structural similarity. To analyze and interpret the differences in

Table 3 Comparative analysis of rhGCP II and rhGCP III inhibition by specific inhibitors

Inhibitor	Molecular formula	K_i for rhGCP II (nmol/L)	K_i for rhGCP III (nmol/L)
I-1		0.9 ± 0.2	0.8 ± 0.1
I-2 (RS)		27 ± 9	8.1 ± 3.2
I-2 (S)		17 ± 4	2.0 ± 1.6
I-2 (R)		480 ± 140	120 ± 53
I-3		7.4 ± 2.9	15 ± 3
I-4		14 ± 6	58 ± 25
I-5		0.12 ± 0.03	0.35 ± 0.28

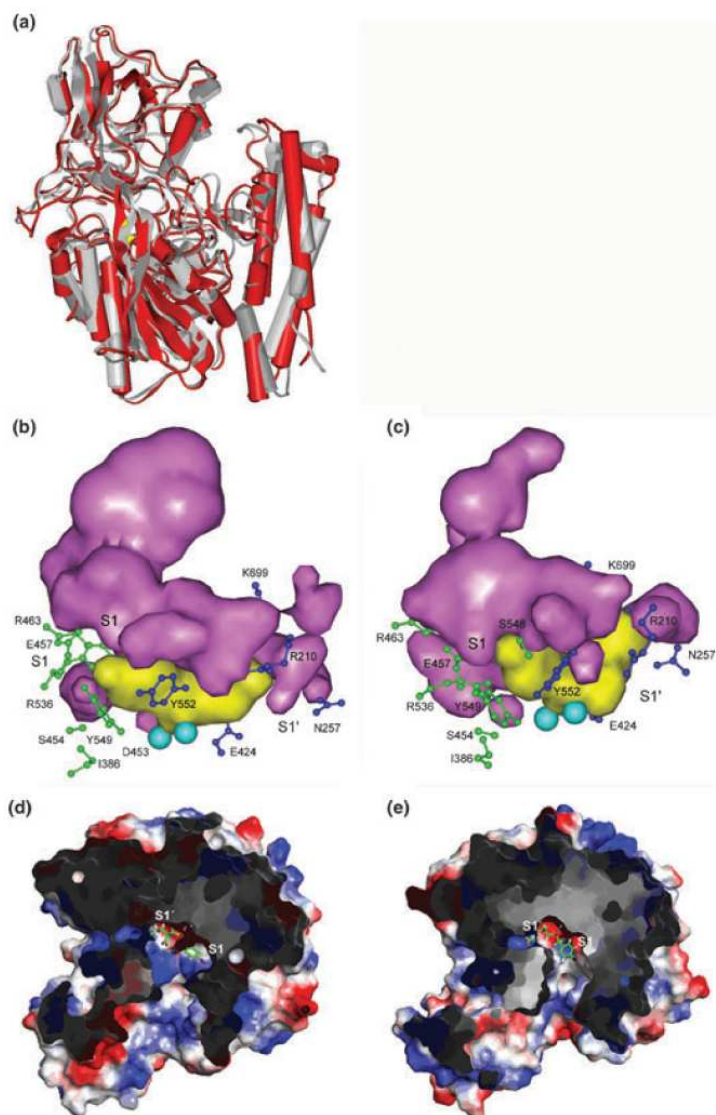
IC_{50} values were used for the calculation of K_i values using the Morrison's formula for competitive inhibitors (Morrison 1969). I-1 is a racemate form of 2-PMPA (Jackson *et al.* 1996), I-2(RS) is the racemate of 2-(hydroxy-pentafluorophenylmethyl-phosphinoylmethyl) pentanedioic acid, while I-2(S) and I-2(R) are its individual enantiomers [compounds RS-2, S-2 and R-2 from (Tsukamoto *et al.* 2005)]. Inhibitor I-3 is 3-(2-carboxy-5-mercapto-pentyl)-benzoic acid [compound 6c in (Majer *et al.* 2006)]. I-4 is 2-(3-mercapto-propyl)pentanedioic acid [compound 4d in (Majer *et al.* 2003)] and I-5 is a phosphinate analog of *N*-acylated γ -glutamylglutamate [compound 4 in (Tsukamoto *et al.* 2002)]. The radiometric assay was used (see Experimental procedures section).

enzymatic activities between GCP II and GCP III, we constructed a model of the 3D structure of GCP III as described in the Experimental procedures section.

The final equilibrium structures of the two proteins obtained from the MD simulations were compared with

respect to the overall fold, RMSD, cavity volume and cavity polarity. The direct comparison of the GCP II and GCP III structures is provided in Fig. 5, panel a. The figure shows a high structural similarity between the two homologous enzymes with an identical overall fold. The backbone RMSD

Fig. 5 Molecular model of GCPIII structure. Panel a: structural model of GCPIII (red) superimposed on the 3D structure of GCPII (gray) in complex with specific inhibitor (Mesters *et al.* 2006) as obtained from MD simulation (see Experimental procedures section for details). Catalytic zinc atoms depicted as yellow spheres. Panels b and c: comparison of active-site clefts of GCPII and GCPIII as seen from molecular modeling. Binding site cavities of GCPII (panel b) and GCPIII (panel c) as compared using program SURFNET. Yellow shows the inhibitor, 2-(4-iodobenzylphosphonomethyl)-pentanedioic acid, bound in the cavity; purple represents the remaining volume of the active-site cavity. The catalytic zinc atoms depicted as light blue spheres, S1 proposed residues in green, S1' residues in blue. The volume of the cavity in GCPIII is smaller by roughly 30% in comparison with GCPII. Panels d and e: A cut through the surface of the GCPII (panel d) and GCPIII (panel e), colored according to the vacuum electrostatics potential in Pymol (DeLano 2002). The surfaces of the binding site cavities of GCPII and GCPIII are shown with charged residues depicted in blue (positive) and red (negative). Inhibitor 2-(4-iodobenzylphosphonomethyl)-pentanedioic acid bound in the cavity.



is 2.17 Å. While the overall fold is preserved in both enzymes, the structure of the substrate/inhibitor binding cavities of GCPII and III significantly differs. The differences are mainly in the size and shape of the cavities as well as in their surface charge. The change of cavity polarity is important as the native substrate of the enzymes, Ac-Asp-Glu, is negatively charged (formal charge -3). The effective charge could be quantified by measuring the solvent accessible surface area (SASA) of the charged groups exposed on the cavity surface. We have identified 15 charged residues on the cavity surface. All of them are preserved in the sequence of GCPIII and are mostly present in the cavity.

The prevailing charge on the surface of the cavity of GCPII is positive. The positive/negative surface ratio is 3.6 (151/42). In case of GCPIII, the positive charge also prevails but the ratio is only 1.7 (114/66) because of decrease in the positive SASA and, at the same time, increase in the negative SASA. Although the charged residues in the PR binding cavity are conserved, the conformation change leads to a considerable decrease in the positively charged surface and minor increase in the negatively charged surface (Fig. 5, panels d and e).

Our model also reveals a change in the shape of the substrate-binding pocket. The accessible volume between the

ligand and the protein is significantly smaller in the case of GCPIII in comparison to GCPII, representing a mere 68% of that in GCPII. (Fig. 5, panels b and c).

Discussion

Glutamate carboxypeptidase II is now becoming widely recognized as an important pharmaceutical target and a diagnostic tool for a number of pathologies ranging from neuropathy to prostate cancer. Therefore, its homologs with the potential to compensate for GCPII enzymatic activity or other potential functions represent a very relevant target of enzymologic research. In this report we analyze GCPIII, a homolog of human GCPII, and address the following questions: (i) what is the substrate specificity of GCPIII? (ii) how do the activities of the two enzymes relate? (iii) could GCPIII compensate for the activity of GCPII and could it be inhibited by the existing inhibitors designed against GCPII?

To answer the first question, a panel of dipeptides of general formulae Ac-X-Glu-OH and Ac-Asp-X-OH was used for direct comparison of the specificity of these two enzymes in the S1 and S1' binding pockets (Barinka *et al.* 2002). As we reported earlier, rhGCPII shows a strong preference for Ac-Asp-Glu-OH (NAAG) and Ac-Glu-Glu-OH, and all other tested substrates (including Ac-Asp-Met-OH) are cleaved at least one order of magnitude less efficiently. In contrast, the substrate specificity of rhGCPIII seems to be less pronounced. While the other substrates in the libraries are cleaved with similar efficiencies by both enzymes, the cognate substrate, Ac-Asp-Glu-OH, is cleaved less effectively by rhGCPIII. Furthermore, in contrast to rhGCPII, rhGCPIII does not cleave Ac-Asp-Ala-OH and Ac-Asp-Met-OH.

To directly compare the catalytic efficiencies of the two enzymes, we determined the kinetic constants of the cleavage of the cognate substrate of GCPII, Ac-Asp-Glu-OH (NAAG), and of two other substrates, Ac-Glu-Glu-OH and β -NAAG. rhGCPIII hydrolyzed all three substrates less efficiently, but only in case of Ac-Glu-Glu-OH did this difference exceed one order of magnitude, suggesting thus different structural preferences for the amino acid occupying the P1 position of the substrate.

This measurement was performed at pH 7.4, which is arguably close to the environment of a neuronal synapse. However, for a meaningful activity comparison, optimal conditions for both enzymes (namely the pH and salt concentration optima) should also be considered, especially when the physiological activity and localization of GCPIII are not known.

An earlier study by Bzdega *et al.* (2004) shows that the pH dependencies of rat GCPII and mouse GCPIII NAAG-hydrolyzing activities are very similar. Nevertheless, the activity measurements were performed at only one substrate

concentration, and the kinetic constants were not determined in their study. Moreover, the quantification of GCPII and GCPIII levels was difficult, as membranes from transfected cells were used in the assay. On the contrary, our measurements with purified rhGCPII and rhGCPIII reveal that the pH dependencies of these two closely homologous enzymes are strikingly different. The pH dependence of rhGCPII forms a typical bell-shaped curve with k_{cat} stable over the neutral and slightly basic region and K_M sharply decreasing with pH. In contrast, the pH optimum of rhGCPIII is shifted to the neutral region, it has a narrower maximum, and the K_M actually increases with pH in the pH range of 6.8–9.0. An interpretation of this dissimilarity can be derived from a structural model of GCPIII, which we constructed on the basis of a recently determined 3D structure of GCPII (Mesters *et al.* 2006). As the native substrates of GCPII are negatively charged, it is not surprising that the prevailing charge on the surface of GCPII's binding cavity is positive. Although the charged residues in the GCPIII binding cavity are conserved, the amino acid exchanges in the vicinity of the binding cavity lead to a considerable decrease in a positively charged surface area and a minor increase of the negatively charged surface in comparison to GCPII. As a result, the prevailing charge on the surface of the GCPIII binding cavity is less positive, which could account for the more acidic pH optimum for rhGCPIII than for rhGCPII. Similarly, this difference in positively charged surface area could have an impact on the substrate specificities of the two homologs.

The GCPII activity determinations reported in the literature have typically been performed in 50 mmol/L Tris buffer pH 7.4 with or without various salt concentrations. We demonstrate that for both enzymes, the kinetic parameters of NAAG hydrolysis can be significantly altered by salt concentration. While the K_M of rhGCPII reaches its minimum at 50 mmol/L NaCl and does not change significantly with increasing salt concentration up to 150 mmol/L NaCl, rhGCPIII has the highest affinity for NAAG at 20 mmol/L NaCl concentration. The k_{cat} value changes significantly only for rhGCPIII and increases with the NaCl concentration. These data are very important when the activities of GCPII and GCPIII are directly compared. For instance, in 20 mmol/L MOPS, 150 mmol/L NaCl, pH 7.4, the catalytic efficiency of rhGCPII is more than 10 \times higher than that of rhGCPIII, while in the same buffer with lower salt concentration (20 mmol/L NaCl, more relevant for intracellular compartments) this efficiency is only 3 \times higher.

The GCPII inhibitors analyzed in this article effectively block the peptidase activity of rhGCPIII. The prototype phosphonate-based inhibitor I-1 exhibits the same K_i against both enzymes, while the inhibitor I-2 with pentafluoro benzyl group in the P1 position is roughly three to eight times more potent against rhGCPIII. The potency increase seems to be slightly higher in the case of the more active enantiomer (I-2(S)). The pentafluoro benzyl group, which is situated at the

edge of the binding pocket and does not make any obvious contacts with the enzyme (Mesters *et al.* 2006) is better tolerated by GCPIII in comparison with rhGCPII. This is likely because of the lower overall positive charge of the surface of GCPIII, which repels the hydrophobic group less than the highly charged surface of GCPII. The situation is reversed in the case of thiol containing inhibitors I-3 and I-4 and the methotrexate-based inhibitor I-5, but here the differences in the values of K_i are not so significant. In addition to the change in polarity of the binding cavities, the structural model of GCPIII also reveals that the binding cavity of GCPIII is smaller than that of GCPII by approximately 30%. Implications of this difference on the geometry of the GCPIII binding cavity with respect to GCPII might also help to explain these differences in inhibitor binding.

Overall, the presented series of inhibitors, which were originally designed for GCPII, showed very similar activities against rhGCPIII regardless of their size and different zinc-binding groups. This finding is relevant in particular with respect to the potential use of GCPII inhibitors for treatment of disorders associated with glutamate excitotoxicity, as potent compounds should effectively block pathological release of glutamate caused by either of the two proteases.

In conclusion, the physiological substrate of GCPII, Ac-Asp-Glu-OH (NAAG), is also hydrolyzed by rhGCPIII but less efficiently and with significantly different pH and salt concentration optima. We believe that this GCPIII activity is significant enough to account for the NAAG-hydrolyzing activity observed in the tissues of GCPII KO mice (Bacich *et al.* 2002) and that GCPIII might thus represent a valid pharmaceutical target. We show on a panel of GCPII inhibitors that the pharmacologic profiles of the two homologs are quite similar. However, as the substrate specificities are distinct and the biological significance of GCPIII is not yet known, our findings might be used for the design of compounds selectively targeting either GCPII or GCPIII. Such inhibitors would be instrumental to evaluate and dissect biological roles of the two individual enzymes.

Acknowledgements

The authors thank Jana Starkova for excellent technical assistance, Martin Hradilek for peptide synthesis and Hillary Hoffman for language corrections and proofreading. Financial assistance of the Grant Agency of the Czech Republic (301/03/0784) and Ministry of Education of the Czech Republic (Research Centre for new Antivirals and Antineoplastics, IM0508) is gratefully acknowledged.

References

Bacich D. J., Ramadan E., O'Keefe D. S. *et al.* (2002) Deletion of the glutamate carboxypeptidase II gene in mice reveals a second enzyme activity that hydrolyzes N-acetylaspartylglutamate. *J. Neurochem.* **83**, 20–29.

- Barinka C., Rinnova M., Sacha P., Rojas C., Majer P., Slusher B. S. and Konvalinka J. (2002) Substrate specificity, inhibition and enzymological analysis of recombinant human glutamate carboxypeptidase II. *J. Neurochem.* **80**, 477–487.
- Barinka C., Mlcochova P., Sacha P., Hilgert I., Majer P., Slusher B. S., Horejsi V. and Konvalinka J. (2004a) Amino acids at the N- and C-termini of human glutamate carboxypeptidase II are required for enzymatic activity and proper folding. *Eur. J. Biochem.* **271**, 2782–2790.
- Barinka C., Sacha P., Sklenar J., Man P., Bezouska K., Slusher B. S. and Konvalinka J. (2004b) Identification of the N-glycosylation sites on glutamate carboxypeptidase II necessary for proteolytic activity. *Protein Sci.* **13**, 1627–1635.
- Bzdega T., Crowe S. L., Ramadan E. R., Sciarretta K. H., Olszewski R. T., Ojeifo O. A., Rafalski V. A., Wroblewska B. and Neale J. H. (2004) The cloning and characterization of a second brain enzyme with NAAG peptidase activity. *J. Neurochem.* **89**, 627–635.
- Case D. A., Darden T. A., Cheatham T. E. III *et al.* (2004) *AMBER 8*. University of California, San Francisco.
- Chang S. S., Reuter V. E., Heston W. D., Bander N. H., Grauer L. S. and Gaudin P. B. (1999) Five different anti-prostate-specific membrane antigen (PSMA) antibodies confirm PSMA expression in tumor-associated neovasculature. *Cancer Res.* **59**, 3192–3198.
- Cornell W. D., Cieplak P., Bayly C. I. *et al.* (1995) A second generation force field for the simulation of proteins, nucleic acids and organic molecules. *J. Am. Chem. Soc.* **117**, 5179–5197.
- Davis M. I., Bennett M. J., Thomas L. M. and Bjorkman P. J. (2005) Crystal structure of prostate-specific membrane antigen, a tumor marker and peptidase. *Proc. Natl Acad. Sci. USA* **102**, 5981–5986.
- DeLano W. L. (2002) *The PyMOL User's Manual*. DeLano Scientific, San Carlos, CA, USA.
- Ghadge G. D., Slusher B. S., Bodner A. *et al.* (2003) Glutamate carboxypeptidase II inhibition protects motor neurons from death in familial amyotrophic lateral sclerosis models. *Proc. Natl Acad. Sci. USA* **100**, 9554–9559.
- Ghosh A. and Heston W. D. (2003) Effect of carbohydrate moieties on the folate hydrolysis activity of the prostate specific membrane antigen. *Prostate* **57**, 140–151.
- Gregorakis A. K., Holmes E. H. and Murphy G. P. (1998) Prostate-specific membrane antigen: current and future utility. *Semin. Urol. Oncol.* **16**, 2–12.
- Harada C., Harada T., Slusher B. S., Yoshida K., Matsuda H. and Wada K. (2000) N-acetylated-alpha-linked-acidic dipeptidase inhibitor has a neuroprotective effect on mouse retinal ganglion cells after pressure-induced ischemia. *Neurosci. Lett.* **292**, 134–136.
- Humphrey W., Dalke A. and Schulten K. (1996) VMD: visual molecular dynamics. *J. Mol. Graph.* **14**, 33–38.
- Israeli R. S., Powell C. T., Corr J. G., Fair W. R. and Heston W. D. (1994) Expression of the prostate-specific membrane antigen. *Cancer Res.* **54**, 1807–1811.
- Jackson P. F., Cole D. C., Slusher B. S., Stetz S. L., Ross L. E., Donzanti B. A. and Trainor D. A. (1996) Design, synthesis, and biological activity of a potent inhibitor of the neuropeptidase N-acetylated alpha-linked acidic dipeptidase. *J. Med. Chem.* **39**, 619–622.
- Kato T., Nagatsu T., Kimura T. and Sakakibara S. (1978) Fluorescence assay of x-prolyl dipeptidyl-aminopeptidase activity with a new fluorogenic substrate. *Biochem. Med.* **19**, 351–359.
- Laskowski R. A. (1995) SURFNET: a program for visualizing molecular surfaces, cavities, and intermolecular interactions. *J. Mol. Graph.* **13**, 323–328.
- Majer P., Jackson P. F., Delahanty G. *et al.* (2003) Synthesis and biological evaluation of thiol-based inhibitors of glutamate carboxypeptidase II: discovery of an orally active GCP II inhibitor. *J. Med. Chem.* **46**, 1989–1996.

- Majer P., Hin B., Stoermer D. *et al.* (2006) Structural optimization of thiol-based inhibitors of glutamate carboxypeptidase II by modification of the P1' side chain. *J. Med. Chem.* **49**, 2876–2885.
- Mesters J. R., Barinka C., Li W., Tsukamoto T., Majer P., Slusher B. S., Konvalinka J. and Hilgenfeld R. (2006) Structure of glutamate carboxypeptidase II, a drug target in neuronal damage and prostate cancer. *EMBO J.* **25**, 1375–1384.
- Morrison J. F. (1969) Kinetics of the reversible inhibition of enzyme-catalysed reactions by tight-binding inhibitors. *Biochim. Biophys. Acta.* **185**, 269–286.
- Murphy G., Ragde H., Kenny G. *et al.* (1995) Comparison of prostate specific membrane antigen, and prostate specific antigen levels in prostatic cancer patients. *Anticancer Res.* **15**, 1473–1479.
- Nan F., Bzdega T., Pshenichkin S., Wroblewski J. T., Wroblewska B., Neale J. H. and Kozikowski A. P. (2000) Dual function glutamate-related ligands: discovery of a novel, potent inhibitor of glutamate carboxypeptidase II possessing mGluR3 agonist activity. *J. Med. Chem.* **43**, 772–774.
- Neale J. H., Olszewski R. T., Gehl L. M., Wroblewska B. and Bzdega T. (2005) The neurotransmitter N-acetylaspartylglutamate in models of pain, ALS, diabetic neuropathy, CNS injury and schizophrenia. *Trends Pharmacol. Sci.* **26**, 477–484.
- Pangalos M. N., Neefs J. M., Somers M., Verhasselt P., Bekkers M., van der Helm L., Fraiponts E., Ashton D. and Gordon R. D. (1999) Isolation and expression of novel human glutamate carboxypeptidases with N-acetylated alpha-linked acidic dipeptidase and dipeptidyl peptidase IV activity. *J. Biol. Chem.* **274**, 8470–8483.
- Pinto J. T., Suffoletto B. P., Berzin T. M., Qiao C. H., Lin S., Tong W. P., May F., Mukherjee B. and Heston W. D. (1996) Prostate-specific membrane antigen: a novel folate hydrolase in human prostatic carcinoma cells. *Clin. Cancer Res.* **2**, 1445–1451.
- Renneberg H., Friedetzky A., Konrad L., Kurek R., Weingartner K., Wennemuth G., Tunn U. W. and Aumuller G. (1999) Prostate specific membrane antigen (PSM) is expressed in various human tissues: implication for the use of PSM reverse transcription polymerase chain reaction to detect hematogenous prostate cancer spread. *Urol. Res.* **27**, 23–27.
- Robinson M. B., Blakely R. D., Couto R. and Coyle J. T. (1987) Hydrolysis of the brain dipeptide N-acetyl-L-aspartyl-L-glutamate. Identification and characterization of a novel N-acetylated alpha-linked acidic dipeptidase activity from rat brain. *J. Biol. Chem.* **262**, 14 498–14 506.
- Schmidt B., Anastasiadis A. G., Seifert H. H., Franke K. H., Oya M. and Ackermann R. (2003) Detection of circulating prostate cells during radical prostatectomy by standardized PSMA RT-PCR: association with positive lymph nodes and high malignant grade. *Anticancer Res.* **23**, 3991–3999.
- Sedo A., Malik R. and Krepela E. (1998) Dipeptidyl peptidase IV in C6 rat glioma cell line differentiation. *Biol. Chem.* **379**, 39–44.
- Serval V., Barbeito L., Pittaluga A., Cheramy A., Lavielle S. and Glowinski J. (1990) Competitive inhibition of N-acetylated-alpha-linked acidic dipeptidase activity by N-acetyl-L-aspartyl-beta-linked L- glutamate. *J. Neurochem.* **55**, 39–46.
- Silver D. A., Pellicer I., Fair W. R., Heston W. D. and Cordon-Cardo C. (1997) Prostate-specific membrane antigen expression in normal and malignant human tissues. *Clin. Cancer Res.* **3**, 81–85.
- Slusher B. S., Vornov J. J., Thomas A. G. *et al.* (1999) Selective inhibition of NAALADase, which converts NAAG to glutamate, reduces ischemic brain injury. *Nat. Med.* **5**, 1396–1402.
- Sokoloff R. L., Norton K. C., Gasior C. L., Marker K. M. and Grauer L. S. (2000) A dual-monoclonal sandwich assay for prostate-specific membrane antigen: levels in tissues, seminal fluid and urine. *Prostate* **43**, 150–157.
- Subasinghe N., Schulte M., Chan M. Y., Roon R. J., Koerner J. F. and Johnson R. L. (1990) Synthesis of acyclic and dehydroaspartic acid analogues of Ac- Asp-Glu-OH and their inhibition of rat brain N-acetylated alpha-linked acidic dipeptidase (NAALAD dipeptidase). *J. Med. Chem.* **33**, 2734–2744.
- Troyer J. K., Beckett M. L. and Wright G. L. Jr (1995) Detection and characterization of the prostate-specific membrane antigen (PSMA) in tissue extracts and body fluids. *Int. J. Cancer* **62**, 552–558.
- Tsai G., Dunham K. S., Drager U., Grier A., Anderson C., Collura J. and Coyle J. T. (2003) Early embryonic death of glutamate carboxypeptidase II (NAALADase) homozygous mutants. *Synapse* **50**, 285–292.
- Tsukamoto T., Flanary J. M., Rojas C., Slusher B. S., Valiaeva N. and Coward J. K. (2002) Phosphonate and phosphinate analogues of N-acetylated gamma-glutamylglutamate. Potent inhibitors of glutamate carboxypeptidase II. *Bioorg. Med. Chem. Lett.* **12**, 2189–2192.
- Tsukamoto T., Majer P., Vitharana D. *et al.* (2005) Enantiospecificity of glutamate carboxypeptidase II inhibition. *J. Med. Chem.* **48**, 2319–2324.
- Vitharana D., France J. E., Scarpetti D., Bonneville G. W., Majer P. and Tsukamoto T. (2002) Synthesis and biological evaluation of (R)- and (S)-2-(phosphonomethyl)pentanedioic acids as inhibitors of glutamate carboxypeptidase II. *Tetrahedron Asymmetry* **13**, 1609–1614.
- Whelan J. (2000) NAALADase inhibitors: a novel approach to glutamate regulation. *Drug Discov. Today* **5**, 171–172.
- Xiao Z., Adam B. L., Cazares L. H., Clements M. A., Davis J. W., Schellhammer P. F., Dalmasso E. A. and Wright G. L. Jr (2001) Quantitation of serum prostate-specific membrane antigen by a novel protein biochip immunoassay discriminates benign from malignant prostate disease. *Cancer Res.* **61**, 6029–6033.
- Zhang W., Slusher B., Murakawa Y., Wozniak K. M., Tsukamoto T., Jackson P. F. and Sima A. A. (2002) GCPII (NAALADase) inhibition prevents long-term diabetic neuropathy in type 1 diabetic BB/Wor rats. *J. Neurol. Sci.* **194**, 21–28.
- Zhou J., Neale J. H., Pomper M. G. and Kozikowski A. P. (2005) NAAG peptidase inhibitors and their potential for diagnosis and therapy. *Nat. Rev. Drug Discov.* **4**, 1015–1026.

6.5 GCPII in human brain

6.5.1 Background information

Even though it is generally accepted that GCPII is expressed in human brain, it is not as well defined as one would expect. Many studies were done on a rat model and GCPII expression and activity was observed in many cases [13, 66, 73, 141, 218, 219]. The situation in human brain seems to be a little bit troublesome in comparison to rat brain, because the studies on GCPII expression in human brain are inconsistent. Several of them detected GCPII expression in human brain [33, 220, 137, 139-141] and several did not [35, 36, 138, 145].

It is surprising that the expression of such an important protein involved in brain disorders (see chapter 3.2) is not well defined and this was also the reason why we decided to analyze expression of GCPII in human brain in detail. It is the first systematic study of GCPII expression in different parts of human brain.

6.5.2 Summary

We quantified GCPII expression in different brain tissue sections using immunoblot and monoclonal antibody GCP-04. This antibody was prepared using recombinant extracellular part of GCPII purified from insect cells' conditioned media. GCPII protein was quantified in various brain compartments (50-300ng GCPII/mg of total protein) and it was the first quantitative analysis of GCPII in human brain.

GCP-04 antibody recognizes epitop comprising of amino acids 100-104 in GCPII sequence. Unfortunately, this epitop is also present in GCPIII (close homolog of GCPII, see chapter 6.4). Even though GCP-04 antibody is 100 times more sensitive to GCPII than to GCPIII, potential interference of GCPIII in immunodetection of GCPII remains plausible.

Data from immunoblot are consistent with enzymatic analysis. The measured activity in brain tissue samples ranged from 1 to 12pmol of cleaved NAAG /min/mg of total protein.

Immunohistochemistry showed that GCPII is mostly expressed in white matter, namely in astrocytes. Nevertheless, not all astrocytes express GCPII and we speculate that GCPII is mostly located in fibrillary astrocytes (type II, present in higher numbers in the white matter).

This paper represents the first systematic study of expression of GCPII in human brain.

I participated in the determination of specificity and selectivity of monoclonal antibody GCP-04.

6.5.3 Publication V

Neuroscience 144 (2007) 1361–1372

EXPRESSION OF GLUTAMATE CARBOXYPEPTIDASE II IN HUMAN BRAIN

P. ŠÁCHA,^{a,b} J. ZÁMEČNÍK,^c C. BAŘINKA,^a
K. HLOUCHOVÁ,^{a,b} A. VÍCHA,^d P. MLČOCHOVÁ,^{a,b}
I. HILGERT,^e T. ECKSCHLAGER^d AND
J. KONVALINKA^{a,b,*}

^aDepartment of Biochemistry, Institute of Organic Chemistry and Biochemistry, Academy of Science of the Czech Republic, Flemingovo n.2, Prague 6, 166 10 Czech Republic

^bDepartment of Biochemistry, Charles University, Faculty of Natural Science, Hlavova 2030, Prague 2, 128 43 Czech Republic

^cDepartment of Pathology and Molecular Medicine, Charles University, 2nd Medical Faculty and University Hospital Motol, V Úvalu 84, Prague 5, 150 06, Czech Republic

^dDepartment of Pediatric Oncology and Hematology, Charles University, 2nd Faculty of Medicine, V Úvalu 84, Prague 5, 150 06, Czech Republic

^eInstitute of Molecular Genetics, Academy of Sciences of the Czech Republic, Vídeňská 1083, Prague 4, 142 20, Czech Republic

Abstract—Glutamate carboxypeptidase II (GCPII) is a transmembrane glycoprotein expressed in various tissues. When expressed in the brain it cleaves the neurotransmitter N-acetylaspartylglutamate (NAAG), yielding free glutamate. In jejunum it hydrolyzes folylpoly-gamma-glutamate, thus facilitating folate absorption. The prostate form of GCPII, known as prostate specific membrane antigen (PSMA), is an established cancer marker. The NAAG-hydrolyzing activity of GCPII has been implicated in a number of pathological conditions in which glutamate is neurotoxic (e.g. amyotrophic lateral sclerosis, Huntington's disease, Alzheimer's disease, epilepsy, schizophrenia, and stroke). Inhibition of GCPII was shown to be neuroprotective in tissue culture and in animal models. GCPII is therefore an interesting putative therapeutic target. However, only very limited and controversial data on the expression and localization of GCPII in human brain are available. Therefore, we set out to analyze the activity and expression of GCPII in various compartments of the human brain using a radiolabeled substrate of the enzyme and the novel monoclonal antibody GCP-04, which recognizes an epitope on the extracellular portion of the enzyme and is more sensitive to GCPII than to the homologous GCPIII. We show that this antibody is more sensitive in immunoblots

*Correspondence to: J. Konvalinka, Department of Biochemistry, Institute of Organic Chemistry and Biochemistry, Academy of Science of the Czech Republic, Flemingovo n.2, Prague 6, 166 10 Czech Republic. Tel: +42–0220183218.

E-mail address: konval@uochb.cas.cz (J. Konvalinka).

Abbreviations: BSA, bovine serum albumin; EDTA, ethylenediaminetetraacetic acid; GCPII/III, human glutamate carboxypeptidase II/III; GFAP, glial fibrillary acidic protein; mAb, monoclonal antibody; NAAG, N-acetyl-L-aspartyl-L-glutamate; NAALADase L, N-acetylated-alpha-linked-acidic dipeptidase L; PSMA, prostate specific membrane antigen; PSM', N-terminally truncated intracellular form of prostate specific membrane antigen; rhGCPII/III, recombinant human glutamate carboxypeptidase II/III; SDS-PAGE, sodium dodecyl sulfate polyacrylamide gel electrophoresis; TBS, Tris-buffered saline; TBST, Tris buffered saline containing 0.1% Triton X-100; 2-PMPA, 2-(phosphonomethyl)pentanedioic acid.

0306-4522/07\$30.00+0.00 © 2006 IBRO. Published by Elsevier Ltd. All rights reserved.
doi:10.1016/j.neuroscience.2006.10.022

than the widely used antibody 7E11. By Western blot, we show that there are approximately 50–300 ng of GCPII/mg of total protein in human brain, depending on the specific area. Immunohistochemical analysis revealed that astrocytes specifically express GCPII in all parts of the brain. GCPII is enzymatically active and the level of activity follows the expression pattern. Using pure recombinant GCPII and homologous GCPIII, we conclude that GCPII is responsible for the majority of overall NAAG-hydrolyzing activity in the human brain. © 2006 IBRO. Published by Elsevier Ltd. All rights reserved.

Key words: NAALADase, PSMA, metallopeptidase, prostate cancer, immunohistochemistry, epitope mapping.

Glutamate carboxypeptidase II (GCPII, EC 3.4.17.21), also known as prostate specific membrane antigen (PSMA) or folate hydrolase I (FOLH1), is a type II transmembrane glycoprotein, the human form of which has a molecular weight of approximately 100 kDa and consists of 750 amino acids. Glycosylation of the enzyme is critical for its proteolytic activity (Barinka et al., 2002, 2004b). GCPII is a zinc metallopeptidase. Recently, its crystal structure has been solved by two groups independently (Davis et al., 2005; Mesters et al., 2006).

In the brain, GCPII cleaves N-acetylaspartylglutamate (N-acetyl-L-aspartyl-L-glutamate, NAAG) to N-acetylaspartate and glutamate. NAAG is a highly abundant peptide neurotransmitter and an agonist of metabotropic glutamate receptor 3 (Wroblewska et al., 1997; Neale et al., 2000). The inhibition of the brain form of GCPII has been demonstrated to be neuroprotective in animal models of ischemic brain injury (Slusher et al., 1999; Lu et al., 2000), to attenuate neuropathic pain (Jackson et al., 2001; Yamamoto et al., 2004), and to prolong survival of the experimental animals in the mouse model of amyotrophic lateral sclerosis (Ghadge et al., 2003; for review, see Neale et al., 2005).

In the jejunum, GCPII cleaves pteroylpoly-gamma-glutamate to folate and glutamate, thus enabling the absorption of dietary folates (Halsted et al., 1998). The physiological function of GCPII in prostate is not known. A GCPII variant called PSM' (N-terminally truncated intracellular form of prostate specific membrane antigen) is transcribed in the prostate. PSM', which lacks the coding sequence for the intracellular and transmembrane domains due to alternative splicing, is a 693 amino acid protein (Su et al., 1995). The PSMA/PSM' mRNA ratio is elevated in prostate cancer (Su et al., 1995), and PSMA could serve as a prostate cancer marker (Murphy, 1995). Furthermore, the mRNA in the rat brain is transcribed in six variants of 3900,

3000, 2800, 2100, 750, and 500 nucleotides. However, the function of those variants is not known (Carter et al., 1996).

There are also reports on expression of GCPII in rat kidney studied by immunohistochemistry (Slusher et al., 1992) or by activity determination (Robinson et al., 1987), but the function of the enzyme in that organ remains unknown.

A human homolog labeled GCPIII which shares 81% similarity with GCPII has been described (Pangalos et al., 1999), and its mouse ortholog has been partially characterized (Bzdega et al., 2004). Little is known about its expression level and activity, and no specific antibodies for GCPIII have been described so far. A report on the phenotype of GCPII knock-out mice suggests that GCPIII activity might compensate for the absent GCPII activity (Bacich et al., 2002). Apart from GCPIII, two other variants of GCPII have been described: N-acetylated- α -linked-acidic dipeptidase L (NAALADase L) and PSMA-like enzyme (Pangalos et al., 1999; O'Keefe et al., 2004). Neither of these gene products seems to exhibit any proteolytic activity, and their physiological role (if any) remains elusive.

Most of the information about the distribution of GCPII in the brain is derived from studies in rats and mice. Considering the wealth of direct and indirect observation suggesting the important role of GCPII in the pathology of various neurological disorders, little is known about its expression and localization in human brain. In the rat brain, NAAG-hydrolyzing activity was reported (Fuhrman et al., 1994), and GCPII was detected immunochemically (Berger et al., 1999). The reports on the immunochemical detection of GCPII in the human brain are more controversial. In their early analysis of 122 human specimens using the antibody 7E11 Horoszewicz et al. (1987) did not observe any GCPII expression in human samples except for prostate and kidney. Similarly, Lopes et al. (1990) and Silver et al. (1997) could not detect any GCPII expression in human brain by using 7E11 antibody. Chang et al. (1999) could not detect GCPII in human brain by immunohistochemistry, although they employed five different monoclonal antibodies.

On the other hand, Troyer et al. (1995) detected low GCPII expression levels by Western blot analysis of membrane preparations of human cerebral cortex using 7E11 antibody. O'Keefe et al. (2004) reported low mRNA and protein expression in human hippocampus and amygdala using monoclonal antibodies. Furthermore, Berger et al. (1995) described localization of GCPII on neuromuscular junctions in rats using immunohistochemical methods. Another report showed strong cytoplasmic staining in the neurons in the hippocampal region of mouse and human brain (Huang et al., 2004). A low level of mRNA was found in human brain by Israeli et al. (1994), Luthi-Carter et al. (1998b), and Renneberg et al. (1999). However, none of these reports analyzed the expression in various segments of human brain systematically. The expression of GCPII in human brain thus remains controversial and poorly characterized. Therefore, we set out to perform a systematic analysis of GCPII expression, enzymatic activity, and lo-

calization in individual segments of human brain using a novel, sensitive monoclonal antibody (mAb).

EXPERIMENTAL PROCEDURES

Tissue samples: dissection and preparation

Samples for the study were obtained from five brains (four males aged 48, 71, 76, and 81 years and one female aged 68 years) during autopsy. The brains were free of metastatic spread of cancer. The autopsies were performed 4–8 h (in one case, 27 h) postmortem. After 2 h at room temperature, the corpses were stored at 5 °C. From one patient (a 48-year-old man who died due to generalized lung cancer and severe bronchopneumonia) samples were taken systematically from different brain compartments as listed in Table 1. Two sets of samples were dissected from each brain location. The first set was fixed in 10% buffered formalin for 24 h at room temperature for the immunohistochemical study. A second set of samples for the quantitative studies was immediately frozen on dry ice and later used for the immunochemical detection by Western blot. In order to analyze the variability in GCPII activity among individuals, additional samples from selected CNS compartments (frontal cerebral cortex, temporal gray matter, temporal white matter, nucleus caudatus, spinal cord and brainstem, see Table 2) were taken from the brains of further four patients and frozen on dry ice. For the activity testing, these frozen samples were thawed, homogenized, and sonicated in the reaction buffer (50 mM Tris-HCl, 5 mM NaCl, pH 7.4) with addition of 1% Triton X-100 and protease inhibitors cocktail (Complete Mini, EDTA-free, Roche, Mannheim, Germany), dialyzed against reaction buffer for 3 days with six exchanges at 4 °C, and centri-

Table 1. Identification of samples taken from various CNS regions

Sample number	CNS compartment
S1	Olfactory bulb
S2	Frontal cerebral cortex
S3	Somatomotoric cerebral cortex
S4	Temporal gray matter
S5	Occipital gray matter
S6	Temporal white matter
S7	Anteroventral thalamic nuclei
S8	Corpus geniculatum lateralis
S9	Ventroposterior thalamic nuclei
S10	Corpus geniculatum mediale
S11	Nucleus caudatus
S12	Globus pallidum
S13	Cerebellum, folia of hemispheres
S14	Nucleus dentatus
S15	Hippocampus
S16	Corpus callosum
S17	Amygdala
S18	Substantia nigra
S19	Pontine nuclei
S20	Cochlear nuclei
S21	Inferior olive
S22	Locus coeruleus
S23	Ventrolateral medulla oblongata
S24	Spinal cord
S25	Supraoptic nucleus
S26	Lateral hypothalamic area
S27	Periventricular nuclei
S28	Nucleus ruber
S29	Superior colliculus
S30	Brainstem regions

Table 2. Specific NAAG-hydrolyzing activity and protein content of individual brain samples

Sample number	CNS compartment	N	GCPII content (ng GCPII/mg total protein)	Activity (pmol/min/mg total protein)	Specific activity (nmol/min/mg)
S2	Frontal cerebral cortex	5	118±50	2.9±1.0	27±11
S4	Temporal gray matter	4	49±30	1.5±0.4	37±13
S6	Temporal white matter	5	282±75	11.8±2.3	43±5
S11	Nucleus caudatus	4	64±29	2.9±0.7	46±7
S24	Spinal cord	5	156±94	6.4±3.1	47±16
S30	Brainstem regions	5	176±61	6.7±1.5	40±8

The sample identification corresponds to the lines in Fig. 3A and B. *N* represents the number of brains from which the samples were taken. Total protein content was determined by Bio-Rad Protein Assay, "GCPII content" represents data from densitometry quantification of the immunoblot intensity of the corresponding sample with ECL detection using a CCD-camera. Pure recombinant GCPII was used as a standard. The activities were measured in duplicates; data represent average values with standard deviation. "Specific activity" represents activity in nanomoles of substrate hydrolyzed per minute divided by GCPII content in mg determined by densitometry as described above.

fused for 10 min at 16,000×*g* at 4 °C. The supernatants were used for further analysis. Determination of protein concentration in the supernatant was performed by BioRad protein assay (BioRad, Munich, Germany) according to the manufacturer's manual.

Preparation of the monoclonal antibodies GCP-04, GCP-02, and 7E11

Hybridomas secreting monoclonal antibodies GCP-04 and GCP-02 (both IgG1) were prepared by standard methods from mice (F1 hybrids of BALB/c and B10.A strains) immunized with recombinant human glutamate carboxypeptidase II (rhGCPII, extracellular portion, i.e. amino acid residues 44–750), as described previously (Barinka et al., 2002). A hybridoma secreting 7E11 antibody was obtained from the American Tissue Culture Collection. Hybridoma cell supernatants were purified by Protein A (Amersham, Pharmacia Biotech, Uppsala, Sweden) affinity chromatography, and the resulting IgG preparation (stock concentration 1 mg/ml of antibody 7E11 and GCP-02, 7 mg/ml in case of GCP-04) was stored at 5 °C until usage.

Phage display

The epitope mapping of the GCP-04 mAb was carried out using Ph.D.-7 Phage Display Peptide Library Kit (NEB, Beverly, MA, USA) according to the manufacturer's protocol. Polysorp tubes (NUNC, Rochester, NY, USA) were coated with 1 ml of purified mAb GCP-04 (100 µg/ml in Tris-buffered saline (TBS)) overnight at 4 °C. The coating solution was discarded and the tubes were blocked with 1.5 ml of bovine serum albumin (BSA, Fluka Chemie, Buchs, Switzerland) solution (5 mg/ml in 0.1 M NaHCO₃ (Lachema, Brno, Czech Republic), 0.02% NaN₃ (Penta, Prague, Czech Republic), pH 8.6) for one hour at 4 °C. The blocking solution was poured off and tubes were washed 6×1 ml with Tris buffered saline containing 0.1% Triton X-100 (TBST). Phages (2×10¹¹) (10 µl of the original library) in 1 ml of TBST were pipetted into the coated tube and rocked gently for 60 min at room temperature. The solution with non-bound phages was discarded and tubes were washed 10×1 ml with TBST. Bound phages were eluted with 1 ml of 200 mM glycine (ICN Biomedicals, Irvine, CA, USA), 1 mg/ml BSA, pH 2.2. The elution proceeded for 10 min at room temperature, and the eluate was then immediately neutralized by addition of 150 µl 1 M Tris-HCl (USB, Cleveland, OH, USA), pH 9.1. The phages were titrated and amplified and the panning procedure was repeated three more times. Following the fourth round of panning, the individual binding clones were amplified and the phage DNA was isolated and sequenced.

Activity assay

One microliter of the supernatant prepared from tissue samples as described above was diluted by reaction buffer (50 mM

Tris-HCl, 5 mM NaCl, pH 7.4) with or without the presence of 100 nM inhibitor 2-(phosphonomethyl)pentanedioic acid (2-PMPA) (Slusher et al., 1999) to a final volume of 180 µl and preincubated at 37 °C for 3 min. The reaction was started by addition of 20 µl of radioactive NAAG (1 µM, 1850 Bq/20 µl, tritium label on the glutamate, PerkinElmer, Boston, MA, USA). After 1–7 h (to achieve conversion between 5% and 30%), the reaction was stopped by the addition of 200 µl chilled 200 mM sodium phosphate (pH 7.4, Lachema). Two hundred microliters of the mixture was separated in a glass column on AG 1-X8 Resin (BioRad), the cleaved glutamate was eluted with 2 ml of 1 M formic acid, mixed with scintillation cocktail (Rotiszint ECO Plus, Roth, Karlsruhe, Germany) and measured in a liquid scintillator (LS 6500, Beckman, Fullerton, CA, USA).

A similar reaction setup was used for a direct comparison of pure recombinant GCPII (extracellular part 44–750, Barinka et al., 2002) and GCPIII (extracellular part 36–740, Hlouchova et al., manuscript in preparation) activities. In the assay, 0.37 ng of rhGCPII and 12.5 ng of rhGCPIII (as determined by active site titration) were used in a total reaction volume of 200 µl, so that after a 20 min reaction the substrate conversion was approximately 20% in both cases.

Active site titrations

Approximately 1.5 µM GCPII was preincubated with differing concentrations of the tight binding inhibitor 2-(phosphonomethyl)pentanedioic acid (10–1000 nM) in 20 mM MOPS, 20 mM NaCl, pH 7.4, for 15 min at 37 °C and reacted with 100 µM Ac-Asp-Met (Barinka et al., 2002) in the total final volume of 110 µl. The reaction products were derivatized by 6-aminoquinolyl-N-hydroxy-succinimidyl carbamate (AccQ)-Fluor reagent (Waters) dissolved in acetonitrile and resolved on a HPLC Luna C18(2)-column (250×4.6 mm, 5 µm, Phenomenex). For the active-site titration of GCPIII, approximately 200 nM enzyme was preincubated with differing concentrations of the tight binding inhibitor 2-(phosphonomethyl)pentanedioic acid (10–3000 nM) in 20 mM MOPS, 20 mM NaCl, pH 7.4, for 15 min at 37 °C, and reacted with 6 µM Ac-Asp-Glu in the total volume of 180 µl. The radioactive assay (see above) was used for product detection. The active-site concentrations of the enzymes were determined from the plots of v_i/v_0 (the ratio of individual reaction rates to rate of uninhibited reaction) against the inhibitor concentration Grafit 5.0 II (Erithacus Software Ltd.), Active Site Titration module.

Western blotting

A defined amount of protein from each sample was resolved on 10% sodium dodecyl sulfate polyacrylamide gel electrophoresis (SDS-PAGE), electroblotted onto a nitrocellulose membrane, and immunostained with an appropriate mouse mAb (GCP-02, 1 mg/ml, diluted 1:5000, GCP-04, 7 mg/ml, diluted 1:35,000 or 7E11, 1

mg/ml, diluted 1:250), followed by incubation with 1:25,000 horseradish peroxidase-conjugated goat anti-mouse antibody (Pierce, Rockford, IL, USA) for 1 h and developed using West Femto mixture (Pierce). The relative intensities of immunoblot bands were quantified by recording the image with a CCD-camera (LAS-1000, Fujifilm, Stamford, CT, USA) followed by analysis using ImageQuant software (version v2003, Amersham Biosciences, Uppsala, Sweden). Alternatively blots were visualized using X-ray film MEDIX XBU (Foma Bohemia, Hradec Králové, Czech Republic) developed by film developer M35-M X-OMAT Processor (Kodak, Hemel Hempstead, UK) by standard procedures.

Deglycosylation

Twenty micrograms of total protein in a total volume of 20 μ l of glycoprotein denaturing buffer (NEB, Boston, MA, USA) was boiled in a water bath for 3 min. Samples were cooled to room temperature. Afterward, 3 μ l of 10% NP-40 (NEB), 3 μ l G7 Reaction Buffer (NEB), and 0.4 μ l peptide N-glycosidase F (500 U/ μ l, EC 3.5.1.52, NEB) were added and the mixture was incubated overnight at 37 °C.

Morphology and immunohistochemistry

Tissues were fixed in 10% buffered formalin (Lachema) for 24 h and embedded in paraffin. To determine the morphological features of the tissue, routine hematoxylin and eosin staining was carried out. All unstained tissue sections were stored at 4 °C until used to minimize antigen deterioration. Thereafter, 4 μ m thick tissue sections aimed for immunohistochemical staining were deparaffinized in xylene and rehydrated through decreasing concentrations of ethanol to water. After blocking of endogenous peroxidase activity, heat-induced epitope retrieval was performed in 10 mM sodium citrate buffer solution (pH 6.0) by warming to 96 °C in a water bath for 40 min. The sections were incubated overnight at 4 °C with anti-GCPII monoclonal mouse antibody GCP-04 (stock concentration 7 mg/ml, diluted 1:1000) or with monoclonal mouse antibody against glial fibrillary acidic protein (GFAP, clone 6F2, DakoCytomation Co., Glostrup, Denmark, diluted 1:1000). The antigen–antibody complexes were visualized by a biotin–streptavidin detection system (ChemMate Detection kit, DakoCytomation Co.) with 3,3'-diaminobenzidine (DAB, Fluka Chemie) as a chromogen. The specificity of staining was confirmed by processing sections cut from the same paraffin block with omission of the primary antibody (data not shown). As a positive control, reactions with the sections of prostate adenocarcinoma were used.

All sections were counterstained with Harris' hematoxylin (Fluka Chemie, Seelze, Germany).

Immunofluorescence

Double immunofluorescence staining was performed using fluorescence-conjugated secondary antibodies. The 5 μ m cryosections were incubated for 1 h at room temperature with antibody to GCP-04 (stock concentration 7 mg/ml, diluted 1:1000) and antibody to GFAP (polyclonal, Dako, Denmark, rabbit IgG, diluted 1:1000). Antibodies were diluted by Antibody Diluent (Dako). Thereafter, the slides were washed in TBS for 5 min and subsequently reacted in the dark for 30 min using a mixture of fluorophore-linked secondary bodies (FITC-conjugated anti-mouse IgG, diluted 1:100 and Cy3-conjugated anti-rabbit IgG, diluted 1:100; Jackson ImmunoResearch, Inc., West Grove, PA, USA). The slides were then washed in TBS for 5 min. The nuclei were visualized by staining with DAPI (1 μ g/ml) for 10 min and washed in TBS. To reduce the autofluorescence of lipofuscin, the sections were then treated with a solution of Sudan Black B (Sigma) in 70% methanol for 5 min. The slides were mounted using mounting medium Mowiol (Calbiochem, La Jolla, CA, USA) containing n-

propylgallate (Sigma-Aldrich, Germany) as an antifading agent. Fluorescence microscopy was then performed sequentially for each field using the Olympus BX51 fluorescent microscope fitted with appropriate filters for FITC, Cy3 and DAPI. The images were captured by Olympus C-5050 in monochrome mode and superimposed using imaging program Analysis D 5.0.

Positive and negative immunohistochemical controls run with each assay; as a positive control, reactions with the sections of prostate adenocarcinoma were used. The specificity of staining was confirmed by processing sections cut from the same block with omission of both primary antibodies. The specificity of the antibodies was further confirmed by preabsorption test. Briefly: antibody GCP-04 (stock concentration 7 mg/ml, diluted 1:1000) or antibody to GFAP (polyclonal, Dako, rabbit IgG, diluted 1:1000) was incubated with excess of recombinant protein GCPII (50 μ g/ml) for 2 h at 37 °C and centrifuged 13,000 \times g/30 min. Subsequently, the sections were incubated with the supernatant showing no positive staining by GCP-04 antibody.

RESULTS

Human brain samples for GCPII immunochemical detection and specific activity

In order to analyze the expression and enzymatic activity of GCPII in individual compartments of the human brain, 30 samples from various loci of the brain were obtained from a 48-year-old male. From each brain region, two sets of samples were prepared: formaldehyde-fixed samples for immunohistochemistry and samples frozen on dry ice for subsequent protein extraction and Western blotting (for sample description, see Table 1). In order to make quantitative comparisons between individual brain regions and to assess the variability of GCPII expression among humans, six samples of selected brain regions from an additional four individuals (three males and one female, aged 68–81) were obtained and used for the parallel determination of protein content, GCPII expression, and NAAG-hydrolyzing activity. For the activity determination, samples were homogenized and thoroughly dialyzed against reaction buffer. The supernatants were then used for further analysis of the total protein concentration, for the activity testing, and for Western blot analysis using a specific mAb raised against GCPII (antibody GCP-04; see Tables 1 and 2 and Fig. 3). The specificity of the NAAG-hydrolyzing activity was confirmed by the fact that all the NAAG-hydrolyzing activity of the supernatants was completely blocked by 2-PMPA, a selective inhibitor of GCPII (data not shown).

Characterization of GCP-04 antibody

The antibody was obtained by immunization of mice with the extracellular part of GCPII prepared by recombinant expression in insect cells (Barinka et al., 2004a). The epitope mapping of the GCP-04 mAb was performed using a library of phage-displayed random heptapeptides (see Experimental Procedures) and revealed that the antibody recognizes the "Φ+–ΨG" linear sequence pattern (where Φ is a hydrophobic amino acid, mainly Trp; + is a positively charged amino acid, Lys or Arg; – is a negatively charged amino acid, Glu or Asp; Ψ is a hydrophobic amino acid, Leu or Phe; G is glycine) that corresponds to amino acids

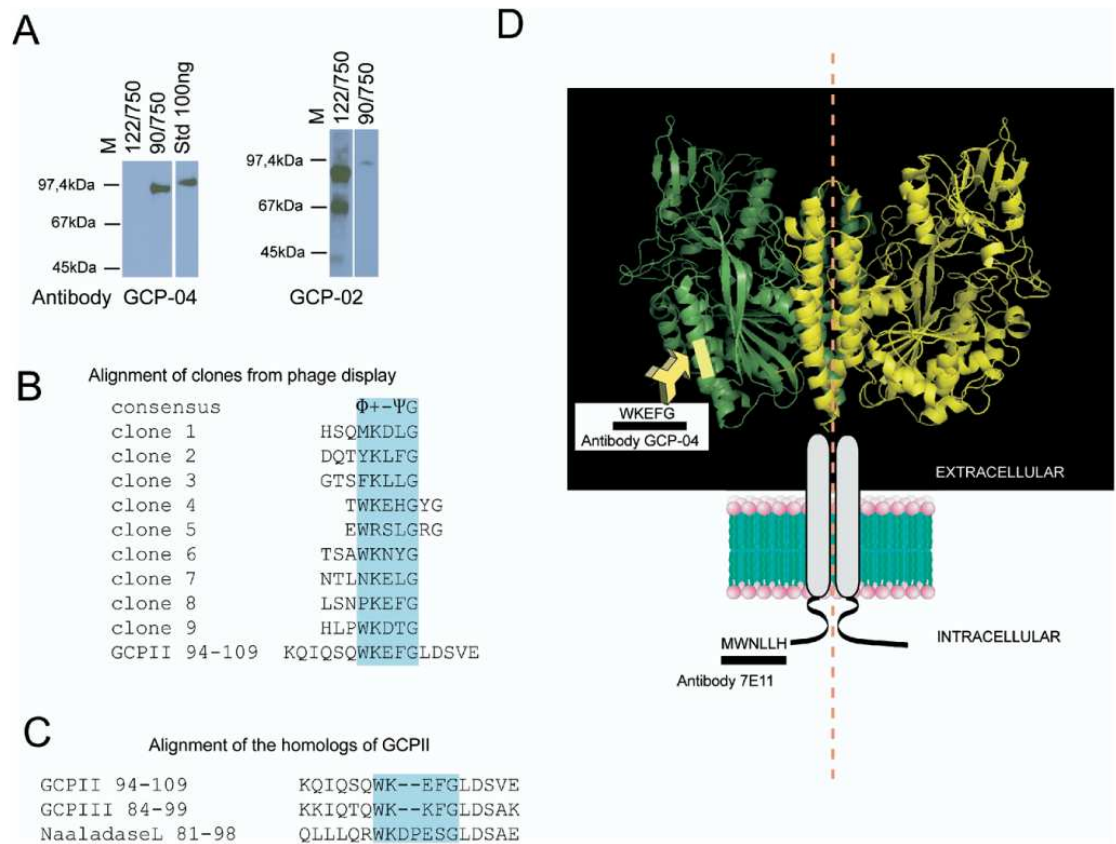


Fig. 1. Epitope mapping of GCP-04 antibody. (A) Western blot analysis comparing immunoreactivity of truncated variants of GCP-II and recombinant ectodomain of GCP-II (amino acids 44–750, Std), using monoclonal antibodies GCP-04 and GCP-02. Purified recombinant proteins comprised of amino acids 44–750 (Std), 90–750, and 122–750 were separated on SDS PAGE, blotted onto nitrocellulose membrane and visualized using the corresponding mAb. (B) Alignment of sequenced phage clones obtained after four rounds of panning to immobilized GCP-04 (for details see the Experimental Procedures). (C) Alignment of the sequences of known GCP-II homologs in the position corresponding to the GCP-04 epitope in GCP-II. (D) Graphic representation of the localization of epitopes recognized by monoclonal antibodies 7E11 and GCP-04 in the 3D structure of GCP-II (Mesters et al., 2006).

100–104 of human GCP-II (see Fig. 1, panel B). A homologous sequence was identified in human GCP-III, suggesting that GCP-04 also recognizes this homologous protein (Fig. 1, panel C). The epitope location is further corroborated by the fact that in the Western blots, GCP-04 gives a positive signal with mutants truncated up to amino acid 90 of GCP-II, but fails to recognize GCP-II mutants missing the first 121 amino acids. On the other hand, mAb GCP-02 recognizes all of the truncated variants of GCP-II tested and could therefore be used as a control for the expression of both variants (see Fig. 1, panel A).

Interestingly, the GCP-04 interacting amino acid segment is a part of an alpha-helix in the native human GCP-II (Mesters et al., 2006, Fig. 1, panel D), and due to this spatial arrangement it is inaccessible to antibody binding. Indeed, the GCP-04 mAb interacts with GCP-II only under denaturing conditions. In direct comparison to 7E11, antibody GCP-04 was at least 10 times more sensitive for

immunochemical detection of the GCP-II antigen. Therefore, SDS PAGE analysis of the brain cell lysates probed with 7E11 yielded only a weak, specific signal (Fig. 2A).

Enzymatic and immunochemical detection of GCP-II in the brain

Fig. 3A demonstrates that GCP-II expression was observed in all 30 samples from individual brain regions. Panel B of the same figure provides additional immunochemical detection of GCP-II in selected brain regions in a total of five human brains: frontal cerebral cortex (lanes S2/1 to S2/4), temporal gray matter (lanes S4/2–S4/4), temporal white matter (lanes S6/1 to S6/4), nucleus caudatus (lanes S11/1, S11/2 and S11/4), spinal cord (lanes S24/1 to S24/4), and the brainstem region (lanes S30/1 to S30/4). In order to provide direct comparison of the GCP-II expression in these brain regions in a single brain, samples from

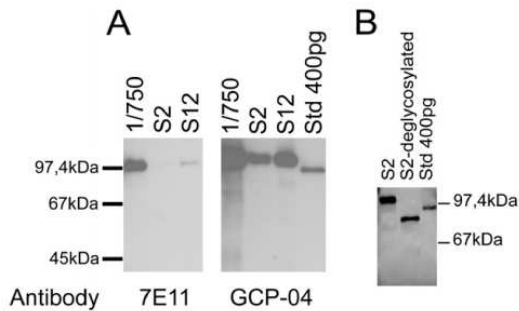


Fig. 2. (A) Comparison of the specificity and selectivity of monoclonal antibodies GCP-04 and 7E11. S2 cells stable transfected by a plasmid encoding the full length (1–750) GCP-II (Barinka et al., 2004a) and human brain samples S2 (frontal cerebral cortex) and S12 (globus pallidum; see Table 1) were analyzed on SDS-PAGE, blotted onto nitrocellulose membrane, and visualized either by GCP-04 or 7E11. Std, 400 pg of pure recombinant GCP-II (amino acids 44–750) was loaded as a control. (B) Glycosylation of GCP-II in human brain. A sample of frontal cerebral cortex was deglycosylated *in vitro* and resolved on 10% SDS PAGE, blotted onto nitrocellulose membrane, and visualized using the mAb GCP-04. Std, 400 pg of pure recombinant GCP-II (amino acids 44–750) was loaded as a control. For experimental details see Experimental Procedures.

individual regions of brain five are displayed in the last six lanes (S2/5 to S30/5). The temporal white matter (samples S6 from both panels), the brainstem (S30) and, to a lesser extent, the frontal cerebral cortex, seem to express the highest amounts of GCP-II.

For the quantification of the expression level of GCP-II in individual samples, we used purified recombinant human GCP-II as a standard, loaded six defined concentrations of the protein on each gel, and analyzed the resulting Western blots by densitometry (see the first two lanes in

panel A and the first lane in panel B). Using this approach, we were able to identify as little as 40 pg of GCP-II in a sample (data not shown). In several samples, small variations in the apparent mobilities of immunoreactive species were observed (e.g. lanes S5 and S6, Fig. 3A). Moreover, additional immunoreactive bands were observed in several samples containing higher amounts of GCP-II. While some additional bands could be explained by the cross-reactivity of the mAb with other cellular proteins, we hypothesized that other bands might mirror different glycosylation patterns in individual human brain cell types. Therefore, we subjected the samples to *in vitro* deglycosylation by the peptide N-glycosidase F. The results of the experiment are depicted in Fig. 2B. Upon deglycosylation *in vitro*, the relative mobility of the immunoreactive band from the frontal cerebral cortex sample decreases by approximately 15 kDa. However, the lower-molecular weight components seen in the original samples are still present in the deglycosylated one, with a corresponding shift in the relative mobility. Thus, the heterogeneity observed in the Western blot analysis cannot be accounted for by different glycosylation patterns alone.

In order to compare the specific NAAG-hydrolyzing activities that we attribute to the enzymatic activities of GCP-II expressed in selected parts of the brain, the cleared cell lysates were tested for their NAAG-hydrolyzing activity using a radiolabeled substrate. The product of the enzymatic hydrolysis, ^3H -labeled free glutamate, was separated and quantified by liquid scintillator. Since the substrate turnover was kept below 30% in all reactions, the product concentrations are directly proportional to the specific enzymatic activities of the individual samples. The results of this analysis are summarized in Table 2. Much higher NAAG-hydrolyzing activities (per mg of total protein)

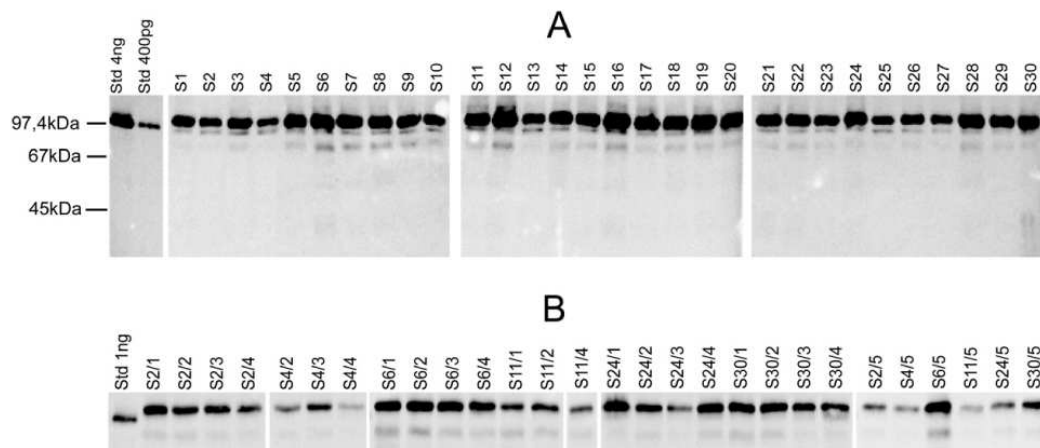


Fig. 3. Western blot analysis of GCP-II expression in individual sections of human brain using GCP-04 antibody. (A) Thirty samples from various loci of a single male brain. For sample identification see Table 1. (B) Immunodetection of GCP-II expression in six brain regions of five human brains: frontal cerebral cortex (lines S2/1 to S2/4), temporal gray matter (lines S4/2–S4/4), temporal white matter (lines S6/1 to S6/4), nucleus caudatus (lines S11/1, S11/2 and S11/4), spinal cord (lines S24/1 to S24/4), and the brainstem region (lines S30/1 to S30/4). For a clear, direct comparison of GCP-II expression within a single brain, samples from all six regions of brain five are displayed in the last six lanes (S2/5 to S30/5). For sample identification see Table 1. Std, different amounts of purified recombinant GCP-II (amino acids 44–750) for quantitative comparison.

are seen in the astrocyte-rich white matter of the brain. The specific activities (per mg of GCPII) were obtained by quantification of the relative intensities of corresponding immunoblot bands in Fig. 3 photographed by a CCD-camera and analyzed by ImageQuant software. Pure recombinant extracellular GCPII (250 pg to 4 ng) was used as a standard for quantification. The results suggest that the specific activity of GCPII is between 27 and 47 nmol/min/mg GCPII.

GCPII and III: antibody specificity and activity comparison

In order to determine the selectivity of the GCP-04 antibody against individual homologs of the enzyme (namely GCPIII), we probed recombinant GCPII and GCPIII proteins, expressed and purified from insect cells (Barinka et al., 2002; Hloučková et al., manuscript in preparation), with GCP-04. These results are shown in Fig. 4A. GCP-04, the mAb that we use for histochemical and immunochemical detection throughout this manuscript, is approximately two orders of magnitude less sensitive toward the recombinant human GCPIII than toward recombinant GCPII. The reason for this difference might be a single amino acid substitution in the sequence of GCPIII (Lys92→Glu102; compare Fig. 1C).

In order to quantify the possible contribution of GCPIII activity to the overall NAAG-hydrolyzing activity observed in the assay, we directly compared the NAAG-hydrolyzing activities of pure recombinant GCPII under the assay conditions used for the analysis of the NAAG-hydrolyzing activities of the samples from the human brain. GCPII is approx. 30 times more active than GCPIII under identical conditions (the specific activity of GCPII is 646 ± 123 nmol of hydrolyzed NAAG/min/mg of GCPII while GCPIII converts 19 ± 0.1 nmol of NAAG/min/mg, see Fig. 4B).

Immunohistochemistry of GCPII in human brain

Since only scarce and controversial data have been available on the expression of GCPII in various structures of the human brain and on its subcellular localization, we set out to analyze GCPII expression by immunohistochemistry using the novel mAb described above. Figs. 5 and 6 exemplify the results that we obtained on both male and female brain slices.

GCPII was reported to be expressed predominantly in astrocytes in a rat model (Berger et al., 1999). Consistent with these observations, we noticed intense immunoreactivity of the astrocyte-containing white matter when compared with that of the gray matter. The expression of GCPII was not observed in any other cell type of the CNS. This observation could be best documented on the inferior temporal gyrus (Fig. 5, panel A), medulla oblongata (Fig. 5, panel B) and basal ganglia (Fig. 5, panel C) where the white matter is closely intermixed with gray matter islands. In all three panels, immunopositive astrocytes in the white matter form clearly distinguishable darker areas around or within the surrounding gray matter that seems to express GCPII very slightly or not at all. In the astrocytes, the expression of GCPII was localized to the cytoplasm of the cell bodies near the cellular membrane; pure membranous positivity was observed only rarely. Focal positivity of astrocytic processes was present in the form of small puncta dispersed in the surrounding white matter. Such an observation was made in each sample analyzed by immunohistochemistry (data not shown).

To find out whether all astrocytes express GCPII, we performed immunohistochemical reactions with the anti-GFAP antibody. Although not quantified, the GFAP positive astrocytes clearly outnumbered the GCPII positive

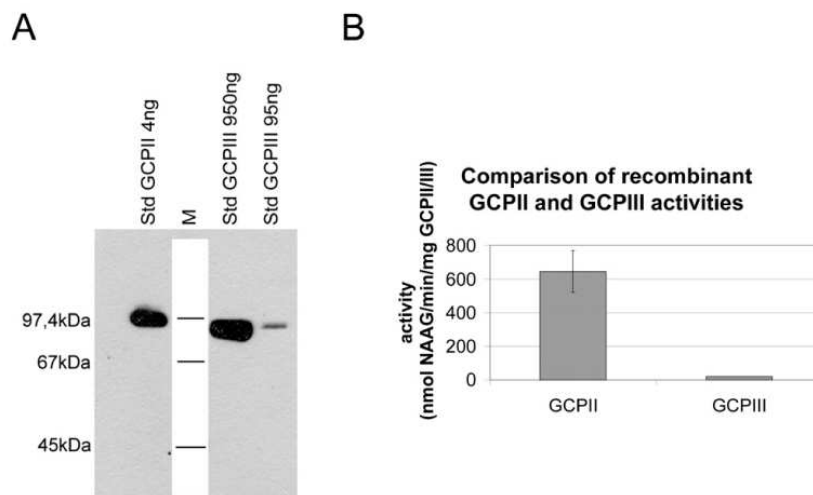


Fig. 4. Comparison of pure recombinant GCPII and GCPIII by Western blot and by activity measurements. (A) Western blot of GCPII and GCPIII: Std GCPII, purified recombinant ectodomain of GCPII (amino acids 44–750), Std GCPIII, different amounts of purified recombinant ectodomain of GCPIII (amino acids 36–740), M, molecular weight marker. Antibody GCP-04 was used for immunodetection. (B) Direct comparison of GCPII and GCPIII NAAG-hydrolyzing activities. For experimental details see Experimental Procedures.

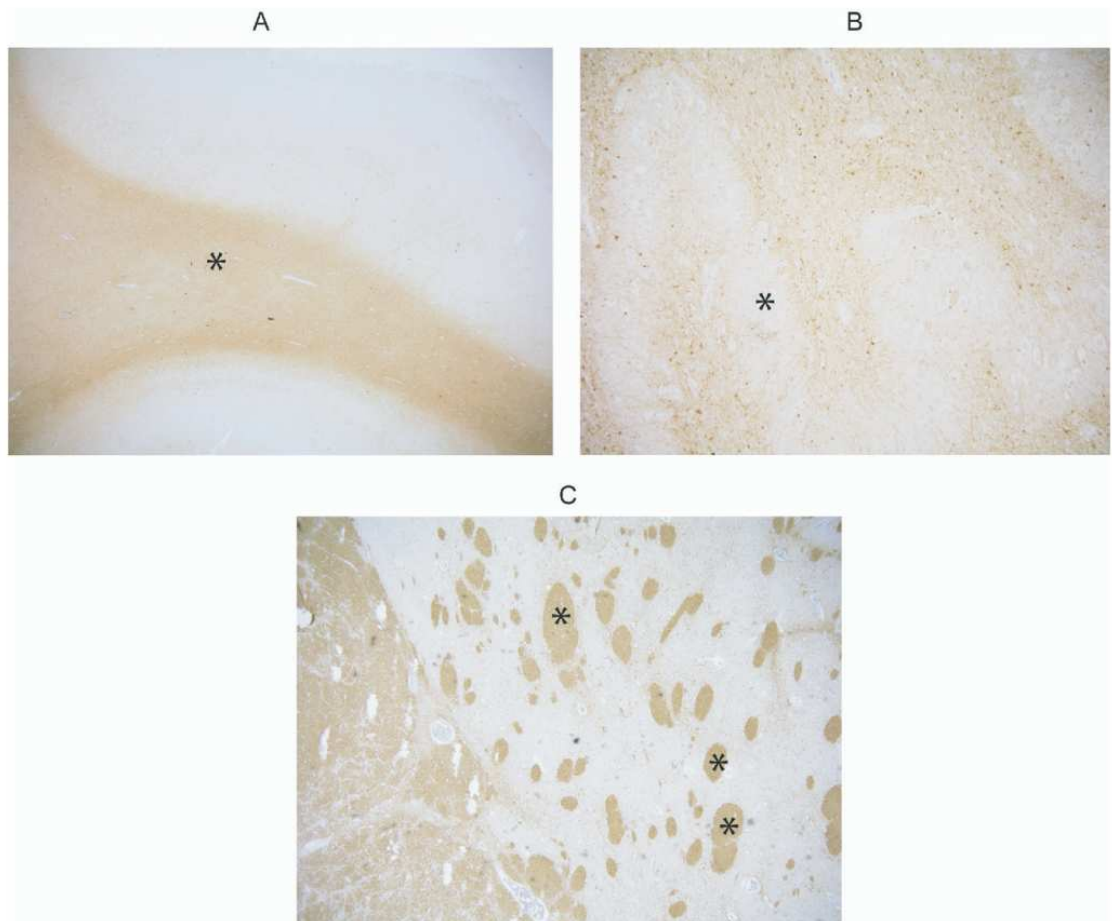


Fig. 5. Localization of GCPII expression in selected regions of the human brain. Immunoperoxidase method, counterstained slightly with hematoxylin. For experimental details see Experimental Procedures. (A) Inferior temporal gyrus. Note the intense immunoreactivity of the white matter (indicated by asterisk *) when compared with that of the cortex. Original magnification 25 \times . (B) Medulla oblongata. The low reactivity of the inferior olivary nucleus (*), in which GCPII-positive astrocytes are scarce, forms the serpentine pale area in the surrounding white matter. Original magnification 40 \times . (C) Basal ganglia—the increased reactivity of the white matter bands (*) inside the gray matter of the basal ganglia. Original magnification 40 \times .

cells in each studied region of the gray matter, indicating that not all astrocytes express GCPII (Fig. 6, panel F). The colocalization of GCPII and GFAP was confirmed by double-labeling immunofluorescence staining using anti-GCPII and anti-GFAP antibodies (Fig. 6, panels C–F). GFAP-positive cells not expressing GCPII are indicated by an asterisk in Fig. 6, panel F.

DISCUSSION

GCPII is a well-established tumor cell marker and a therapeutic target for prostate cancer. It is also a very attractive target for therapeutic intervention in pathological processes in which excessive glutamate is neurotoxic. Therefore, it is surprising that only limited information on the expression of the enzyme in the human CNS is available. Most of the literature reports analyze only the

NAAG-hydrolyzing activity in human brain or determine expression of the enzyme detected immunochemically in rodent tissues. Several authors failed to detect the expression of GCPII in the human CNS by immunochemical or immunohistochemical methods using various monoclonal antibodies.

The outcome of the immunochemical protein determination obviously depends on the antibody available. The mAb GCP-04 used throughout this study was prepared using the extracellular part of GCPII, obtained by heterologous expression in a *Drosophila* cell line. Recombinant proteins expressed by insect cells might differ from the authentic, native proteins. Namely, they may show different glycosylation patterns in comparison to their human counterparts. However, analyses of the glycosylation of recombinant GCPII revealed the N-glycosylation sites are

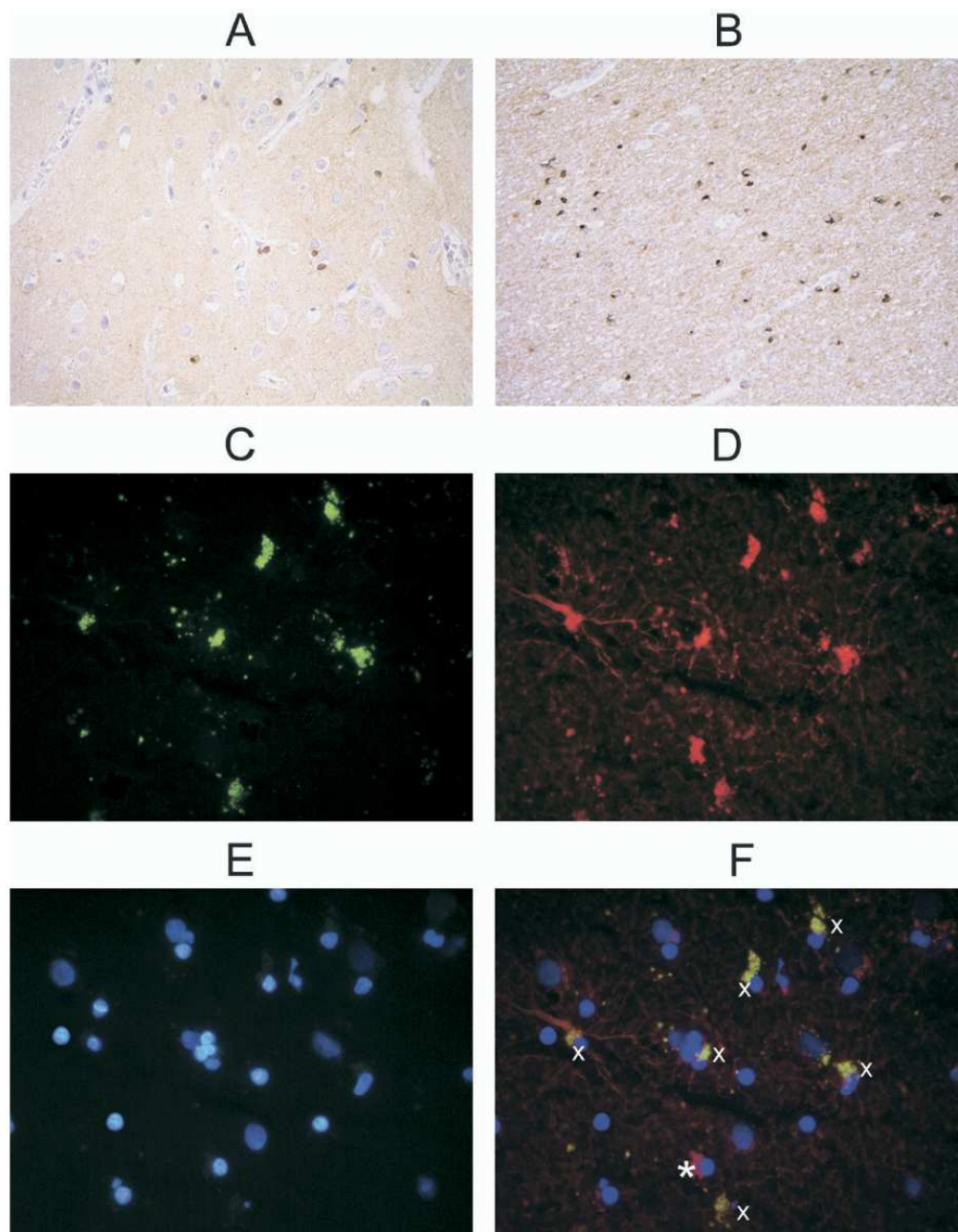


Fig. 6. Localization of GCP II expression in frontal cortex in comparison with GFAP expression. Immunoperoxidase method, counterstained slightly with hematoxylin. Original magnification 400 \times . (A) Frontal cortex: the immunopositive astrocytes (detected by GCP-04 antibody) are scarce in the gray matter. (B) White matter, stained with GCP-04 antibody. The number of GCP II immunoreactive cells is higher in the white matter than in the cortex (A). (C–F) The double-labeling GCP-04/GFAP immunofluorescence in the human frontal cortex. (C, D) The GCP II (visualized by FITC-labeled GCP-04 antibody, green) is localized to the cytoplasm of a portion of GFAP- positive astrocytes (Cy3, red). (E) The nuclei of the cells are visualized by DAPI staining. (F) The cytoplasmic co-localization of GCP II and GFAP in the superimposed image is indicated by a cross (x); the GFAP positive but GCP-04 negative astrocytes are indicated by asterisks (*). Original magnification 600 \times .

identical to those of human GCPII and that both proteins show equivalent activity (Ghosh and Heston, 2003; Barinka et al., 2004b).

In an attempt to quantify GCPII expression in individual tissue sections, we performed Western blot analysis using GCP-04. The semi-quantitative analysis of the signal intensities in the blots using a standard calibration curve of known concentrations of rhGCPII yielded concentrations of GCPII in various sections of the CNS ranging from approximately 50–300 ng per mg of total protein. No other quantitative value is available for GCPII expression in human brain; however, this value is slightly lower than the numbers published by Murphy et al. (2000) for GCPII expression in normal human prostate and than values reported by Sokoloff et al. (2000), who reported 519–4254 ng/mg protein in the normal prostate and 1.8–51 ng/mg protein in other tissues.

At least two other homologs of GCPII, GCPIII (formerly referred to as NAALADase II) and NAALADase L (Pangalos et al., 1999), have been described. Since these homologs differ in the N-terminal parts of their amino acid sequence, they lack the epitope recognized by the 7E11 antibody and thus should not cross-react with GCPII in immunochemical determination using this antibody. Epitope mapping using a phage display approach revealed that GCP-04 interacts with the linear epitope comprising amino acids 100–104 of human GCPII. In human NAALADase L, a close homolog of GCPII with 54% sequence similarity, this linear epitope is disrupted by the insertion of two amino acids (see Fig. 1 panel C), and consequently, GCP-04 might not be able to recognize the protein. Another GCPII-like protein described in the literature is PSMA-like protein. Its sequence starts at amino acid 309 (GCPII numbering) (Pangalos et al., 1999; O'Keefe et al., 2004); it thus lacks the epitope recognized by GCP-04. Furthermore, since it also lacks the active-site domain of GCPII, as determined by X-ray crystallography (Mesters et al., 2006), it is highly improbable that it shows any peptidase activity whatsoever.

The closest homolog of GCPII in human is GCPIII. In order to dissect the contributions of GCPII and GCPIII to the overall NAAG-hydrolyzing activity in the human brain, we cloned and expressed human GCPIII in insect cells (Hloučová et al., manuscript in preparation). As shown in Fig. 4A, antibody GCP-04 is at least 100 times more sensitive to recombinant purified GCPII than to purified GCPIII. A single amino acid substitution in the epitope sequence of GCPIII (Lys92→Glu102) seems to be responsible for a profound decrease in the affinity of GCP-04 mAb toward GCPIII. As the NAAG-hydrolyzing activity is concerned, in the assay conditions used in this paper, GCPII is approx. 30 times more active than GCPIII. A more detailed analysis of the enzymatic activity of GCPIII will be given elsewhere (Hloučová et al., manuscript in preparation).

It should be noted that these results do not suggest that GCPIII expression and/or activity in human brain is irrelevant. Enzymatic activities of metalloenzymes are highly dependent on the exact assay conditions. Furthermore, no direct comparison has been reported for

the antibodies used in previous studies, and it remains questionable as to what extent the GCPII-homologs have interfered with the immunologic detection of GCPII in human tissues in the studies published by other authors previously.

Western blots of brain sections (Fig. 3) show one major and two minor immunoreactive bands. The electrophoretic mobility of the major band corresponds to the expected molecular weight of GCPII. Lower bands are much weaker in intensity and might thus represent a degradation product, cross-reactive human protein, or a truncated GCPII variant (Bzdega et al., 1997). In order to analyze whether or not these two bands represent alternatively glycosylated GCPII species, we deglycosylated the corresponding samples by PNGase F *in vitro* (Fig. 2B). Equivalent heterogeneity of the samples was shown after the deglycosylation, suggesting that the immunoreactive bands do not differ solely in glycosylation state.

The specific expression of GCPII in studied tissues was further confirmed by its enzymatic activity, analyzed as the ability to hydrolyze radiolabeled NAAG. The values summarized in Table 2 range from 1 to 12 pmol/min/mg of total protein. These values are higher than those reported by Tsai et al. (1991) in several sections of CNS (ranging from 0.3 pmol/h/mg in spinal cord to 8.5 pmol/h/mg in the motor cortex). On the other hand, the values reported for the NAAG-hydrolyzing activities in the rat CNS are approximately 10 times higher than the activities reported in this paper (Fuhrman et al., 1994; Blakely et al., 1988; Robinson et al., 1987). These discrepancies could be explained by the fact that these authors analyzed the activity of an isolated membrane fraction of rat CNS (and obtained thus much higher specific activities per milligram of the protein. Furthermore, sample preparation, storage, and assay conditions (especially buffer and salt concentration) strongly influence the activities of GCPII.

It should be noted that the NAAG-hydrolyzing activities of the cleared samples steadily increased with prolonged dialysis in our hands (data not shown). It could be argued that an endogenous inhibitor, slowly dissociating from the enzyme upon dialysis, might be present in the crude sample preparation. The exact method of sample preparation might thus considerably influence the outcome of the analysis and make direct comparison of the enzymatic activities reported by different groups very difficult.

In general, our data support the observations made by Slusher et al. (1992) and Berger et al. (1999) in a rodent model, suggesting that GCPII is mostly expressed in the white matter, specifically in the astrocytes. However, not all of the GFAP-positive astrocytes were immunopositive in our samples, as suggested by Berger et al. (1999) in the rat model. Based on our observations, we can speculate that GCPII is expressed mostly in fibrillary astrocytes (i.e. type II astrocytes), which are known to be present in higher numbers in the white matter when compared with the type I protoplasmic astrocytes of the gray matter. Accordingly, we did not observe a tight link between the expression of GFAP and GCPII, as was proposed by Luthi-Carter et al. (1998a).

CONCLUSION

In conclusion, in this study we report the first systematic analysis of the expression of GCPII in human brain using immunochemical detection. Using the specific mAb GCP-04, we have detected GCPII expression in all parts of the human brain. GCPII seems to be expressed exclusively in astrocytes, especially in those localized in the white matter. The presented immunochemical and histochemical data are generally in agreement with the enzymatic analyses of the corresponding brain samples.

Acknowledgments—The financial support of the Grant Agency of the Czech Republic 301/03/0784, the Ministry of Education of the Czech Republic No. MSM 0021620813 and 1M0508, and the Ministry of Health of the Czech Republic No. VZ FNM 0064203 is gratefully acknowledged. The authors thank Jana Starková and Adrian Cibula for their excellent technical help and Hillary Hoffman for the critical proofreading of the manuscript.

REFERENCES

- Bacich DJ, Ramadan E, O'Keefe DS, Bukhari N, Węgorzewska I, Ojeifo O, Olszewski R, Wrenn CC, Bzdega T, Wroblewska B, Heston WD, Neale JH (2002) Deletion of the glutamate carboxypeptidase II gene in mice reveals a second enzyme activity that hydrolyzes N-acetylaspartylglutamate. *J Neurochem* 83: 20–29.
- Barinka C, Rinnova M, Sacha P, Rojas C, Majer P, Slusher BS, Konvalinka J (2002) Substrate specificity, inhibition and enzymological analysis of recombinant human glutamate carboxypeptidase II. *J Neurochem* 80:477–487.
- Barinka C, Mlcochova P, Sacha P, Hilgert I, Majer P, Slusher BS, Horejsi V, Konvalinka J (2004a) Amino acids at the N- and C-termini of human glutamate carboxypeptidase II are required for enzymatic activity and proper folding. *Eur J Biochem* 271: 2782–2790.
- Barinka C, Sacha P, Sklenar J, Man P, Bezouska K, Slusher BS, Konvalinka J (2004b) Identification of the N-glycosylation sites on glutamate carboxypeptidase II necessary for proteolytic activity. *Protein Sci* 13:1627–1635.
- Berger UV, Carter RE, Coyle JT (1995) The immunocytochemical localization of N-acetylaspartyl glutamate, its hydrolysing enzyme NAALADase, and the NMDAR-1 receptor at a vertebrate neuromuscular junction. *Neuroscience* 64:847–850.
- Berger UV, Luthi-Carter R, Passani LA, Elkabes S, Black I, Konradi C, Coyle JT (1999) Glutamate carboxypeptidase II is expressed by astrocytes in the adult rat nervous system. *J Comp Neurol* 415:52–64.
- Blakely RD, Robinson MB, Thompson RC, Coyle JT (1988) Hydrolysis of the brain dipeptide N-acetyl-L-aspartyl-L-glutamate: subcellular and regional distribution, ontogeny, and the effect of lesions on N-acetylated-alpha-linked acidic dipeptidase activity. *J Neurochem* 50:1200–1209.
- Bzdega T, Turi T, Wroblewska B, She DW, Chung HS, Kim H, Neale JH (1997) Molecular cloning of a peptidase against N-acetylaspartylglutamate from a rat hippocampal cDNA library. *J Neurochem* 69:2270–2277.
- Bzdega T, Crowe SL, Ramadan ER, Sciarretta KH, Olszewski RT, Ojeifo OA, Rafalski VA, Wroblewska B, Neale JH (2004) The cloning and characterization of a second brain enzyme with NAAG peptidase activity. *J Neurochem* 89:627–635.
- Carter RE, Feldman AR, Coyle JT (1996) Prostate-specific membrane antigen is a hydrolase with substrate and pharmacologic characteristics of a neuropeptidase. *Proc Natl Acad Sci U S A* 93: 749–753.
- Chang SS, Reuter VE, Heston WD, Bander NH, Grauer LS, Gaudin PB (1999) Five different anti-prostate-specific membrane antigen (PSMA) antibodies confirm PSMA expression in tumor-associated neovasculature. *Cancer Res* 59:3192–3198.
- Davis MI, Bennett MJ, Thomas LM, Bjorkman PJ (2005) Crystal structure of prostate-specific membrane antigen, a tumor marker and peptidase. *Proc Natl Acad Sci U S A* 102:5981–5986.
- Fuhrman S, Palkovits M, Cassidy M, Neale JH (1994) The regional distribution of N-acetylaspartylglutamate (NAAG) and peptidase activity against NAAG in the rat nervous system. *J Neurochem* 62:275–281.
- Ghadge GD, Slusher BS, Bodner A, Dal Canto M, Wozniak K, Thomas AG, Rojas C, Tsukamoto T, Majer P, Miller RJ, Monti AL, Roos RP (2003) Glutamate carboxypeptidase II inhibition protects motor neurons from death in familial amyotrophic lateral sclerosis models. *Proc Natl Acad Sci U S A* 100:9554–9559.
- Ghosh A, Heston WD (2003) Effect of carbohydrate moieties on the folate hydrolysis activity of the prostate specific membrane antigen. *Prostate* 57:140–151.
- Halsted CH, Ling EH, Luthi-Carter R, Villanueva JA, Gardner JM, Coyle JT (1998) Folylpolypoly-gamma-glutamate carboxypeptidase from pig jejunum. Molecular characterization and relation to glutamate carboxypeptidase II. *J Biol Chem* 273:20417–20424.
- Horoszewicz JS, Kawinski E, Murphy GP (1987) Monoclonal-antibodies to a new antigenic marker in epithelial prostatic cells and serum of prostatic-cancer patients. *Anticancer Res* 7:927–936.
- Huang XM, Bennett M, Thorpe PE (2004) Anti-tumor effects and lack of side effects in mice of an immunotoxin directed against human and mouse prostate-specific membrane antigen. *Prostate* 61: 1–11.
- Israeli RS, Powell CT, Corr JG, Fair WR, Heston WDW (1994) Expression of the prostate-specific membrane antigen. *Cancer Res* 54:1807–1811.
- Jackson PF, Tays KL, Maclin KM, Ko YS, Li W, Vitharana D, Tsukamoto T, Stoermer D, Lu XC, Wozniak K, Slusher BS (2001) Design and pharmacological activity of phosphinic acid based NAALADase inhibitors. *J Med Chem* 44:4170–4175.
- Lopes AD, Davis WL, Rosenstraus MJ, Uveges AJ, Gilman SC (1990) Immunohistochemical and pharmacokinetic characterization of the site-specific immunoconjugate Cyt-356 derived from antiprostata monoclonal antibody-7E11-C5. *Cancer Res* 50:6423–6429.
- Lu XM, Tang Z, Liu W, Lin Q, Slusher BS (2000) N-acetylaspartylglutamate protects against transient focal cerebral ischemia in rats. *Eur J Pharmacol* 408:233–239.
- Luthi-Carter R, Berger UV, Barczak AK, Enna M, Coyle JT (1998a) Isolation and expression of a rat brain cDNA encoding glutamate carboxypeptidase II. *Proc Natl Acad Sci U S A* 95:3215–3220.
- Luthi-Carter R, Barczak AK, Speno H, Coyle JT (1998b) Molecular characterization of human brain N-acetylated alpha-linked acidic dipeptidase (NAALADase). *J Pharmacol Exp Ther* 286: 1020–1025.
- Mesters JR, Barinka C, Li W, Tsukamoto T, Majer P, Slusher BS, Konvalinka J, Hilgenfeld R (2006) Structure of glutamate carboxypeptidase II, a drug target in neuronal damage and prostate cancer. *EMBO J* 25:1375–1384.
- Murphy GP (1995) Radioscintiscanning of prostate-cancer. *Cancer* 75:1819–1822.
- Murphy GP, Su S, Jarisch J, Kenny GM (2000) Serum levels of PSMA [letter]. *Prostate* 42:318–319.
- Neale JH, Bzdega T, Wroblewska B (2000) N-Acetylaspartylglutamate: the most abundant peptide neurotransmitter in the mammalian central nervous system. *J Neurochem* 75:443–452.
- Neale JH, Olszewski RT, Gehl LM, Wroblewska B, Bzdega T (2005) The neurotransmitter N-acetylaspartylglutamate in models of pain, ALS, diabetic neuropathy, CNS injury and schizophrenia. *Trends Pharmacol Sci* 26:477–484.

- O'Keefe DS, Bacich DJ, Heston WDW (2004) Comparative analysis of prostate-specific membrane antigen (PSMA) versus a prostate-specific membrane antigen-like gene. *Prostate* 58:200–210.
- Pangalos MN, Neefs JM, Somers M, Verhasselt P, Bekkers M, van der Helm L, Fraiponts E, Ashton D, Gordon RD (1999) Isolation and expression of novel human glutamate carboxypeptidases with N-acetylated alpha-linked acidic dipeptidase and dipeptidyl peptidase IV activity. *J Biol Chem* 274:8470–8483.
- Renneberg H, Friedetzky A, Konrad L, Kurek R, Weingartner K, Wennenmuth G, Tunn UW, Aumuller G (1999) Prostate specific membrane antigen (PSM) is expressed in various human tissues: implication for the use of PSM reverse transcription polymerase chain reaction to detect hematogenous prostate cancer spread. *Urol Res* 27:23–27.
- Robinson MB, Blakely RD, Couto R, Coyle JT (1987) Hydrolysis of the brain dipeptide N-acetyl-L-aspartyl-L-glutamate. Identification and characterization of a novel N-acetylated alpha-linked acidic dipeptidase activity from rat brain. *J Biol Chem* 262:14498–14506.
- Silver DA, Pellicer I, Fair WR, Heston WD, Cordon-Cardo C (1997) Prostate-specific membrane antigen expression in normal and malignant human tissues. *Clin Cancer Res* 3:81–85.
- Slusher BS, Tsai G, Yoo G, Coyle JT (1992) Immunocytochemical localization of the N-acetyl-aspartyl- glutamate (NAAG) hydrolyzing enzyme N-acetylated alpha-linked acidic dipeptidase (NAALADase). *J Comp Neurol* 315:217–229.
- Slusher BS, Vormov JJ, Thomas AG, Hurn PD, Harukuni I, Bhardwaj A, Traystman RJ, Robinson MB, Britton P, Lu XC, Tortella FC, Wozniak KM, Yudkoff M, Potter BM, Jackson PF (1999) Selective inhibition of NAALADase, which converts NAAG to glutamate, reduces ischemic brain injury. *Nat Med* 5:1396–1402.
- Sokoloff RL, Norton KC, Gasior CL, Marker KM, Grauer LS (2000) A dual-monoclonal sandwich assay for prostate-specific membrane antigen: levels in tissues, seminal fluid and urine. *Prostate* 43:150–157.
- Su SL, Huang IP, Fair WR, Powell CT, Heston WD (1995) Alternatively spliced variants of prostate-specific membrane antigen RNA: ratio of expression as a potential measurement of progression. *Cancer Res* 55:1441–1443.
- Troyer JK, Beckett ML, Wright GL Jr (1995) Detection and characterization of the prostate-specific membrane antigen (PSMA) in tissue extracts and body fluids. *Int J Cancer* 62:552–558.
- Tsai GC, Stauch-Slusher B, Sim L, Hedreen JC, Rothstein JD, Kuncel R, Coyle JT (1991) Reductions in acidic amino-acids and N-acetylaspartylglutamate in amyotrophic-lateral-sclerosis CNS. *Brain Res* 556:151–156.
- Wroblewska B, Wroblewski JT, Pshenichkin S, Surin A, Sullivan SE, Neale JH (1997) N-acetylaspartylglutamate selectively activates mGluR3 receptors in transfected cells. *J Neurochem* 69:174–181.
- Yamamoto T, Hirasawa S, Wroblewska B, Grajkowska E, Zhou J, Kozikowski A, Wroblewski J, Neale JH (2004) Antinociceptive effects of N-acetylaspartylglutamate (NAAG) peptidase inhibitors ZJ-11, ZJ-17 and ZJ-43 in the rat formalin test and in the rat neuropathic pain model. *Eur J Neurosci* 20:483–494.

(Accepted 7 October 2006)
(Available online 5 December 2006)

6.6 Full length form of GCPII – PSMA and the origin of its truncated form

6.6.1 Background information

In the human prostate full length form of GCPII (=PSMA) and other three spliced variants were identified [7] (see chapter 3.1.1).

PSM' is the most intensively studied spliced form of GCPII. It lacks 266 nucleotides from the 5' end [8] and thus it does not have any intracellular nor transmembrane domain. The expressed protein was observed as a 95kDa cytosolic protein [221]. Moreover, NAAG hydrolyzing activity was detected in cytosolic fraction from GCPII expressing cells and prostate tissues [221-223].

All studies on PSM' protein assumed that this cytosolic protein arises from alternatively spliced mRNA. We found that N-glycosylation is indispensable for GCPII enzyme activity [17, 224, 225]. Since cytosolic proteins are not supposed to be N-glycosylated, we hypothesize that PSM' might in fact represent a product of posttranslation cleavage of GCPII.

6.6.2 Summary

The expression of PSM' was investigated in different cell lines. Surprisingly, it was detected in HEK293 (Human Embryonal Kidney) cells transfected with a plasmid coding only for full length GCPII, thus no alternative splicing could occur.

We confirmed that PSM' is located into cytosol, possesses hydrolytic activity and it is N-glycosylated. Interestingly, it does not contain any signal peptide to be guided into glycosylation pathways into endoplasmatic reticulum. From that we conclude that PSM' is not a product of translation from an open reading frame of GCPII, nor the product of alternative splicing.

GCPII contains an internalization signal and internalizes into the cell. It is possible that after internalization the protein undergoes endoproteolytic cleavage. To investigate this hypothesis we biotinylated cell surface proteins (including GCPII), allowed internalization to proceed and investigated cytosol for biotinylated PSM'. We observed PSM' in the cytosol but it was not biotinylated.

Our data suggest that PSM' might not arise from alternative splicing. We have not found evidence suggesting that it could arise from proteolytic cleavage during internalization. We can only speculate that this truncated protein form of GCPII might be produced by a proteolytic processing on its way through trafficking pathway into the cytoplasm.

6.6.3 Publication VI

Prostate-Specific Membrane Antigen and its Truncated Form PSM'

Petra Mlčochová^{1,2}, Cyril Bařinka^{1#}, and Jan Konvalinka^{1,2*}

¹Gilead Sciences and IOCB Research Centre, Institute of Organic Chemistry and Biochemistry, Academy of Sciences of the Czech Republic, Flemingovo n. 2, Prague 6, 166 10 Czech Republic

²Dept. of Biochemistry, Faculty of Science, Charles University, Hlavova 2030, Prague 2, 128 43 Czech Republic

[#]Current address: National Cancer Institute at Frederick, 539 Boyles Street, Frederick, MD 21702, USA

*to whom correspondence should be addressed

Abbreviations:

ER, endoplasmic reticulum; HEK 1-750, Human Embryonic Kidney cell line transfected with plasmid encoding PSMA (amino acids 1-750); IMDM, Iscove's Modified Dulbecco's Medium; IP, immunoprecipitation; LNCaP, Lymph-Node Carcinoma of the Prostate cell line; NAAG, N-acetyl-L-aspartyl-L-glutamate; NA-HRP, neutravidin-horseradish peroxidase; PBS, Phosphate Buffered Saline; PSM', N-terminally truncated form of PSMA; PSMA, prostate specific membrane antigen

INTRODUCTION

Prostate specific membrane antigen (PSMA) is a 100kDa type II membrane glycoprotein expressed in all types of prostatic tissues, including normal epithelial cells, benign prostatic hyperplasia, prostatic intraepithelial neoplasia, and cancerous tissue [1,2]. In the prostate tissues, several alternatively spliced variants of PSMA have been identified, namely PSM', PSM-C, PSM-D, and PSM-E [3-5].

In PSM' bases 114-379 of the genomic PSMA sequence are absent due to alternative splicing [3,4]. PSM-C has the same splice donor site as PSM' (nucleotide 114) but an alternative acceptor site is located in intron one of PSMA; the mRNA contains an additional 133 nucleotides. PSM-D has the same splice donor site as PSM' and a unique acceptor site within intron one. It includes a novel exon [3]. PSM-E mRNA contains a unique exon (97 nucleotides), which is inserted between nucleotides 379 and 380 of PSMA cDNA. Furthermore, PSM-E lacks a 93-nucleotide region, nucleotides 2232-2324 of PSMA [5].

It has been shown that PSM' mRNA is predominantly expressed in normal prostate. The ratio of PSMA/PSM' mRNA levels can be used as a tumor index, which increases during prostate cancer (with increasing Gleason score) and can therefore be a useful indicator for diagnosis of prostate cancer and tumor progression [3,4]. PSM-C expression remains unchanged in normal prostate, primary prostate tumor, and metastasis; PSM-D is mainly expressed in metastasis [3]; and PSM-E mRNA expression levels vary significantly in normal prostate, benign prostatic hyperplasia, and prostate cancer [5].

PSM' is the most frequently described alternatively spliced variant of PSMA. Its cDNA lacks nucleotides at the 5' end [3,4], which encode the intracellular and transmembrane domain in PSMA. PSM' was identified in LNCaP cells as a 95kDa cytosolic protein with the amino acid sequence starting at alanine in position 60 of the full length PSMA sequence [6,7].

The cytosolic fractions of LNCaP cells and prostate tissues have been analyzed, and PSM' shows equivalent enzymatic activity to PSMA [7-9].

All studies performed on PSM' have assumed that the protein arises from alternatively spliced mRNA. However, at the same time, data have been presented that PSMA is N-glycosylated [10-12] and that glycosylation is indispensable for its enzymatic activity. This seems contradictory in the case of PSM', since cytosolic proteins are generally not N-glycosylated. Therefore, in this report we set out to analyze the glycosylation, intracellular localization, and possible origin of PSM'.

MATERIALS AND METHODS

Western Blotting

Proteins were resolved by SDS-PAGE and electroblotted onto a nitrocellulose membrane. The membrane was probed with an anti-GCPII mouse antibody (GCP-04, 1mg/ml, 1:5,000 dilution;[11]) overnight at room temperature, followed by incubation with a goat anti-mouse horseradish peroxidase conjugated secondary antibody (1:25,000; Pierce, Rockford, IL, USA) for 1 hour. The blot was developed using SuperSignal West Dura Chemiluminiscence Substrate (Pierce).

Immunoprecipitation

Cells were lysed in RIPA buffer (50mM Tris, 150mM NaCl, 2% NP-40, 0.5% NaDOC, 0.1% SDS, pH 8.0) with protease inhibitor cocktail (Complete Mini, EDTA-free; Roche, Indianapolis, IN, USA) added, for 30min at 4°C. The cell lysate was pre-cleared with Protein G Sepharose (GE Healthcare Bio-Science, Uppsala, Sweden) and incubated with anti-GCPII mouse antibody 7E11 (3 µg) for 2 hrs. The antibody(7E11)-GCPII complex was incubated with Protein G Sepharose (GE Healthcare Bio-Science) for 1 hr at 4°C. The flow-through fraction was mixed with the anti-GCPII mouse antibody GCP-05 (3 µg) overnight at 4°C. The antibody(GCP-05)-GCPII complex was further incubated with Protein G Sepharose (GE Healthcare Bio-Science) for 4 hrs. Both resins were washed with RIPA buffer, and proteins were eluted with 8M guanidinium hydrochloride. The eluted proteins were precipitated by addition of 5% trichloroacetic acid and centrifuged. The pellet was dissolved in 1x SDS PAGE sample buffer.

Endoglycosidase digestion

Immunoprecipitated proteins and cell lysates were treated with 100U of PNGase F (New England Biolabs, Mississauga, ON, Canada) or 400U of Endo H (New England Biolabs) overnight at 37°C in a total volume of 20µL.

Differential centrifugation

LNCaP and HEK 1-750 cells were harvested in 20mM Tris, 130mM NaCl, pH 7.4, with added protease inhibitor cocktail (Roche, Indianapolis, IN, USA), frozen and thawed three times, and homogenized with 50 up and down strokes in a glass homogenizer. The homogenate was centrifuged at 600xg for 5min (the pellet contained whole cells, large debris, and nuclei). The supernatant was then centrifuged at 3,000xg for 20min to spin down mitochondria. Another centrifugation was performed at 10,000xg for 20min (pelleting lysosomes, peroxisomes), followed by centrifugation at 100,000xg for 1 hour (pelleting the microsomal fraction) and a final centrifugation at 300,000xg for 3 hrs (pelleting macromolecules). The remaining supernatant consisted of the soluble cytoplasmatic fraction.

Radioenzymatic Assay

The radioenzymatic assay using ³H-NAAG as a substrate (radiolabeled on the terminal glutamate) was performed as previously described [10].

Monoclonal antibody GCP-05

Hybridomas secreting monoclonal antibodies were prepared by standard methods from mice (F1 hybrids of BALB/c and B10.A strains) immunized with recombinant human PSMA as described previously [10].

Cell surface biotinylation

LNCaP cells were grown to 90% confluency, the medium was removed, and the cells were washed with precooled PBS. Cells were treated with 0.5mg water-soluble Sulfo-NHS-SS-Biotin (Pierce, Rockford, IL, USA) dissolved in PBS for 30min at 4°C and then washed with PBS. Biotinylation was stopped by 10mM glycine (in PBS), and cells were transferred back to

IMDM complete medium and incubated at 37°C for 1 hour to allow internalization of membrane proteins. The incubation was stopped by transferring the dishes to 4°C, biotins on cell surface proteins were stripped in a reducing solution (50mM glutathione, 75mM NaCl, 75mM NaOH in PBS) for 30min at 4°C. Cells were washed thrice in PBS. PSMA/PSM' proteins were immunoprecipitated and analyzed by Western blot using GCP-04 antibody (1:5,000) and Neutravidin-horseradish peroxidase conjugated antibody (1:2,500; Pierce, Rockford, IL, USA), specific for biotin.

RESULTS

N-glycosylation of PSM'

The expression of PSM' was studied in LNCaP cells, which endogenously express PSMA, as well as in HEK 293 cells transfected with a plasmid encoding full-length PSMA (amino acids 1-750; HEK1-750). Two protein species of approximately 100kDa and 96kDa were detected in the lysates of both cell lines, albeit in different ratios, using Western blot analysis. The lower molecular weight protein was the minor form in both cell lines studied (Fig.1A).

The lower molecular weight protein (approx. 96kDa) was identified as a N-terminally truncated PSMA (most likely PSM') using two specific antibodies, 7E11 and GCP-05, which recognize epitopes at the N-terminus and in the extracellular region of PSMA, respectively (Fig. 1B). The identification of PSM' was confirmed by mass spectroscopy (data not shown).

The nature and the extent of N-glycosylation of PSMA/PSM' in LNCaP and HEK1-750 cells was studied using PNGase F and endoglycosidase H (Endo H), two N-glycosidases with differing specificities, (Figure 2). While PNGase F removes N-linked oligosaccharides indiscriminately, Endo H cleaves within the chitobiose core of high-mannose and some hybrid-oligosaccharides from N-linked glycoproteins. Our data show that both PSMA and PSM' are sensitive to the PNGase F treatment and therefore both forms are N-glycosylated (Fig. 2: panel A, lines 1,3; panel B, lines 4,6 and Fig. 2: panel C,D). Endo H treatment also results in a partial shift of sample mobility, suggesting that the proteins are posttranslationally modified by a mixture of high-mannose or hybrid and complex type oligosaccharides (Fig. 2; panel A, B, lines 2 and 5) and are therefore trafficked beyond the *cis*-Golgi.

Subcellular localization of PSM'

Differential centrifugation analysis revealed that PSM' is localized predominantly in cytoplasm of both LNCaP and HEK 1-750 cells (Fig. 3, panel A,B). The fractions containing the highest amounts of PSM' were treated with PNGaseF to yield a lower molecular weight protein product corresponding to deglycosylated PSM' (Fig. 3, panel B). Individual fractions obtained by differential centrifugation were subsequently analyzed for proteolytic activity using *N*-acetyl-aspartyl-glutamate, a natural substrate of the brain form of PSMA [9]. The activity measurements confirmed that PSM' possesses hydrolytic activity comparable to that of PSMA (Fig. 3, panel C, D).

PSMA trafficking

To test the hypothesis that PSM' is a product of posttranslational processing of PSMA, cell surface biotinylation experiments were performed. The biotinylated cell surface PSMA protein was internalized into the cells, and lysates prepared from these cells were inspected for the presence of PSMA/PSM' proteins by immunoprecipitation and Western blotting (Fig. 4). Detection with GCP-04 (specific for PSMA/PSM'; Fig. 4A) showed the presence of PSMA (immunoprecipitated with 7E11 antibody) and PSM' (immunoprecipitated with GCP-05). On the other hand, detection with NA-HRP (specific for any biotinylated protein present; Fig. 4B) did not reveal a biotinylated PSM' form. This observation challenges the hypothesis that the truncated form PSM' arises from processing of PSMA during endosomal trafficking. A band of higher molecular weight was observed in these experiments (Fig. 4). Cross-linking experiments revealed that this band is a homodimer of PSMA and PSM' (data not shown).

To complement the cell surface biotinylation experiment, we analyzed the internalization of a PSMA variant with a mutation in the internalization signal. Internalization is regulated by the internalization signal LL(4,5), and a mutation in this signal resulted in impaired internalization of PSMA into the cell [13]. We therefore transfected HEK 293 cells

with plasmid 1-750 containing a specific mutation in the internalization signal (LL(4,5)AA). Cells expressing this mutant protein showed the same PSM' content as HEK 293 cells transfected with the wild type plasmid 1-750 (data not shown).

DISCUSSION

In this study we investigated the N-terminally truncated form of PSMA known as PSM' at the protein level. PSM' expression was observed in LNCaP cells, which is in agreement with previously reported observations [6]. Surprisingly, it was also detected in HEK293 cells transfected with a plasmid encoding the full length form, PSMA. This observation suggests that PSM' could be generated by a mechanism that is distinct from the generally accepted notion of an alternative splicing of the PSMA gene. We hypothesized that the truncated form might be generated *via* post-translational endoproteolytic cleavage of PSMA. A similar hypothesis was made for adaptor protein FE65, which is now known to be converted into an N-terminally truncated fragment through endoproteolysis [14].

The hypothetical PSM' protein arising from alternative translation (or from alternative splicing) would not contain the cytosolic and transmembrane domain and would therefore lack the signal sequence necessary to drive the newly synthesized protein into the endoplasmic reticulum and through the glycosylation process. Previous reports on PSM' did not include analysis of glycosylation [6]. Our experiments using endoglycosidases with different specificities showed that PSM' is N-glycosylated and contains a mixture of high mannose or hybrid and complex types of oligosaccharides. Even though O-glycosylation of PSMA has been reported [15] it was not analyzed in this study. We aimed our effort only to N-glycosylation, which is known to be indispensable for enzymatic activity of PSMA [10].

The observation of N-glycosylation in PSM' indicates that this truncated protein is trafficked not only into the ER but also to the Golgi apparatus. This trafficking is difficult to imagine without a signal sequence. Indeed, we have previously shown that insect cells transfected with cDNA encoding PSM' expressed a cytosolic protein that was not glycosylated and which showed no NAAG-hydrolysing activity [10]. Furthermore, mammalian cells transfected with cDNA encoding PSM' also expressed inactive, deglycosylated protein (data

not shown). The above mentioned results are difficult to reconcile with the notion of PSM' being a product of alternative translation or alternative splicing of the PSMA gene and our data suggest that the PSM' protein more likely originates from the endoproteolytic cleavage of the full-length PSMA.

The localization of PSM' to the cytosol as well as its NAAG-hydrolyzing activity were reported several times [6-9]. However, since the N-glycosylation of PSMA is indispensable for the hydrolytic activity of the enzyme [10], it is difficult to imagine that a cytosolic protein not secreted *via* the ER would be proteolytically active. In this report we confirm that PSM' is indeed localized in the cytosol and possesses hydrolytic activity. It is very rare to find N-linked glycoproteins existing in cytosol, yet there are some exceptions, such as a Na⁺-pump alpha subunit with N-linked carbohydrates facing the cytoplasm. Furthermore, studies have identified 14 glycoproteins containing high mannose and/or hybrid type N-glycans in the cytosolic fraction during aging in the brain [16,17]. PSM' could be another such exception.

Even if we accept that PSM' arises from the post-translational endoproteolytic cleavage of full length PSMA, the question of where this process takes place remains. Even though PSMA possesses a known internalization signal [13] and can undergo constitutive and antibody-induced internalization into the cell [18], our study of biotinylated PSMA processing during endocytosis and internalization does not provide evidence that PSM' originates from PSMA degradation during such a process. Moreover, cells expressing recombinant PSMA with a mutation in the internalization signal also expressed PSM', just as cells transfected with the wild type PSMA.

In conclusion, our experiments suggest that PSM' is a proteolytically active glycoprotein that is neither a product of alternatively spliced mRNA nor a product of proteolytic processing of the full length PSMA upon internalization and endosomal

trafficking. We can only speculate that this species might be produced by a proteolytic processing event inside the Golgi apparatus and then translocated by an unknown mechanism into the cytosol.

Insights into PSMA processing and the origin of its truncated form PSM' will heighten our understanding of the behavior of PSMA, a therapeutic target for prostate cancer, as well as our general understanding of N-glycosylation and the trafficking of cytosolic proteins.

Acknowledgement

We would like to thank Jana Starková for outstanding technical assistance, Václav Hořejší for the monoclonal antibodies and Hillary Hoffman for the critical proofreading of the manuscript.. This work has been supported by grants from the Ministry of Education of the Czech Republic (Research Center for New Antivirals and Antineoplastics-1M0508 and Research Center for Complex Molecular Systems and Biomolecules LC 512).

Reference List

1. Bostwick DG, Pacelli A, Blute M, Roche P, Murphy GP. Prostate specific membrane antigen expression in prostatic intraepithelial neoplasia and adenocarcinoma: a study of 184 cases. *Cancer* 1998;82:2256-2261.
2. Sokoloff RL, Norton KC, Gasior CL, Marker KM, Grauer LS. A dual-monoclonal sandwich assay for prostate-specific membrane antigen: levels in tissues, seminal fluid and urine. *Prostate* 2000;43:150-157.
3. Schmittgen TD, Tiske S, Vessella RL, True LD, Zakrajsek BA. Expression of prostate specific membrane antigen and three alternatively spliced variants of PSMA in prostate cancer patients. *International Journal of Cancer* 2003;107:323-329.
4. Su SL, Huang IP, Fair WR, Powell CT, Heston WD. Alternatively spliced variants of prostate-specific membrane antigen RNA: ratio of expression as a potential measurement of progression. *Cancer Res* 1995;55:1441-1443.
5. Cao KY, Mao XP, Wang DH, Xu L, Yuan GQ, Dai SQ, Zheng BJ, Qiu SP. High expression of PSM-E correlated with tumor grade in prostate cancer: A new alternatively spliced variant of prostate-specific membrane antigen. *Prostate* 2007;67:1791-1800.
6. Grauer LS, Lawler KD, Marignac JL, Kumar A, Goel AS, Wolfert RL. Identification, purification, and subcellular localization of prostate-specific membrane antigen PSM' protein in the LNCaP prostatic carcinoma cell line. *Cancer Res* 1998;58:4787-4789.
7. Williams T, Kole R. Analysis of prostate-specific membrane antigen splice variants in LNCap cells. *Oligonucleotides* 2006;16:186-195.
8. Lapidus RG, Tiffany CW, Isaacs JT, Slusher BS. Prostate-specific membrane antigen (PSMA) enzyme activity is elevated in prostate cancer cells. *Prostate* 2000;45:350-354.
9. Tiffany CW, Lapidus RG, Merion A, Calvin DC, Slusher BS. Characterization of the enzymatic activity of PSM: comparison with brain NAALADase. *Prostate* 1999;39:28-35.
10. Barinka C, Rinnova M, Sacha P, Rojas C, Majer P, Slusher BS, Konvalinka J. Substrate specificity, inhibition and enzymological analysis of recombinant human glutamate carboxypeptidase II. *J Neurochem* 2002;80:477-487.
11. Barinka C, Sacha P, Sklenar J, Man P, Bezouska K, Slusher BS, Konvalinka J. Identification of the N-glycosylation sites on glutamate carboxypeptidase II necessary for proteolytic activity. *Protein Sci* 2004;13:1627-1635.
12. Ghosh A, Heston WD. Effect of carbohydrate moieties on the folate hydrolysis activity of the prostate specific membrane antigen. *Prostate* 2003;57:140-151.

13. Rajasekaran SA, Anilkumar G, Oshima E, Bowie JU, Liu H, Heston W, Bander NH, Rajasekaran AK. A novel cytoplasmic tail MXXXL motif mediates the internalization of prostate-specific membrane antigen. *Mol Biol Cell* 2003;14:4835-4845.
14. Hu Q, Wang L, Yang Z, Cool BH, Zitnik G, Martin GM. Endoproteolytic cleavage of FE65 converts the adaptor protein to a potent suppressor of the sAPPalpha pathway in primates. *J Biol Chem* 2005;280:12548-12558.
15. Castelletti D, Fracasso G, Alfalah M, Cingarlini S, Colombatti M, Naim HY. Apical transport and folding of prostate-specific membrane antigen occurs independent of glycan processing. *J Biol Chem* 2006;281:3505-3512.
16. Pedemonte CH, Sachs G, Kaplan JH. An intrinsic membrane glycoprotein with cytosolically oriented n-linked sugars. *Proc Natl Acad Sci U S A* 1990;87:9789-9793.
17. Sato Y, Suzuki Y, Ito E, Shimazaki S, Ishida M, Yamamoto T, Yamamoto H, Toda T, Suzuki M, Suzuki A, Endo T. Identification and characterization of an increased glycoprotein in aging: Age-associated translocation of cathepsin D. *Mechanisms of Ageing and Development* 2006;127:771-778.
18. Liu H, Rajasekaran AK, Moy P, Xia Y, Kim S, Navarro V, Rahmati R, Bander NH. Constitutive and antibody-induced internalization of prostate-specific membrane antigen. *Cancer Res* 1998;58:4055-4060.

Figure 1.: Expression of PSMA/PSM' proteins in two cell lines. **Panel A:** Lysates from LNCaP and HEK1-750 cells (untreated or deglycosylated using PNGase F) were subjected to SDS-PAGE, electroblotted on a nitrocellulose membrane, probed using the GCP-04 antibody (1:5,000). **Panel B:** Sequential immunoprecipitation of PSMA from LNCaP cells with 7E11 (against N-terminus), followed by immunoprecipitation with GCP-05 antibody (against extracellular domain). Immunoprecipitated proteins were separated on SDS-PAGE and electroblotted onto a nitrocellulose membrane, then probed with GCP-04 antibody.

Figure 2.: Effect of endoglycosidases on PSMA/PSM' proteins. Lysates from LNCaP (**Panel A**) and HEK1-750 cells (**Panel B**) were either untreated or deglycosylated using PNGase F or Endo H. Protein samples were resolved by SDS-PAGE, electroblotted on a nitrocellulose membrane, and the membrane was probed with the GCP-04 antibody (1: 5,000). **Panels C, D:** PSMA/PSM' from LNCaP (**Panel C**) and HEK1-750 (**Panel D**) lysates were sequentially immunoprecipitated using monoclonal antibodies 7E11 and GCP-05, and proteins were subsequently deglycosylated with PNGase F or Endo H. Samples were resolved by SDS-PAGE, electroblotted on a nitrocellulose membrane, and the membrane was probed with the GCP-04 antibody (1: 5,000)

Figure 3.: PSM' localization to cytosol. Lysates from LNCaP and HEK1-750 cells were subjected to differential centrifugation and individual fractions were inspected for the presence of PSMA/PSM' proteins (Western blotting using the GCP-04 antibody; **Panels A, B**) and the NAAG-hydrolyzing activity (**Panels C, D**). **Panel A:** Immunodetection of PSMA/PSM' in different cellular fractions. **Panel B:** Immunodetection of untreated or PNGase F treated macromolecule (Ma) and cytosolic (Cyt) fractions. **Panels C, D:** Individual fractions from the differential centrifugation of LNCaP (**Panel C**) and HEK1-750 (**Panel D**) lysates were assayed for the NAAG-hydrolyzing activity using the radioenzymatic assay.

Figure 4.: Cell surface biotinylation. Cell surface proteins were biotinylated with Sulfo-NHS-SS-Biotin and then incubated 1h at 37°C to allow internalization of plasma membrane molecules. Biotin labels were stripped from proteins remaining at the cell surface, cells were lysed and cell lysates subjected to sequential immunoprecipitation using monoclonal antibodies 7E11 (recognizing the N-terminus) and GCP-05 (to the extracellular domain). Proteins were resolved by SDS-PAGE and electroblotted on a nitrocellulose membrane. **Panel A:** The immunoblot probed with the GCP-04 antibody (1: 5,000). **Panel B:** The immunoblot probed with NeutrAvidin conjugated to horseradish peroxidase (1:2,500) specific for biotin.

Figure 1

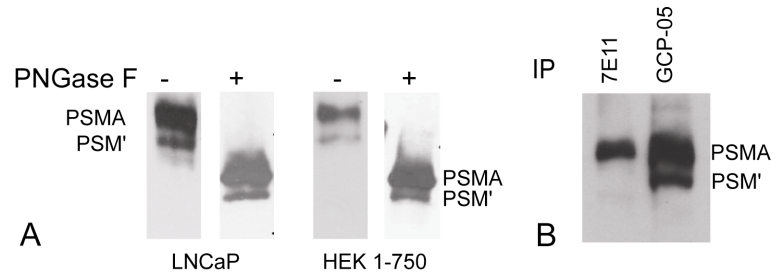


Figure 2

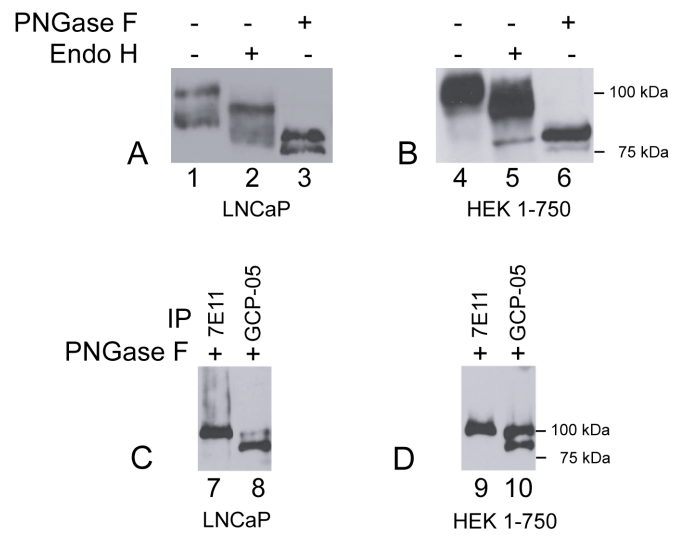


Figure 3

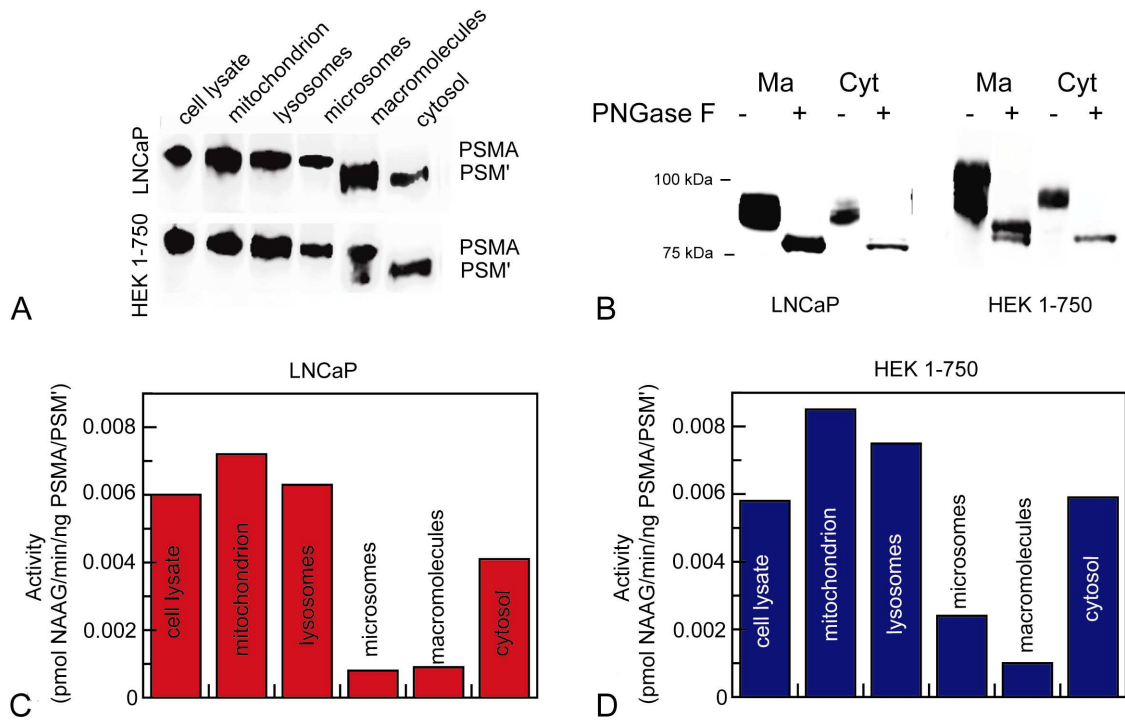
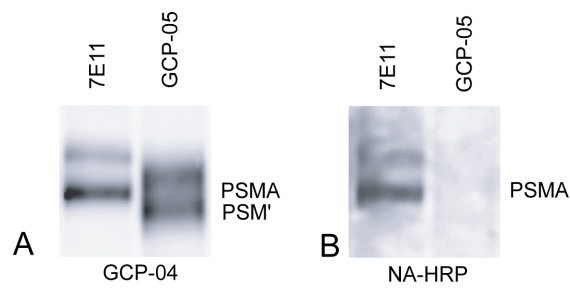


Figure 4



7 CONCLUSIONS AND PERSPECTIVES

Recently reported crystal structures of GCPII provide structural insight into the organization of the substrate binding cavity and highlight residues implicated in substrate / inhibitor binding in the S1' site of the enzyme. To complement and extend the structural studies, we constructed a QMMM model of GCPII in complex with its substrate, N-acetyl-aspartyl-glutamate, which enabled us to predict additional amino acid residues interacting with the bound substrate, and used site-directed mutagenesis to assess the contribution of individual residues for substrate / inhibitor binding and enzymatic activity of GCPII. We prepared and characterized 12 GCPII mutants targeting the amino acids in the vicinity of substrate/inhibitor binding pockets. The experimental results suggest that residues (especially Arg210) in the S1' site are critical for substrate / inhibitor binding, whereas the residues forming the S1 pocket might be more important for the 'fine-tuning' of GCPII substrate specificity and appear to be relevant for substrate turnover and may play a role in the enzyme's mechanism of action.

Even though the QMMM calculations of the NAAG binding mode in the GCPII active site enabled us to predict the structure and enzyme-substrate interactions in the S1 binding site, the complete description of reaction mechanism of GCPII is beyond the scope of our study. We would like to look more closely into the catalytic mechanism of glutamate carboxypeptidase II. An interesting approach is a study of a putative proton shuttle Glu424, located near zinc ions in the active site of GCPII. The mutation of this residue might show us its role in enzyme catalysis; moreover, we might obtain a crystal structure of GCPII with bound unsplit substrate N-acetyl-aspartyl-glutamate.

Human GCPII consists of 750 amino acids, and six individual domains were predicted to constitute the protein structure. We reported the analysis of the contribution of these putative domains to the structure and function of recombinant human GCPII. We cloned 13 mutants of human GCPII that are truncated or extended at one or both the N- and C-termini of the GCPII sequence. The clones were used to generate stably transfected *Drosophila* Schneider's cells, and the expression and carboxypeptidase activities of the individual protein products were determined. The results clearly show that the amino acids at the extreme C-terminus of GCPII are crucial for the hydrolytic activity of the enzyme and, furthermore, that no more than 60 amino acids can be deleted from the N-terminus without compromising the carboxypeptidase activity of GCPII.

We undertook this study before the first crystal structure of GCPII was determined. X-ray structures provided evidence that the ectodomain of GCPII is composed of three domains.

All these domains form active site of the enzyme and are indispensable for the GCPII enzymatic activity, which explains why changes on both N- and C- terminus are so detrimental to protein stability and activity.

We report crystal structures of the human GCPII complexed with three glutamate mimetics/derivatives, 2-(phosphonomethyl)pentanedioic acid, quisqualic acid, and L-serine *O*-sulfate. Despite the structural differences between the distal parts of the inhibitors, all three compounds share similar binding modes in the S1' site (pharmacophore pocket) of GCPII, where they are stabilized by a combination of polar and van der Waals interactions. The structural variety of the distal parts of the inhibitors leads to rearrangements of the S1' site that are necessary for efficient interactions between the enzyme and an inhibitor.

The set of structures presented here, in connection with the available biochemical data, illustrates a flexibility of the GCPII pharmacophore pocket and underlines the structural features required for potent GCPII inhibition.

Our data could be used for the development of the new GCPII inhibitors using the rational structure-based drug design approach and could draw attention to the modification in the inhibitor structure, which can improve the pharmacokinetic profile and potency towards GCPII.

Experiments with GCPII knock-out mice showed that GCPII is not the only one NAAG-hydrolyzing enzyme in the brain. We presumed that glutamate carboxypeptidase III (GCPIII), a close homolog of GCPII, might complement for GCPII activity in these knock-out mice.

While human GCPII is an important pharmacological target in the neurotransmission and degenerative diseases, no biochemical study of human GCPIII is available at present. We cloned, expressed and characterized a recombinant human GCPIII.

We show that GCPIII lacks dipeptidylpeptidase IV-like activity, its activity is dependent on N-glycosylation, and is sensitive to several known inhibitors of GCPII effectively inhibit it. In comparison to GCPII, GCPIII has lower N-acetyl-aspartyl-glutamate-hydrolyzing activity, different pH and salt concentration dependence, and distinct substrate specificity.

We created a molecular model of GCPIII and provided interpretation of the distinct substrate specificity of both enzymes, and examine the amino acid residues responsible for the differences by site-directed mutagenesis. These results may help to design potent and

selective inhibitors of both enzymes. Such inhibitors would be helpful to evaluate and distinguish biological roles of the two individual enzymes.

We believe that GCPIII activity is significant enough to account for the NAAG-hydrolyzing activity observed in the tissues of GCPII knock-out mice and that GCPIII might thus represent a valid pharmaceutical target.

Why would brain harbour two similar enzymes with the same enzymatic activity? The honest answer is: we do not know. The possible explanation might be that GCPII and GCPIII possess different biological roles in the brain. One of our goals is to find GCPIII molecular partner and to clarify the function of GCPIII.

Only very limited and controversial data on the expression and localization of GCPII in human brain are available. Therefore, we set out the first systematic analysis of the expression of GCPII in human brain using immunochemical detection. We used a novel monoclonal antibody GCP-04, which recognizes an epitope on the extracellular part of the enzyme and is more sensitive to GCPII than to the homologous protein GCPIII. We also showed that this antibody is more sensitive in immunoblots than the widely used antibody 7E11. Immunohistochemical analysis revealed GCPII expression in all parts of the human brain. GCPII seems to be expressed exclusively in astrocytes, especially in those localized in the white matter. Our published results are only starting point in further studies on the role of GCPII in the human brain.

It is generally known that GCPII is expressed in prostate and overexpressed during the prostate cancer. Analogically, we showed GCPII expression in astrocytes and we would like to investigate further the GCPII expression in brain tumors, especially in the astrocytomas.

In the benign prostate PSM' mRNA is overexpressed over GCPII. Interestingly enough, in the case of prostate cancer this expression pattern is reversed. Very few information is known about protein designated PSM', a truncated form of GCPII. We investigated the origin of PSM' and its trafficking in the cells.

Our experiments revealed that PSM' is a proteolytically active N-linked glycoprotein. Surprisingly, it is not a product of alternatively spliced GCPII mRNA, which is generally accepted fact. We hypothesize that it might be a product of proteolytic processing of the full length GCPII upon internalization and endosomal trafficking, but our data suggest it is also not the case. We can only speculate that this species might be produced by a proteolytic

processing event inside the Golgi apparatus and then translocated by an unknown mechanism into the cytosol.

Insights into GCPII processing and the origin of its truncated form PSM' might improve our understanding of the behavior of GCPII, a therapeutic target for prostate cancer, as well as our general understanding of N-glycosylation and the trafficking of cytosolic proteins.

8 REFERENCES

1. O'Keefe DS, Su SL, Bacich DJ, Horiguchi Y, Luo Y, Powell CT, Zandvliet D, Russell PJ, Molloy PL, Nowak NJ, Shows TB, Mullins C, Vonder Haar RA, Fair WR, Heston WD. Mapping, genomic organization and promoter analysis of the human prostate-specific membrane antigen gene. *Biochim Biophys Acta* 1998;1443:113-127.
2. Leek J, Lench N, Maraj B, Bailey A, Carr IM, Andersen S, Cross J, Whelan P, MacLennan KA, Meredith DM, . Prostate-specific membrane antigen: evidence for the existence of a second related human gene. *Br J Cancer* 1995;72:583-588.
3. Pangalos MN, Neefs JM, Somers M, Verhasselt P, Bekkers M, van der HL, Fraiponts E, Ashton D, Gordon RD. Isolation and expression of novel human glutamate carboxypeptidases with N-acetylated alpha-linked acidic dipeptidase and dipeptidyl peptidase IV activity. *J Biol Chem* 1999;274:8470-8483.
4. Good D, Schwarzenberger P, Eastham JA, Rhoads RE, Hunt JD, Collins M, Batzer M, Theodossiou C, Kolls JK, Grimes SR. Cloning and characterization of the prostate-specific membrane antigen promoter. *J Cell Biochem* 1999;74:395-405.
5. Watt F, Martorana A, Brookes DE, Ho T, Kingsley E, O'Keefe DS, Russell PJ, Heston WD, Molloy PL. A tissue-specific enhancer of the prostate-specific membrane antigen gene, FOLH1. *Genomics* 2001;73:243-254.
6. Noss KR, Wolfe SA, Grimes SR. Upregulation of prostate specific membrane antigen/folate hydrolase transcription by an enhancer. *Gene* 2002;285:247-256.
7. Schmittgen TD, Teske S, Vessella RL, True LD, Zakrajsek BA. Expression of prostate specific membrane antigen and three alternatively spliced variants of PSMA in prostate cancer patients. *Int J Cancer* 2003;107:323-329.
8. Su SL, Huang IP, Fair WR, Powell CT, Heston WD. Alternatively spliced variants of prostate-specific membrane antigen RNA: ratio of expression as a potential measurement of progression. *Cancer Res* 1995;55:1441-1443.
9. Bzdega T, Turi T, Wroblewska B, She D, Chung HS, Kim H, Neale JH. Molecular cloning of a peptidase against N-acetylaspartylglutamate from a rat hippocampal cDNA library. *J Neurochem* 1997;69:2270-2277.
10. Williams T, Kole R. Analysis of prostate-specific membrane antigen splice variants in LNCap cells. *Oligonucleotides* 2006;16:186-195.
11. Cao KY, Mao XP, Wang DH, Xu L, Yuan GQ, Dai SQ, Zheng BJ, Qiu SP. High expression of PSM-E correlated with tumor grade in prostate cancer: A new alternatively spliced variant of prostate-specific membrane antigen. *Prostate* 2007;67:1791-1800.

12. Rawlings ND, Barrett AJ. Structure of membrane glutamate carboxypeptidase. *Biochim Biophys Acta* 1997;1339:247-252.
13. Robinson MB, Blakely RD, Couto R, Coyle JT. Hydrolysis of the brain dipeptide N-acetyl-L-aspartyl-L-glutamate. Identification and characterization of a novel N-acetylated alpha-linked acidic dipeptidase activity from rat brain. *J Biol Chem* 1987;262:14498-14506.
14. Pinto JT, Suffoletto BP, Berzin TM, Qiao CH, Lin S, Tong WP, May F, Mukherjee B, Heston WD. Prostate-specific membrane antigen: a novel folate hydrolase in human prostatic carcinoma cells. *Clin Cancer Res* 1996;2:1445-1451.
15. Heston WD. Characterization and glutamyl preferring carboxypeptidase function of prostate specific membrane antigen: a novel folate hydrolase. *Urology* 1997;49:104-112.
16. Mhaka A, Gady AM, Rosen DM, Lo KM, Gillies SD, Denmeade SR. Use of methotrexate-based peptide substrates to characterize the substrate specificity of prostate-specific membrane antigen (PSMA). *Cancer Biol Ther* 2004;3:551-558.
17. Barinka C, Rinnova M, Sacha P, Rojas C, Majer P, Slusher BS, Konvalinka J. Substrate specificity, inhibition and enzymological analysis of recombinant human glutamate carboxypeptidase II. *J Neurochem* 2002;80:477-487.
18. Subasinghe N, Schulte M, Chan MY, Roon RJ, Koerner JF, Johnson RL. Synthesis of acyclic and dehydroaspartic acid analogues of Ac-Asp-Glu-OH and their inhibition of rat brain N-acetylated alpha-linked acidic dipeptidase (NAALA dipeptidase). *J Med Chem* 1990;33:2734-2744.
19. Serval V, Barbeito L, Pittaluga A, Cheramy A, Lavielle S, Glowinski J. Competitive inhibition of N-acetylated-alpha-linked acidic dipeptidase activity by N-acetyl-L-aspartyl-beta-linked L-glutamate. *J Neurochem* 1990;55:39-46.
20. Jackson PF, Cole DC, Slusher BS, Stetz SL, Ross LE, Donzanti BA, Trainor DA. Design, synthesis, and biological activity of a potent inhibitor of the neuropeptidase N-acetylated alpha-linked acidic dipeptidase. *J Med Chem* 1996;39:619-622.
21. Kozikowski AP, Nan F, Conti P, Zhang J, Ramadan E, Bzdega T, Wroblewska B, Neale JH, Pshenichkin S, Wroblewski JT. Design of remarkably simple, yet potent urea-based inhibitors of glutamate carboxypeptidase II (NAALADase). *J Med Chem* 2001;44:298-301.
22. Jackson PF, Tays KL, Maclin KM, Ko YS, Li W, Vitharana D, Tsukamoto T, Stoermer D, Lu XC, Wozniak K, Slusher BS. Design and pharmacological activity of phosphinic acid based NAALADase inhibitors. *J Med Chem* 2001;44:4170-4175.

23. Majer P, Jackson PF, Delahanty G, Grella BS, Ko YS, Li W, Liu Q, Maclin KM, Polakova J, Shaffer KA, Stoermer D, Vitharana D, Wang EY, Zakrzewski A, Rojas C, Slusher BS, Wozniak KM, Burak E, Limsakun T, Tsukamoto T. Synthesis and biological evaluation of thiol-based inhibitors of glutamate carboxypeptidase II: discovery of an orally active GCP II inhibitor. *J Med Chem* 2003;46:1989-1996.
24. Majer P, Hin B, Stoermer D, Adams J, Xu W, Duvall BR, Delahanty G, Liu Q, Stathis MJ, Wozniak KM, Slusher BS, Tsukamoto T. Structural optimization of thiol-based inhibitors of glutamate carboxypeptidase II by modification of the P1' side chain. *J Med Chem* 2006;49:2876-2885.
25. Davis MI, Bennett MJ, Thomas LM, Bjorkman PJ. Crystal structure of prostate-specific membrane antigen, a tumor marker and peptidase. *Proc Natl Acad Sci U S A* 2005;102:5981-5986.
26. Mesters JR, Barinka C, Li W, Tsukamoto T, Majer P, Slusher BS, Konvalinka J, Hilgenfeld R. Structure of glutamate carboxypeptidase II, a drug target in neuronal damage and prostate cancer. *EMBO J* 2006;25:1375-1384.
27. Schulke N, Varlamova OA, Donovan GP, Ma D, Gardner JP, Morrissey DM, Arrigale RR, Zhan C, Chodera AJ, Surowitz KG, Maddon PJ, Heston WD, Olson WC. The homodimer of prostate-specific membrane antigen is a functional target for cancer therapy. *Proc Natl Acad Sci U S A* 2003;100:12590-12595.
28. Barinka C, Starkova J, Konvalinka J, Lubkowski J. A high-resolution structure of ligand-free human glutamate carboxypeptidase II. *Acta Crystallograph Sect F Struct Biol Cryst Commun* 2007;63:150-153.
29. Holz RC, Bzymek KP, Swierczek SI. Co-catalytic metallopeptidases as pharmaceutical targets. *Curr Opin Chem Biol* 2003;7:197-206.
30. Fundoiano-Hershcovitz Y, Rabinovitch L, Langut Y, Reiland V, Shoham G, Shoham Y. Identification of the catalytic residues in the double-zinc aminopeptidase from *Streptomyces griseus*. *FEBS Lett* 2004;571:192-196.
31. Dumas F, Gala JL, Berteau P, Brasseur F, Eschwege P, Paradis V, Lacour B, Philippe M, Loric S. Molecular expression of PSMA mRNA and protein in primary renal tumors. *Int J Cancer* 1999;80:799-803.
32. Gala JL, Loric S, Guiot Y, Denmeade SR, Gady A, Brasseur F, Heusterspreute M, Eschwege P, De Nayer P, Van Cangh P, Tombal B. Expression of prostate-specific membrane antigen in transitional cell carcinoma of the bladder: prognostic value? *Clin Cancer Res* 2000;6:4049-4054.

33. Kinoshita Y, Kuratsukuri K, Landas S, Imaida K, Rovito PM, Jr., Wang CY, Haas GP. Expression of prostate-specific membrane antigen in normal and malignant human tissues. *World J Surg* 2006;30:628-636.
34. Liu H, Moy P, Kim S, Xia Y, Rajasekaran A, Navarro V, Knudsen B, Bander NH. Monoclonal antibodies to the extracellular domain of prostate-specific membrane antigen also react with tumor vascular endothelium. *Cancer Res* 1997;57:3629-3634.
35. Lopes AD, Davis WL, Rosenstraus MJ, Uveges AJ, Gilman SC. Immunohistochemical and pharmacokinetic characterization of the site-specific immunoconjugate CYT-356 derived from antiprostata monoclonal antibody 7E11-C5. *Cancer Res* 1990;50:6423-6429.
36. Silver DA, Pellicer I, Fair WR, Heston WD, Cordon-Cardo C. Prostate-specific membrane antigen expression in normal and malignant human tissues. *Clin Cancer Res* 1997;3:81-85.
37. Sokoloff RL, Norton KC, Gasior CL, Marker KM, Grauer LS. A dual-monoclonal sandwich assay for prostate-specific membrane antigen: levels in tissues, seminal fluid and urine. *Prostate* 2000;43:150-157.
38. Raine CS. Neurocellular Anatomy. In: Siegel GJ, Agranoff BW, Albers RW, Fisher SK, Uhler MD, editors. *Basic Neurochemistry: molecular, cellular and medical aspects*, edn 6th: New York: Lippincott-Raven; 1999. p 691-709.
39. Bruno V, Battaglia G, Copani A, D'Onofrio M, Di IP, De BA, Melchiorri D, Flor PJ, Nicoletti F. Metabotropic glutamate receptor subtypes as targets for neuroprotective drugs. *J Cereb Blood Flow Metab* 2001;21:1013-1033.
40. Thompson GA, Kilpatrick IC. The neurotransmitter candidature of sulphur-containing excitatory amino acids in the mammalian central nervous system. *Pharmacology & Therapeutics* 1996;72:25-36.
41. Thomsen C, Suzdak PD. Serine-O-Phosphate Has Affinity for Type-Iv, But Not Type-I, Metabotropic Glutamate-Receptor. *Neuroreport* 1993;4:1099-1101.
42. Boss V, Nutt KM, Conn PJ. L-Cysteine Sulfinic Acid As An Endogenous Agonist of A Novel Metabotropic Receptor-Coupled to Stimulation of Phospholipase-D Activity. *Mol Pharmacol* 1994;45:1177-1182.
43. Curatolo A, Darcange P, Lino A, Brancati A. Distribution of N-Acetyl-Aspartic and N-Acetyl-Aspartyl-Glutamic Acids in Nervous Tissue. *J Neurochem* 1965;12:339-342.
44. Neale JH, Bzdega T, Wroblewska B. N-Acetylaspartylglutamate: the most abundant peptide neurotransmitter in the mammalian central nervous system. *J Neurochem* 2000;75:443-452.

45. Koller KJ, Coyle JT. Ontogenesis of N-acetyl-aspartate and N-acetyl-aspartyl-glutamate in rat brain. *Brain Res* 1984;317:137-140.
46. Moffett JR, Namboodiri MAA, Cangro CB, Neale JH. Immunohistochemical Localization of N-Acetylaspartate in Rat-Brain. *Neuroreport* 1991;2:131-134.
47. Moffett JR, Namboodiri MA, Neale JH. Enhanced carbodiimide fixation for immunohistochemistry: application to the comparative distributions of N-acetylaspartylglutamate and N-acetylaspartate immunoreactivities in rat brain. *J Histochem Cytochem* 1993;41:559-570.
48. Passani LA, Vonsattel JP, Coyle JT. Distribution of N-acetylaspartylglutamate immunoreactivity in human brain and its alteration in neurodegenerative disease. *Brain Res* 1997;772:9-22.
49. Tieman SB, Tieman DG. N-acetylaspartylglutamate immunoreactivity in human retina. *Vision Res* 1996;36:941-947.
50. Kowalski MM, Cassidy M, Namboodiri MA, Neale JH. Cellular localization of N-acetylaspartylglutamate in amphibian retina and spinal sensory ganglia. *Brain Res* 1987;406:397-401.
51. Anderson KJ, Borja MA, Cotman CW, Moffett JR, Namboodiri MA, Neale JH. N-acetylaspartylglutamate identified in the rat retinal ganglion cells and their projections in the brain. *Brain Res* 1987;411:172-177.
52. Tieman SB, Cangro CB, Neale JH. N-acetylaspartylglutamate immunoreactivity in neurons of the cat's visual system. *Brain Res* 1987;420:188-193.
53. Tieman SB, Neale JH, Tieman DG. N-acetylaspartylglutamate immunoreactivity in neurons of the monkey's visual pathway. *J Comp Neurol* 1991;313:45-64.
54. Cassidy M, Neale JH. N-acetylaspartylglutamate catabolism is achieved by an enzyme on the cell surface of neurons and glia. *Neuropeptides* 1993;24:271-278.
55. Renno WM, Lee JH, Beitz AJ. Light and electron microscopic immunohistochemical localization of N-acetylaspartylglutamate (NAAG) in the olivocerebellar pathway of the rat. *Synapse* 1997;26:140-154.
56. Williamson LC, Neale JH. Ultrastructural localization of N-acetylaspartylglutamate in synaptic vesicles of retinal neurons. *Brain Res* 1988;456:375-381.
57. Tsai G, Forloni G, Robinson MB, Stauch BL, Coyle JT. Calcium-dependent evoked release of N-[3H]acetylaspartylglutamate from the optic pathway. *J Neurochem* 1988;51:1956-1959.

58. Zollinger M, Brauchlithetokis J, Gutteckamsler U, Do KQ, Streit P, Cuenod M. Release of N-Acetylaspartylglutamate from Slices of Rat Cerebellum, Striatum, and Spinal-Cord, and the Effect of Climbing Fiber Deprivation. *J Neurochem* 1994;63:1133-1142.
59. Riveros N, Orrego F. A study of possible excitatory effects of N-acetylaspartylglutamate in different in vivo and in vitro brain preparations. *Brain Res* 1984;299:393-395.
60. Cassidy M, Neale JH. Localization and transport of N-acetylaspartylglutamate in cells of whole murine brain in primary culture. *J Neurochem* 1993;60:1631-1638.
61. Valivullah HM, Lancaster J, Sweetnam PM, Neale JH. Interactions Between N-Acetylaspartylglutamate and Ampa, Kainate, and Nmda Binding-Sites. *J Neurochem* 1994;63:1714-1719.
62. Westbrook GL, Mayer ML, Namboodiri MA, Neale JH. High concentrations of N-acetylaspartylglutamate (NAAG) selectively activate NMDA receptors on mouse spinal cord neurons in cell culture. *J Neurosci* 1986;6:3385-3392.
63. Trombley PQ, Westbrook GL. Excitatory Synaptic Transmission in Cultures of Rat Olfactory-Bulb. *J Neurophysiol* 1990;64:598-606.
64. Burlina AP, Skaper SD, Mazza MR, Ferrari V, Leon A, Burlina AB. N-Acetylaspartylglutamate Selectively Inhibits Neuronal Responses to N-Methyl-D-Aspartic Acid In-Vitro. *J Neurochem* 1994;63:1174-1177.
65. Coyle JT. The nagging question of the function of N-acetylaspartylglutamate. *Neurobiol Dis* 1997;4:231-238.
66. Fuhrman S, Palkovits M, Cassidy M, Neale JH. The regional distribution of N-acetylaspartylglutamate (NAAG) and peptidase activity against NAAG in the rat nervous system. *J Neurochem* 1994;62:275-281.
67. Bergeron R, Coyle JT, Tsai GC, Greene RW. NAAG reduces NMDA receptor current in CA1 hippocampal pyramidal neurons of acute slices and dissociated neurons. *Neuropsychopharmacology* 2005;30:7-16.
68. Wroblewska B, Wroblewski JT, Pshenichkin S, Surin A, Sullivan SE, Neale JH. N-acetylaspartylglutamate selectively activates mGluR3 receptors in transfected cells. *J Neurochem* 1997;69:174-181.
69. Wroblewska B, Wroblewski JT, Saab OH, Neale JH. N-Acetylaspartylglutamate Inhibits Forskolin-Stimulated Cyclic-Amp Levels Via A Metabotropic Glutamate-Receptor in Cultured Cerebellar Granule Cells. *J Neurochem* 1993;61:943-948.
70. Sanabria ER, Wozniak KM, Slusher BS, Keller A. GCP II (NAALADase) inhibition suppresses mossy fiber-CA3 synaptic neurotransmission by a presynaptic mechanism. *J Neurophysiol* 2004;91:182-193.

71. Bruno V, Wroblewska B, Wroblewski JT, Fiore L, Nicoletti F. Neuroprotective activity of N-acetylaspartylglutamate in cultured cortical cells. *Neuroscience* 1998;85:751-757.
72. Ghose S, Wroblewska B, Corsi L, Grayson DR, Deblas AL, Vicini S, Neale JH. N-acetylaspartylglutamate stimulates metabotropic glutamate receptor 3 to regulate expression of the GABA(A) alpha 6 subunit in cerebellar granule cells. *J Neurochem* 1997;69:2326-2335.
73. Blakely RD, Robinson MB, Thompson RC, Coyle JT. Hydrolysis of the brain dipeptide N-acetyl-L-aspartyl-L-glutamate: subcellular and regional distribution, ontogeny, and the effect of lesions on N-acetylated-alpha-linked acidic dipeptidase activity. *J Neurochem* 1988;50:1200-1209.
74. Guarda AS, Robinson MB, Ory-Lavollee L, Forloni GL, Blakely RD, Coyle JT. Quantitation of N-acetyl-aspartyl-glutamate in microdissected rat brain nuclei and peripheral tissues: findings with a novel liquid phase radioimmunoassay. *Brain Res* 1988;427:223-231.
75. Berger UV, Carter RE, McKee M, Coyle JT. N-acetylated alpha-linked acidic dipeptidase is expressed by non-myelinating Schwann cells in the peripheral nervous system. *J Neurocytol* 1995;24:99-109.
76. Berger UV, Schwab ME. N-acetylated alpha-linked acidic dipeptidase may be involved in axon-Schwann cell signalling. *J Neurocytol* 1996;25:499-512.
77. Williamson LC, Neale JH. Uptake, metabolism, and release of N-[3H]acetylaspartylglutamate by the avian retina. *J Neurochem* 1992;58:2191-2199.
78. Berger UV, Luthi-Carter R, Passani LA, Elkabes S, Black I, Konradi C, Coyle JT. Glutamate carboxypeptidase II is expressed by astrocytes in the adult rat nervous system. *J Comp Neurol* 1999;415:52-64.
79. Arundine M, Tymianski M. Molecular mechanisms of calcium-dependent neurodegeneration in excitotoxicity. *Cell Calcium* 2003;34:325-337.
80. Slusher BS, Vornov JJ, Thomas AG, Hurn PD, Harukuni I, Bhardwaj A, Traystman RJ, Robinson MB, Britton P, Lu XC, Tortella FC, Wozniak KM, Yudkoff M, Potter BM, Jackson PF. Selective inhibition of NAALADase, which converts NAAG to glutamate, reduces ischemic brain injury. *Nat Med* 1999;5:1396-1402.
81. Cai Z, Lin S, Rhodes PG. Neuroprotective effects of N-acetylaspartylglutamate in a neonatal rat model of hypoxia-ischemia. *Eur J Pharmacol* 2002;437:139-145.
82. Lu XM, Tang Z, Liu W, Lin Q, Slusher BS. N-acetylaspartylglutamate protects against transient focal cerebral ischemia in rats. *Eur J Pharmacol* 2000;408:233-239.

83. Bacich DJ, Wozniak KM, Lu XC, O'Keefe DS, Callizot N, Heston WD, Slusher BS. Mice lacking glutamate carboxypeptidase II are protected from peripheral neuropathy and ischemic brain injury. *J Neurochem* 2005;95:314-323.
84. Harada C, Harada T, Slusher BS, Yoshida K, Matsuda H, Wada K. N-acetylated-alpha-linked-acidic dipeptidase inhibitor has a neuroprotective effect on mouse retinal ganglion cells after pressure-induced ischemia. *Neurosci Lett* 2000;292:134-136.
85. Long JB, Yourick DL, Slusher BS, Robinson MB, Meyerhoff JL. Inhibition of glutamate carboxypeptidase II (NAALADase) protects against dynorphin A-induced ischemic spinal cord injury in rats. *Eur J Pharmacol* 2005;508:115-122.
86. Thomas AG, Olkowski JL, Slusher BS. Neuroprotection afforded by NAAG and NAALADase inhibition requires glial cells and metabotropic glutamate receptor activation. *Eur J Pharmacol* 2001;426:35-38.
87. Thomas AG, Liu W, Olkowski JL, Tang Z, Lin Q, Lu XC, Slusher BS. Neuroprotection mediated by glutamate carboxypeptidase II (NAALADase) inhibition requires TGF-beta. *Eur J Pharmacol* 2001;430:33-40.
88. Bruno V, Battaglia G, Copani A, D'Onofrio M, Di Iorio P, De Blasi A, Melchiorri D, Flor PJ, Nicoletti F. Metabotropic glutamate receptor subtypes as targets for neuroprotective drugs. *J Cereb Blood Flow Metab* 2001;21:1013-1033.
89. Faden AI, Demediuk P, Panter SS, Vink R. The Role of Excitatory Amino-Acids and Nmda Receptors in Traumatic Brain Injury. *Science* 1989;244:798-800.
90. Neale JH, Olszewski RT, Gehl LM, Wroblewska B, Bzdega T. The neurotransmitter N-acetylaspartylglutamate in models of pain, ALS, diabetic neuropathy, CNS injury and schizophrenia. *Trends Pharmacol Sci* 2005;26:477-484.
91. Zhong C, Zhao X, Sarva J, Kozikowski A, Neale JH, Lyeth BG. NAAG peptidase inhibitor reduces acute neuronal degeneration and astrocyte damage following lateral fluid percussion TBI in rats. *J Neurotrauma* 2005;22:266-276.
92. Zhong C, Zhao X, Van KC, Bzdega T, Smyth A, Zhou J, Kozikowski AP, Jiang J, O'Connor WT, Berman RF, Neale JH, Lyeth BG. NAAG peptidase inhibitor increases dialysate NAAG and reduces glutamate, aspartate and GABA levels in the dorsal hippocampus following fluid percussion injury in the rat. *J Neurochem* 2006;97:1015-1025.
93. Gracely RH, Lynch SA, Bennett GJ. Painful Neuropathy - Altered Central Processing Maintained Dynamically by Peripheral Input. *Pain* 1992;51:175-194.

94. Laird JMA, Mason GS, Webb J, Hill RG, Hargreaves RJ. Effects of a partial agonist and a full antagonist acting at the glycine site of the NMDA receptor on inflammation-induced mechanical hyperalgesia in rats. *Br J Pharmacol* 1996;117:1487-1492.
95. Yamamoto T, Nozaki-Taguchi N, Sakashita Y. Spinal N-acetyl-alpha-linked acidic dipeptidase (NAALADase) inhibition attenuates mechanical allodynia induced by paw carrageenan injection in the rat. *Brain Res* 2001;909:138-144.
96. Yamamoto T, Nozaki-Taguchi N, Sakashita Y, Inagaki T. Inhibition of spinal N-acetylated-alpha-linked acidic dipeptidase produces an antinociceptive effect in the rat formalin test. *Neuroscience* 2001;102:473-479.
97. Yamamoto T, Saito O, Aoe T, Bartolozzi A, Sarva J, Zhou J, Kozikowski A, Wroblewska B, Bzdega T, Neale JH. Local administration of N-acetylaspartylglutamate (NAAG) peptidase inhibitors is analgesic in peripheral pain in rats. *Eur J Neurosci* 2007;25:147-158.
98. Chen SR, Wozniak KM, Slusher BS, Pan HL. Effect of 2-(phosphono-methyl)-pentanedioic acid on allodynia and afferent ectopic discharges in a rat model of neuropathic pain. *J Pharmacol Exp Ther* 2002;300:662-667.
99. Nagel J, Belozertseva I, Greco S, Kashkin V, Malyshkin A, Jirgensons A, Shekunova E, Eilbacher B, Bepalov A, Danysz W. Effects of NAAG peptidase inhibitor 2-PMPA in model chronic pain - relation to brain concentration. *Neuropharmacology* 2006;51:1163-1171.
100. Carlsson A. The Current Status of the Dopamine Hypothesis of Schizophrenia. *Neuropsychopharmacology* 1988;1:179-186.
101. Tsai GC, Passani LA, Slusher BS, Carter R, Baer L, Kleinman JE, Coyle JT. Abnormal Excitatory Neurotransmitter Metabolism in Schizophrenic Brains. *Arch Gen Psychiatry* 1995;52:829-836.
102. Tsai GC, Coyle JT. Glutamatergic mechanisms in schizophrenia. *Annu Rev Pharmacol Toxicol* 2002;42:165-179.
103. Javitt DC, Zukin SR. Recent Advances in the Phencyclidine Model of Schizophrenia. *Am J Psychiatry* 1991;148:1301-1308.
104. Krystal JH, Anand A, Moghaddam B. Effects of NMDA receptor antagonists: Implications for the pathophysiology of schizophrenia. *Arch Gen Psychiatry* 2002;59:663-664.
105. Moghaddam B, Adams BW. Reversal of phencyclidine effects by a group II metabotropic glutamate receptor agonist in rats. *Science* 1998;281:1349-1352.
106. Olszewski RT, Bukhari N, Zhou J, Kozikowski AP, Wroblewski JT, Shamimi-Noori S, Wroblewska B, Bzdega T, Vicini S, Barton FB, Neale JH. NAAG peptidase inhibition reduces locomotor

- activity and some stereotypes in the PCP model of schizophrenia via group II mGluR. *J Neurochem* 2004;89:876-885.
107. Flores C, Coyle JT. Regulation of glutamate carboxypeptidase II function in corticolimbic regions of rat brain by phencyclidine, haloperidol, and clozapine. *Neuropsychopharmacology* 2003;28:1227-1234.
108. Cameron NE, Cotter MA, Maxfield EK. Antioxidant Treatment Prevents the Development of Peripheral-Nerve Dysfunction in Streptozotocin-Diabetic Rats. *Diabetologia* 1993;36:299-304.
109. Montal M. Mitochondria, glutamate neurotoxicity and the death cascade. *Biochim Biophys Acta* 1998;1366:113-126.
110. Rosson GD, Dellon AL. Vascular risk factors and diabetic neuropathy. *N Engl J Med* 2005;352:1925.
111. Berent-Spillson A, Robinson AM, Golovoy D, Slusher B, Rojas C, Russell JW. Protection against glucose-induced neuronal death by NAAG and GCP II inhibition is regulated by mGluR3. *J Neurochem* 2004;89:90-99.
112. Zhang W, Slusher B, Murakawa Y, Wozniak KM, Tsukamoto T, Jackson PF, Sima AA. GCPII (NAALADase) inhibition prevents long-term diabetic neuropathy in type 1 diabetic BB/Wor rats. *J Neurol Sci* 2002;194:21-28.
113. Rakhit R, Chakrabartty A. Structure, folding, and misfolding of Cu,Zn superoxide dismutase in amyotrophic lateral sclerosis. *Biochim Biophys Acta* 2006;1762:1025-1037.
114. Rothstein JD, Tsai G, Kuncl RW, Clawson L, Cornblath DR, Drachman DB, Pestronk A, Stauch BL, Coyle JT. Abnormal excitatory amino acid metabolism in amyotrophic lateral sclerosis. *Ann Neurol* 1990;28:18-25.
115. Tsai GC, Stauch-Slusher B, Sim L, Hedreen JC, Rothstein JD, Kuncl R, Coyle JT. Reductions in acidic amino acids and N-acetylaspartylglutamate in amyotrophic lateral sclerosis CNS. *Brain Res* 1991;556:151-156.
116. Ghadge GD, Slusher BS, Bodner A, Canto MD, Wozniak K, Thomas AG, Rojas C, Tsukamoto T, Majer P, Miller RJ, Monti AL, Roos RP. Glutamate carboxypeptidase II inhibition protects motor neurons from death in familial amyotrophic lateral sclerosis models. *Proc Natl Acad Sci U S A* 2003;100:9554-9559.
117. Epidemiology of malignant tumors-analyses (2007). Retrieved October 20, 2007, from Epidemiology of malignant tumors in the Czech Republic Web site: <http://www.svod.cz/?sec=analyzy>
118. Gao X, Porter AT, Grignon DJ, Pontes JE, Honn KV. Diagnostic and prognostic markers for human prostate cancer. *Prostate* 1997;31:264-281.

119. Schultz WA. Prostate cancer. *Molecular Biology of Human Cancers*: Springer; 2007. p 383-402.
120. Ostrowski WS, Kuciel R. Human Prostatic Acid-Phosphatase - Selected Properties and Practical Applications. *Clin Chim Acta* 1994;226:121-129.
121. Yam LT, Janckila AJ, Lam WKW, Li CY. Immunohistochemistry of Prostatic Acid-Phosphatase. *Prostate* 1981;2:97-107.
122. Thompson IM, Ankerst DP. Prostate-specific antigen in the early detection of prostate cancer. *CMAJ* 2007;176:1853-1858.
123. Wang MC, Valenzuela L, Murphy GP, Chu TM. Tissue Specific and Tumor Specific Antigens in Human Prostate. *Fed Proc* 1977;36:1254.
124. Wang MC, Valenzuela LA, Murphy GP, Chu TM. Purification of A Human-Prostate Specific Antigen. *Investig Urol* 1979;17:159-163.
125. Papotti M, Paties C, Peveri V, Moscuzza L, Bussolati G. Immunocytochemical Detection of Prostate-Specific Antigen (Psa) in Skin Adnexal and Breast Tissues and Tumors. *Basic Appl Histochem* 1989;33:25-29.
126. Pummer K, Wirnsberger G, Pustner P, Stettner H, Wandschneider G. False positive prostate specific antigen values in the sera of women with renal cell carcinoma. *J Urol* 1992;148:21-23.
127. Smith MR, Biggar S, Hussain M. Prostate-specific antigen messenger RNA is expressed in non-prostate cells: implications for detection of micrometastases. *Cancer Res* 1995;55:2640-2644.
128. van Krieken JH. Prostate marker immunoreactivity in salivary gland neoplasms. A rare pitfall in immunohistochemistry. *Am J Surg Pathol* 1993;17:410-414.
129. Yu H, Giai M, Diamandis EP, Katsaros D, Sutherland DJ, Levesque MA, Roagna R, Ponzzone R, Sismondi P. Prostate-specific antigen is a new favorable prognostic indicator for women with breast cancer. *Cancer Res* 1995;55:2104-2110.
130. Frazier HA, Humphrey PA, Burchette JL, Paulson DF. Immunoreactive prostatic specific antigen in male periurethral glands. *J Urol* 1992;147:246-248.
131. Kamoshida S, Tsutsumi Y. Extraprostatic localization of prostatic acid phosphatase and prostate-specific antigen: distribution in cloacogenic glandular epithelium and sex-dependent expression in human anal gland. *Hum Pathol* 1990;21:1108-1111.
132. Yu H, Diamandis EP. Measurement of serum prostate specific antigen levels in women and in prostatectomized men with an ultrasensitive immunoassay technique. *J Urol* 1995;153:1004-1008.

133. Wu JT. Assay for prostate specific antigen (PSA): problems and possible solutions. *J Clin Lab Anal* 1994;8:51-62.
134. Stamey TA, Yang N, Hay AR, McNeal JE, Freiha FS, Redwine E. Prostate-specific antigen as a serum marker for adenocarcinoma of the prostate. *N Engl J Med* 1987;317:909-916.
135. Murphy WM, Soloway MS, Barrows GH. Pathologic changes associated with androgen deprivation therapy for prostate cancer. *Cancer* 1991;68:821-828.
136. Israeli RS, Powell CT, Corr JG, Fair WR, Heston WD. Expression of the prostate-specific membrane antigen. *Cancer Res* 1994;54:1807-1811.
137. Troyer JK, Beckett ML, Wright GL, Jr. Detection and characterization of the prostate-specific membrane antigen (PSMA) in tissue extracts and body fluids. *Int J Cancer* 1995;62:552-558.
138. Chang SS, Reuter VE, Heston WD, Bander NH, Grauer LS, Gaudin PB. Five different anti-prostate-specific membrane antigen (PSMA) antibodies confirm PSMA expression in tumor-associated neovasculature. *Cancer Res* 1999;59:3192-3198.
139. Mhawech-Fauceglia P, Zhang S, Terracciano L, Sauter G, Chadhuri A, Herrmann FR, Penetrante R. Prostate-specific membrane antigen (PSMA) protein expression in normal and neoplastic tissues and its sensitivity and specificity in prostate adenocarcinoma: an immunohistochemical study using multiple tumour tissue microarray technique. *Histopathology* 2007;50:472-483.
140. O'Keefe DS, Bacich DJ, Heston WD. Comparative analysis of prostate-specific membrane antigen (PSMA) versus a prostate-specific membrane antigen-like gene. *Prostate* 2004;58:200-210.
141. Luthi-Carter R, Barczak AK, Speno H, Coyle JT. Hydrolysis of the neuropeptide N-acetylaspartylglutamate (NAAG) by cloned human glutamate carboxypeptidase II. *Brain Res* 1998;795:341-348.
142. Chang SS, O'Keefe DS, Bacich DJ, Reuter VE, Heston WD, Gaudin PB. Prostate-specific membrane antigen is produced in tumor-associated neovasculature. *Clin Cancer Res* 1999;5:2674-2681.
143. Bubendorf L, Nocito A, Moch H, Sauter G. Tissue microarray (TMA) technology: miniaturized pathology archives for high-throughput in situ studies. *J Pathol* 2001;195:72-79.
144. Douglas TH, Morgan TO, McLeod DG, Moul JW, Murphy GP, Barren R, III, Sesterhenn IA, Mostofi FK. Comparison of serum prostate specific membrane antigen, prostate specific antigen, and free prostate specific antigen levels in radical prostatectomy patients. *Cancer* 1997;80:107-114.
145. Horoszewicz JS, Kawinski E, Murphy GP. Monoclonal antibodies to a new antigenic marker in epithelial prostatic cells and serum of prostatic cancer patients. *Anticancer Res* 1987;7:927-935.

146. Rochon YP, Horoszewicz JS, Boynton AL, Holmes EH, Barren RJ, III, Erickson SJ, Kenny GM, Murphy GP. Western blot assay for prostate-specific membrane antigen in serum of prostate cancer patients. *Prostate* 1994;25:219-223.
147. Beckett ML, Cazares LH, Vlahou A, Schellhammer PF, Wright GL, Jr. Prostate-specific membrane antigen levels in sera from healthy men and patients with benign prostate hyperplasia or prostate cancer. *Clin Cancer Res* 1999;5:4034-4040.
148. Cunha AC, Weigle B, Kiessling A, Bachmann M, Rieber EP. Tissue-specificity of prostate specific antigens: comparative analysis of transcript levels in prostate and non-prostatic tissues. *Cancer Lett* 2006;236:229-238.
149. Nagao K, Hisatomi H, Hirata H, Yamamoto S, Hikiji K, Yamamoto M, Kanamaru T. Expression of molecular marker genes in various types of normal tissue: implication for detection of micrometastases. *Int J Mol Med* 2002;10:307-310.
150. Renneberg H, Friedetzky A, Konrad L, Kurek R, Weingartner K, Wennemuth G, Tunn UW, Aumuller G. Prostate specific membrane antigen (PSM) is expressed in various human tissues: implication for the use of PSM reverse transcription polymerase chain reaction to detect hematogenous prostate cancer spread. *Urol Res* 1999;27:23-27.
151. Cama C, Olsson CA, Raffo AJ, Perlman H, Buttyan R, O'Toole K, McMahon D, Benson MC, Katz AE. Molecular staging of prostate cancer. II. A comparison of the application of an enhanced reverse transcriptase polymerase chain reaction assay for prostate specific antigen versus prostate specific membrane antigen. *J Urol* 1995;153:1373-1378.
152. Corey E, Corey MJ. Detection of disseminated prostate cells by reverse transcription-polymerase chain reaction (RT-PCR): technical and clinical aspects. *Int J Cancer* 1998;77:655-673.
153. Israeli RS, Miller WH, Jr., Su SL, Powell CT, Fair WR, Samadi DS, Huryk RF, DeBlasio A, Edwards ET, Wise GJ, . Sensitive nested reverse transcription polymerase chain reaction detection of circulating prostatic tumor cells: comparison of prostate-specific membrane antigen and prostate-specific antigen-based assays. *Cancer Res* 1994;54:6306-6310.
154. Loric S, Dumas F, Eschwege P, Blanchet P, Benoit G, Jardin A, Lacour B. Enhanced detection of hematogenous circulating prostatic cells in patients with prostate adenocarcinoma by using nested reverse transcription polymerase chain reaction assay based on prostate-specific membrane antigen. *Clin Chem* 1995;41:1698-1704.
155. Miyake H, Kurahashi T, Hara I, Takenaka A, Fujisawa M. Significance of micrometastases in pelvic lymph nodes detected by real-time reverse transcriptase polymerase chain reaction in patients with clinically localized prostate cancer undergoing radical prostatectomy after neoadjuvant hormonal therapy. *BJU Int* 2007;99:315-320.

156. Wright GL, Jr., Grob BM, Haley C, Grossman K, Newhall K, Petrylak D, Troyer J, Konchuba A, Schellhammer PF, Moriarty R. Upregulation of prostate-specific membrane antigen after androgen-deprivation therapy. *Urology* 1996;48:326-334.
157. Murphy GP, Elgamal AA, Su SL, Bostwick DG, Holmes EH. Current evaluation of the tissue localization and diagnostic utility of prostate specific membrane antigen. *Cancer* 1998;83:2259-2269.
158. Zhang Y, Zippe CD, Van Lente F, Klein EA, Gupta MK. Combined nested reverse transcription-PCR assay for prostate-specific antigen and prostate-specific membrane antigen in detecting circulating prostatic cells. *Clin Cancer Res* 1997;3:1215-1220.
159. Mitsiades CS, Lembessis P, Sourla A, Milathianakis C, Tsintavis A, Koutsilieris M. Molecular staging by RT-pCR analysis for PSA and PSMA in peripheral blood and bone marrow samples is an independent predictor of time to biochemical failure following radical prostatectomy for clinically localized prostate cancer. *Clin Exp Metastasis* 2004;21:495-505.
160. Kurek R, Nunez G, Tselis N, Konrad L, Martin T, Roeddiger S, Aumuller G, Zamboglou N, Lin DW, Tunn UW, Renneberg H. Prognostic value of combined "triple"-reverse transcription-PCR analysis for prostate-specific antigen, human kallikrein 2, and prostate-specific membrane antigen mRNA in peripheral blood and lymph nodes of prostate cancer patients. *Clin Cancer Res* 2004;10:5808-5814.
161. Thomas J, Gupta M, Grasso Y, Reddy CA, Heston WD, Zippe C, Dreicer R, Kupelian PA, Brainard J, Levin HS, Klein EA. Preoperative combined nested reverse transcriptase polymerase chain reaction for prostate-specific antigen and prostate-specific membrane antigen does not correlate with pathologic stage or biochemical failure in patients with localized prostate cancer undergoing radical prostatectomy. *J Clin Oncol* 2002;20:3213-3218.
162. Burger MJ, Tebay MA, Keith PA, Samaratunga HM, Clements J, Lavin MF, Gardiner RA. Expression analysis of delta-catenin and prostate-specific membrane antigen: their potential as diagnostic markers for prostate cancer. *Int J Cancer* 2002;100:228-237.
163. Kawakami M, Nakayama J. Enhanced expression of prostate-specific membrane antigen gene in prostate cancer as revealed by in situ hybridization. *Cancer Res* 1997;57:2321-2324.
164. Perner S, Hofer MD, Kim R, Shah RB, Li H, Moller P, Hautmann RE, Gschwend JE, Kuefer R, Rubin MA. Prostate-specific membrane antigen expression as a predictor of prostate cancer progression. *Hum Pathol* 2007;38:696-701.
165. Bostwick DG, Pacelli A, Blute M, Roche P, Murphy GP. Prostate specific membrane antigen expression in prostatic intraepithelial neoplasia and adenocarcinoma: a study of 184 cases. *Cancer* 1998;82:2256-2261.

166. Wright GL Jr, Haley C, Beckett ML, Schellhammer PF. Expression of prostate-specific membrane antigen in normal, benign, and malignant prostate tissues. *Urol Oncol* 1995;1:18-28.
167. Ross JS, Sheehan CE, Fisher HA, Kaufman RP, Jr., Kaur P, Gray K, Webb I, Gray GS, Mosher R, Kallakury BV. Correlation of primary tumor prostate-specific membrane antigen expression with disease recurrence in prostate cancer. *Clin Cancer Res* 2003;9:6357-6362.
168. Kahn D, Williams RD, Seldin DW, Libertino JA, Hirschhorn M, Dreicer R, Weiner GJ, Bushnell D, Gulfo J. Radioimmunoscinigraphy with 111indium labeled CYT-356 for the detection of occult prostate cancer recurrence. *J Urol* 1994;152:1490-1495.
169. Hinkle GH, Burgers JK, Neal CE, Texter JH, Kahn D, Williams RD, Maguire R, Rogers B, Olsen JO, Badalament RA. Multicenter radioimmunoscinigraphic evaluation of patients with prostate carcinoma using indium-111 capromab pendetide. *Cancer* 1998;83:739-747.
170. Polascik TJ, Manyak MJ, Haseman MK, Gurganus RT, Rogers B, Maguire RT, Partin AW. Comparison of clinical staging algorithms and 111indium-capromab pendetide immunoscintigraphy in the prediction of lymph node involvement in high risk prostate carcinoma patients. *Cancer* 1999;85:1586-1592.
171. Thomas CT, Bradshaw PT, Pollock BH, Montie JE, Taylor JM, Thames HD, McLaughlin PW, DeBiose DA, Hussey DH, Wahl RL. Indium-111-capromab pendetide radioimmunoscinigraphy and prognosis for durable biochemical response to salvage radiation therapy in men after failed prostatectomy. *J Clin Oncol* 2003;21:1715-1721.
172. Ballangrud AM, Yang WH, Charlton DE, McDevitt MR, Hamacher KA, Panageas KS, Ma D, Bander NH, Scheinberg DA, Sgouros G. Response of LNCaP spheroids after treatment with an alpha-particle emitter (²¹³Bi)-labeled anti-prostate-specific membrane antigen antibody (J591). *Cancer Res* 2001;61:2008-2014.
173. Li Y, Tian Z, Rizvi SM, Bander NH, Allen BJ. In vitro and preclinical targeted alpha therapy of human prostate cancer with Bi-213 labeled J591 antibody against the prostate specific membrane antigen. *Prostate Cancer Prostatic Dis* 2002;5:36-46.
174. McDevitt MR, Barendsward E, Ma D, Lai L, Curcio MJ, Sgouros G, Ballangrud AM, Yang WH, Finn RD, Pellegrini V, Geerlings MW, Jr., Lee M, Brechbiel MW, Bander NH, Cordon-Cardo C, Scheinberg DA. An alpha-particle emitting antibody ([²¹³Bi]J591) for radioimmunotherapy of prostate cancer. *Cancer Res* 2000;60:6095-6100.
175. Morris MJ, Divgi CR, Pandit-Taskar N, Batraki M, Warren N, Nacca A, Smith-Jones P, Schwartz L, Kelly WK, Slovin S, Solit D, Halpern J, Delacruz A, Curley T, Finn R, O'donoghue JA, Livingston P, Larson S, Scher HI. Pilot trial of unlabeled and indium-111-labeled anti-prostate-specific

- membrane antigen antibody J591 for castrate metastatic prostate cancer. *Clin Cancer Res* 2005;11:7454-7461.
176. Bander NH, Trabulsi EJ, Kostakoglu L, Yao D, Vallabhajosula S, Smith-Jones P, Joyce MA, Milowsky M, Nanus DM, Goldsmith SJ. Targeting metastatic prostate cancer with radiolabeled monoclonal antibody J591 to the extracellular domain of prostate specific membrane antigen. *J Urol* 2003;170:1717-1721.
177. Smith-Jones PM, Vallabhajosula S, Navarro V, Bastidas D, Goldsmith SJ, Bander NH. Radiolabeled monoclonal antibodies specific to the extracellular domain of prostate-specific membrane antigen: preclinical studies in nude mice bearing LNCaP human prostate tumor. *J Nucl Med* 2003;44:610-617.
178. Vallabhajosula S, Smith-Jones PM, Navarro V, Goldsmith SJ, Bander NH. Radioimmunotherapy of prostate cancer in human xenografts using monoclonal antibodies specific to prostate specific membrane antigen (PSMA): studies in nude mice. *Prostate* 2004;58:145-155.
179. Vallabhajosula S, Goldsmith SJ, Kostakoglu L, Milowsky MI, Nanus DM, Bander NH. Radioimmunotherapy of prostate cancer using 90Y- and 177Lu-labeled J591 monoclonal antibodies: effect of multiple treatments on myelotoxicity. *Clin Cancer Res* 2005;11:7195s-7200s.
180. Murphy G, Tjoa B, Ragde H, Kenny G, Boynton A. Phase I clinical trial: T-cell therapy for prostate cancer using autologous dendritic cells pulsed with HLA-A0201-specific peptides from prostate-specific membrane antigen. *Prostate* 1996;29:371-380.
181. Harada M, Matsueda S, Yao A, Ogata R, Noguchi M, Itoh K. Prostate-related antigen-derived new peptides having the capacity of inducing prostate cancer-reactive CTLs in HLA-A2+ prostate cancer patients. *Oncol Rep* 2004;12:601-607.
182. Kobayashi H, Omiya R, Sodey B, Yanai M, Oikawa K, Sato K, Kimura S, Senju S, Nishimura Y, Tateno M, Celis E. Identification of naturally processed helper T-cell epitopes from prostate-specific membrane antigen using peptide-based in vitro stimulation. *Clin Cancer Res* 2003;9:5386-5393.
183. Kobayashi K, Noguchi M, Itoh K, Harada M. Identification of a prostate-specific membrane antigen-derived peptide capable of eliciting both cellular and humoral immune responses in HLA-A24+ prostate cancer patients. *Cancer Sci* 2003;94:622-627.
184. Lu J, Celis E. Recognition of prostate tumor cells by cytotoxic T lymphocytes specific for prostate-specific membrane antigen. *Cancer Res* 2002;62:5807-5812.

185. Matsueda S, Takedatsu H, Yao A, Tanaka M, Noguchi M, Itoh K, Harada M. Identification of peptide vaccine candidates for prostate cancer patients with HLA-A3 supertype alleles. *Clin Cancer Res* 2005;11:6933-6943.
186. Salgaller ML, Tjoa BA, Lodge PA, Ragde H, Kenny G, Boynton A, Murphy GP. Dendritic cell-based immunotherapy of prostate cancer. *Crit Rev Immunol* 1998;18:109-119.
187. Schroers R, Shen L, Rollins L, Xiao Z, Sonderstrup G, Slawin K, Huang XF, Chen SY. Identification of MHC class II-restricted T-cell epitopes in prostate-specific membrane antigen. *Clin Cancer Res* 2003;9:3260-3271.
188. Lodge PA, Childs RA, Monahan SJ, McLean JG, Sehgal A, Boynton AL, Salgaller ML, Murphy GP. Expression and purification of prostate-specific membrane antigen in the baculovirus expression system and recognition by prostate-specific membrane antigen-specific T cells. *J Immunother* 1999;22:346-355.
189. Mincheff M, Zoubak S, Altankova I, Tchakarov S, Makogonenko Y, Botev C, Ignatova I, Dimitrov R, Madarzhieva K, Hammett M, Pomakov Y, Meryman H, Lissitchkov T. Human dendritic cells genetically engineered to express cytosolically retained fragment of prostate-specific membrane antigen prime cytotoxic T-cell responses to multiple epitopes. *Cancer Gene Ther* 2003;10:907-917.
190. Waeckerle-Men Y, Uetz-von AE, Fopp M, von MR, Bohme C, Schmid HP, Ackermann D, Cerny T, Ludwig B, Groettrup M, Gillessen S. Dendritic cell-based multi-epitope immunotherapy of hormone-refractory prostate carcinoma. *Cancer Immunol Immunother* 2006;55:1524-1533.
191. Gong MC, Latouche JB, Krause A, Heston WD, Bander NH, Sadelain M. Cancer patient T cells genetically targeted to prostate-specific membrane antigen specifically lyse prostate cancer cells and release cytokines in response to prostate-specific membrane antigen. *Neoplasia* 1999;1:123-127.
192. Ma Q, Safar M, Holmes E, Wang Y, Boynton AL, Junghans RP. Anti-prostate specific membrane antigen designer T cells for prostate cancer therapy. *Prostate* 2004;61:12-25.
193. Maher J, Brentjens RJ, Gunset G, Riviere I, Sadelain M. Human T-lymphocyte cytotoxicity and proliferation directed by a single chimeric TCRzeta /CD28 receptor. *Nat Biotechnol* 2002;20:70-75.
194. Gade TP, Hassen W, Santos E, Gunset G, Saudemont A, Gong MC, Brentjens R, Zhong XS, Stephan M, Stefanski J, Lyddane C, Osborne JR, Buchanan IM, Hall SJ, Heston WD, Riviere I, Larson SM, Koutcher JA, Sadelain M. Targeted elimination of prostate cancer by genetically directed human T lymphocytes. *Cancer Res* 2005;65:9080-9088.

195. Ren J, Zheng L, Chen Q, Li H, Zhang L, Zhu H. Co-administration of a DNA vaccine encoding the prostate specific membrane antigen and CpG oligodeoxynucleotides suppresses tumor growth. *J Transl Med* 2004;2:29.
196. Medin JA, Liang SB, Hou JW, Kelley LS, Peace DJ, Fowler DH. Efficient transfer of PSA and PSMA cDNAs into DCs generates antibody and T cell antitumor responses in vivo. *Cancer Gene Ther* 2005;12:540-551.
197. Todorova K, Zoubak S, Mincheff M, Kyurkchiev S. Biochemical nature and mapping of PSMA epitopes recognized by human antibodies induced after immunization with gene-based vaccines. *Anticancer Res* 2005;25:4727-4732.
198. Mincheff M, Zoubak S, Makogonenko Y. Immune responses against PSMA after gene-based vaccination for immunotherapy-A: results from immunizations in animals. *Cancer Gene Ther* 2006;13:436-444.
199. Kuratsukuri K, Wang CY, Sone T, Nishisaka N, Jones RF, Haas GP. Induction of antibodies against prostate-specific membrane antigen (PSMA) by vaccination with a PSMA DNA vector. *Eur Urol* 2002;42:67-73.
200. Todorova K, Ignatova I, Tchakarov S, Altankova I, Zoubak S, Kyurkchiev S, Mincheff M. Humoral immune response in prostate cancer patients after immunization with gene-based vaccines that encode for a protein that is proteasomally degraded. *Cancer Immun* 2005;5:1:1-8.
201. Smith S. Technology evaluation: C242-DM1, ImmunoGen Inc. *Curr Opin Mol Ther* 2001;3:198-203.
202. Henry MD, Wen S, Silva MD, Chandra S, Milton M, Worland PJ. A prostate-specific membrane antigen-targeted monoclonal antibody-chemotherapeutic conjugate designed for the treatment of prostate cancer. *Cancer Res* 2004;64:7995-8001.
203. Fracasso G, Bellisola G, Cingarlini S, Castelletti D, Prayer-Galetti T, Pagano F, Tridente G, Colombatti M. Anti-tumor effects of toxins targeted to the prostate specific membrane antigen. *Prostate* 2002;53:9-23.
204. Huang X, Bennett M, Thorpe PE. Anti-tumor effects and lack of side effects in mice of an immunotoxin directed against human and mouse prostate-specific membrane antigen. *Prostate* 2004;61:1-11.
205. Wolf P, Gierschner D, Buhler P, Wetterauer U, Elsasser-Beile U. A recombinant PSMA-specific single-chain immunotoxin has potent and selective toxicity against prostate cancer cells. *Cancer Immunol Immunother* 2006;55:1367-1373.
206. Zeng H, Wu Q, Li H, Wei Q, Lu Y, Li X, Wang F, Zhao F, Ding Z, Yang Y. Construction of prostate-specific expressed recombinant plasmids with high transcriptional activity of prostate-specific membrane antigen (PSMA) promoter/enhancer. *J Androl* 2005;26:215-221.

207. O'Keefe DS, Uchida A, Bacich DJ, Watt FB, Martorana A, Molloy PL, Heston WD. Prostate-specific suicide gene therapy using the prostate-specific membrane antigen promoter and enhancer. *Prostate* 2000;45:149-157.
208. Uchida A, O'Keefe DS, Bacich DJ, Molloy PL, Heston WD. In vivo suicide gene therapy model using a newly discovered prostate-specific membrane antigen promoter/enhancer: a potential alternative approach to androgen deprivation therapy. *Urology* 2001;58:132-139.
209. Ikegami S, Tadakuma T, Ono T, Suzuki S, Yoshimura I, Asano T, Hayakawa M. Treatment efficiency of a suicide gene therapy using prostate-specific membrane antigen promoter/enhancer in a castrated mouse model of prostate cancer. *Cancer Sci* 2004;95:367-370.
210. Speno HS, Luthi-Carter R, Macias WL, Valentine SL, Joshi AR, Coyle JT. Site-directed mutagenesis of predicted active site residues in glutamate carboxypeptidase II. *Mol Pharmacol* 1999;55:179-185.
211. Mahadevan D, Saldanha JW. The extracellular regions of PSMA and the transferrin receptor contain an aminopeptidase domain: implications for drug design. *Protein Sci* 1999;8:2546-2549.
212. Stoermer D, Liu Q, Hall MR, Flanary JM, Thomas AG, Rojas C, Slusher BS, Tsukamoto T. Synthesis and biological evaluation of hydroxamate-based inhibitors of glutamate carboxypeptidase II. *Bioorg Med Chem Lett* 2003;13:2097-2100.
213. Rinker-Schaeffer CW, Hawkins AL, Su SL, Israeli RS, Griffin CA, Isaacs JT, Heston WD. Localization and physical mapping of the prostate-specific membrane antigen (PSM) gene to human chromosome 11. *Genomics* 1995;30:105-108.
214. Shneider BL, Thevananther S, Moyer MS, Walters HC, Rinaldo P, Devarajan P, Sun AQ, Dawson PA, Ananthanarayanan M. Cloning and characterization of a novel peptidase from rat and human ileum. *J Biol Chem* 1997;272:31006-31015.
215. Bacich DJ, Ramadan E, O'Keefe DS, Bukhari N, Wegorzewska I, Ojeifo O, Olszewski R, Wrenn CC, Bzdega T, Wroblewska B, Heston WD, Neale JH. Deletion of the glutamate carboxypeptidase II gene in mice reveals a second enzyme activity that hydrolyzes N-acetylaspartylglutamate. *J Neurochem* 2002;83:20-29.
216. Bzdega T, Crowe SL, Ramadan ER, Sciarretta KH, Olszewski RT, Ojeifo OA, Rafalski VA, Wroblewska B, Neale JH. The cloning and characterization of a second brain enzyme with NAAG peptidase activity. *J Neurochem* 2004;89:627-635.
217. Bacich DJ, Pinto JT, Tong WP, Heston WD. Cloning, expression, genomic localization, and enzymatic activities of the mouse homolog of prostate-specific membrane antigen/NAALADase/folate hydrolase. *Mamm Genome* 2001;12:117-123.

218. Slusher BS, Robinson MB, Tsai G, Simmons ML, Richards SS, Coyle JT. Rat brain N-acetylated alpha-linked acidic dipeptidase activity. Purification and immunologic characterization. *J Biol Chem* 1990;265:21297-21301.
219. Slusher BS, Tsai G, Yoo G, Coyle JT. Immunocytochemical localization of the N-acetyl-aspartyl-glutamate (NAAG) hydrolyzing enzyme N-acetylated alpha-linked acidic dipeptidase (NAALADase). *J Comp Neurol* 1992;315:217-229.
220. Passani LA, Vonsattel JP, Carter RE, Coyle JT. N-acetylaspartylglutamate, N-acetylaspartate, and N-acetylated alpha-linked acidic dipeptidase in human brain and their alterations in Huntington and Alzheimer's diseases. *Mol Chem Neuropathol* 1997;31:97-118.
221. Grauer LS, Lawler KD, Marignac JL, Kumar A, Goel AS, Wolfert RL. Identification, purification, and subcellular localization of prostate-specific membrane antigen PSM' protein in the LNCaP prostatic carcinoma cell line. *Cancer Res* 1998;58:4787-4789.
222. Lapidus RG, Tiffany CW, Isaacs JT, Slusher BS. Prostate-specific membrane antigen (PSMA) enzyme activity is elevated in prostate cancer cells. *Prostate* 2000;45:350-354.
223. Tiffany CW, Lapidus RG, Merion A, Calvin DC, Slusher BS. Characterization of the enzymatic activity of PSM: comparison with brain NAALADase. *Prostate* 1999;39:28-35.
224. Barinka C, Sacha P, Sklenar J, Man P, Bezouska K, Slusher BS, Konvalinka J. Identification of the N-glycosylation sites on glutamate carboxypeptidase II necessary for proteolytic activity. *Protein Sci* 2004;13:1627-1635.
225. Ghosh A, Heston WD. Effect of carbohydrate moieties on the folate hydrolysis activity of the prostate specific membrane antigen. *Prostate* 2003;57:140-151.

9 GLOSSARY

1 *FISH*

Fluorescent *in situ* hybridization is a cytogenetic technique, which is used for detection and localization of presence or absence of specific DNA sequences on chromosomes. It uses fluorescent probes, which bind only to those parts of the chromosome with which they show a high degree of sequence similarity. Fluorescence microscopy can be used to find out where the fluorescent probe bound to the chromosome.

2 *agonist*

In pharmacology it is a substance that binds to a specific receptor and triggers a response in the cell. It mimics the action of an endogenous ligand (such as hormone or neurotransmitter) that binds to the same receptor.

3 *G-proteins*

Guanine nucleotide binding proteins are a family of proteins involved in second messenger cascades. They are so called, because of their signaling mechanism, which uses the exchange of guanosine diphosphate (GDP) for guanosine triphosphate (GTP) as a general molecular "switch" function to regulate cell processes.

4 *antagonist*

A molecule that blocks the ability of a given chemical to bind to its receptor, it prevents a biological response.

5 *glia (glial cells)*

Non-neuronal cells that provide support and nutrition, maintain homeostasis, form myelin, and participate in signal transmission in the nervous system.

Types of glia:

Microglia

Specialized macrophages capable of phagocytosis that protect neurons of the central nervous system.

Astrocytes

Characteristic star-shaped glial cells in the brain. They perform many functions, including the formation of the blood-brain barrier, the provision of nutrients to the nervous tissue, and play a principal role in the repair and scarring process in the brain.

Oligodendrocytes

Cells that coat axons in the central nervous system with their cell membrane, called myelin, producing the so-called myelin sheath.

Ependymal cells

Cell which line the cavities of the CNS and make up the walls of the ventricles. These cells create and secrete cerebrospinal fluid.

Schwann cells

They are similar in function to oligodendrocytes and provide myelination to axons in the peripheral nervous system. They also have phagocytotic activity.

6 *transient middle cerebral artery occlusion*

It is an animal model of ischemic stroke where the middle cerebral artery is surgically dissected and subsequently transiently occluded. After defined period of time the middle cerebral artery is being reperfused again.

7 *ganglion*

Type of neuron located in the retina of the eye that receives visual information from photoreceptors via various intermediate cells such as bipolar cells, amacrine cells, and horizontal cells.

8 *traumatic brain injury*

Traumatic injuries to the brain occur when a sudden trauma causes brain damage. Symptoms of a traumatic brain injury can be mild, moderate, or severe, depending on the extent of the damage to the brain. Outcome can be anything from complete recovery to permanent disability or death.

9 *lateral fluid percussion*

A model of mild-moderate concussion, which leads to the temporary loss of the capacity for experience-dependent plasticity in developing organism.

10 *afferent nerves*

Nerve fibers (usually sensory) that carry impulses from an organ or tissue toward the brain and spinal cord, or the information processing centers of the enteric nervous system, which is located within the walls of the digestive tract.

11 *ectopic discharges*

The ectopic afferent activity is largely responsible for the development of hypersensitivity of dorsal horn neurons and neuropathic pain. Afferent ectopic discharges from the site of nerve injury constitute a source of abnormal sensory input to the spinal dorsal horn.

12 *hyperalgesia*

An extreme sensitivity to pain, which in one form is caused by damage to nociceptors in the body's soft tissues.

A nociceptor is a sensory receptor that sends signals that cause the perception of pain in response to potentially damaging stimulus.

13 *allodynia*

An exaggerated response to otherwise non-noxious stimuli and can be either static or mechanical. For example, a person with allodynia may perceive light pressure or the movement of clothes over the skin as painful, whereas a healthy individual will not feel pain.

14 *carrageenan injection*

In this method carrageenan is injected subcutaneously into the plantar surface of the hind paw.

15 *diabetic neuropathy*

Disorders associated with diabetes mellitus, which result from diabetic microvascular injury involving small blood vessels that supply nerves. The first pathological change in the microvasculature is vasoconstriction. As the disease progresses, neuronal dysfunction correlates closely with the development of vascular abnormalities, which contribute to diminished oxygen tension and hypoxia. Microvascular dysfunction occurs early in diabetes, parallels the progression of neural dysfunction, and may be sufficient to support the severity of structural, functional, and clinical changes observed in diabetic neuropathy.

16 *carcinoma*

Any cancer that arises from epithelial cells. It is malignant by definition: carcinomas invade surrounding tissues and organs, and may spread to lymph nodes and distal sites (metastasis).

17 *benign prostatic hyperplasia (BPH)*

Increase in size of the prostate in middle-aged and elderly men. It is characterized by hyperplasia of prostatic stromal and epithelial cells, resulting in the formation of large, fairly discrete nodules in the

periurethral region of the prostate. Although prostate specific antigen levels may be elevated in these patients, because of increased organ volume and inflammation due to urinary tract infections, BPH is not considered to be a premalignant lesion.

18 *adenocarcinoma*

Form of carcinoma that originates in glandular tissue. To be classified as adenocarcinoma, the cells do not necessarily need to be part of a gland, as long as they have secretory properties. This form of carcinoma can occur in some higher mammals, including humans.

19 *tissue microarrays*

A paraffin blocks in which up to 1000 separate tissue cores are assembled in array fashion to allow simultaneous histological analysis. The major limitations in molecular clinical analysis of tissues include the cumbersome nature of procedures, limited availability of diagnostic reagents and limited patient sample size. The technique of tissue microarray was developed to address these issues.

20 *metastasis*

Spread of a disease from one organ or part to another non-contiguous organ or part. Only malignant tumor cells and infections have the capacity to metastasize.

21 *Gleason score*

A Gleason score is given to prostate cancer based upon its microscopic appearance. The Gleason score is important because higher Gleason scores are associated with worse prognosis. This is because higher Gleason scores are given to cancer, which is more aggressive. To assign a Gleason score, a piece of prostatic tissue must be obtained (a biopsy). This is done either by removing the gland (prostatectomy) or by sampling the gland with a needle introduced through the rectum.

Grade 1: The cancerous prostate closely resembles normal prostate tissue. The glands are small, well formed, and closely packed

Grade 2: The tissue still has well-formed glands, but they are larger and have more tissue between them.

Grade 3: The tissue still has recognizable glands, but the cells are darker. At high magnification, some of these cells have left the glands and are beginning to invade the surrounding tissue.

Grade 4: The tissue has few recognizable glands. Many cells are invading the surrounding tissue

Grade 5: The tissue does not have recognizable glands. There are often just sheets of cells throughout the surrounding tissue.

22 *prostatic intraepithelial neoplasia (PIN)*

A non-invasive lesion in the prostate gland that is thought to be a precursor to prostate cancer. PIN does not require specific therapy, but close follow-up with additional biopsies is warranted. PIN may disappear, remain unchanged, or progress to prostate cancer, often over as many as ten years.